



Evaluation of YB-1 transcriptional factor, DNA glycosylase hNTH1 and human topoisomerase I functions in relation to drug resistance and DNA repair mechanisms

Muge Senarisoy

► To cite this version:

Muge Senarisoy. Evaluation of YB-1 transcriptional factor, DNA glycosylase hNTH1 and human topoisomerase I functions in relation to drug resistance and DNA repair mechanisms. Biochemistry, Molecular Biology. Université Grenoble Alpes; Ege Üniversitesi (Izmir, Turquie), 2018. English. NNT : 2018GREAV064 . tel-02110791

HAL Id: tel-02110791

<https://theses.hal.science/tel-02110791>

Submitted on 25 Apr 2019

HAL is a multi-disciplinary open access archive for the deposit and dissemination of scientific research documents, whether they are published or not. The documents may come from teaching and research institutions in France or abroad, or from public or private research centers.

L'archive ouverte pluridisciplinaire **HAL**, est destinée au dépôt et à la diffusion de documents scientifiques de niveau recherche, publiés ou non, émanant des établissements d'enseignement et de recherche français ou étrangers, des laboratoires publics ou privés.



THÈSE

Pour obtenir le grade de

**DOCTEUR DE LA COMMUNAUTE UNIVERSITE
GRENOBLE ALPES**

**préparée dans le cadre d'une cotutelle entre la
*Communauté Université Grenoble Alpes et Ege
University***

Spécialité : **Biotechnology**

Arrêté ministériel : le 6 janvier 2005 – 25 mai 2016

Présentée par **Muge SENARISOY**

Thèse dirigée par **Dr. Joanna Timmins**

Codirigée par **Prof. Dr. Zeki Topcu**

Préparée au sein de l'**Institut de Biologie Structurale et de la
Faculté de Pharmacie d'Egée**

dans **les Écoles Doctorales Chimie et Science du Vivant
(Grenoble) et Graduate School of Natural and Applied
Sciences (Izmir)**

**Evaluation of YB-1 Transcriptional Factor, DNA
Glycosylase hNTH1 and Human Topoisomerase I
Functions in Relation to Drug Resistance and
DNA Repair Mechanisms**

Thèse soutenue publiquement le **27 September 2018**,
devant le jury composé de :

Dr. Dominique Bourgeois

Président

Dr. Xavier Morelli

Rapporteur

Prof. Dr. Meltem Muftuoglu

Rapporteur

Prof. Dr. Hilmi Orhan

Membre

Dr. Joanna Timmins

Membre

Prof. Dr. Zeki Topcu

Membre





THÈSE

Pour obtenir le grade de

**DOCTEUR DE LA COMMUNAUTE UNIVERSITE
GRENOBLE ALPES**

**préparée dans le cadre d'une cotutelle entre la
*Communauté Université Grenoble Alpes et Ege
University***

Spécialité : **Biotechnologie**

Arrêté ministériel : le 6 janvier 2005 – 25 mai 2016

Présentée par **Muge SENARISOY**

Thèse dirigée par **Dr. Joanna Timmins**

Codirigée par **Prof. Dr. Zeki Topcu**

Préparée au sein de l'**Institut de Biologie Structurale et de la
Faculté de Pharmacie d'Egée**

dans les **Écoles Doctorales Chimie et Science du Vivant
(Grenoble) et Graduate School of Natural and Applied
Sciences (Izmir)**

**Etudes des Fonctions du Facteur de
Transcription YB-1, de l'ADN Glycosylase NTH1
et de la Topoisomérase I dans le Contexte de la
Résistance aux Drogues et en Relation avec les
Voies de Réparation de l'ADN**

Thèse soutenue publiquement le **27 septembre 2018**,
devant le jury composé de :

Dr. Dominique Bourgeois

Président

Dr. Xavier Morelli

Rapporteur

Prof. Dr. Meltem Muftuoglu

Rapporteur

Prof. Dr. Hilmi Orhan

Membre

Dr. Joanna Timmins

Membre

Prof. Dr. Zeki Topcu

Membre



ABSTRACT**EVALUATION OF YB-1 TRANSCRIPTIONAL FACTOR, DNA GLYCOSYLASE hNTH1 AND HUMAN TOPOISOMERASE I FUNCTIONS IN RELATION TO DRUG RESISTANCE AND DNA REPAIR MECHANISMS**

SENARISOY, Müge

PhD in Biotechnology

Supervisor: Dr. Joanna TIMMINS

Co-Supervisor: Prof. Dr. Zeki TOPCU

September 2018, 209 pages

Acquired resistance to anti-cancer therapy is common and is a major clinical issue. Functional DNA repair pathways provide a common mechanism for drug resistance, but it can also result from mutations or reduced expression of the targeted protein. The overexpression or nuclear localisation of the multifunctional Y-box binding protein (YB-1) is considered as a prognostic marker for drug resistance in tumours. YB-1 has several interaction partners in cells; in this study, we have focused on its interaction with the human DNA repair enzyme NTH1 (hNTH1) and human DNA topoisomerase I (hTopoI), two enzymes that have been shown to be stimulated by YB-1. The abundance of the hNTH1/YB-1 complex was shown to increase in cisplatin-resistant tumour cells. Human TopoI is an essential enzyme involved in cellular regulation of DNA supercoiling and is the target of several anti-cancer agents. YB-1 enhances the activity of hTopoI and its sensitivity to hTopoI inhibitor, camptothecin in tumour cells. We have characterised the YB-1/hNTH1 and YB-1/hTopoI complexes *in vitro* and *in vivo* using Fluorescence Resonance Energy Transfer (FRET) measurements to identify and develop new strategies for the treatment of drug-resistant tumours. We also designed and optimised an original FRET-based biosensor to screen two medium-sized chemical libraries in order to find potential inhibitors of the hNTH1/YB-1 complex. Several “hits” were identified that significantly reduced the FRET level of our biosensor. For some of these compounds, we have reproduced these results starting from powders, have performed dose-response curves and have validated their actions as inhibitors of the hNTH1/YB-1 interface using alternative binding assays. Taken together, our results demonstrate that YB-1 directly interacts and stimulates a DNA repair and a DNA relaxing enzyme and targeting the YB-1/hNTH1 interface represents an interesting new strategy for the development of anti-cancer drugs.

Keywords: Cancer, DNA Repair, Topoisomerase I, Protein-protein interactions, FRET

RÉSUMÉ

ETUDES DES FONCTIONS DU FACTEUR DE TRANSCRIPTION YB-1, DE L'ADN GLYCOSYLASE hNTH1 ET DE LA TOPOISOMERASE HUMAINE I DANS LE CONTEXTE DE LA RÉSISTANCE AUX DROGUES ET EN RELATION AVEC LES VOIES DE RÉPARATION DE L'ADN

SENARISOY, Müge

Doctorat en Biotechnologie

Directeur: Dr. Joanna TIMMINS

Co-Directeur: Prof. Dr. Zeki TOPCU

Septembre 2018, 209 pages

La résistance acquise aux traitements anticancéreux représente un problème clinique majeur. Les voies de réparation de l'ADN fournissent un mécanisme de résistance, mais celle-ci peut aussi résulter de mutations ou d'une expression réduite de la protéine ciblée. La surexpression ou la localisation nucléaire de la Y-Box binding (YB-1) protéine est considérée comme un marqueur pronostique de chimiorésistance de la tumeur. YB-1 interagit avec plusieurs partenaires ; dans cette étude, nous nous sommes concentrés sur son interaction avec l'enzyme de réparation de l'ADN NTH1 (hNTH1) et l'ADN topoisomérase I (hTopoI), deux enzymes stimulées par YB-1. L'abondance du complexe hNTH1/YB-1 est accrue dans les cellules tumorales résistantes au cisplatine. La TopoI humaine est une enzyme essentielle impliquée dans la régulation cellulaire du surenroulement de l'ADN et est la cible de plusieurs agents anticancéreux. YB-1 augmente la sensibilité à l'inhibiteur de TopoI, la camptothécine, dans les tumeurs. Nous avons caractérisé les complexes YB-1/hNTH1 et YB-1/hTopoI *in vitro* et *in vivo* en utilisant des mesures de transfert d'énergie par résonance en fluorescence (ou FRET) pour identifier et développer de nouvelles stratégies pour le traitement de tumeurs chimio-résistantes. Nous avons développé et optimisé un biosenseur original basé sur le FRET pour cribler deux chimiothèques de taille moyenne afin d'identifier des inhibiteurs potentiels du complexe hNTH1/YB-1. Plusieurs «hits» ont été identifiés qui réduisent de façon significative le niveau de FRET de notre biosenseur. Pour certains de ces composés, nous avons reproduit ces résultats à partir de poudres, effectué des courbes dose-réponse et validé leurs actions en tant qu'inhibiteurs de l'interface hNTH1/YB-1 en utilisant d'autres tests d'interactions. Ensemble nos résultats démontrent que YB-1 interagit directement et stimule des enzymes de la réparation de l'ADN et du relaxation de l'ADN, et que cibler l'interface YB-1/hNTH1 représente une nouvelle stratégie intéressante pour le développement de traitements anticancéreux.

Mots clés: Cancer, Réparation de l'ADN, Topoisomérase I, Interactions protéines-protéines, FRET

ÖZET**YB-1 TRANSKRİPSİYON FAKTÖRÜ, DNA GLİKOZİL AZ hNTH1
VE İNSAN TOPOİZOMERAZ I ENZİMİ İŞLEVLERİNİN İLAÇ
DİRENCİ VE DNA TAMİR MEKANİZMASI KAPSAMINDA
DEĞERLENDİRİLMESİ**

ŞENARISOY, Müge

Doktora Tezi, Biyoteknoloji Anabilim Dalı

Tez Danışmanı: Prof. Dr. Zeki TOPÇU

İkinci Danışmanı: Dr. Joanna TIMMINS

Eylül 2018, 209 sayfa

Anti-kanser tedavisine karşı kazanılan direnç yaygın ve önemli bir klinik sorundur. Fonksiyonel DNA onarım yolları, ilaç direnci için yaygın bir mekanizma sağlamaktadır, ancak aynı zamanda, hedeflenen proteinin mutasyonlarından veya ekspresyonunun azalmasından da kaynaklanabilmektedir. Çok işlevli Y-box bağlanma proteinin (YB-1) aşırı ekspresyonu veya nükleer lokalizasyonu, tümörlerde ilaç direnci için bir prognostik belirteç olarak kabul edilmektedir. YB-1'in hücrelerde birkaç etkileşim partneri vardır; bu çalışmada, YB-1 ile aktiviteleri uyarıldığı gösterilen insan DNA onarım enzimi NTH1 (hNTH1) ve insan DNA topoizomera z I (hTopoI) ile olan etkileşimleri üzerine odaklandık. Cisplatin-dirençli tümör hücrelerinde hNTH1/YB-1 kompleks oluşumunun arttığı gösterilmiştir. İnsan TopoI, DNA süpersarmallarının hücre sel regülasyonunda yer alan ve birkaç anti-kanser ajanının hedefi olan önemli bir enzimdir. YB-1, hTopoI aktivitesini ve tümör hücrelerinin hTopoI inhibitörü Camptothecin'e olan duyarlılığını artırmaktadır. Bu çalışmada YB-1/hNTH1 ve YB-1/hTopoI komplekslerini *in vitro* ve *in vivo* olarak, ilaca dirençli tümörlerin tedavisi için yeni stratejiler tanımlamak ve geliştirmek için Fluoresans Rezonans Enerji Transferi (FRET) ölçümlerini kullanarak karakterize ettik. Ayrıca, hNTH1/YB-1 kompleksinin potansiyel inhibitörlerini bulmak için iki orta ölçekli kimyasal kütüphaneyi taramak üzere orijinal bir FRET-bazlı biyosensör tasarladık ve optimize ettik. Biyosensörümüzün FRET seviyesini önemli ölçüde azaltan birkaç "hit" tespit ettik. Bu bileşiklerin bazıları için, to z bileşiklerden başlayarak bu sonuçları tekrar ürettik, doz-cevap eğrileri gerçekleştirdik ve alternatif bağlama deneyleri kullanarak hNTH1/YB-1 arayüzünün inhibitörleri olarak onayladık. Birlikte ele alındığında, sonuçlarımız YB-1'in DNA onarımı ve DNA relakse edici enzimleriyle doğrudan etkileşime girip uyardığını ve YB-1/hNTH1 arayüzünü hedef almanın, anti-kanser ilaçlarının geliştirilmesi için ilginç yeni bir stratejiyi temsil ettiğini göstermektedir.

Anahtar sözcükler: Kanser, DNA tamiri, Topoizomera z I, Protein-protein etkileşimleri, FRET

ACKNOWLEDGEMENTS

I am very grateful to my thesis advisor, Dr. Joanna Timmins, for giving me the opportunity to do my PhD work in her laboratory. I also want to thank her for her valuable and constructive suggestions in every step of my research. I would like to express my deep gratitude to Prof. Dr. Zeki Topcu, my thesis co-advisor, for his guidance since my bachelor degree and his encouragements about my career.

I would like to thank my rapporteurs Dr. Xavier Morelli and Prof. Dr. Meltem Müftüoğlu, for giving their precious time to evaluate my thesis work, and the President of my jury, Dr. Dominique Bourgeois and the examiner Prof. Dr. Hilmi Orhan, for accepting to take part in my jury and assessing my work. I also want to thank my thesis progress committee members Assoc. Prof. Dr. Serap Evran and Dr. Jean-Philippe Kleman, for their feedback and guidance during my PhD.

I wish to thank various people for their contribution to this project; Dr. Jean-Philippe Kleman for his advice and help in analyzing the *in vitro* and *in vivo* FRET data; François Lacroix for her valuable technical support on the M4D platform; Dr. Caroline Barette, for the high-throughput screening on the CMBA platform; Dr. Meike Stelter, for preliminary results on the hNTH1/YB-1 complex characterisation; Dr. Joanna Timmins, for performing the AlphaScreen dose-response assays.

I am also very thankful to all my past and present lab mates; from the VIC Group at IBS: Kevin Floc'h, Dr. Mizar Oliva, Salvatore DeBonis, Marjolaine Noirclerc-Savoye, Fabienne Hans, Anne-Sophie Banneville, Anna Seck, Anthoula Mettou; from Zeki's lab at EGE: Dr. Sevil Zencir, Gizem Çalışkan, Dr. Mustafa Kotmakçı, Dr. Esra Öztürk Yiğit, Ezgi Öner, Dr. Pakize Cantürk Kılıçkaya and my bachelor friend Pelin Dinsel.

I wish to thank my colleagues and friends; Ana Sosa Fajardo, Quentin Bertrand, Laura Lemel, Lynda Djerbal, Rana Elmasri, Silvia Achilli, Marko Nedelkovich, Daniel Thedie, Tomas Hosek, Simon Harris, Raleb Taher, Clarissa Liesche, Joël Beaudouin, and Joyce Woodhouse for their pleasant company in Grenoble during my PhD and further.

This work is dedicated to my mother, Deniz Durgut and my dearest brother, Hakan Şenarisoğlu who always love me and believe in me. They supported me in any case. I would also like to thank my aunt Şeniz Tosun, my uncle Oğuz Durgut, and my cousins Gizem and Nerin Tosun for their valuable support.

My PhD study was supported by The Scientific and Technological Research Council of Turkey (TUBITAK) 2214/B International Joint PhD Fellowship Programme and by the Labex GRAL.

TABLE OF CONTENTS

	PAGE
ABSTRACT	iii
RÉSUMÉ	v
ÖZET... ..	vii
ACKNOWLEDGEMENTS	ix
LIST OF FIGURES	xv
LIST OF TABLES.....	xxi
LIST OF ABBREVIATIONS	xxiii
Chapter 1. Introduction	1
Summary	3
1.1 Cancer and its treatment.....	11
1.2. Acquired resistance to chemotherapy	13
1.2.1. Alterations of drug metabolism and membrane transport.....	14
1.2.2. Failure to induce apoptosis	15
1.2.3. Enhanced DNA repair pathways.....	16
1.2.4. Changes in drug target or drug target level	18
1.3. Y-box Binding Protein 1 as a prognostic marker of drug resistance	19
1.3.1. Protein properties of YB-1	20
1.3.2. Functions of YB-1 in cells.....	22
1.4. Importance of protein-protein interactions in cellular processes.....	24
1.4.1. Methods for identification of PPI	24
1.4.2. Chemical library screening in order to find PPI inhibitors.....	25
1.4.2.1. Fluorescence Resonance Energy Transfer.....	26
1.4.2.2. Homogeneous Time-Resolved Fluorescence (HTRF) Assay.....	28
1.4.2.3. Amplified Luminescent Proximity Homogeneous (AlphaScreen) Assay.....	29
1.5. Human Endonuclease III (hNTH1) and its role in Base Excision Repair	30

1.5.1. Base Excision Repair Pathway.....	30
1.5.2. Human Endonuclease III (hNTH1)	34
1.6. Preliminary data obtained for the study of YB-1/hNTH1 complex	38
1.7. DNA topoisomerase I as an anticancer drug target.....	39
1.7.1. DNA Topology.....	40
1.7.2. DNA Topoisomerases	41
1.7.3. Human Topoisomerase I (hTopoI)	44
Objectives	49
Chapter 2. Materials and Methods	51
Summary	53
2.1. Cloning	57
2.1.1. Mammalian Expression Vector.....	59
2.1.2. Bacterial Expression Vector	60
2.1.2.1. Fluorescent Protein Coupled Constructs	61
2.1.2.2. Biosensor constructs	61
2.2. Protein expression and purification.....	63
2.2.1. Expression and purification of fluorescent proteins.....	63
2.2.2. Expression and purification of fluorescent protein fusion proteins, Biosensor constructs and human Topoisomerase I (hTopoI)	63
2.2.3. Large-scale purification of Biosensor 1 for chemical library screening ...	67
2.2.4. Preparation of proteins for AlphaScreen Assay	67
2.3. <i>In vitro</i> Fluorescence Resonance Energy Transfer (FRET) measurements .	68
2.4. <i>In vitro</i> high-throughput screening with Biosensor 1.....	71
2.4.1. Optimization of Biosensor 1 FRET measurements.....	71
2.4.2. Chemical library screening at CMBA platform	72
2.5. AlphaScreen Assay	75
2.6. DNA relaxation activity assays.....	76
2.7. Maintenance and transfection of mammalian cells	77
2.8. FRET measurements in mammalian cells	78

Chapter 3. Results.....	81
Summary	83
<u>Part I. YB-1/hNTH1 complex</u>	91
3.1. YB-1/hNTH1 interaction in mammalian cells.....	91
3.1.1. FRET measurements in hNTH1-mTQ2 expressing MCF7 cells.....	92
3.1.2. Design of Biosensor construct	94
3.2. YB-1 Δ C/hNTH1 interaction <i>in vitro</i>	95
3.2.1. Purification of fluorescent protein fusion constructs	95
3.2.1.1. Fluorescent proteins	95
3.2.1.2. YB-1 Δ C fusion constructs	96
3.2.1.3. hNTH1 fusion constructs.....	97
3.2.1.4. Biosensor constructs.....	99
3.2.2. FRET measurements	101
3.2.2.1. Mixture of individual proteins	101
3.2.2.2. Biosensors.....	103
3.3. High-throughput chemical library screening with Biosensor 1.....	107
3.3.1. Optimization of Biosensor 1	108
3.3.2. Life Chemicals Protein-Protein Interaction Fragment Library.....	111
3.3.3. Prestwick Chemical Library	113
3.4. Validation of hits from screening	117
3.4.1. Autofluorescence of compounds	117
3.4.2. Effect of compounds on the FRET signal of the Fusion construct.....	118
3.4.3. Effect of compounds on the FRET signal of Biosensor 1	119
3.4.4. AlphaScreen Assay	126
<u>Part II. YB-1-hTopoI complex</u>	128
3.5. YB-1-hTopoI interaction <i>in vitro</i>	128
3.5.1. Expression and purification of human Topoisomerase I (hTopoI).....	128
3.5.2. DNA relaxation activity assays.....	131
3.5.3. Stimulation of hTopoI's relaxation activity by YB-1	132
3.5.4. <i>In vitro</i> FRET measurements.....	133

3.5.4.1. Expression and purification of hTopoI fusion constructs	133
3.5.4.2. Mixture of individual proteins	135
3.6. YB-1/hTopoI interaction in mammalian cells	137
3.6.1. FRET measurements in HeLa cells	137
3.6.2. FRET measurements in MCF7 cells	140
3.6.3. FRET measurements in PC-3 cells.....	142
Chapter 4. Discussion.....	145
Summary	147
<u>Part I. YB-1/hNTH1 complex</u>	155
<u>Part II. YB-1/hTopoI complex</u>	163
<u>Part III. Both hNTH1 and hTopoI complexes with YB-1</u>	168
<u>Part IV. Conclusions and Future Prospects</u>	169
ANNEX	171
REFERENCES	193
CURRICULUM VITAE	213

LIST OF FIGURES

FIGURE	PAGE
1.1. Hallmarks of tumour cells	12
1.2. Illustration of the different mechanisms of chemotherapeutic drug resistance in tumour cells.....	14
1.3. Overview of DNA repair pathways involved in repairing toxic DNA lesions formed by cancer treatments	17
1.4. Schematic diagram of YB-1 domain organization	21
1.5. Structural information about YB-1	21
1.6. Schematic diagram showing the numerous functions of YB-1 that affect all hallmarks of cancer	22
1.7. Jablonski diagram showing the various steps involved in fluorescence excitation and emission	26
1.8. Illustration of FRET principle	27
1.9. Principle of HTRF assay	28
1.10. Illustration of AlphaScreen Assay	30
1.11. Schematic diagram illustrating the various steps and enzymes involved in Base Excision Repair.....	33
1.12. Schematic diagram of hNTH1 domain organization	34
1.13. The 3D structure of EndoIII-1 from <i>Deinococcus radiadurans</i>	35
1.14. Pyrimidine-derived lesions excised by hNTH1	36
1.15. Schematic illustration of the bifunctional reaction mechanism catalyzed by hNTH1 and the effect of XPG, APE1, and YB-1 on the regulation of its activity.....	37
1.16. Stimulation of hNTH1 AP-lyase activity by YB-1.....	38
1.17. AlphaScreen binding assays of YB-1 and hNTH1	39
1.18. Illustration of the different DNA topologies.	41
1.19. Reactions of Type I and Type II topoisomerases	43
1.20. Mechanism of Human Topoisomerase I targeting drugs	44
1.21. The structure and domain organization of hTopoI	45

1.22. Active site of hTopoI and its reaction	46
1.23. hTopoI-mediated DNA relaxation by controlled rotation	47
1.24. Schematic illustration of the complex and diverse roles of YB-1 in regulating the sensitivity and resistance of tumour cells to chemotherapeutic drugs	49
2.1. Illustration of the domain organisation of YB1, hNTH1 and hTopoI and their various constructs used in this study	57
2.2. Strategies used to assemble the complete <i>hTopoI</i> gene using the three fragments obtained from Eurofins MWG	58
2.3. Maps of pEGFP-C1 and N-1 mammalian expression vectors	59
2.4. Maps of bacterial expression vectors used for protein expressions	60
2.5. Illustration of the purification protocol steps used in our various protein purifications.....	64
2.6. Excitation and emission spectra of mTQ2 and sYFP2 fluorescent proteins used in this study	68
2.7. Schematic representation of the FRET measurements performed in order to calculate the FRET efficiency	69
2.8. Fluorescence spectra showed spill-over factors between channels.....	70
2.9. Illustration of screening plates	73
2.10. Representative agarose gel image to show the mobility of the supercoiled substrate, the nicked circles, and the relaxed topoisomers	76
2.11. Illustration of the confocal, spinning disk microscopy platform setup used for the acceptor photobleaching experiments on fixed cells.....	78
3.1. MCF7 cells transfected with hNTH1-mTQ2, YB-1-sYFP2 and YB-1 Δ C- sYFP2.....	92
3.2. hNTH1-YB-1 FRET measurements in transfected MCF7 cells	93
3.3. Biosensor design	94
3.4. Example of a hNTH1-YB-1 FRET measurement in MCF7 cells transfected with Biosensor 1	95
3.5. Illustration of fluorescent proteins used in our work	95
3.6. Example of Stain-Free gel image of fluorescent proteins	96
3.7. Illustration of YB-1 Δ C constructs fused to sYFP2 used in our work	96

3.8. Illustration of the different chromatographic steps used to purify YB-1ΔC fusion constructs.....	97
3.9. Illustration of hNTH1 constructs fused to mTQ2 used in our work.....	97
3.10. Illustration of the different chromatographic steps used to purify hNTH1 fusion constructs.....	98
3.11. NtailhNTH1-mTQ2 ion-exchange chromatography.	98
3.12. Illustration of the Biosensor constructs used in our work	99
3.13. Representative gels and chromatograms of Biosensor 1 purification.....	100
3.14. Stain-free gel analysis of purified Biosensor constructs	100
3.15. mTQ2 and sYFP2 spectra of the sYFP2 and mTQ2 alone and mixed in a 1:1 ratio, and sYFP2-mTQ2 fusion construct at 1.5μM in 200mM NaCl GF buffer	101
3.16. FRET efficiencies of individual protein mixes of hNTH1 and YB-1ΔC constructs	102
3.17. FRET measurements of Biosensor 1 and its comparison with Fusion construct.....	103
3.18. FRET measurements of all Biosensors and Fusion construct at different NaCl concentrations	104
3.19. FRET efficiencies of Fusion and Biosensor constructs at 1 μM concentration in 50 mM NaCl in the presence of 6 M urea.....	105
3.20. FRET measurements in order to find a potential competitor of YB-1/hNTH1 interaction for Biosensor 1 construct.....	106
3.21. FRET measurements of Fusion and Biosensor constructs at different protein concentrations in buffer containing 50mM NaCl.....	107
3.22. Stability of FRET signal of 0.2 μM Fusion and Biosensor 1 construct in presence of increasing amounts of DMSO	108
3.23. Inhibition of Biosensor 1 FRET by addition of hNTH1 DNA substrate ..	109
3.24. Stability of FRET signal of Biosensor 1 construct during 2 hours	109
3.25. Equation of Z' factor and categorization of screening assay by the value of the Z' factor	110
3.26. Overall results obtained from the first HTS of Life Chemicals PPI library	111
3.27. Overall results obtained from the second HTS of Life Chemicals PPI library with selected 30 compounds.....	112

3.28. Potential hits identified in Life Chemicals PPI library.....	113
3.29. Overall results obtained from the first HTS of Prestwick Chemical library	114
3.30. Overall results obtained from the secondary HTS of Prestwick Chemical library with 30 selected compounds	115
3.31. Characterisation of the top 8 hits identified from the Prestwick chemical library.....	115
3.32. Effect of selected compounds on the FRET efficiency of the Fusion construct.....	119
3.33. Inhibition of Biosensor 1 FRET by Life Chemicals test compounds	120
3.34. Inhibition of Biosensor 1 FRET by seven Prestwick compounds	121
3.35. Comparison of the extent of inhibition of seven selected Prestwick compounds from different sources	122
3.36. Spectral analysis of Prestwick compounds.....	123
3.37. Dose response curves of selected Prestwick hits ordered from Sigma, dissolved in DMSO and stored at 4°C for 2 days or 3 months prior to measurements	124
3.38. Dose response curves of seven Prestwick hits provided by CMBA platform.....	125
3.39. Dose response curves of selected Prestwick hits ordered from Sigma and stored at 4°C for 2 days determined by AlphaScreen assay.....	127
3.40. Illustration of hTopoI constructs used in our work.....	128
3.41. Purification of hTopoI-FL and hTopoI-70	129
3.42. Mass spectrometry analysis of hTopoI-FL and hTopoI-70 fractions.....	130
3.43. DNA relaxation activity of purified hTopoI	131
3.44. DNA relaxation activity of wild-type and K172A hTopoI.....	131
3.45. Inhibition of the DNA relaxation activity of hTopoI by CPT	132
3.46. Stimulation of hTopoI DNA relaxation activity by YB-1ΔC	133
3.47. Illustration of hTopoI fusion constructs used in our work	134
3.48. Purification of hTopoI-mTQ2.....	134
3.49. Representative gel of the purified proteins for <i>in vitro</i> FRET measurements	135

3.50. FRET efficiencies of individual protein mixes of hTopoI and YB-1ΔC constructs	136
3.51. Effect of salt concentration on YB-1/hTopoI interaction.....	137
3.52. Schematic illustration of mammalian expression vector constructs used for <i>in vivo</i> FRET experiments.....	137
3.53. Nuclear localisation of hTopoI-mTQ2 in HeLa cells	138
3.54. Schematic illustration of 2A co-expression constructs used in mammalian cells.....	139
3.55. FRET measurements between YB-1ΔC and hTopoI in HeLa cells.....	139
3.56. FRET measurements between YB-1ΔC and hTopoI in MCF7 cells using the 2A constructs.....	140
3.57. FRET measurements in MCF7 cells co-transfected with YB-1ΔC and hTopoI	142
3.58. Cellular distribution of sYFP2 and mTQ2 signals in PC-3 cells transfected with 2A constructs.....	143
3.59. FRET measurements in PC-3 cells co-transfected with YB-1ΔC and hTopoI	143
4.1. The steps of high throughput chemical library screening with Biosensor 1 in order to find potential inhibitors of YB-1/hNTH1 complex.....	158

LIST OF TABLES

TABLE	PAGE
1.1. Classification of human DNA topoisomerases and their properties, activities, and mechanisms	42
2.1. Alpha Factor calculation with mTQ2 and sYFP2 fluorescent proteins	71
3.1. Properties of purified hNTH1 fusion proteins	99
3.2. Properties of purified Biosensor proteins	101
3.3. Z' factor values obtained for our Biosensor 1 assay	110
3.4. List of compounds from Prestwick Chemical Library after second screening	116
3.5. The level of intrinsic fluorescence of potential hits from Life Chemicals and Prestwick Chemical Library at 50 μ M concentration	118
3.6. IC ₅₀ values of Prestwick hits ordered from Sigma	125
3.7. IC ₅₀ values of Prestwick hits provided by CMBA platform	125
3.8. IC ₅₀ values of Prestwick hits determined by AlphaScreen assay	127
3.9. Properties of purified hTopoI proteins	130
3.10. Properties of purified hTopoI fused to mTQ2 proteins	134

LIST OF ABBREVIATIONS

3D	Three-dimensional
8-oxoG	8-oxo-7,8-dihydroguanine
β ME	β -mercaptoethanol
BSA	Bovine serum albumin
cDNA	Complementary Deoxyribonucleic Acid
CV	Column Volume
DABCO	1,4-Diazabicyclo[2.2.2]octane
DMSO	Dimethyl sulfoxide
dsDNA	Double Stranded Deoxyribonucleic Acid
ECACC	European Collection of Authenticated Cell Cultures
EDTA	Ethylenediaminetetraacetic acid
EMA	European Medicines Agency
EMSA	Electrophoretic Mobility Shift Assay
FDA	Food and Drug Administration
FMDV	Foot-and-mouth disease virus
FPLC	Fast Protein Liquid Chromatography
GF	Gel Filtration
IC ₅₀	Half Maximal Inhibitory Concentration
IPTG	Isopropyl β -D-1-thiogalactopyranoside
mRNA	Messenger Ribonucleic Acid
mRNP	Messenger Ribonucleoprotein
PCR	Polymerase Chain Reaction
ROI	Region of Interest
SDS	Sodium dodecyl sulfate
TCEP	Tris(2-carboxyethyl)phosphine
Tg	Thymine glycol
THF	Tetrahydrofuran
UV	Ultraviolet

Chapter 1. Introduction

Summary

FRENCH

Le cancer tue des millions de personnes chaque année. C'est une maladie génétique dans laquelle un groupe de cellules anormales se multiplie de façon incontrôlable en ne tenant pas compte des règles normales de la division cellulaire et peuvent envahir les tissus voisins. Il existe différents types de thérapies anticancéreuses : chirurgie, radiothérapie, chimiothérapie, immunothérapie, endocrinothérapie et thérapie génique. La chimiothérapie est l'un des principaux modes de traitement contre le cancer et peut être définie comme l'utilisation de médicaments ayant une toxicité sélective contre les cellules tumorales. Le développement de la résistance aux médicaments dans les cellules tumorales est un problème majeur de chimiothérapie et provoque des échecs de traitement du cancer. La résistance acquise peut se développer pendant le traitement de tumeurs initialement sensibles et peut être causée par des mutations survenant pendant le traitement, ainsi que par diverses autres réponses adaptatives. Il existe de nombreux mécanismes de résistance aux médicaments anticancéreux dans les cellules tumorales, tels que le transport membranaire altéré impliquant la p-glycoprotéine produite par le gène de résistance multiple (MDR), les modifications du métabolisme des médicaments et l'interaction médicamenteuse avec d'autres molécules subcellulaires, des protéines du cycle cellulaire mutées telles que p53, une réparation améliorée de l'ADN ou une enzyme cible altérée.

La protéine multifonctionnelle Y-box Binding 1 (YB-1) est un marqueur métastatique établi, et une expression élevée de YB-1 est en corrélation avec l'agressivité tumorale et la faible survie des patients dans divers types de tumeurs. YB-1 est un membre de la famille de protéines se liant à l'ADN/ARN avec des domaines de choc froid (CSD) évolutifs. La protéine YB-1 humaine comprend trois domaines fonctionnels: (i) Le domaine N-terminal variable est riche en résidus alanine et proline et est donc également appelé domaine A / P, (ii) Le CSD agit comme un domaine de liaison d'acide nucléique, (iii) la région C-terminale hydrophile de YB-1 contient des répétitions alternées de groupes d'acides aminés acides et basiques et a été décrite comme se liant à la fois aux acides nucléiques et

à un certain nombre des protéines différentes y compris YB-1 elle-même. Le plus souvent, une majorité de YB-1 est dans le cytoplasme en association avec l'ARN. Cependant, en réponse à certains signaux intra- et extracellulaires, une partie significative de YB-1 peut se déplacer vers le noyau de la cellule. Lorsque YB-1 se retrouve dans le noyau, elle devient impliquée dans la transcription de divers gènes, dans la réparation et la réplication de l'ADN, et dans l'épissage de pré-ARNm. Il a été montré qu'YB-1 peut interagir avec l'ADN glycosylase hNTH1 à travers un criblage double-hybride de levure et une augmentation de l'association YB-1/hNTH1 a été observée dans la lignée cellulaire de tumeur mammaire MCF7 dans des conditions spécifiques d'endommagement de l'ADN. YB-1 peut également interagir directement avec la Topoisomérase I humaine (hTopoI) et stimuler l'activité de relaxation de l'ADN de celle-ci. Cette interaction améliore la sensibilité à la Camptothécine (CPT) dans les cellules PC-3 du cancer de la prostate humain, mais pas dans les cellules HeLa du cancer du col de l'utérus. Pendant mes études de doctorat, je me suis concentrée sur les interactions de YB-1 avec la protéine de réparation de l'ADN NTH1 et l'ADN Topoisomérase I, et leurs implications dans la résistance aux médicaments anticancéreux.

La NTH1 humaine est une ADN glycosylase bifonctionnelle, responsable de l'élimination des pyrimidines oxydées à l'étape initiale de réparation d'excision de base. Les ADN glycosylases bifonctionnelles, en plus de leur activité glycosylase, ont une activité AP-lyase. Après l'élimination de la base lésée, elles clivent le brin d'ADN 3' au site AP par β -élimination, ce qui nécessite un traitement final avant la réparation ultérieure. Les produits finaux de la β -élimination peuvent être traités par APE1 générant une extrémité 3'-OH, ou par l'ADN polymérase β , l'enzyme qui effectue également la tâche de remplacer la base manquante. La réparation est ensuite complétée par ligature, une étape qui est généralement catalysée par l'ADN ligase III en association avec son partenaire de liaison XRCC1. hNTH1 est une protéine de 34 kDa, constituée d'un domaine catalytique composé de deux sous-domaines α -hélicoïdaux contenant un motif hélice-tour-hélice et une boucle groupée [4Fe-4S], et un domaine N-terminal spécifique des mammifères. La réaction enzymatique de hNTH1 est régulée par XPG, APE1 et YB-1. L'interaction directe de YB-1 avec hNTH1 entraîne une augmentation de l'activité de la lyase de hNTH1.

L'ADN Topoisomérase I est un membre de la famille des enzymes ADN topoisomérases. Ce sont des enzymes essentielles, qui sont responsables de la régulation de la topologie de l'ADN dans les cellules. Elles sont impliquées dans des fonctions cellulaires vitales telles que la réplication, la transcription, la recombinaison et la réparation de l'ADN. Ces enzymes catalysent les changements de conformation de la topologie de l'ADN en générant la rupture concertée et le retour des brins d'ADN sans modifier la structure chimique de l'ADN. En raison de leur rôle crucial dans la prolifération des cellules, elles sont la cible de médicaments anticancéreux. Les topoisomérases sont divisées en deux classes principales: les type I, qui clivent l'ADN simple brin, et les type II, qui clivent l'ADN double brin. Les topoisomérases de type I sont subdivisées en deux sous-groupes mécaniquement différents: les type IA, s'attachent à la cassure simple brin au niveau du groupe 5'-phosphate, et les enzymes de type IB se lient au groupe 3'-phosphate du site de rupture. hTopoI est une topoisomérase de type IB et résout les problèmes topologiques de l'ADN en générant des brins d'ADN uniques réversibles. hTopoI est une enzyme monomérique de 91 kDa qui forme une pince protéique asymétrique qui entoure l'ADN double brin. hTopoI contient quatre domaines: un domaine N-terminal mal conservé, un domaine central hautement conservé, un domaine lieur formé par une paire étendue d'hélices α et un domaine C-terminal conservé. L'activité de relaxation de l'ADN de hTopoI est régulée par p53, NKX3.1, PARP-1 et YB-1. YB-1 peut interagir directement avec hTopoI et stimuler son activité de relaxation.

Les objectifs de mon travail de thèse étaient d'étudier la formation des complexes YB-1/hNTH1 et YB-1/hTopoI *in vitro* et *in vivo* (dans diverses lignées cellulaires de mammifères) en utilisant des approches FRET et de concevoir et optimiser un Biosenseur à base de FRET, qui pourrait être utilisé pour le criblage haut débit de chimiothèques afin d'identifier des inhibiteurs potentiels de ces complexes pour une utilisation en thérapie combinée.

Özet

TURKISH

Kanser, her yıl milyonlarca insanın ölümüne neden olmaktadır. Bir grup anormal hücrenin, hücre bölünmesi kurallarını göz ardı ederek kontrolsüz bir şekilde bölündüğü ve yakın dokuları istila edebildiği bir genetik hastalıktır. Farklı türde antikanser tedavileri vardır. Bunlara bazı örnekler; cerrahi, radyoterapi, kemoterapi, immünoterapi, endokrin tedavisi ve gen tedavisidir. Kemoterapi, kansere karşı başlıca tedavi yöntemlerinden biridir ve tümör hücrelerine karşı seçici toksisiteli ilaçların kullanımı olarak tanımlanabilir. Tümör hücrelerinde ilaç direncinin gelişmesi önemli bir sorundur ve kanser tedavisi başarısızlıklarına neden olmaktadır. Kazanılmış ilaç direnci, başlangıçta duyarlı olan tümörlerin tedavisi sırasında gelişmektedir ve tedavi sırasında oluşan mutasyonların yanı sıra çeşitli diğer adaptif yanıtlar yoluyla da ortaya çıkabilmektedir. Tümör hücrelerinde antikanser ilaç direncinin gelişmesinde birçok mekanizma rol oynar. Çoklu ilaç direnci geninin ürünü p-glikoproteini içeren değiştirilmiş membran taşınması, ilaç metabolizmalarındaki değişiklikler ve diğer alt-hücrel moleküller ile ilaç etkileşimi, mutasyona uğramış p53 gibi hücre döngüsü proteinlerinin sonucunda apoptoz uyarımının başarısızlığa uğraması, geliştirilmiş DNA onarımı veya değiştirilmiş hedef enzim bunlar arasındadır. Çok fonksiyonlu Y-box bağlanma proteini 1 (YB-1) bir metastatik belirteçtir. YB-1'in yüksek ifadesi, tümör agresivitesi ve çeşitli tümör tiplerinde zayıf hasta sağkalımı ile ilişkilendirilmiştir.

YB-1, evrimsel eski soğuk şok domainlerine (CSD) sahip DNA/RNA bağlayıcı ailesi proteinlerinin bir üyesidir. İnsan YB-1 proteini üç fonksiyonel domainden oluşur: (i) Değişken N-terminal domaini alanin ve prolin kalıntıları bakımından zengindir ve bu nedenle de A/P domaini olarak adlandırılır, (ii) CSD, bir nükleik asit bağlama alanı olarak davranır (iii) YB-1'in hidrofilik C-terminal bölgesi, asidik ve bazik amino asit kümelerinin dönüşümlü tekrarlarını içerir ve hem nükleik asitlere hem de YB-1'in kendisi de dahil olmak üzere bir dizi farklı proteinlere bağlandığı belirlenmiştir. Çoğu zaman, YB-1'in büyük bir kısmı, RNA ile bağlantılı olarak sitoplazmadadır. Bununla birlikte, bazı hücre içi ve hücre dışı

sinyallere cevap olarak YB-1'in önemli bir kısmı hücre çekirdeğine hareket edebilir. YB-1 çekirdeğe yer değiştirdiğinde, çeşitli genlerin transkripsiyonunda, DNA onarımında ve replikasyonunda ve mRNA uç birleştirmede yer alır. YB-1'in, maya iki hibrit taraması ile DNA glikozilazı hNTH1 ile etkileştiği bulunmuştur ve spesifik DNA hasarı koşulları altında MCF7 meme tümörü hücre hattında YB-1/hNTH1 kompleksinde bir artış gözlenmiştir. YB-1'in İnsan Topoizomeraz I (hTopoI) ile doğrudan etkileştiği ve DNA relaksasyon aktivitesini arttırdığı bulunmuştur. Bu etkileşim, insan prostat kanseri PC-3 hücrelerinde Camptothecin (CPT) duyarlılığını artırır, ancak servikal kanser HeLa hücrelerinde bu artış gözlenmemiştir. Çalışmamızda YB-1'in insan DNA onarım proteini NTH1 ve insan DNA topoizomeraz I ile etkileşimlerine ve bunların antikanser ilaç direncindeki etkilerine odaklanılmıştır.

İnsan NTH1, baz eksizyon onarımının ilk basamağında oksitlenmiş pirimidinlerin çıkarılmasından sorumlu iki fonksiyonlu bir DNA glikozilazdır. Glikosilaz aktivitelerinin yanı sıra iki fonksiyonlu DNA glikozilazlar, AP-liyaz aktivitesine sahiptirler. Baz lezyonunun çıkarılmasından sonra, AP bölgesinin 3' ucunu β -eliminasyonu ile sonraki onarımdan önce son işlem gerektiren DNA uçları oluşturarak keserler. Beta-eliminasyonunun son ürünleri, APE1 tarafından 3'-OH ucu oluşturacak şekilde işlenir. DNA polimeraz β , oluşan tek baz boşluğunu doldurma görevini yerine getiren enzimdir. Onarım daha sonra bağlanma partneri XRCC1 ile birlikte DNA ligaz III ile katalize edilen çentiğin ligasyonu ile tamamlanır. hNTH1, bir sarmal-hairpin-sarmal motifi ve bir [4Fe-4S] küme döngüsü ve ilave bir memelilere özgü N-terminal domaini içeren iki α -sarmal alt domainden oluşan bir katalitik domainden oluşan bir 34 kDa proteindir. hNTH1'in enzimatik aktivitesi XPG, APE1 ve YB-1 tarafından düzenlenir. hNTH1'in YB-1 ile doğrudan etkileşiminin, hNTH1'in liyaz aktivitesini arttırdığı gösterilmiştir.

DNA topoizomeraz I, DNA topoizomeraz enzim ailesinin bir üyesidir. Bunlar, hücrelerdeki DNA topolojisini düzenlemekten sorumlu olan temel enzimlerdir. Replikasyon, transkripsiyon, rekombinasyon ve DNA onarımı gibi hayati hücresel işlevlerde rol alırlar. Bu enzimler, DNA topolojisindeki yapısal değişiklikleri, DNA'nın kimyasal yapısını değiştirmeden, DNA zincirlerinin

kontrollü kırılmasını ve yeniden birleşmesini sağlayarak katalize ederler. Proliferatif hücrelerde önemli rolleri nedeniyle, bunlar antikanser ilaçlarının hedefleri olmuşlardır. Topoizomerazlar iki ana sınıfa ayrılır: tek zincirli DNA'yı kesen tip I ve çift zincirli DNA'yı kesen tip II. Tip I topoizomerazlar, mekanik olarak farklı iki alt gruba ayrılır: tek zincir kırıklarında 5'-fosfata bağlanan tip IA, ve kırılma bölgesindeki 3'-fosfata bağlanan IB enzimleri. hTopoI, bir Tip IB topoizomerazdır ve geri dönüşümlü tek DNA zinciri kırıkları üreterek DNA'nın topolojik problemlerini çözer. hTopoI, çift zincirli DNA'yı çevreleyen bir asimetric protein kelepçesi oluşturan 91 kDa'lık bir monomerik enzimdir. hTopoI, dört domain içerir. Zayıf olarak korunmuş bir N-terminal domaini, yüksek ölçüde korunmuş bir çekirdek domain, uzatılmış bir çift heliks ile oluşturulan bir bağlayıcı domain ve korunmuş bir C-terminal domaini. hTopoI'nin DNA relaksasyon aktivitesi p53, NKX3.1, PARP-1 ve YB-1 ile düzenlenir. YB-1'in hTopoI ile doğrudan etkileştiği ve relaksasyon aktivitesini uyardığı gösterilmiştir.

Tez çalışmamın amacı, FRET yaklaşımını kullanarak *in vitro* ve *in vivo* (çeşitli memeli hücre hatlarında) YB-1/hNTH1 ve YB-1/hTopoI komplekslerinin oluşumunu araştırmak ve kombinasyon terapisinde kullanım için bu komplekslerin potansiyel inhibitörlerini tanımlamak amacıyla yüksek verimli kimyasal kütüphane taraması için kullanılabilir bir FRET-bazlı biyosensörü tasarlamak ve optimize etmektir.

1.1 Cancer and its treatment

Cancer causes millions of people to die each year. It is a genetic disease in which a group of abnormal cells grow uncontrollably by disregarding the normal rules of cell division and can invade nearby tissues (Bertram, 2000). Normal cells in the human body are constantly subject to signals that dictate whether the cell should divide, differentiate into another cell or die. But cancer cells develop a degree of autonomy from these signals, resulting in uncontrolled growth and proliferation. If this uncontrolled proliferation is allowed to continue and spread, it can be fatal. In fact, almost 90% of cancer-related deaths are due to a tumour spreading - a process called metastasis (Hanahan and Weinberg, 2011).

The development of cancer called carcinogenesis/oncogenesis is a complex multi-step process involving the accumulation of genetic and epigenetic alterations over time. These alterations can cause genomic instability and mutations in genes critical for the control of cell growth. At the end of this process, a normal cell is transformed into a cancer cell (Hoeijmakers, 2001). Several molecular pathways take part in this complex transformation. Cancer cells acquire several biological capabilities during this process, which are referred to as hallmarks of cancer providing a concept for understanding the complex cancer biology (Hanahan and Weinberg, 2011). The six principle hallmarks of cancer are: (i) growth signal autonomy, (ii) evasion of growth suppressors, (iii) resistance to cell death, (iv) replicative immortality, (v) induction of angiogenesis, and (vi) activation of invasion and metastasis (Figure 1.1). There are two other emerging hallmarks: the ability to avoid the immune system and to reprogram energy metabolism (Hanahan and Weinberg, 2011).

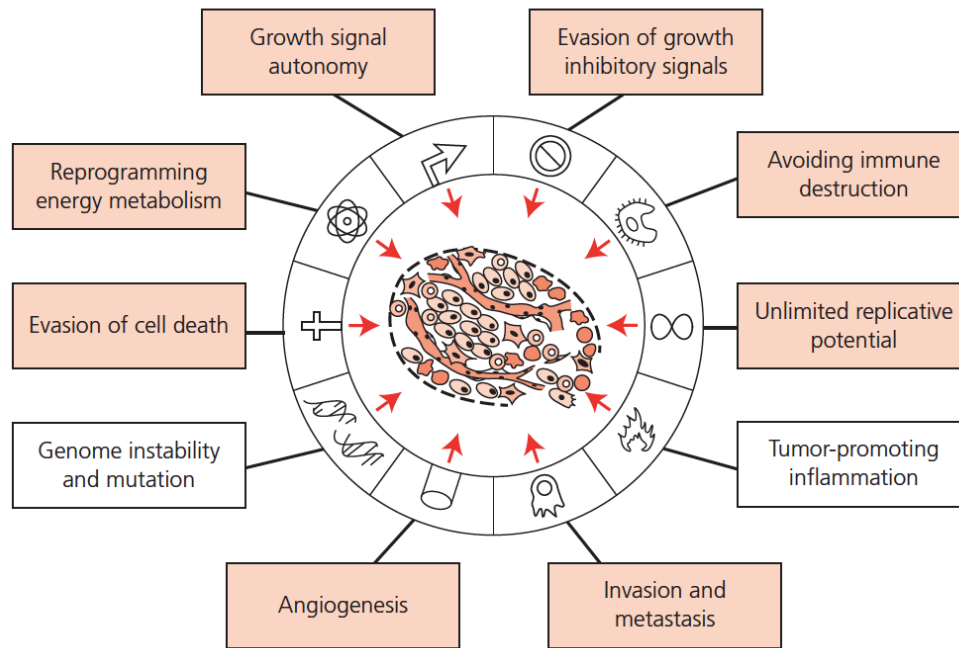


Figure 1.1. Hallmarks of tumour cells. Light pink rectangles specify the eight hallmarks; white rectangles specify two enabling characteristics that are necessary for obtaining the hallmarks of cancer. Taken from Pecorino, 2008.

Because cancer is a result of genomic instability caused by random mutations, each patient harbours a different cancer regarding which genes are mutated, regarding the nature of each mutation and regarding the sequence of appearance of these mutations. This can explain why different patients suffering from the same cancer may respond differently to a same treatment (Marin et al., 2012; Gerlinger et al., 2012). To treat human cancer, drugs that interfere with each of the acquired capabilities necessary for tumour growth and progression have been developed and are in clinical trials or in some cases approved for clinical use (Hanahan and Weinberg, 2011). It is thus useful to understand molecular pathways in cells in order to understand carcinogenesis but also to develop new, more efficient therapeutic strategies (Farrell, 2011).

There are different types of anticancer therapies: surgery, radiotherapy, chemotherapy, immunotherapy, endocrine therapy and gene therapy (Urruticoechea et al., 2010). Depending on the type of cancer, one or more of these treatments are selected and applied to patients. Surgery is not applicable for

all cases, making chemotherapy one of the principal modes of treatment against cancer.

Chemotherapy can be defined as the use of drugs with selective toxicity against tumour cells. These chemotherapeutic agents, such as EGFR, cyclin-dependent kinase, telomerase, PARP and topoisomerase inhibitors, selectively target one or more hallmarks of cancer. Such therapies mostly kill highly proliferating cells by generating DNA damage. DNA damage causes cell-cycle arrest and leads to apoptosis. However, cancer cells manage to find ways to escape from death after exposure to therapeutic agents.

Development of drug resistance in tumour cells is a major problem of chemotherapy and causes cancer treatment failures. Resistance to anticancer drugs can be divided into two categories: intrinsic and acquired. Intrinsic resistance occurs in the tumour cells, which have genetic alterations existing before treatment that make the therapy ineffective. Acquired drug resistance can develop during treatment of tumours that were initially sensitive and can be caused by mutations arising during treatment, as well as through various other adaptive responses (Zahreddine and Borden, 2013).

1.2. Acquired resistance to chemotherapy

There are many mechanisms of anticancer drug resistance in tumour cells, such as altered membrane transport involving p-glycoprotein product of multidrug resistance gene (MDR), changes in drug metabolisms and drug interaction with other subcellular molecules, failure to induce apoptosis as a result of mutated cell cycle proteins such as p53, enhanced DNA repair or altered target enzyme (Figure 1.2) (Housman et al., 2014; Rebucci and Michiels, 2013). Mechanisms of resistance can change according to the action of the cytotoxic agent and mutations and/or epigenetic changes acquired in the genome of tumour cells.

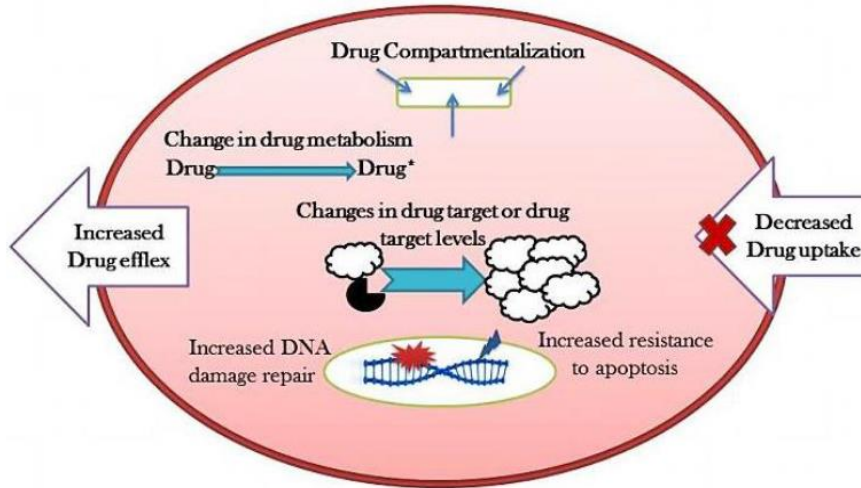


Figure 1.2. Illustration of the different mechanisms of chemotherapeutic drug resistance in tumour cells. Taken from (Mansoori et al., 2017).

There are lots of studies aiming to find a solution to overcome drug resistance. The use of combination drug therapy using different classes of drugs, inhibition of essential enzymes involved in DNA repair pathway, gene knockout using antisense molecules are some examples of approaches used in order to block drug resistance. In my study, my work focused on anticancer drug resistance mechanisms involving enhanced DNA repair and alterations of the target molecule.

1.2.1. Alterations of drug metabolism and membrane transport

Lack of prodrug activation or epigenetic silencing of genes involved in drug processing are examples of potential causes of resistance and are frequently tumour-specific. Drug-metabolizing enzymes take part in the activation and deactivation of drugs, and can therefore affect the susceptibility of organs and tissues to their therapeutic and toxic effects. Drug-metabolizing enzymes include the cytochrome P450 (CYP) system, glutathione-*S*-transferase (GST) superfamily, and uridine diphospho-glucuronosyltransferase (UGT) superfamily (Michael and Doherty, 2005). Drugs such as fluorouracil (5-FU) and irinotecan (CPT-11) must be converted to their active metabolites to exert their anticancer effects. CPT-11 is converted to SN-38 by carboxylesterase (Xu and Villalona-Calero, 2002), and

several *in vitro* studies have indicated that the level of carboxylesterase activity in cancer cells is an important determinant of CPT-11 sensitivity (Kojima et al., 1998; Longley and Johnston, 2005). For many DNA interacting agents, *e.g.* alkylating agents, anthracyclines, and platinum drugs, an important mechanism of inactivation is related to the overexpression of GSTs that metabolize the drugs into inactive molecules (Kauvar et al., 1998).

The most studied drug resistance mechanism is the increased drug efflux by ATP binding cassette (ABC) membrane transporters. Increasing the release of drugs outside the cells results in insufficient accumulation of drug inside the cells and decrease in drug efficiency. This mechanism provides a resistance to various anticancer drugs that are structurally and functionally different from the initial anticancer drug (Glavinas et al., 2004). Three membrane transporters—multidrug resistance protein 1 (MDR1), multidrug resistance-associated protein 1 (MRP1), and breast cancer resistance protein (BCRP)—are implicated in many drug resistant cancers. All three transporters have broad substrate specificity and are able to efflux many xenobiotics, including vinca alkaloids, epipodophyllotoxins, anthracyclines, taxanes, and kinase inhibitors, from cells (Housman et al., 2014). One of the well-known members of ABC transporter is *MDR1* gene product P-glycoprotein. Increased expression of P-glycoprotein has been correlated with drug resistance to various anticancer agents (Gottesman et al., 2002). The Y-box Binding Protein 1 (YB-1), which is the focus of my study, binds to *MDR1* gene promoter containing Y-boxes and regulates its expression in drug resistant tumours (Kuwano et al., 2004).

1.2.2. Failure to induce apoptosis

The resistance to anticancer drugs can also be due to the fact that in cancer cells, apoptotic pathways are frequently dysfunctional. Anti-apoptotic BCL-2 family members, inhibitors of apoptosis proteins and caspases are key proteins of this mechanism (Colmegna et al., 2017). The caspases are a large group of proteins that play a central role in apoptosis. They work at two levels: initiator caspases (*e.g.* caspase-2, -8, -9, and -10) are responsible for the initiation of the apoptotic pathway and effector caspases (caspase-3, -6, and -7) are responsible for

the actual cleavage of cellular components during apoptosis. Decreased levels of these proteins or impaired functions can block apoptosis thus contributing to resistance.

The p53 protein is one of the best-known tumour suppressor proteins whose mutation acquired oncogenic property. Defects in the p53 tumour suppressor gene have been linked to more than 50% of human cancers (Bai and Zhu 2006) because it is not only involved in the induction of apoptosis, but it is also a key player in cell cycle regulation, development, differentiation, gene amplification, DNA recombination, chromosomal segregation, and cellular senescence. Mutations in the p53 gene impair the connection between DNA damage (caused by chemotherapeutic agents) and activation of apoptosis (Mansoori et al., 2017), thereby leading to drug resistance.

1.2.3. Enhanced DNA repair pathways

The most common non-surgical cancer treatments function by generating DNA damage. Many anticancer drugs induce DNA damage either directly (for example, platinum-based drugs) or indirectly (for example, topoisomerase inhibitors). Damage to DNA induces several cellular responses that enable the cell either to eliminate or cope with the damage or to activate a programmed cell death process, presumably to eliminate cells with potentially catastrophic mutations (Sancar et al., 2004). DNA double-strand breaks (DSBs) are generally considered to be the most toxic of all DNA lesions. Enhanced DNA repair pathways provide a resistance to initially effective cytotoxicity of these therapies (Helleday et al., 2008).

There are 5 main DNA repair pathways in mammals: Base-excision repair (BER), Nucleotide-excision repair (NER), Homolog recombination (HR), Non-homologous end joining (NHEJ) and Mismatch repair (Hoeijmakers, 2001). Each pathway deals with different types of DNA damage and together are responsible for genomic stability. Deficiencies in any of these pathways may accelerate the process of carcinogenesis and at the same time may cause drug resistance to therapies targeting them (Tubbs and Nussenzweig, 2017). Enhanced DNA repair

can also cause drug resistance against DNA-damaging agents (Helleday et al., 2008), since efficient repair of toxic lesions in tumour cells can prevent cell death. Cancer cells deficient in one or more DNA repair pathways may be more sensitive to therapeutic agents targeting one of the remaining pathways than the neighbouring healthy cells. On the other hand, deficiency in the targeted repair pathway may result in a loss of sensitivity to the therapeutic agent.

An overview of the toxic lesions occurring after cancer treatments and the major repair pathways involved in reducing their cytotoxicity is provided in Figure 1.3 (Helleday et al., 2008).

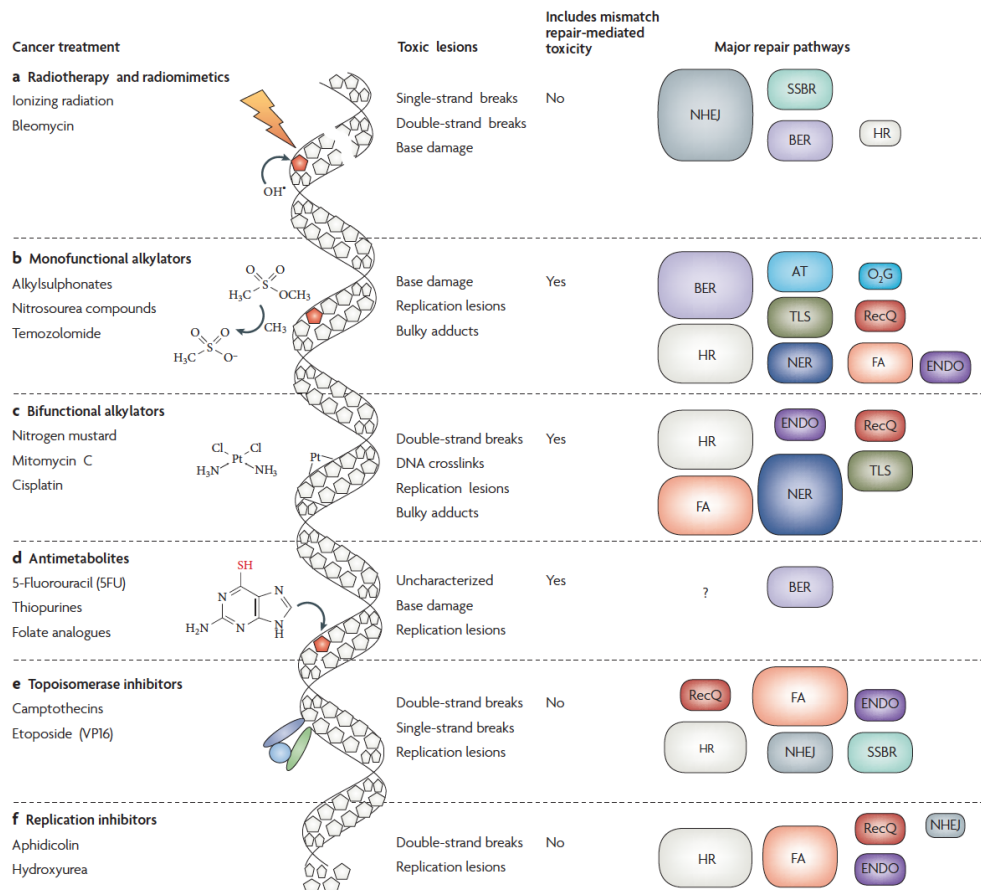


Figure 1.3. Overview of DNA repair pathways involved in repairing toxic DNA lesions formed by cancer treatments taken from Helleday et al., 2008. NHEJ, non-homologous end joining; SSBR, DNA single-strand break repair; HR, homologous recombination; AT, alkyltransferase; TLS, translesion synthesis; O₂G, DNA dioxygenases; RecQ, RecQ-mediated repair; FA, Fanconi anaemia repair pathway; ENDO, endonuclease mediated repair.

Ionizing radiation, UV radiation and several anticancer drugs induce oxidative stress in tumour cells. Base excision repair is mostly responsible for repair of oxidatively induced DNA modifications (Dizdaroglu, 2015). Some of DNA repair proteins are promising targets in cancer treatments (Sánchez-Pérez, 2006) and the proteins involved in BER are increasingly considered as targets for cancer treatment (Dianov, 2011). One of the proteins I studied during my PhD, the DNA glycosylase hNTH1, plays a role in the early steps of the BER pathway.

1.2.4. Changes in drug target or drug target level

Acquired drug resistance may also occur as a result of the alteration of the target molecule. During treatment, target proteins can be subjected to several mutations and the expression levels of target proteins can increase or decrease. These changes in turn affect the efficiency of cytotoxic therapy (Rebucci and Michiels, 2013). Resistance to tyrosine kinase inhibitors is an example of this mechanism. Imatinib is a specific inhibitor of the kinase resulting from the fusion of *Bcr* and *Abl* genes. Because of the reactivation of the kinase due to a point mutation in the ATP binding domain of the kinase preventing imatinib binding, the treatment of patients becomes inefficient (O'Hare et al., 2005). On the other hand, *in vitro*, resistance is most often related to Bcr-Abl mRNA and protein overexpression.

Topoisomerases solve topological problems in DNA ahead of the replication fork and of the RNA polymerase during transcription by transiently inducing single or double-strand breaks. They are important anticancer agent targets (Holden, 2001). The most toxic topoisomerase inhibitors function by stabilizing the formation of a DNA-enzyme complex. Mutations occurring in the enzyme can influence the formation of the cleavable complex leading to reduce efficiencies of the inhibitors. Reduced levels of topoisomerases also play an important role in cellular sensitivity to their inhibitors (Beck et al., 1999; Beretta et al., 2013). Human topoisomerase I (hTopoI) is also one of the proteins I studied during the course of my work. Cellular resistance to hTopoI inhibitor Camptothecin (CPT) has been associated with the post-translational modifications of hTopoI and its interaction with other proteins that modulate its enzymatic activity

(Bandyopadhyay et al., 2012; Horie et al., 2002). Low hTopoI activity may also cause a resistance to CPT (Pommier, 2006). hTopoI directly interacts with different proteins involved in DNA replication, transcription and repair (Czubaty et al., 2005). Some of these interaction partners affect hTopoI's activity and in turn these interactions modulate cellular sensitivity to CPT (Das et al., 2016; Wu et al., 2014).

1.3. Y-box Binding Protein 1 as a prognostic marker of drug resistance

The multifunctional Y-box binding protein 1 (YB-1) is now an established metastatic marker, and high expression of YB-1 correlates with tumour aggressiveness and poor patient survival in diverse tumour types (Kohno et al., 2003; Lasham et al., 2013). Many reports associated with drug resistance have also shown a possible link between the multifunctional YB-1 and drug resistance both in cell cultures and in clinical human tumour samples. It has been shown that the extent of YB-1 expression and its localisation correlate with cellular sensitivities to the cytotoxic effects of cisplatin and other DNA-damaging agents (Ohga et al., 1996, Stavrovskaya et al., 2012). Several studies have indeed indicated that the level of nuclear expression of YB-1 is predictive of drug resistance and poor prognosis in breast tumours, ovarian cancers, and synovial sarcomas (Bargou et al., 1997; Janz et al., 2002; Oda et al., 2003; Rubinstein et al., 2002; Yahata et al., 2002; Dahl et al., 2009).

The mode of action of YB-1 is still unclear. YB-1 regulates the activity of the MDR genes *MDR1* and *LRP* and has been suggested to be an early and global marker of MDR in tumours (Saji et al., 2003; Vaiman et al., 2006). Several forms of p53 have also been shown to cause YB-1 to accumulate in the nucleus, which in turn inhibits p53 activity and makes cells more resistant to apoptosis (Zhang et al., 2003). The nuclear localisation of YB-1 has also been shown to be induced by UV irradiation and a C-terminally truncated form of YB-1 was mainly localized in the nucleus (Koike et al., 1997). These studies suggest that YB-1 may itself have a key role in self-defence signalling mechanisms, being initiated in response to environmental poisons such as oxidative stress or DNA damaging reagents, such

as chemotherapeutic agents.

1.3.1. Protein properties of YB-1

YB-1 is a member of the DNA/RNA-binding family of proteins with evolutionally ancient cold shock domains (CSD). It is a 324 amino acid-long protein (35.9kDa), that exhibits, however, an aberrant electrophoretic mobility close to 50kDa (Cohen et al., 2010). It binds to the Y-box, a cis-acting element, which regulates gene expression, containing an inverted CCAAT box (Didier et al., 1988). Several eukaryotic genes including genes encoding major histocompatibility class II antigens, thymidine kinase, proliferating cell nuclear antigen, DNA polymerase α , epidermal growth factor receptor, DNA topoisomerase II α and multidrug resistance I protein contain the Y-box binding consensus sequence in their regulatory regions (Wolffe et al., 1992; Wolffe, 1994; Ladomery and Sommerville, 1995; Asakuno et al., 1994). YB-1 gene is comprised of 8 exons and 7 introns spanning 19kb of genomic DNA and is located on chromosome 1 p 34 (Toh et al., 1998).

The human YB-1 protein comprises three functional domains (Wolffe, 1994) (Figure 1.4). The variable N-terminal domain is rich in alanine and proline residues and is therefore also termed A/P domain. The CSD acts as a nucleic acid binding domain being involved in both specific and unspecific interactions with DNA and RNA (Eliseeva et al., 2011). Structurally, CSD is comprised of a five-stranded β -barrel (Wistow, 1990; Kloks et al., 2002) (Figure 1.5) containing RNP-1 and RNP-2 like consensus motifs (Landsman, 1992) and belongs to the β -sheet RNA-binding protein group (Graumann and Marahiel, 1996). The hydrophilic C-terminal region (CTD) of YB-1 contains alternating repeats of acidic and basic amino acid clusters and has been described to bind to both nucleic acids and a number of different proteins including YB-1 itself (Das et al., 2016; Ise et al., 1999; Okamoto et al., 2000; Skabkin et al., 2004). Furthermore, the CTD contains sequences governing the nucleo-cytoplasmic distribution of YB-1: a non-canonical nuclear localization signal (NLS, amino acids 186–205) and a cytoplasmic retention site (CRS, amino acids 267–293), which prevails over the NLS and therefore leads to a mainly cytoplasmic localization of YB-1 (Eliseeva et

al., 2011; Lasham et al., 2013). It contains a cleavage site for the 20S proteasome, which provides a regulatory mechanism for nuclear-cytoplasmic transport of YB-1 when cells are exposed to genotoxic stress (Sorokin et al., 2005).

The N- and C-terminal domains of YB-1 are predicted to be largely disordered. Such proteins are unable to fold spontaneously into stable, well-defined globular three-dimensional structures but are dynamically disordered and fluctuate rapidly over an ensemble of conformations that cover a continuum of conformational space ranging from extended statistical coils to collapsed globules (Dyson and Wright, 2005). Probably this is the reason why there has been no success in determining the three-dimensional structure of the intact YB-1.

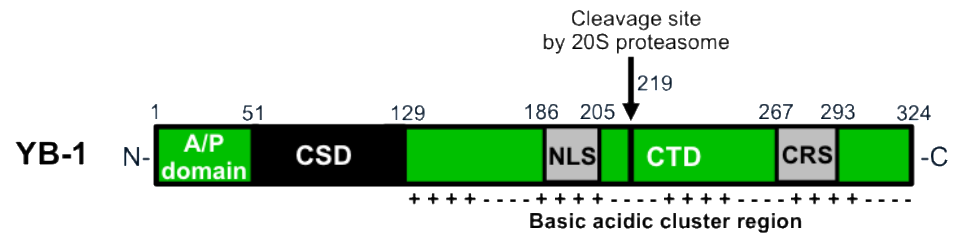


Figure 1.4. Schematic diagram of YB-1 domain organization. A/P domain: Alanine and proline rich N-terminal domain. CSD: A cold shock domain. The C-terminal domain (CTD) of YB-1 consists of four alternating clusters of positively (basic) and negatively charged (acidic) amino acids, each about 30 amino acids in length (indicated by pluses and minuses). NLS: A nuclear localization signal, CRS: A cytoplasmic retention site. Reviewed in Eliseeva et al., 2011.

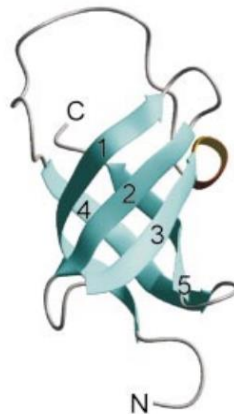


Figure 1.5. Structural information about YB-1. Ribbon diagram of the lowest energy structure of CSD from Kloks et al., 2002.

YB-1 and its homologs form oligomers with a mass up to 800 kDa in the absence of RNA (18 S) (Evdokimova et al., 1995). Oligomerization may occur due to interaction with oppositely charged amino acids clusters of the C- terminal domain from different protein molecules (Tafuri and Wolffe, 1992).

1.3.2. Functions of YB-1 in cells

YB-1 plays a role in the regulation of several different pathways due to its ability to interact with nucleic acids and other proteins (Figure 1.6)

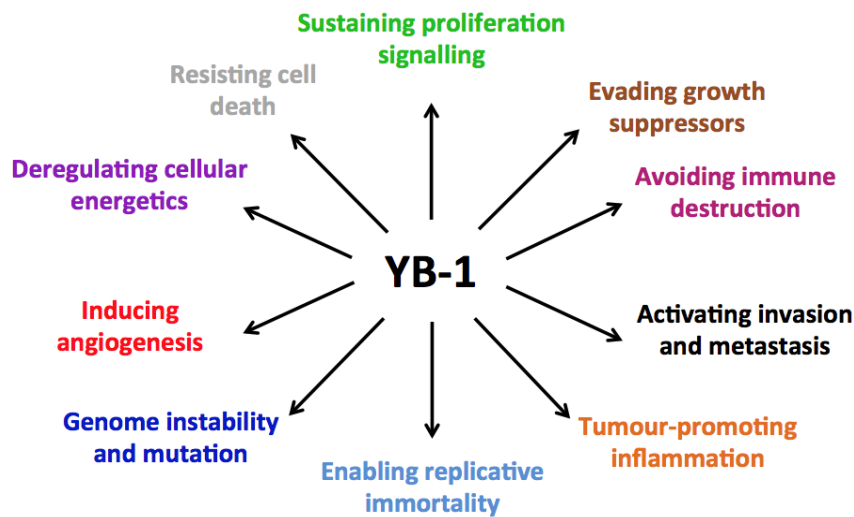


Figure 1.6. Schematic diagram showing the numerous functions of YB-1 that affect all hallmarks of cancer (Lasham et al., 2013).

At most times, a majority of YB-1 is within the cytoplasm in association with RNA. It is the major packing protein of messenger ribonucleoproteins (mRNPs) (Wu et al., 2015), regulates mRNA translation, provides for its stability, and is involved in its localization. However, in response to some intra- and extracellular signals a significant portion of YB-1 can move to the cell nucleus. When YB-1 translocates into the nucleus, it becomes involved in transcription of various genes, in DNA repair and replication, and in pre-mRNA splicing (Eliseeva et al., 2011).

YB-1 both enhances and represses the expression of genes, which contain the specific Y-box-containing regions in their promoters as well as with single stranded regions that can have no Y-box sequence. YB-1 also interacts with proteins involved in transcription and regulates their functions. hTopoI regulates gene transcription by controlling supercoils in DNA during this process (Puc et al., 2015; Baranello et al., 2016). YB-1 has been found to interact directly with hTopoI and enhance its DNA relaxation activity (Wu et al., 2014). This interaction enhances CPT sensitivity in human prostate cancer PC-3 cells, but not in cervical cancer HeLa cells.

There are indications that YB-1 may also be involved in DNA repair. Its high affinity for damaged DNA, its weak 3'-5'-exonuclease activity on single-stranded DNA and weak endonuclease activity on double-stranded DNA are features that support its possible implication in DNA repair (Hasegawa et al., 1991; Izumi et al., 2001). It has been shown that YB-1 can separate DNA duplex of different oligonucleotides less than 36bp long and this activity is increased when duplex molecules contain either mispaired bases or cisplatin modifications (Gaudreault et al., 2004). In addition, YB-1 interacts with several proteins involved in repair and can regulate the activity of some of them (Das et al., 2007; Chattopadhyay et al., 2008). PARP1, the key regulator of DNA repair events, was stimulated by YB-1 and this interaction decreased sensitivity to PARP1 inhibitors (Alemasova et al., 2018). YB-1 was found to interact with the DNA glycosylase hNTH1 through a yeast two hybrid (Y2H) screen and in this same study YB-1 was shown to stimulate the lyase activity of hNTH1 by enhancing the formation of an Schiff base intermediate between enzyme and apurinic/aprimidinic (AP) site (Marenstein et al., 2001). Another study showed an increase in YB-1-hNTH1 association in the MCF7 breast tumour cell line under specific DNA-damaging conditions (Guay et al., 2008). Interestingly, knockdown of one or the other of the two proteins results in restored sensitivity to both cisplatin and UV light.

During my PhD studies, I focused on the interactions of YB-1 with the human DNA repair protein NTH1 and human DNA topoisomerase I, and their implications in anticancer drug resistance.

1.4. Importance of protein-protein interactions in cellular processes

Protein-protein interactions (PPIs) constitute a complex network and take part in many cellular processes. Most pathological conditions of mammalian cells result from dis-functioning or variations in these interactions. The identification of interacting partners can shed light on a protein's cellular function and can provide new therapeutic strategies in case of disease. PPIs represent specific physical contacts between proteins in particular biological conditions (De Las Rivas and Fontanillo, 2010).

1.4.1. Methods for identification of PPI

Large-scale genomics and proteomics programs have identified complete networks of protein interactions within a cell (called the interactome) and have led to major breakthroughs in understanding biological pathways, host–pathogen interactions and cancer development (Lievens et al., 2010). There are two approaches to obtain information about molecular interactions: computational and experimental. A number of experimental methods, based on distinct, physical principles have been developed to identify PPIs such as the yeast two-hybrid method (Y2H) (Topcu and Borden, 2000), affinity purification-mass spectrometry approaches and protein microarrays (Ruffner et al., 2007).

For verification of these interactions, confocal microscopy, coimmunoprecipitation, surface plasmon resonance and spectroscopic studies are useful methods (Berggård et al., 2007). Fluorescence (Föster) Resonance Energy Transfer (FRET) is also a routinely used biophysical method for the study of protein-protein interactions. FRET is non-radiative energy transfer from a donor fluorophore (coupled to protein X) to an acceptor fluorophore (coupled to a protein Y) if protein X and Y are close enough to each other (Föster radius). This method can be applied both *in vivo* and *in vitro* with resolution in the nanometer range (Ngounou Wetie et al., 2014).

1.4.2. Chemical library screening in order to find PPI inhibitors

In recent years, targeting PPIs represents a new avenue for drug development (Wells and McClendon, 2007). PPIs are druggable, but discovering small-molecules that disrupt PPIs is very challenging. The analysis of PPI interfaces is important in order to facilitate the identification of potential inhibitors of protein complexes (Milhas et al., 2016).

The nature of PPIs differs depending on the type of complexes (obligate and non-obligate). The minimum protein surface for non-obligate protein-protein complexes is suggested to be around 900 Å² (about 500 Å² provided by each partner) and consists of around 12 residues on each partner (Villoutreix et al., 2014). Most atoms in non-obligate interfaces are in contact with the solvent. These interfaces are lacking residues such as glutamic acid, aspartic acid and lysine and contain mostly methionine, tyrosine and tryptophan (Villoutreix et al., 2014). The interface of obligate protein-protein complexes is more hydrophobic, and aliphatic and aromatic residues are abundant compared to non-obligate protein complexes. In these interfaces, some residues are directly involved in the stabilization of the complex by largely contributing to the binding energy of the interaction, and are referred to as hotspots (Chakrabarti and Janin, 2002). Tryptophan, arginine and tyrosine are often found at hotspots in contrast leucine, serine, threonine and valine are unfavourable (Bogan and Thorn, 1998). Hydrogen bonding, but also electrostatic and hydrophobic interactions formed at PPIs can be disrupted by small chemical compounds (Arkin and Wells, 2004).

Several databases and chemical libraries have recently been developed taking into account the specific properties of PPIs in order to facilitate the search for potential inhibitors of PPIs (Basse et al., 2016; Milhas et al., 2016) and various experimental approaches, described below, are used to identify initial lead compounds.

1.4.2.1. Fluorescence Resonance Energy Transfer

Fluorescence Resonance Energy Transfer or FRET is a fluorescence-based technique. Fluorescence is a type of luminescence, and corresponds to the emission of light by a particular chemical compound or protein (fluorophore) within nanoseconds after the absorption of light. In this process, an electron from the fluorophore is excited to a higher energy state and then returns to a lower energy state accompanied by the emission of a photon. The difference between the excitation and emission wavelengths, called the Stokes shift, is the important feature that makes fluorescence so useful. The outermost electron orbitals in the fluorophore molecule determine both its efficiency and the wavelengths of absorption and emission. The efficiency of the fluorescence process is defined by its quantum yield, which is the ratio of the number of photons emitted to the number of photons absorbed. When fluorophores in their so-called ‘ground state’ (S_0) absorb light energy (photons), alterations in the electronic, vibrational and rotational states of the molecules can occur. If the absorbed photon’s energy is greater than that needed for the transfer from the ground state to the lowest energy level of S_1 , the molecule will also undergo a change in vibration, rotation and/or move into an even higher electronic orbital. This transition to an ‘excited state’ (S_2) arises in femtoseconds (Lichtman and Conchello, 2005). The molecule uses several different pathways, like vibrational relaxation and fluorescence emission, to shed the absorbed energy and return to its low-energy ground state. The processes, which occur between the absorption and emission of light are illustrated in the Jablonski diagram (Lakowicz, 2006) (Figure 1.7).

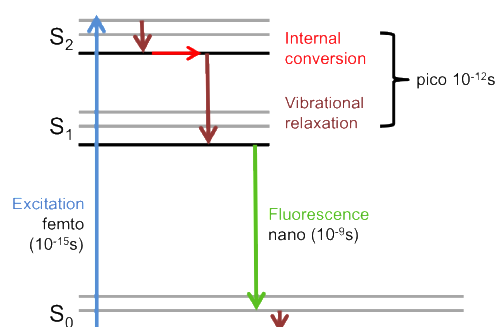


Figure 1.7. Jablonski diagram showing the various steps involved in fluorescence excitation and emission. Adapted from Lichtman and Conchello, 2005.

FRET involves a non-radiative transfer of energy from an excited donor fluorophore to an adjacent acceptor fluorophore. Due to the nature of the transition dipole interaction between the two fluorophores, energy transfer is more efficient when they are in close proximity than when they are further apart, allowing one to measure relative distances of up to 10 nm between donor and acceptor, making FRET extremely sensitive to small changes in distance (Piston and Kremers, 2007). The donor molecules typically emit at shorter wavelengths, which overlap with the absorption spectrum of the acceptor.

In our study, fluorescent proteins-based FRET was used, which is suitable for both *in vivo* and *in vitro* studies of PPIs. Fluorescence microscopy is a very useful technique to explore processes in live or fixed cells, and fluorescent proteins (FPs) are commonly used as markers for such studies (Day and Davidson, 2009). Recent developments in fluorescence microscopy and in FPs have greatly widened the capabilities of cellular imaging (eg. high resolution imaging) and have significantly contributed to a better understanding of various biological processes (Adam et al., 2009; Bourgeois, 2017). FPs suitable for FRET measurements are known as FRET pairs, and numerous of these have been described that display different properties, such as spectral overlap between FPs, the brightness of FPs, donor:acceptor stoichiometry (Bajar et al., 2016). We used the CFP (Cyan Fluorescent Protein) and YFP (Yellow Fluorescent Protein) variants, mTurquoise2 and sYFP2, two bright colour variants of GFP (Green Fluorescent Protein), as donor and acceptor fluorophores (Figure 1.8). All proteins used for *in vitro* FRET measurements were expressed as fusion proteins with either of these two fluorescent proteins. FRET can be either intra- or inter-molecular.

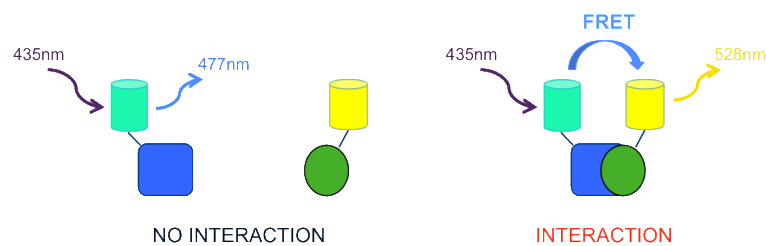


Figure 1.8. Illustration of FRET principle. The blue square and the green circle represent two interacting proteins. The cyan and yellow cylinders represent mTQ2 and sYFP2 respectively.

FRET signal is detected when the two fluorescent proteins are within 10nm proximity of each other.

In the literature, several protein-based fluorescent biosensors have been developed to study cellular processes, like enzyme-substrate relation, post-translational modifications, and protease activity (Tamura and Hamachi, 2014). In such biosensors, intramolecular FRET is usually measured.

1.4.2.2. Homogeneous Time-Resolved Fluorescence (HTRF) Assay

The homogeneous time-resolved fluorescence (HTRF) system from CisBio International (Bagnols/Cèze Cedex, France) is one of a family of technologies based on time-resolved fluorescence resonance energy transfer (TR-FRET) (Newton et al., 2008). This method uses rare-earth lanthanides with long emission half-lives as donor fluorophores. The method provides significant advantages to drug discovery researchers in high throughput screening (HTS), including assay flexibility, reliability, increased assay sensitivity, higher throughput, and fewer false positive/false negative results (Figure 1.9) (Degorce et al., 2009).

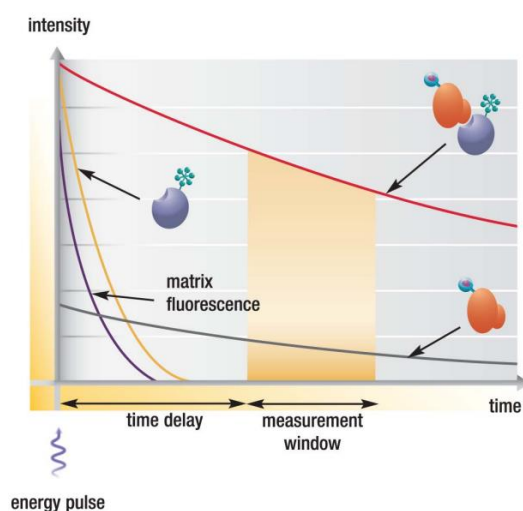


Figure 1.9. Principle of HTRF assay. The energy pulse from the excitation source (flash lamp, laser) is followed by a time delay, allowing interfering short-lived fluorescence (compounds, proteins, medium etc.) to decay. The red line: FRET signal intensity generated at 665 nm; black line, emission of donor cryptate at 620 nm; orange line, fluorescent signal generated from acceptor fluorophores. Taken from (Degorce et al., 2009).

1.4.2.3. Amplified Luminescent Proximity Homogeneous (AlphaScreen) Assay

Alpha Technology (Amplified Luminescent Proximity Homogeneous Assay) is a highly flexible, homogeneous no-wash assay ideal for the measurement of protein interactions and complexes. The technology of AlphaScreen was originally developed under the name of LOCI® (Luminescent Oxygen Channeling Immunoassay) by Dade Behring, Inc. of Germany (Ullman *et al.*, 1994). This technique is a bead-based proximity assay and relies on excited emission of luminescence upon proximity of donor and acceptor beads, which are coupled to the respective interaction partners. Excitation of the donor bead leads to the formation of singlet oxygen, which diffuses to the acceptor and stimulates emission. Unlike FRET, acceptor emission occurs at a higher energy (lower wavelength) than donor excitation.

Donor beads contain a photosensitizer, phthalocyanine, which converts ambient oxygen to an excited form of O₂, singlet oxygen, upon illumination at 680 nm. Like other excited molecules, singlet oxygen has a limited lifetime prior to returning to ground state. Within its 4μsec half-life, singlet oxygen can diffuse approximately 200 nm in solution. If an acceptor bead is within that distance, energy is transferred from the singlet oxygen to thioxene derivatives within the acceptor bead, resulting in light production. Without the interaction between donor and acceptor bead, singlet oxygen falls to ground state and no signal is produced. AlphaScreen acceptor beads use rubrene as the final fluorophore, emitting light between 520 and 620 nm. AlphaLISA acceptor beads use a Europium chelate as the final fluorophore, emitting light in a narrower peak at 615 nm (Figure 1.10) (Arkin *et al.*, 2004).

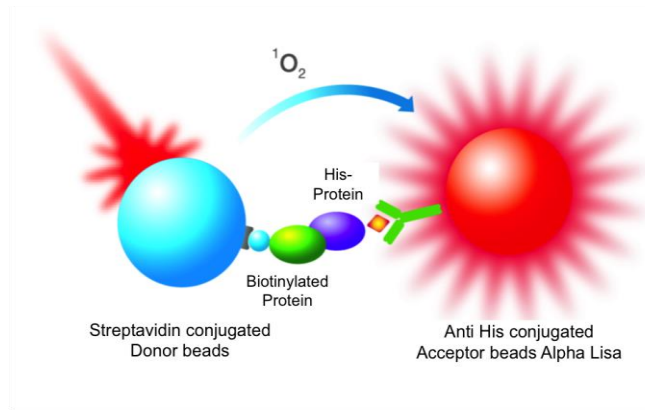


Figure 1.10. Illustration of AlphaScreen Assay. Binding of biological partners (represented by purple and green ovals) brings Donor and Acceptor beads (represented by the large blue and red circles) into close proximity (≤ 200 nm) and thus a fluorescent signal between 520–620 nm is produced in the case of AlphaScreen. When there is no binding between biological partners, Donor and Acceptor beads are not in close proximity. Singlet oxygen decays and no signal is produced.

1.5. Human Endonuclease III (hNTH1) and its role in Base Excision Repair

1.5.1. Base Excision Repair Pathway

The Base Excision Repair (BER) pathway (Figure 1.11) removes small base lesions that do not significantly distort the DNA helix structure. Such damage typically results from deamination, oxidation, or methylation (Krokan and Bjørås, 2013). Tomas Lindahl, the 2015 Nobel Prize winner in Chemistry, was the first to decipher the fundamental steps in the BER pathway in 1974. The initial step of BER is the recognition and removal of the damaged base by DNA glycosylases. Base removal generates an abasic site in DNA, which is then further processed by the DNA glycosylases themselves in the case of bifunctional enzymes or by an AP endonuclease, before *de novo* synthesis by the DNA polymerase together with a DNA ligase to fix the DNA (Figure 1.11).

There are 11 determined mammalian DNA glycosylases, which are responsible for excision of different types of base lesions (Jacobs and Schär, 2012). The initial recognition by DNA glycosylases occurs by diffusion of the enzyme along the DNA. Minor backbone distortions and the H-bond acceptor and

donor changes that occur as a result of base damage are recognized at low specificity and affinity, which is followed by base flipping to generate a high-specificity and -affinity complex. DNA glycosylases are divided into two groups according to their catalytic activities. Monofunctional DNA glycosylases cleave the N-glycosidic bond between the damaged base and the deoxyribose sugar and release the substrate base by creating an apurinic/aprimidinic (AP) site. After excision of the damaged base by a monofunctional DNA glycosylase, an AP endonuclease (APE1 in humans) cleaves the phosphodiester backbone on the 5' side of the AP site via a hydrolytic mechanism (Madhusudan et al., 2005). Bifunctional DNA glycosylases, besides their glycosylase activity, have AP-lyase activity. After removal of the base lesion, they cleave the DNA strand 3' to the AP site by β -elimination or β/δ -elimination leaving ends that require end processing before subsequent repair. The end products of the β -elimination are an unsaturated hydroxyaldehyde linked to the 3' end (3'-dRP) and 5'-P, which can be processed by APE1 generating a 3'-OH end. β/δ -elimination releases an unsaturated deoxyribose as trans-4-hydroxy-2,4-pentadienal generating a one-nucleotide gap surrounded by 3'-P and 5'-P ends. The 3'-P can be removed by polynucleotide kinase/phosphatase (PNKP), preparing the intermediate for the polymerase step.

The action of APE1 on an AP site generates a single-strand break with a 3'-hydroxyl terminus, which can prime DNA repair synthesis, and a 5'-deoxyribose phosphate (5'dRp) terminus. The 5'dRp residue must be removed in order for the repair process to be completed. This task is accomplished by the dRp lyase domain present in DNA polymerase β , the enzyme that also performs the task of filling in the single base gap thus formed (Prasad et al., 1998; Beard et al., 2006). Repair is then completed by ligation of the nick, which is generally catalysed by DNA ligase III in association with its binding partner XRCC1. This pathway has been termed 'short patch' BER. In some types of short-patch BER, poly(ADPribose) polymerase I (PARP1) also participates.

The long-patch BER pathway involves strand displacement repair synthesis of at least two nucleotides and the excision of the 5'-dRP residue as part of a flap oligonucleotide released by the FEN1 nuclease with the help of PCNA (Klungland and Lindahl, 1997). Strand elongation is then performed by DNA polymerase δ/ϵ ,

which is expressed in proliferating cells (Akbari et al., 2009).

Human NTH1 is a bifunctional DNA glycosylase, responsible for the removal of oxidized pyrimidines together with two other DNA glycosylases, the endonuclease VIII-like (NEIL) enzymes NEIL1 and NEIL2 (Dizdaroglu, 2005). These enzymes possess an AP-lyase activity with β/δ -elimination and a 5'-phosphodiesterase activity that removes the 5'-dRP residue. They also excise 4,6-diamino-5-formamidopyrimidine (FapyAde) lesion (Aamann et al., 2014).

The choice between 'short patch' and 'long patch' repair pathways is defined by the initiating DNA glycosylase, the cell type and availability of BER factors (Krokan and Bjørås, 2013).

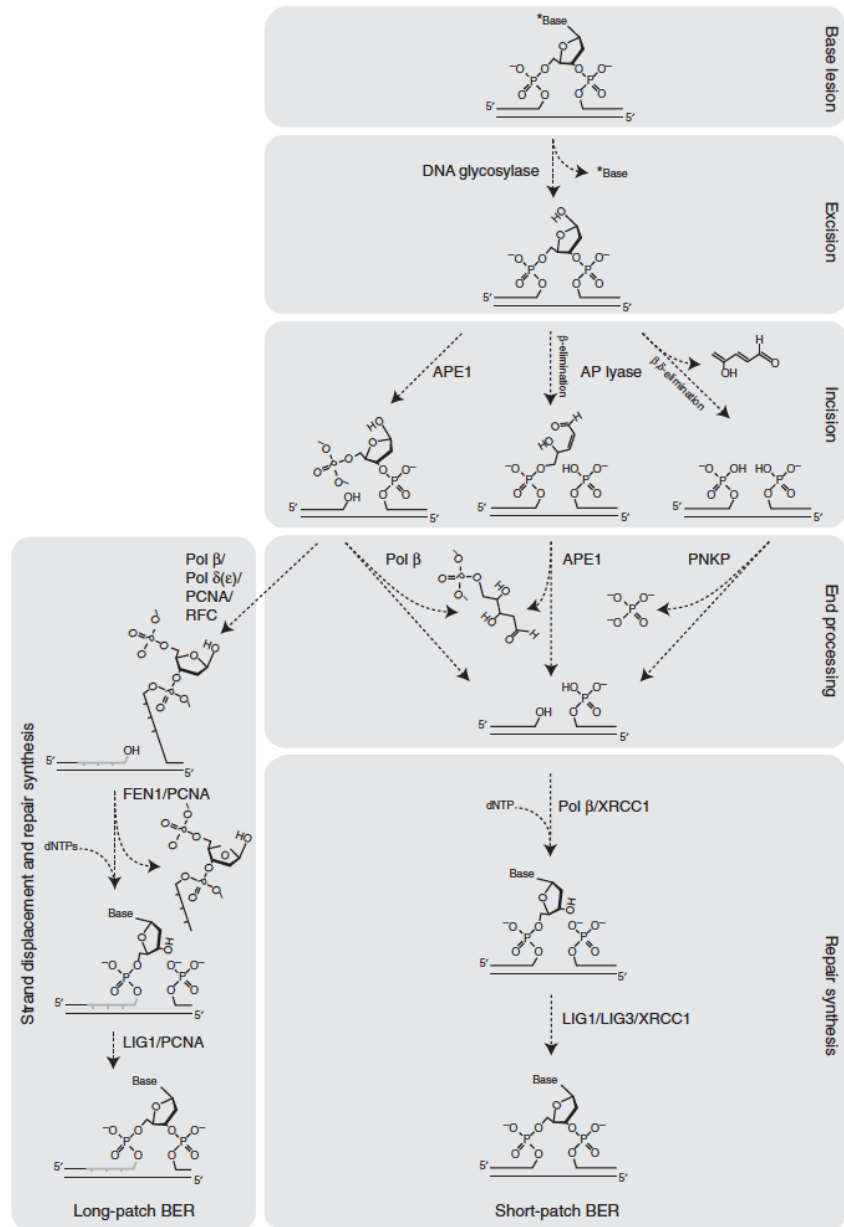


Figure 1.11. Schematic diagram illustrating the various steps and enzymes involved in Base Excision Repair. Taken from Krokan and Bjørås, 2013.

BER and its closely associated pathways play key roles in prevention of cancer, neurodegeneration, aging and resistance to anticancer agents. The cytotoxic effects of anticancer drugs, which introduce base modifications and in particular base oxidation and alkylation, can be reduced by the efficient repair of DNA by the BER pathway. Because of its necessity for cell survival, several BER proteins such as APE1 or PARP1 are targets of therapeutic drugs (Madhusudan et al., 2005; Malyuchenko et al., 2015).

1.5.2. Human Endonuclease III (hNTH1)

Human NTH1, a homologue of *Escherichia coli* endonuclease III (Nth), was first purified and identified from calf thymus (Hilbert et al., 1996). The *hnth1* gene is localized on chromosome 16p13.2-.3. It encodes a 34kDa protein, which consists of a catalytic domain composed of two α -helical subdomains containing an helix-hairpin-helix motif and a [4Fe-4S] cluster loop, and an additional mammalian-specific N-terminal domain, or NTD (Figure 1.12) (Ikeda et al., 1998).

Escherichia coli Endonuclease III (EndoIII) is a bifunctional DNA glycosylase/AP lyase, which repairs a series of structurally diverse toxic or mutagenic oxidized pyrimidines. This enzyme was first identified not on the basis of its DNA glycosylase activity, but rather because it nicked UV-irradiated DNA. For this reason it was termed an endonuclease, because it was thought that nicking resulted from enzyme-catalyzed hydrolysis of internucleotide phosphodiester bonds at sites of DNA damage (Hilbert et al., 1996). It has since been determined that the enzyme nicks DNA not via hydrolysis, but by catalyzing β -elimination of the 3'-P group at the AP site formed as a result of the enzyme's DNA glycosylase activity (Mazumder et al., 1991). The modified base that was enzymatically released from UV-irradiated DNA proved to be cytosine and/or uracil hydrate (Boorstein et al., 1989). Enzymes that catalyse both base release and strand cleavage via β -elimination are now termed DNA glycosylase/AP lyases (Hilbert et al., 1997).

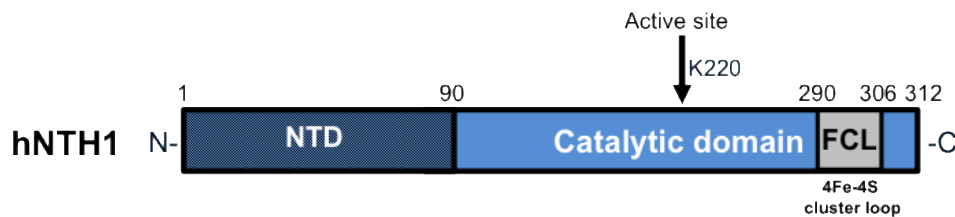


Figure 1.12. Schematic diagram of hNTH1 domain organization.

The 3D structure of hNHT1 is unknown, but several structures of its homologs from bacteria have been reported (Thayer et al., 1995; Fromme and Verdine, 2003; Sarre et al., 2015) (Figure 1.13). These structures, however, only

correspond to the catalytic domain, which is highly conserved from bacteria to humans (~30% sequence identity).

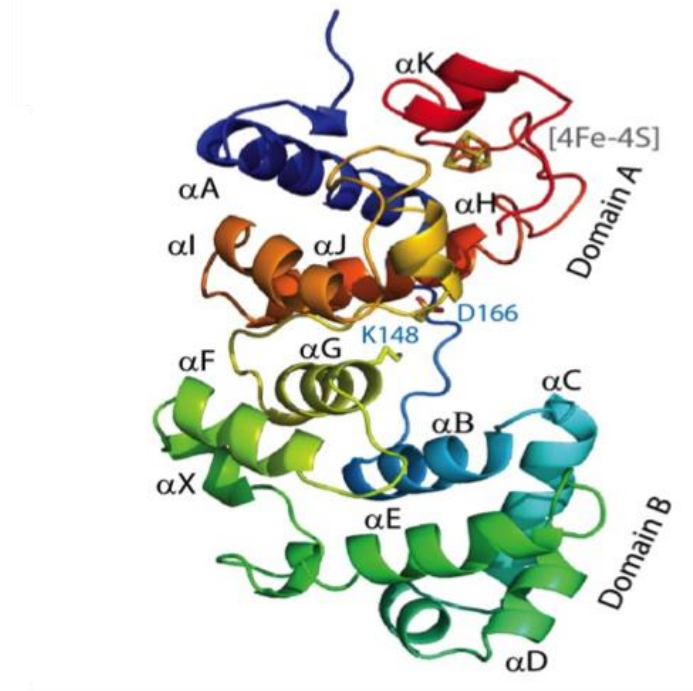


Figure 1.13. The 3D structure of EndoIII-1 from *Deinococcus radiadurans* (Sarre et al., 2015) illustrated in rainbow colours (dark blue: N-terminus; Red: C-terminus). EndoIII enzymes are composed of two domains separated by a DNA-binding cleft in which are located the two canonical catalytic residues: Lysine and Aspartate. A [4Fe-4S] cluster is present at the C-terminus.

E. coli EndoIII displays a broader substrate specificity than hNTH1. The substrate specificity of hNTH1 protein is similar to that of *Schizosaccharomyces pombe* Nth protein (Dizdaroglu et al., 2000) (Figure 1.14).

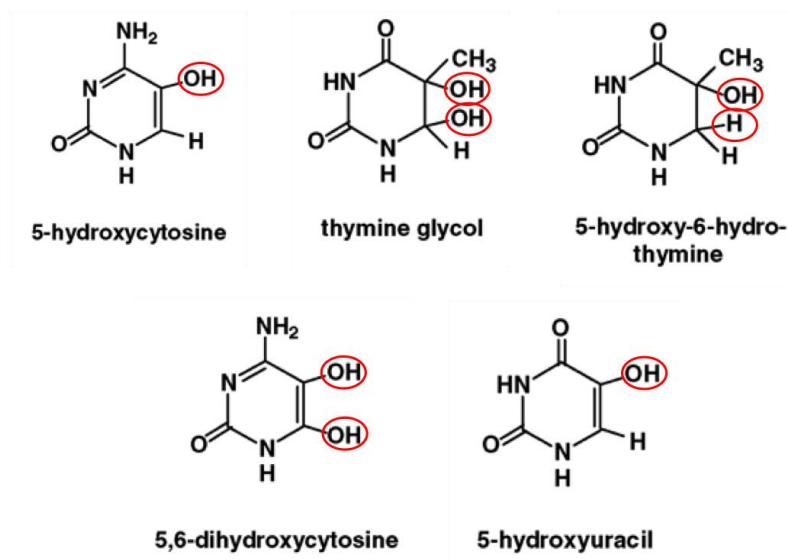


Figure 1.14. Pyrimidine-derived lesions excised by hNTH1. Base modifications are encircled with red colour. Adapted from Dizdaroglu et al., 1999.

hNTH1's catalytic activity is tightly regulated and several mechanisms are involved in this process (Liu et al., 2003) (Figure 1.15). It has been shown that its N-terminal tail (NTD) plays an auto-inhibitory role, which could explain the low activity of hNTH1 compared to that of its *E. coli* homologue (Liu and Roy, 2002). The hNTH1 dimer was detected *in vivo* and *in vitro* at high protein concentrations. The dimerization of hNTH1 occurs via NTD interactions and masks the inhibitory effect of this tail (Liu et al., 2003).

hNTH1 also has several interaction partners, which regulate its enzymatic reaction (Figure 1.15). The nucleotide excision repair enzyme XPG binds directly to hNTH1 and enhances its binding to damaged DNA. The stimulation of hNTH1 activity by XPG does not require XPG's catalytic activity in nucleotide excision repair (Bessho, 1999; Klungland et al., 1999). It has been reported that APE1 also stimulates hNTH1's glycosylase activity against Tg:A -containing 2'-deoxyribose oligonucleotide duplex and increases hNTH1's lyase activity against Tg:A -containing substrate (Marenstein et al., 2003). As mentioned before, the direct interaction of hNTH1 with YB-1 has been shown to enhance the lyase activity of hNTH1 (Marenstein et al., 2001).

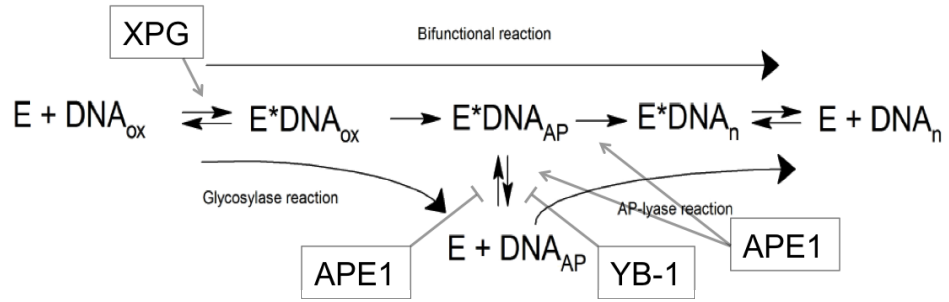


Figure 1.15. Schematic illustration of the bifunctional reaction mechanism catalyzed by hNTH1 and the effect of XPG, APE1, and YB-1 on the regulation of its activity. In the case of coupled bifunctional activities, the enzyme and the substrate ($E+DNA_{ox}$) generate an enzyme-substrate complex ($E*DNA_{ox}$), which leads to the removal of the oxidized base and the formation of an enzyme-abasic site complex ($E*DNA_{AP}$). In turn, this complex is further processed by the lyase activity to an enzyme-nicked DNA complex ($E*DNA_n$) and finally, the fully processed DNA product after β -elimination is released from the enzyme ($E+DNA_n$). In case the two reaction steps are uncoupled, the enzyme dissociates from the abasic site DNA ($E+DNA_{AP}$) after the glycosylase reaction, thereby creating a mixture of DNA substrates containing either abasic sites or oxidized bases. The enzyme can then engage in either one of the two sub-pathways: (i) a new round of DNA glycosylase activity on DNA_{ox} or (ii) AP-lyase activity on DNA_{AP} . The relative engagement into one or the other pathway depends on the concentrations of the various species (E , DNA_{ox} , DNA_{AP} and DNA_n) in the reaction. Various factors as indicated act at different reaction steps to regulate the hNTH1 activity. \rightarrow and \perp denote stimulation and inhibition, respectively. Adapted from Liu et al., 2003.

Other DNA glycosylases' repair activities are also regulated by co-factors. The 8-Oxoguanine DNA glycosylase 1, which is responsible for the repair of the most frequent oxidized DNA lesion pre-mutagenic 8-oxo-7,8-dihydroguanine (8-oxoG), is controlled by APE1, XRCC1, and PARP1 (Ba and Boldogh, 2018). NEIL1 and NEIL2 are stimulated by Cockayne Syndrome group B protein (Muftuoglu et al., 2009; Aamann et al., 2014).

The knockdown of a gene is one of the methods to study the physiological importance of proteins. Knocking-down NTH1 alone ($Nth1^{-/-}$) did not cause significant consequences in mice. However, targeted deletion of *hNTH1* and *NEIL1* ($Nth1^{-/-}Neil1^{-/-}$) results in increased tumorigenesis in comparison to $Nth1^{-/-}$ or $Neil1^{-/-}$ mice, which is the first demonstration of the carcinogenicity of

oxidative damage to DNA other than 8-oxoG and highlights the importance of hNTH1 (Chan et al., 2009).

1.6. Preliminary data obtained for the study of YB-1/hNTH1 complex

Before my arrival in Dr. Timmins' team, some activity and interaction experiments had already been performed to characterise the YB-1/hNTH1 complex, which are described below. The glycosylase and lyase activities of hNTH1 were measured on specific oligonucleotide substrates containing thymine glycol (a commonly used EndoIII substrate) paired with adenine in the absence and presence of YB-1 (Figure 1.16). YB-1 did not appear to affect the DNA glycosylase activity of hNTH1, but instead was found to specifically stimulate (27% increase) the rate of AP lyase activity of hNTH1, as reported in the literature (Figure 1.16; Marenstein et al., 2001).

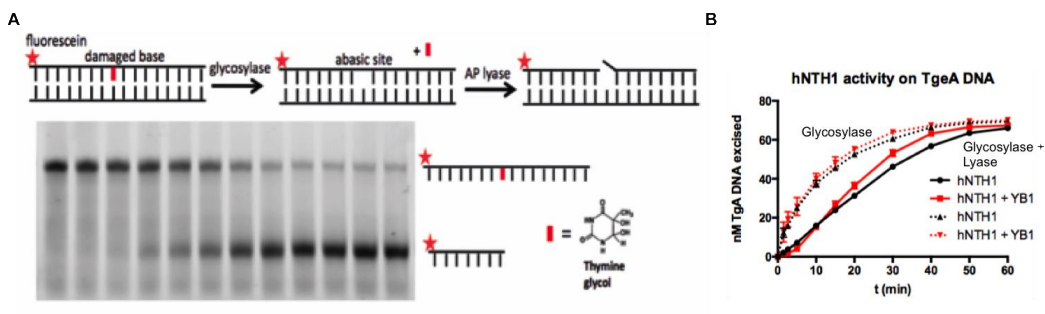


Figure 1.16. Stimulation of hNTH1 AP-lyase activity by YB-1. (A) DNA substrate used in this work: a 35 mer dsDNA containing thymine glycol (Tg) in position 14 and a fluorescein labelled DNA strand for detection on gel and representative gel of hNTH1 activity reaction. (B) Time course experiments of the DNA glycosylase (dotted line) and lyase activities (full line) of 3 nM hNTH1 on 75 nM DNA substrate in the absence (black) and presence (red) of 30 nM YB-1.

AlphaScreen assays were also performed to characterize the interaction between YB-1 and hNTH1 (Figure 1.17). For this, His-tagged hNTH1 was bound to Anti-His coated acceptor beads and biotinylated YB-1 was bound to streptavidin-coated donor beads. By combining different constructs of hNTH1 and YB-1 in such an assay, Dr. J. Timmins' team could show that the NTD of hNTH1 is critical for interaction with YB-1 and the C-terminal region of YB-1, which is missing in the nuclear form of YB-1, is dispensable for this interaction. The C-

terminal residues of YB-1 between 182 and 219 may also play a role in the interaction between YB-1 and hNTH1, since the slightly shorter construct (YB1-C182) showed reduced AlphaScreen signal compared to the nuclear form (YB1-C219, later referred to as YB-1 Δ C).

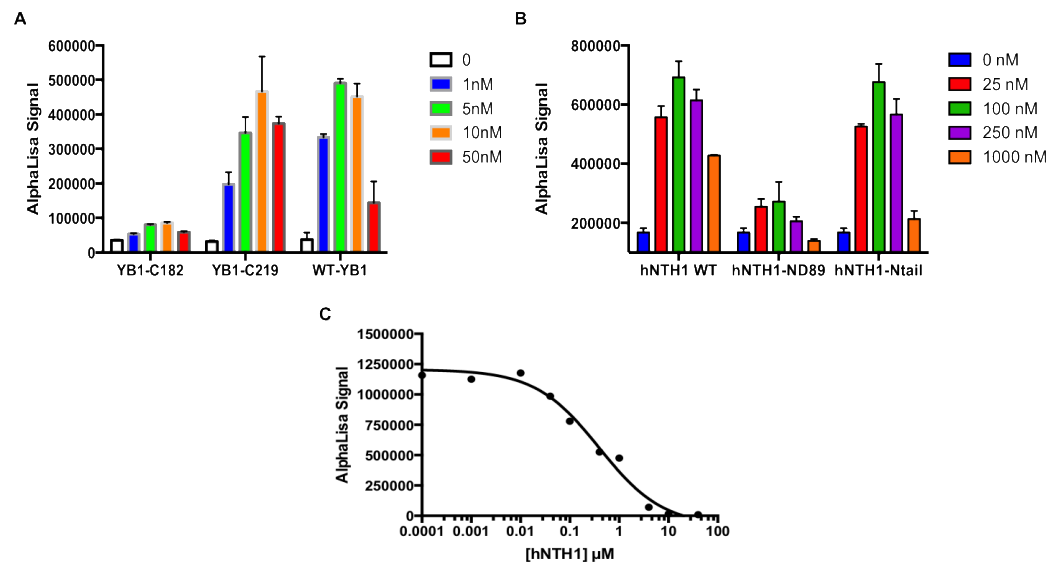


Figure 1.17. AlphaScreen binding assays of YB-1 and hNTH1. **(A)** AlphaScreen measurements obtained from a titration of increasing amounts (0, 1, 5, 10 and 50 nM) of YB-1 (wild-type, WT; residues 1-182, YB1-C182; residues 1-219, YB1-C219) into reactions containing 100 nM His-tagged hNTH1. The binding profiles are typical of specific binding. The reduced signal obtained at the highest concentration of YB1 is due to a saturation of the binding sites on the streptavidin coated donor beads. **(B)** AlphaScreen measurements obtained from a titration of increasing amounts (0, 25, 100, 250 and 1000 nM) of hNTH1 (wild-type, WT; residues 90-326, hNTH1-ND89; residues 1-89, hNTH1-Ntail) into reactions containing 10 nM biotinylated YB1-C219, which was the concentration producing the best signal in (A). **(C)** AlphaScreen competition assay. Increasing concentrations of hNTH1 (without His-tag) were added to an AlphaScreen reaction containing 10 nM biotinylated YB1-C219 and 100 nM His-hNTH1. The untagged hNTH1 replaces the His-tagged hNTH1 in the complex leading to a decrease in the Alpha Screen signal. The IC_{50} derived from this data provides us with an estimate of the binding affinity of the YB-1/hNTH1 complex and was found to be $\sim 0.5 \mu$ M.

1.7. DNA topoisomerase I as an anticancer drug target

DNA topoisomerase I is a member of the DNA topoisomerase enzyme family. These are essential enzymes, which are responsible for regulating the topology of DNA in cells. They are involved in vital cellular functions such as

replication, transcription, recombination and DNA repair. These enzymes catalyze the conformational changes in DNA topology by generating the concerted breakage and rejoining of DNA strands without changing the chemical structure of DNA (Champoux, 2001; Wang, 2002). Because of their crucial role in proliferating cells, they are targets of anticancer drugs.

1.7.1. DNA Topology

In cells, DNA is packed into the nucleus. Supercoiling of the genomic DNA is essential and helps to pack the genome into a small volume to fit into the nucleus. Topological forms of DNA result from its structure composed of two DNA strands that are repeatedly intertwined. Opening these two strands, which occurs in all major genetic processes like replication and transcription may cause a torsional stress on DNA. If this stress is not taken care of, it can result in DNA double-strand breaks (Wang, 2002). To maintain genome integrity, DNA topoisomerases avoid this stress by changing the topology of DNA.

Supercoiling can occur when DNA ends are not able to perform free rotation, as is the case inside living cells. Closed circular DNAs like plasmids, bacterial chromosomes, genomes of mitochondria and chloroplasts are good examples of supercoiling because they have no DNA ends. Although eukaryotic chromosomes consist of linear DNA, they are organized into constrained domains or loops attached to proteins and nuclear matrix, which block free rotation during strand separation (Mirkin, 2001).

The fundamental topological parameter of a constrained DNA molecule or domain is called the linking number (Lk). The linking number is defined as the number of times that one DNA strand crosses an imaginary surface, which is formed by the other DNA strand. The only way to change Lk is to introduce a break in one or both DNA strands, rotate the two DNA strands relative to each other and seal the break. There are two geometrical functions in closed circular DNA: the twist (Tw) represents the total number of helical repeats by describing how the individual strands of DNA wrap around the axis of the DNA helix, and the writhe (Wr) is a measure of the coiling of the helix axis in space. Linking

number is the sum of Tw and Wr. The shape of the DNA called ‘supercoiled’ is a higher helix formation with normal double-stranded DNA. In living cells, the characteristic organization of the DNA is a negative supercoil, in which the Wr is increased and Tw is lowered compared to a relaxed DNA and has the same Lk (Bates and Maxwell, *DNA Topology*, 2005) (Figure 1.18).

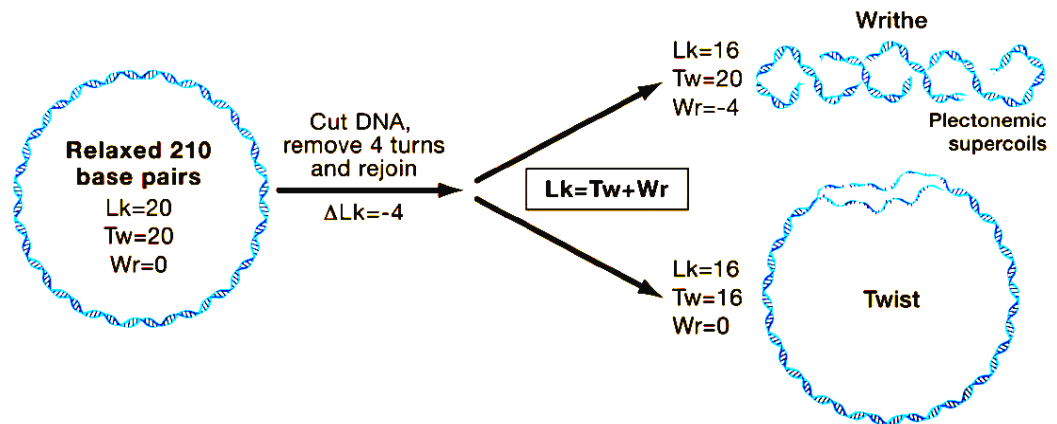


Figure 1.18. Illustration of the different DNA topologies. Example of a torsionally relaxed DNA molecule with a length of 210 base pairs containing 20 turns (10.5 bp/turn) or $Tw = 20$. If the DNA were cut and one end was twisted by four turns in the direction opposite to the natural helicity of the DNA, and subsequently resealed, the resulting linking number of the DNA would be equal to $Lk = 20 - 4 = 16$. (Right) The upper and lower panels show the topology of the DNA molecule when the removal of these turns is at the expense of twist ($Tw = 20 - 4 = 16$) and writhe ($Wr = 0 - 4 = -4$), respectively. Taken from Koster et al., 2010.

1.7.2. DNA Topoisomerases

DNA topoisomerases catalyze topological changes by generating controlled transient strand breakage on DNA (Pommier et al., 2016). The first DNA topoisomerase was discovered in 1971 in *Escherichia coli* by James Wang who was studying the supercoiling of *E. coli* DNA (Wang, 1971).

DNA topoisomerases carry out the strand breakage by the tyrosine residue in their active site. This key residue attacks the phosphodiester bond of DNA leading to the formation of a covalent bond by a transesterification reaction (Champoux, 2001). Topoisomerases are divided into two major classes: type I, which cleave single-stranded DNA, and type II, which cleave double-stranded DNA. Type I

topoisomerases are further subdivided into two mechanistically different subgroups: type IA, which attach the single-strand break to the 5'-phosphate, and type IB enzymes, which bind the 3'-phosphate at the break site (Table 1.1) (Nitiss et al., 2012).

Table 1.1. Classification of human DNA topoisomerases and their properties, activities, and mechanisms. rel: relaxation activity, -: negative supercoils, +: positive supercoils, cat/decat: catenation and decatenation activity.

Type	Name	DNA Cleavage	Polarity	Size (kDa) Composition	Activity	Mechanism
IA	Top3 α Top3 β	Single strand	5'	112 Monomer	rel -	Strand passage
IB	Top1 Top1mt	Single strand	3'	91 Monomer	rel - +	Rotation
II	Top2 α Top2 β	Double strand	5'	174 Homodimer	rel - + cat/decat	Strand passage ATPase

Type I topoisomerases mainly catalyse relaxation of supercoiled DNA, but in some cases, they can also perform knotting/unknotting and duplex formation with single-stranded DNA, and catenation/decatenation of nicked circular DNAs. Type II topoisomerases can catalyse relaxation/supercoiling, knotting/unknotting, and catenation/decatenation reactions by generating double-strand breaks using ATP. The reactions performed by type I and type II topoisomerases are summarized in Figure 1.19.

Type IA topoisomerases can only relax negatively supercoiled DNA reducing one linking number at each reaction by a strand passage mechanism. In contrast, type IB topoisomerases can relax both positively and negatively supercoiled DNA by controlled rotation allowing to reduce more than one linking number for each reaction. Type II topoisomerases possess an ATPase activity to perform strand passage of double-stranded DNA between double-strand breaks.

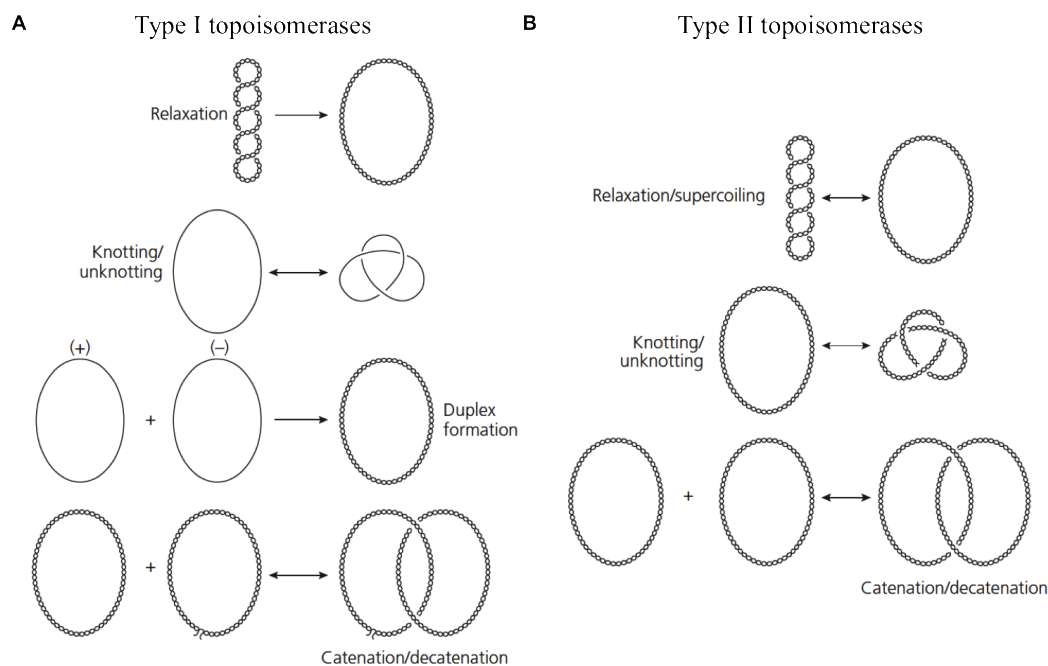


Figure 1.19. Reactions of Type I (A) and Type II (B) topoisomerases. Taken from (DNA Topology, 2005).

Because of their essential roles in cellular processes, topoisomerases are well-defined anticancer drug targets. Overexpression of topoisomerases in tumour cells provides selectivity for drugs. There are two types of topoisomerase inhibitors that differ in their mechanism of actions: (i) trapping of topoisomerase-DNA complexes and (ii) catalytic inhibition of topoisomerases (Topcu, 2001; Pommier, 2014).

CPT, an alkaloid from *Camptotheca acuminata*, is one of the most known hTopoI targeting anticancer drug. Camptothecin derivatives, such as Topotecan and Irinotecan are the only FDA-approved hTopoI-targeted anticancer drugs (Pommier, 2014). CPT blocks hTopoI's rejoining step of the cleavage/religation reaction, resulting in accumulation of hTopoI-cleavable complex (Figure 1.20 A) (Liu et al., 2000). Accumulation of hTopoI-cleavable complex impairs several important cellular processes such as replication and transcription which are blocked by the torsional stress on the DNA and leads to the formation of cytotoxic strand breaks (Figure 1.20 B) (Koster et al., 2007).

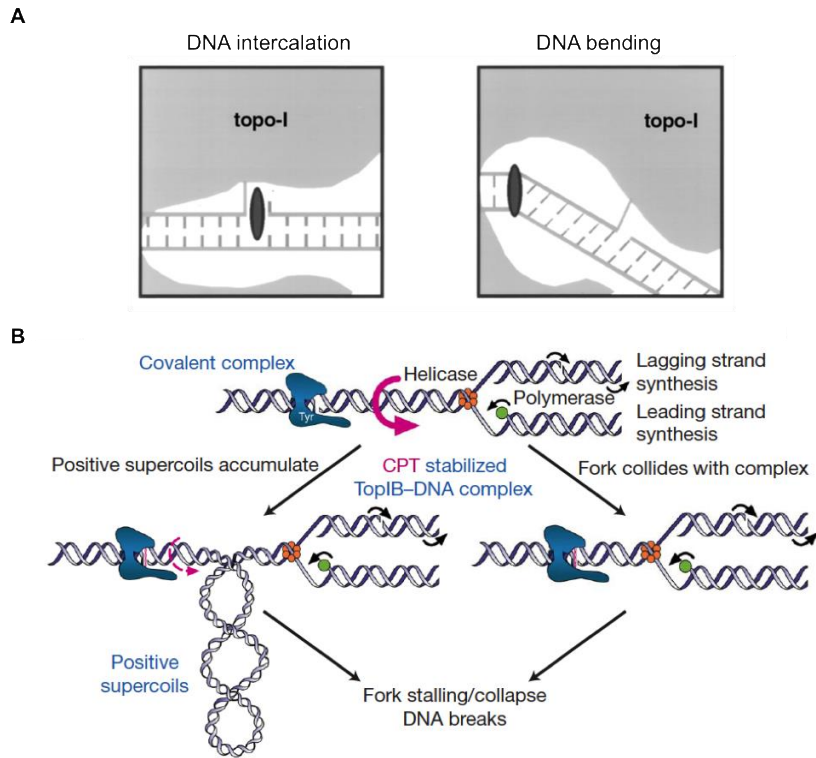


Figure 1.20. Mechanism of Human Topoisomerase I targeting drugs. **(A)** Two possible modes of formation of hTopoI-cleavable complex by either drug intercalation into DNA (like Camptothecin) or drug binding to DNA (like Nogalamycin). Taken from Liu et al., 2000. **(B)** Cytotoxic effect of CPT stabilized hTopoI-cleavable complex. A replication fork creates positive supercoils, which are removed (pink arrow) by hTopoI (blue). When CPT stabilizes hTopoI-cleavable complex in the DNA, DNA breaks can occur as a result of the accumulation of positive supercoils (left). Another possibility is the collision of the replication fork with CPT stabilized hTopoI-cleavable complex, and the formation of DNA breaks at the end (right). Taken from Koster et al., 2007.

hTopoI-mediated DNA damage can be repaired by reversal of hTopoI-cleavable complex, by Tyrosyl-DNA-phosphodiesterase (Tdp1) and endonucleases (Pommier et al., 2006).

1.7.3. Human Topoisomerase I (hTopoI)

Human Topoisomerase I (hTopoI) is a Type IB topoisomerase (Wang, 2002) and solves the topological problems of DNA in replication, transcription and other cellular processes by generating reversible single DNA strands (Pommier, 2006). hTopoI is encoded by a single copy gene located in chromosome region 20q12-13.2 (Juan et al., 1988).

hTopoI is a 91kDa monomeric enzyme that forms an asymmetric protein clamp, which encircles double-stranded DNA. hTopoI contains four domains: a poorly conserved N-terminal domain, a highly conserved core domain, a linker domain formed by an extended pair of α -helices, and a conserved C-terminal domain (Figure 1.21) (Pommier, 2006). The N-terminal domain is highly charged, protease sensitive and contains targeting signals. The core domain contains three subdomains: core subdomain I (residues 215–232 and 319–433); core subdomain II (residues 233–318); core subdomain III (residues 434–635). The C-terminal and core domains are involved in enzymatic activity. The C-terminus contains the active site tyrosine described above (Tyr 723 in hTopoI) involved in the catalytic reaction illustrated in Figure 1.22.

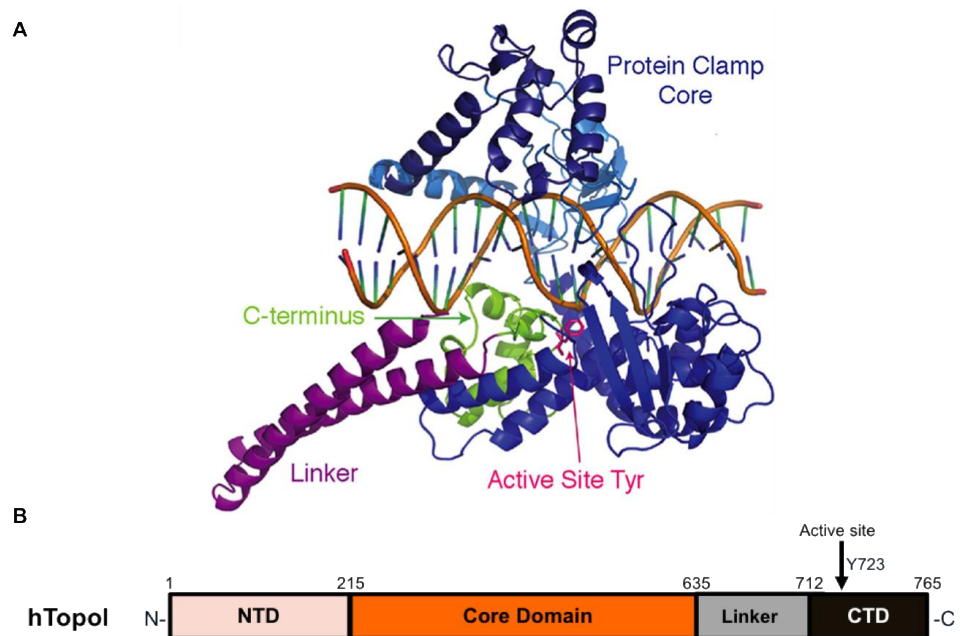


Figure 1.21. The structure and domain organization of hTopoI **(A)** The structure of a C-terminal 70-kDa fragment of human DNA topoisomerase I (Topo70) in a noncovalent complex with a 22-base pair DNA duplex. Ribbon diagram of PDB file 1A36 (Stewart et al., 1998), viewed perpendicular to helical axis of the DNA duplex (backbone is in orange), the core domain of Topo70 forms a protein clamp (shades of blue). The linker domain (purple) extends from the core at an oblique angle to the DNA, and the C-terminal domain is in green. The active site Tyr is mutated to Phe to render the enzyme inactive for structural studies (indicated in magenta). Taken from Wright et al., 2015. **(B)** Schematic diagram of hTopoI domain organization. NTD: N-terminal domain. CTD: C-terminal domain.

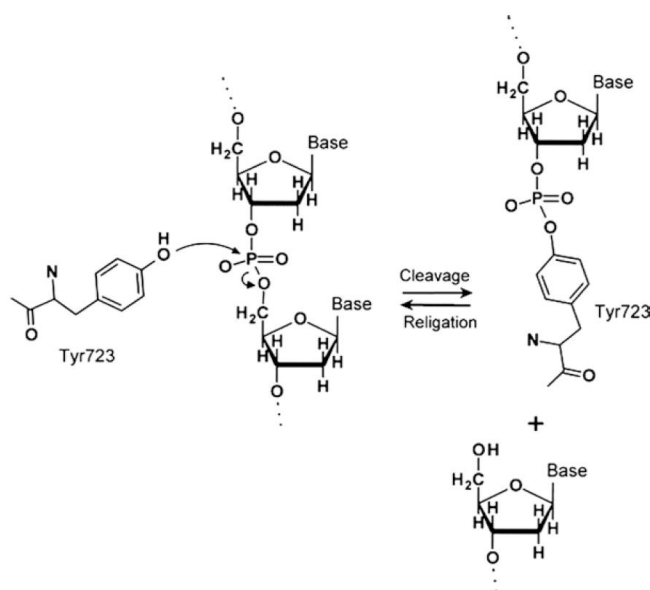


Figure 1.22. Active site of hTopoI and its reaction. In the cleavage reaction, the O-4 atom of the active site Tyr723 is shown as the nucleophile that attacks a phosphodiester bond in DNA to generate a phosphodiester linkage between itself and the 3' end of the broken strand. The religation reaction involves nucleophilic attack by the free 5' hydroxyl group of the broken strand on the tyrosine-DNA linkage to restore the phosphodiester bond in the DNA and release the active site tyrosine. Taken from (Pommier, 2012).

hTopoI can relax both negatively and positively supercoiled DNA by a controlled rotation mechanism (Figure 1.23). In the strand-breakage reaction, a tyrosyl oxygen of the enzyme attacks a DNA phosphorus, forming a covalent phosphotyrosine link and breaking a DNA phosphodiester bond at the same time (Figure 1.22). Rejoining of the DNA strand occurs by a second transesterification, which is basically the reverse of the first — the oxygen of the DNA hydroxyl group that is generated in the first reaction attacks the phosphorus of the phosphotyrosine link, breaking the covalent bond between the protein and DNA, and reforming the DNA backbone bond (Figure 1.22). These reactions create transient enzyme-mediated gates in the DNA for the passage of another DNA strand.

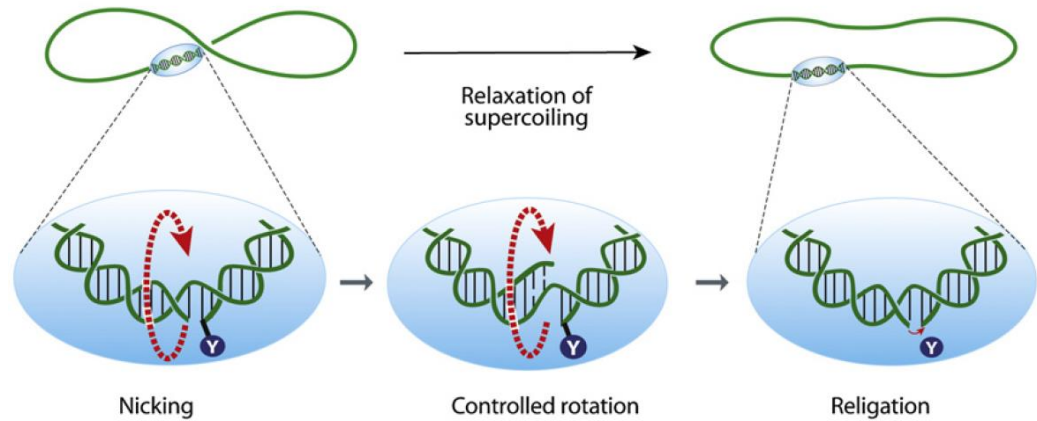


Figure 1.23. hTopoI-mediated DNA relaxation by controlled rotation. Taken from Pommier et al. 2010.

The tumour suppressor protein p53 and hTopoI form complexes *in vitro* and *in vivo*. p53 accumulates in the nucleus and stimulates hTopoI DNA relaxation activity in DNA-alkylating agent Mitomycin C-treated MCF7 cells (Gobert et al., 1996). p53 enhances hTopoI activity by facilitating the clamp structure opening of hTopoI in order to release its substrate DNA. Monomeric form of p53 is enough to increase the catalytic activity of hTopoI but the tetrameric form of p53 is necessary for the stimulation of the topoisomerase I-induced recombination repair reaction (Søe and Grosse, 2003).

Another tumour suppressor, the prostate-specific homeodomain protein NKX3.1, also interacts with hTopoI and stimulates its activity by enhancing hTopoI-DNA complex formation and increasing its cleavage activity. Down regulation of NKX3.1 decreases hTopoI activity in prostates (Bowen et al., 2007). It has been shown that the effect of NKX3.1 on hTopoI sensitizes cells to the cellular toxicity of CPT. The knockdown of hTopoI had an effect on the DNA damage response in PC-3 cells (Song et al., 2013).

Topo I has been identified as the major non-histone substrate of PARP-1 and its catalytic activity was inhibited by pADP-ribosylation *in vitro* (Kasid et al., 1989). For this reason, using PARP inhibitors in clinical trials enhances the cytotoxicity of CPT. It has been shown that subnuclear localization of hTopoI changed during PARP inhibitor treatment by live-cell imaging, which was not the result of hTopoI/PARP-1 interaction (Das et al., 2016). As mentioned earlier, YB-

1 has been shown to interact directly with hTopoI and stimulate its relaxation activity (Wu et al., 2014).

There is also some evidence that hTopoI is involved in DNA repair process. Decreased expression levels of hTopoI by anti-sense RNA negatively affects the ability of cells to induce DNA repair following UV radiation (Mao and Muller, 2003). The rapid recruitment of hTopoI to UVA-irradiated DNA sites may result from its binding to DNA lesions but it may also play additional roles in the repair of these lesions (Mielke et al., 2007). Several DNA lesions have been shown to trap the hTopoI-cleavable complex (Pourquier et al., 1997; Leshner et al., 2002). hTopoI may be required to adjust DNA topology during repair processes or it may help to recruit DNA repair proteins to DNA lesions.

Objectives

In the light of the studies presented above, it is clear that YB-1 plays a key role in modulating the sensitivity of tumour cells to chemotherapeutic agents via its interactions with various proteins, including hNTH1 and hTopoI, as illustrated in Figure 1.24.

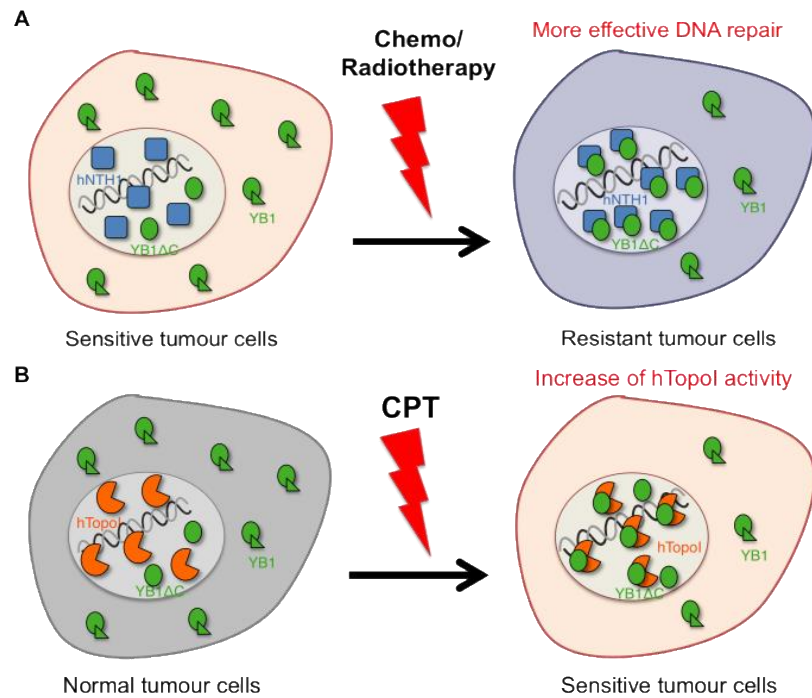


Figure 1.24. Schematic illustration of the complex and diverse roles of YB-1 in regulating the sensitivity and resistance of tumour cells to chemotherapeutic drugs. **(A)** The increased abundance of nuclear YB-1 in response to genotoxic stress has been shown to lead to enhanced YB1/hNTH1 complex formation and increased resistance to anticancer therapies, in particular cisplatin, in solid tumours. **(B)** In tumour cells treated with the hTopoI inhibitor, CPT, YB-1 has been shown to stimulate hTopoI activity thereby increasing the sensitivity of these cells to the anticancer agent by trapping more hTopoI-DNA complexes.

The first objective of my thesis work was to investigate the formation of the YB-1/hNTH1 complex *in vitro* and in MCF7 cells using FRET approaches and to design and optimise a FRET-based biosensor, which could be used for high-throughput chemical library screening in order to identify potential inhibitors of this complex for use in combined therapy. In addition, a second objective was to study YB-1/hTopoI complex *in vitro* and in various mammalian cell lines using

FRET method and to find potent enhancers of this interaction in order to potentiate the effects of Camptothecin treatment.

Chapter 2. Materials and Methods

Summary

FRENCH

Les gènes codant pour les protéines d'intérêt utilisées pour des expériences de FRET ont été amplifiés par PCR et insérés dans des vecteurs d'expression pour cellules mammifères et pour bactéries, soit par des méthodes de clonage classique (digestion par enzyme de restriction suivie de ligation), soit par assemblage de l'ADN de type Gibson. Toutes les protéines recombinantes utilisées dans ce travail ont été surexprimées dans des cellules BL21 (DE3) d'*Escherichia coli* avec une étiquette His clivable en N-terminal ou une étiquette His non-clivable en C-terminal (pour plusieurs constructions de topoisomérase I humaine). Le protocole de purification est composé de trois étapes: (i) chromatographie d'affinité pour le nickel, (ii) chromatographie d'affinité pour l'héparine et (iii) chromatographie d'exclusion de taille. Les mesures de fluorescence avec des protéines purifiées ont été effectuées sur un lecteur de microplaques Clariostar (BMG Labtech) dans des plaques à puits à fond plat Corning 384 (Merck) à température ambiante. Nous avons optimisé notre Biosenseur 1 pour le criblage de la chimiothèque. Un criblage à haut débit (HTS) a été réalisé sur la plateforme de Criblage pour des Molécules BioActives (CMBA) au CEA de Grenoble. Deux chimiothèques ont été criblées: la chimiothèque PPI de Life Chemicals (800 composés) et la chimiothèque Prestwick (1280 composés). Les hits potentiels identifiés à partir de notre HTS avec le Biosenseur 1 ont été validés avec une autre technique connue sous le nom d'AlphaScreen. Des dosages de relaxation du plasmide superenroulé ont été réalisés pour étudier l'effet de YB-1 sur hTopoI. Plusieurs lignées cellulaires de mammifères ont été utilisées pour des expériences de FRET *in vivo*. Le microscope à épifluorescence sur la plateforme d'imagerie M4D de l'IBS a été utilisé pour vérifier la localisation des cellules et l'efficacité de la transfection avant les expériences de photoblanchiment accepteur effectuée sur le microscope confocal.

Özet

TURKISH

FRET deneyleri için kullanılan ilgili proteinleri kodlayan genler, PCR ile amplifiye edildi ve geleneksel klonlama yöntemleri (restriksiyon enzimi kesimi takiben ligasyon) veya Gibson DNA'nın bir araya getirilmesi ile memeli ve bakteriyel hücre ekspresyon vektörlerine klonlandı. Bu çalışmada kullanılan tüm rekombinant proteinler, ya uzaklaştırılabilir bir N-terminal His-etiketi ya da ayrılmaz bir C-terminal His-etiketi (birkaç insan Topoizomera I için) ile *Escherichia coli* BL21 (DE3) hücrelerinde aşırı eksprese edilmiştir. Saflaştırma protokolü üç aşamadan oluşur: (i) nikel afinite kromatografisi, (ii) heparin afinite kromatografisi ve (iii) boyut dışlama kromatografisi. Saflaştırılmış proteinlerle floresans ölçümleri, oda sıcaklığında siyah düz tabanlı Corning 384 kuyucuklu plakalarda (Merck) bir Clariostar (BMG Labtech) mikroparka okuyucusu üzerinde gerçekleştirilmiştir. Kimyasal kütüphane taraması için Biosensör 1 optimize edilmiştir. Yüksek verimli kimyasal kütüphane taraması (HTS), CEA, Grenoble'da BioAktif Molekül Taraması (CMBA) platformunda gerçekleştirildi. İki kimyasal kütüphane taranmıştır: Life Chemicals PPI kütüphanesi (800 bileşik) ve Prestwick kütüphanesi (1280 bileşik). HTS'mizden Biosensör 1 ile tanımlanan potansiyel inhibitörler, AlphaScreen olarak bilinen başka bir teknikte daha da doğrulanmıştır. YB-1'in hTopoI üzerindeki etkisini araştırmak için süper sarmal plasmid relaksasyon deneyleri gerçekleştirilmiştir. Çeşitli memeli hücre hatları *in vivo* FRET deneyleri için kullanılmıştır. IBS'nin M4D görüntüleme platformundaki epifloresans mikroskopunda hücreler, akseptör foto-ağartma deneylerinden önce protein lokalizasyonunu ve transfeksiyon etkinliğini kontrol etmek için gözlenmişlerdir. Akseptör foto-ağartma deneyleri için, IBS'nin M4D görüntüleme platformunda bir FRAPPA cihazı ile donatılmış bir Olympus IX81 konfokal mikroskobu kullanılmıştır.

2.1. Cloning

The cDNAs encoding human YB1, NTH1 and TopoI were codon optimized for expression in both bacteria and mammalian cells (in particular, removal of rare codons) and were synthesized by Eurofins MWG (see Annex for original and optimized sequences) (Figure 2.1).

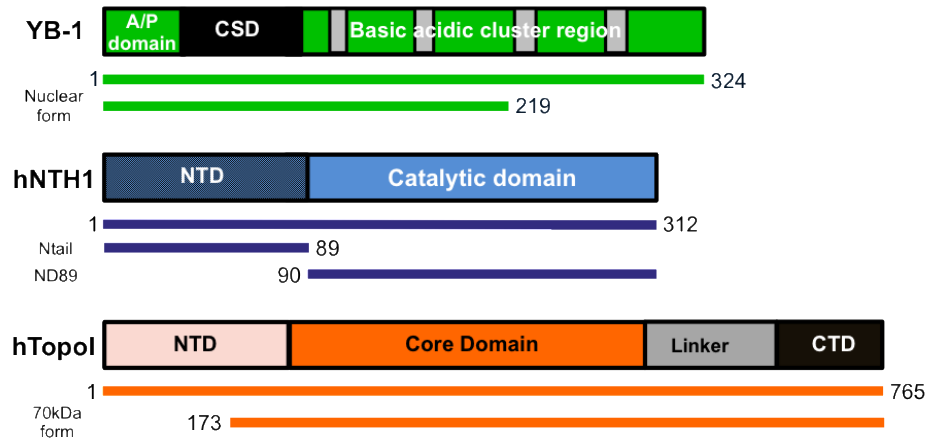


Figure 2.1. Illustration of the domain organisation of YB1, hNTH1 and hTopoI and their various constructs used in this study.

The optimized cDNAs of *hnth1* and *ybl* were provided as cloned fragments in the pEX-A2 plasmid. For *htopoI* the cDNA was delivered as three fragments of equal size (766 bp for each, cloned into pEX-A2 plasmid). Two strategies were used to assemble these three parts into the full-length gene using the NEBuilder HiFi DNA Assembly kit (New England Biolabs; NEB). First, we tried to assemble the three *htopoI* fragments for further amplification by PCR (Figure 2.2 A). Second, we created a pEX-A2 plasmid containing the full-length gene by direct assembly of the plasmid and the three fragments with overlapping sequences (Figure 2.2 B). The second strategy was successful, and we obtained full-length *htopoI* gene and confirmed this construct by DNA sequencing (Genewiz).

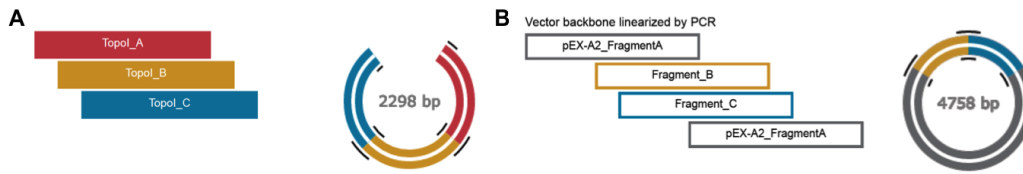


Figure 2.2. Strategies used to assemble the complete *hTopoI* gene using the three fragments obtained from Eurofins MWG. **(A)** Assembly of three linear *hTopoI* fragments for PCR amplification. **(B)** Assembly of three fragments into pEX-A2 plasmid.

PCR reactions were performed using Phusion® High-Fidelity PCR Master Mix (Thermo Scientific) (100 ng template DNA, 500 nM forward/reverse primers, 2 X Phusion Master Mix in a total volume of 40 µl) with the following reaction conditions:

Step	Temperature	Time
Initial Denaturation	98°C	30 seconds
30 Cycles	98°C 50-65°C 72°C	5-10 seconds 10-30 seconds 15-30 seconds per kb
Final Extension	72°C	5-10 minutes (min)
Hold	4°C	

After amplification, 6 X DNA loading dye (Thermo Scientific) was added to PCR reactions before electrophoresis on a 1% agarose gel containing GelGreen (Biotium) in 1xTBE buffer (89 mM Tris-borate, pH 8.0, 2mM EDTA). GeneRuler 1 kb DNA ladder (Thermo Scientific) was used for comparison. The gel was visualized on a Chemidoc MP Gel Imaging System (Biorad). PCR products were excised and recovered from the agarose with the NucleoSpin® Gel and PCR Clean-up kits (Macherey-Nagel).

PCR products and plasmids were then incubated with appropriate restriction enzymes (obtained from NEB) at 37°C for 1 hour. To insert restriction-digested

fragments into plasmids, T4 DNA ligase (Fermentas) was used. Ligation was carried out at room temperature (RT) for 1 hour using the Rapid Ligation kit (Fermentas).

E. coli DH5 α competent cells (NEB) were transformed with 2 μ l ligation reaction mixture using the heat shock method. After transformation, the cells were transferred to LB-agar plates containing an appropriate antibiotic (100 μ g/ μ l Ampicillin or 50 μ g/ μ l Kanamycin) and incubated at 37°C overnight (o/n).

Liquid cultures (5 ml) in LB containing appropriate antibiotic were started from colonies obtained after transformation for plasmid DNA purification using NucleoSpin® Plasmid QuickPure (Macherey-Nagel). Purified plasmids were controlled by restriction enzyme digestion. Positive clones were verified by DNA sequencing (Genewiz). The verified clones were used for further experiments. PCR primers used for cloning all constructs and cloning fragments are provided in the Annex.

2.1.1. Mammalian Expression Vector

For *in vivo* FRET measurements, all genes were cloned into mammalian expression vectors derived from either pEGFP-C1 or pEGFP-N1 (Figure 2.3 A and B).

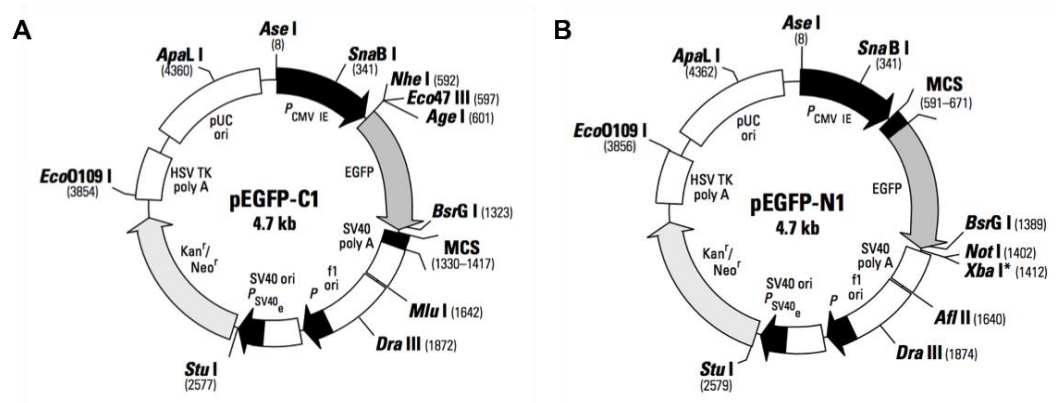


Figure 2.3. Maps of pEGFP-C1 (A) and N-1 (B) mammalian expression vectors that were modified in this study to replace eGFP by either sYFP2 or mTQ2 for *in vivo* FRET experiments.

The EGFP gene was replaced with sYFP2 or mTQ2 genes (kindly provided by J.P. Kleman from the M4D imaging platform at IBS) to create pmTQ2-C1/N1 and psYFP2-C1/N1 vectors. Then the *hnth1* gene was cloned into pmTQ2-C1 and N1 vectors and the *yb1ΔC* gene was cloned into psYFP2-C1 and N1 vectors. To overcome low transfection efficiency, we decided to fuse the two protein constructs sYFP2-YB1ΔC and hNTH1-mTQ2 with a 10 amino acid long linker SGGGASGGGT. The *NheI* restriction site was added in the middle of the linker to facilitate the cloning.

The *htop1* gene was also cloned into mammalian expression vectors pmTQ2-C1 by ligation and pmTQ2-N1 by DNA assembly using NEBuilder® HiFi DNA Assembly kit (NEB). We additionally created a co-expression plasmid with a self-cleaving Foot-and-mouth disease virus (FMDV) 2A peptide (Kim et al., 2011). For this, we amplified the mTQ2-hTopoI and the YB1ΔC-sYFP2 constructs with overlapping regions encoding the 2A peptide and then assembled these two fragments by NEBuilder® HiFi DNA Assembly kit to create the YB1ΔC-sYFP2-2A-mTQ2-hTopoI construct.

2.1.2. Bacterial Expression Vector

For expression in *E. coli* we also cloned target genes of interest into bacterial expression vectors pProEX HTb and pET21d (Figure 2.4 A and B).

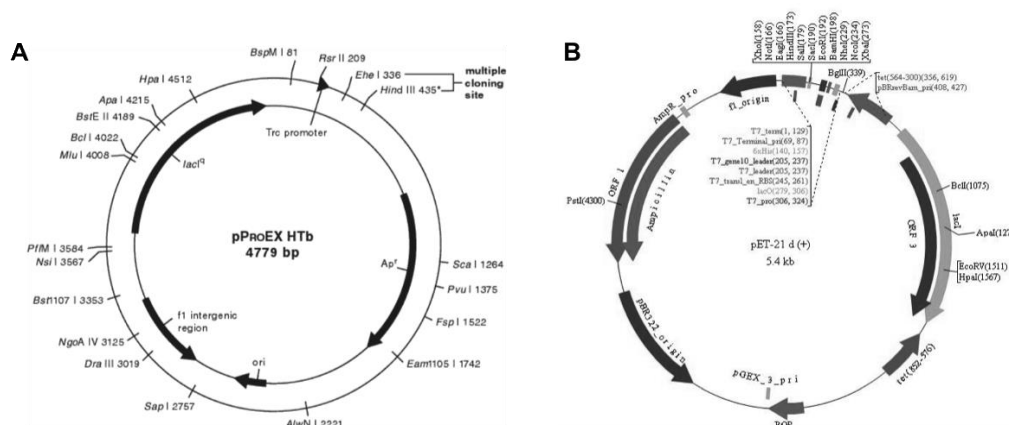


Figure 2.4. Maps of bacterial expression vectors used for protein expressions. **(A)** pProEX-HTb, and **(B)** pET21d vectors.

The optimized cDNAs encoding for hNTH1, YB1 and hTopoI were cloned into pProEX-HTb (Invitrogen) plasmid and placed under the control of an isopropyl β -D-1-thiogalactopyranoside (IPTG)-inducible pTrc promoter. In addition, the pProEX-HTb vector introduces a hexa-histidine (6x His) affinity tag followed by a highly specific tobacco etch virus (TEV) protease cleavage site at the amino (N-) terminus of the expressed protein (Figure 2.4 A). To obtain a carboxy-(C-)terminal 6x His-tagged form, the *htopoI* gene was cloned into pET21d (Novagen) plasmid under the control of a T7/Lac operon with *NcoI* and *XhoI* restriction enzymes (Figure 2.4 B). Both bacterial expression vectors contain an ampicillin resistance gene.

2.1.2.1. Fluorescent Protein Coupled Constructs

To express and purify fluorescent protein coupled proteins in *E. coli*, sYFP2-YB1 Δ C and hNTH1-mTQ2 were amplified from psYFP2-C1-YB1 Δ C and pmTQ2-N1-hNTH1 constructs, respectively and subcloned into pProEX-HTb plasmid. To create the new individual constructs by changing the position of fluorescent proteins (YB1 Δ C-sYFP2 and mTQ2-hNTH1), YB1 Δ C and hNTH1 were ligated into digested pProEX-HTb-sYFP2 and pProEX-HTb-mTQ2, respectively. To determine the interaction domains of hNTH1, we created two different hNTH1 constructs (NtailhNTH1 and ND89hNTH1) fused with mTQ2 (Figure 2.1).

For bacterial protein expression, fluorescent protein coupled hTopoI constructs (mTQ2-hTopoI and hTopoI-mTQ2) were subcloned from pmTQ2-C1-hTopoI and pmTQ2-N1-hTopoI into pProEX-HTb and pET21d plasmids, respectively.

2.1.2.2. Biosensor constructs

For bacterial expression of the Biosensor 1 (sYFP2-YB1 Δ C-hNTH1-mTQ2) construct, sYFP2-YB1 Δ C (~1360 bp) and hNTH1-mTQ2 (~1660 bp) were amplified by PCR using respectively psYFP2-C1-YB1 and pmTQ2-N1-hNTH1 as

templates. A 3-piece ligation was set up with digested PCR products sYFP2-YB1ΔC, mTQ2-hNTH1 and digested pProEX-HTb plasmid.

For making the Biosensor 2 (sYFP2-YB1ΔC-NtailhNTH1-mTQ2) and Biosensor 3 (sYFP2-YB1ΔC-ND89hNTH1-mTQ2) constructs, NtailhNTH1-mTQ2 and ND89hNTH1-mTQ2 were amplified by PCR using pmTQ2-N1-hNTH1-Ntail and pmTQ2-N1-ND89hNTH1 as templates, respectively. Then both of them were ligated into digested pProEX-HTb-sYFP2-YB1ΔC.

To create the Biosensor 4 (sYFP2-YB1ΔC-drEndoIII2-mTQ2) construct, drEndoIII2 (~675 bp) was amplified by PCR using *Deinococcus radiodurans* genomic DNA as a template. It was ligated into digested pProEX-HTb-mTQ2. Then drEndoIII2-mTQ2 (~1400bp) was ligated with digested pProEX-HTb - sYFP2-YB1ΔC.

For making the Biosensor 5 (sYFP2-YB1ΔC-mTQ2) and Biosensor 6 (sYFP2- hNTH1-mTQ2) constructs, mTQ2 and sYFP2 were amplified by PCR using pProEX-HTb-mTQ2 and pProEX-HTb-sYFP2 as templates, respectively. Then both of them were ligated into digested pProEX-HTb-sYFP2-YB1ΔC and pProEX-HTb-hNTH1-mTQ2, respectively.

To create the Biosensor 7 (mTQ2-hNTH1-YB1ΔC-sYFP2) construct, mTQ2-hNTH1 (~1660 bp) and YB1ΔC-sYFP2 (~1360 bp) were amplified by PCR using psYFP2-N1-YB1 and pmTQ2-C1-hNTH1 as templates, respectively and cloned using the same strategy as Biosensor 1.

To create the Biosensor 9 (mTQ2-hTopoI-YB1ΔC-sYFP2) construct, mTQ2-hTopoI (~3000 bp), YB1ΔC-sYFP2 (~1360 bp) and pET21d plasmid (~5500 bp) were amplified by PCR using pProEX-HTb mTQ2-hTopoI, psYFP2-N1-YB1 and pET21d-hTopoI as templates, respectively. A 3-piece DNA assembly was performed with PCR products mTQ2-hTopoI, sYFP2-YB1ΔC and pET21d by NEBuilder HiFi DNA Assembly kit.

A list of all the constructs prepared in this work is provided in the Annex.

2.2. Protein expression and purification

All recombinant proteins used in this work were overexpressed in *Escherichia coli* (*E.coli*) BL21 (DE3) cells with either a cleavable N-terminal His-tag or an uncleavable C-terminal His-tag (for several human Topoisomerase I constructs). Bacterial cultures were grown in LB medium (Sigma) containing 100 µg/ml Ampicillin at 37°C until they reached OD₆₀₀ between 1.0 - 1.3. The cultures were then induced with 1 mM IPTG.

2.2.1. Expression and purification of fluorescent proteins

All fluorescent proteins (mTQ2, sYFP2 and sYFP2-mTQ2 fusion) were overexpressed in BL21 (DE3) cells with a cleavable N-terminal His-tag. 1 liter (L) cell cultures were induced with 1 mM IPTG at 20°C with agitation o/n. The cell pellets were resuspended in 20 mL/liter Lysis Buffer containing 50 mM Tris pH 8.0, 200 mM NaCl, 2 mM MgCl₂, 0.5 mM EDTA, 0.02 % Triton. After lysis by sonication, the lysates were then centrifuged (30 min, 20000 rpm, 4°C) to remove cell debris. The supernatant was loaded on a 2 ml Ni-IDA sepharose and purified by gravity-flow on bench. The fractions containing fluorescent proteins eluted from the Ni-IDA with buffer containing 250 mM imidazole were pooled and concentrated using Millipore Amicon® Ultra centrifugal filter concentrators (Merck) before injection onto a Superdex 75 10/300 GL gel filtration column equilibrated in a 50 mM Tris pH 8.0, 200 mM NaCl. After determination of the protein concentration, aliquots of the proteins were flash-frozen in liquid nitrogen and then stored at -20°C.

2.2.2. Expression and purification of fluorescent protein fusion proteins, Biosensor constructs and human Topoisomerase I (hTopoI)

1 or 2 L cell cultures of YB-1ΔC and hNTH1 fusion proteins were induced with 1 mM IPTG at 20°C with agitation o/n. The cell pellets obtained after centrifugation (20 min, 6000 rpm, 4°C) were resuspended in 20 mL/liter Lysis Buffer containing 50 mM Tris pH 8.0, 2 M NaCl, 2 mM MgCl₂, 0.5 mM EDTA, 0.02 % Triton and 10 % Sucrose, supplemented with EDTA-free complete

protease inhibitor tablets (1 tablet for 2 L culture; Roche). We flash froze pellets in liquid nitrogen and stored them at -80°C .

6 or 12 L cell cultures of N- or C-terminally his-tagged hTopoI were induced with 1mM IPTG at 18°C o/n. The cell pellets were resuspended in 10 mL/liter Lysis Buffer composed of 50 mM Tris pH 8.0, 1 M NaCl, 2 mM MgCl_2 , 0.5 mM EDTA supplemented with EDTA-free complete protease inhibitor tablets (1 tablet for 2 L culture; Roche). hTopoI cell pellets were used directly for lysis without freezing.

Before cell lysis, we added a few mg lysozyme and DNaseI (Roche) into thawed pellets and incubated for 5 min on ice before continuing. We also added PMSF and β -mercaptoethanol (β ME) at final concentration of 1mM. For constructs containing YB1 Δ C, we added 20 μl S7 nuclease (1mg/ml stock solution, Roche) to further eliminate nucleic acid contamination. The cell lysis was performed by sonication (Pulse ON 10 sec_Pulse OFF 30 sec_Time 2:00_Amp 70%). For constructs containing YB1 Δ C, we added 1 M Urea to the sonicated lysates to facilitate the release of nucleic acids from proteins. The lysates were then centrifuged (30 min, 20000 rpm, 4°C) to remove cell debris.

For testing the interaction between two proteins, it is essential to have a sufficient amount of high quality protein that is stable and can be reproducibly prepared. Therefore, we optimized the purification protocols for each of our target proteins (Figure 2.5).

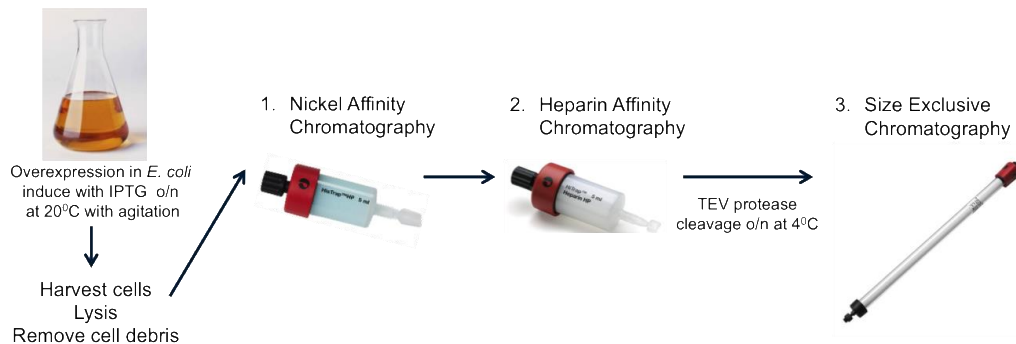


Figure 2.5. Illustration of the purification protocol steps used in our various protein purifications.

The first step of the purification was performed on a 5 ml HisTrap FF affinity column (GE Healthcare) on an ÄKTA Purifier FPLC (Fast Protein Liquid Chromatography) system (GE Healthcare) controlled by the Unicorn software. The column was equilibrated with Ni Buffer A (50 mM Tris pH 8.0, 0.5 M NaCl, 2 mM MgCl₂, 0.5 mM EDTA, 0.02 % Triton, 10 % Glycerol, 1 mM β ME). All buffers used for FPLC were filtered and degased. The supernatant obtained from the lysis was loaded onto the column manually using a syringe and the column was then connected to the FPLC and washed extensively to elute weakly bound contaminants. The first wash was done with Ni Buffer A. Then other washes were performed with Ni Buffer A supplemented with 10 mM (2 % Ni Buffer B = Ni Buffer A with 500 mM imidazole) and 50 mM (10 % Ni Buffer B) imidazole. The protein was eluted with Ni Buffer A and a gradient of imidazole (100 % Ni Buffer B, during 50 min) and collected in 1.5 ml fractions in 96-well plates. After analysing fractions from chromatogram peaks on 10 or 12 % TGX Stain-Free Gels (Biorad), sample-containing fractions were pooled and centrifuged (13000 rpm at 4°C for 5 min) to remove the precipitated protein. The TGX Stain-Free Gels contain unique trihalo compounds, which in the presence of UV-light react with tryptophan residues producing fluorescence that allow rapid fluorescent detection of proteins using the Chemidoc MP Gel Imaging System (Biorad). The protein concentration was determined by Bio-Rad protein assay using BSA as a standard following the manufacturer's procedures. The nickel column was able to remove most cellular contaminants.

The second step of the purification was a Heparin affinity chromatography for eliminating nucleic acid contamination. The structure and negative charge of heparin enable it to mimic DNA in its overall binding properties so it is useful for purification of DNA binding proteins. Prior to loading onto Heparin columns, samples were diluted to lower the NaCl concentration to 200 mM. The protein was then loaded on a 5 ml HiTrap Heparin HP column (GE Healthcare), which was equilibrated with Heparin Buffer A (50 mM Tris pH 8.0, 100 mM NaCl, 0.5 mM EDTA, 10 % Glycerol). First, the column was washed with 5 column volumes (CV) Heparin Buffer A, then the proteins were eluted with a linear NaCl gradient (0 to 100% Heparin Buffer B=Heparin Buffer A with 1 M NaCl, during 60 min) and collected in 1 ml fractions. Ntail-hNTH1-mTQ2 construct was not

contaminated with nucleic acids so we performed an ion-exchange chromatography instead of a heparin affinity purification. The sample was diluted to 50 mM NaCl for loading onto a HiTrapQ FF column (GE Healthcare) and eluted with a NaCl gradient using the same buffers as for the Heparin chromatography. The protein containing samples were identified by 10 or 12 % TGX Stain-Free Gel (Biorad) analysis and were pooled. TEV (Tobacco Etch Virus) protease produced inhouse was added to the protein at a ratio of 1 mg to 20 mg protein for cleavage of N-terminally His-tagged pProEX-HTb constructs. Cleavage was performed overnight at 4°C.

The final purification step was a size-exclusion chromatography. This chromatography serves as a quality control of our proteins. The sample was concentrated using Millipore Amicon® Ultra centrifugal filter concentrators (Merck). PMSF was added to the protein samples prior to injection onto a Superdex 200 10/300 GL column (GE Healthcare) or a SEC650 (BioRad) column equilibrated in a buffer containing 20 mM Tris pH 8.0, 1 M NaCl, 0.2 mM EDTA, 1 mM Tris(2-carboxyethyl)phosphine hydrochloride (TCEP), 10 % glycerol (GF Buffer). 0.5 ml fractions were collected. This size-exclusion step was then repeated, this time with a GF Buffer containing 500 mM NaCl instead of 1 M NaCl. hNTH1 and hTopoI constructs were injected onto a Superdex 200 10/300 GL gel filtration column equilibrated in a GF Buffer containing 200 mM NaCl. The elution peak containing the sample was pooled after checking on 10 or 12 % TGX Stain-Free Gel. The protein was concentrated and the final protein concentrations were measured using ultraviolet absorbance at 280 nm and the theoretical molar extinction coefficients of each construct on a NanoPhotometer TM UV/Vis Spectrophotometer (Implen). The molar extinction coefficients of the various proteins were calculated using the ProtParam tool on the ExPASy Proteomics Server (<http://ca.expasy.org/tools/protparam.html>), which bases its calculation on protein amino acid composition in conjunction with the molar extinction coefficients of tyrosine, tryptophan, and cystine (see Annex for details of all protein constructs). After determination of the protein concentration, aliquots of the proteins were flash-frozen in liquid nitrogen and then stored at -80°C.

2.2.3. Large-scale purification of Biosensor 1 for chemical library screening

To obtain large amounts of Biosensor 1 for use in chemical library screening, 6 L of bacterial culture were prepared. The supernatant containing Biosensor 1 was obtained as described above. Four sequential Nickel column purifications were carried out. Biosensor constructs were eluted with a 150 mM imidazole step based on the elution profiles observed previously using gradient elution. Sample-containing fractions were pooled, and their salt concentrations were adjusted to 200 mM in order to perform three sequential Heparin column purifications. After eliminating DNA contamination, we performed several gel filtration purifications with SEC650 column first equilibrated in a GF Buffer containing 1 M NaCl, then equilibrated in a GF Buffer containing 500 mM NaCl. The elution peak containing the Biosensor 1 was pooled after checking on 10 % TGX Stain-Free Gel. Only highly pure fractions were conserved to minimise contamination by degradation products of Biosensor 1, which could interfere with FRET measurements. The protein concentration was measured on a NanoPhotometer™ UV/Vis Spectrophotometer (Implen). Aliquots of the proteins (1 ml / 0.5 ml) were flash-frozen in liquid nitrogen and then stored at -80°C.

2.2.4. Preparation of proteins for AlphaScreen Assay

For AlphaScreen measurements (see section 2.5), we used hNTH1 with its N-terminal His-tag (no cleavage with the TEV protease) and biotinylated YB1ΔC. To biotinylate YB1ΔC, we first used a 5 ml HiTrap Desalting column (GE Healthcare) to transfer 0.5mg YB1ΔC into a phosphate buffer (20 mM NaPhosphate pH 8.0, 0.5 M NaCl, 1 mM MgCl₂, 5 % glycerol, 0.005 % Triton X-100 and 1 mM βME) instead of the Tris-based GF buffer, since the NHS-Biotin (Sigma) reacts with amine groups. YB1ΔC was then incubated with 0.25 mM NHS-Biotin at 25°C for 2 hours before the reaction was stopped by the addition of 50 mM Tris pH 8.0. The excess of NHS-Biotin was then removed by a second run on the desalting column equilibrated this time in Tris GF buffer. Fractions containing biotinylated YB1ΔC were pooled, aliquoted and stored at -80°C.

2.3. *In vitro* Fluorescence Resonance Energy Transfer (FRET) measurements

FRET involves a non-radiative transfer of energy from an excited donor fluorophore to an adjacent acceptor fluorophore. Due to the nature of the transition dipole interaction between the two fluorophores, energy transfer is more efficient when they are in close proximity than when they are further apart, allowing one to measure relative distances of up to 10 nm between donor and acceptor, making FRET extremely sensitive to small changes in distance (Piston and Kremers, 2007). The donor molecules typically emit at shorter wavelengths, which overlap with the absorption spectrum of the acceptor. We used CFP (Cyan Fluorescent Protein) and YFP (Yellow Fluorescent Protein) variants (mTurquoise2 and sYFP2), two colour variants of GFP (Green Fluorescent Protein), as donor and acceptor fluorophores (Figure 2.6). All proteins used for FRET measurements were expressed as fusions with either of these two fluorescent proteins. In Biosensor constructs containing both sYFP2 and mTQ2, we measured intramolecular FRET.

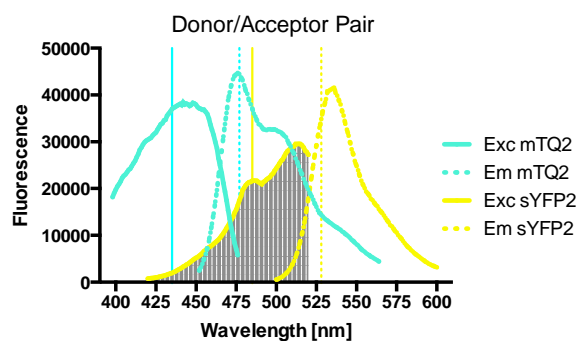


Figure 2.6. Excitation (full line) and emission (dashed line) spectra of mTQ2 (cyan) and sYFP2 (yellow) fluorescent proteins used in this study. The emission of mTQ2 overlaps extensively (grey) with the excitation spectrum of sYFP2. Vertical cyan and yellow full lines indicate the excitation wavelengths used for mTQ2, and sYFP2, respectively. Vertical cyan and yellow dashed lines indicate the emission wavelengths used for mTQ2, and sYFP2, respectively.

Fluorescence measurements were carried out on a Clariostar (BMG Labtech) microplate reader in black flat bottom Corning 384 well plates (Merck) at room temperature. Reaction mixtures were prepared in 50 μ l final volume in GF buffer (20 mM Tris pH 8.0, 0.2 mM EDTA, 1 mM TCEP, 10 % glycerol)

containing different concentrations of NaCl or urea (6 M). Protein concentrations in protein mixes with hNTH1 constructs were at 5 μ M final concentration for each protein. Protein mixes with hTopoI constructs were prepared at 1 μ M final concentration for each protein. Analysis of all biosensors was performed at 1 μ M final concentration. All *in vitro* FRET measurements were performed in triplicate.

FRET efficiencies were calculated by performing three different measurements (Figure 2.7). First, the donor molecule (mTQ2) was excited at its absorption wavelength (435/15 nm) and the fluorescence intensity of mTQ2 was recorded at its emission wavelength (477/20 nm). The measurement corresponds to the donor channel, which we refer to as I_{DD} . Second, the acceptor molecule (sYFP2) was excited at its absorption wavelength (485/15 nm) and the fluorescence intensity of sYFP2 was measured at its emission wavelength (528/20 nm) (Figure 2.7 A). This measurement corresponds to the acceptor channel, referred to as I_{AA} . Finally, a third measurement was performed in which mTQ2 was excited at 435/15 nm, and the fluorescence intensity at sYFP2's emission wavelength was recorded. We called this filter combination the FRET channel or I_{DA} . If two fluorescent proteins are close enough to FRET, a decrease of mTQ2 fluorescence intensity and an increase of sYFP2 fluorescence intensity will be observed in the FRET channel (Figure 2.7 B).

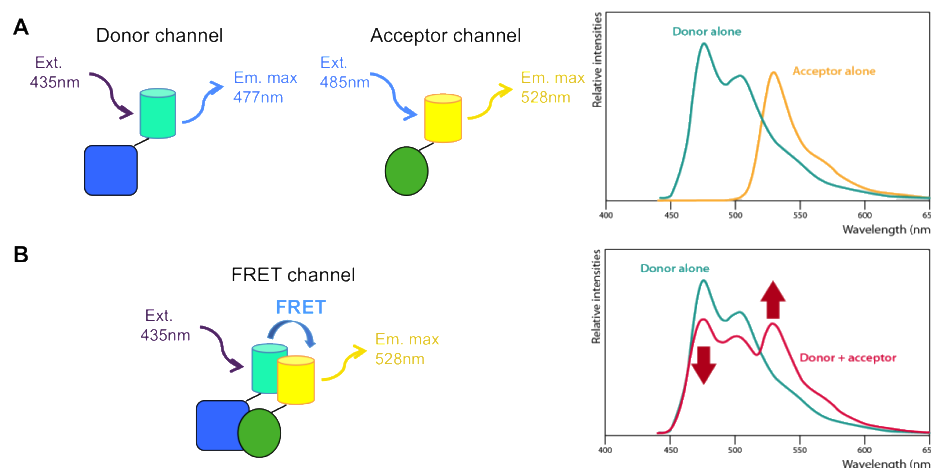


Figure 2.7. Schematic representation of the FRET measurements performed in order to calculate the FRET efficiency. **(A)** Fluorescence spectra of donor only (blue) and acceptor only (yellow) samples recorded using respectively donor and acceptor channels. **(B)** Fluorescence spectra of donor alone (blue) and of mixed donor and acceptor labeled samples (red) using the FRET channel. Ext.: Excitation, Em. max: Emission maximum.

Ratiometric FRET efficiency calculations were performed using various correction factors (Roszik et al., 2009). These spill-over factors reflect spectral crosstalk between the donor, the acceptor and the FRET channel and were calculated with donor only and acceptor only samples (Figure 2.8). S_1 is the contribution of the donor alone to the FRET signal (I_{DA}/I_{DD}) and was calculated to be 0.42 for mTQ2. S_2 is the contribution of the acceptor alone to the FRET signal (I_{DA}/I_{AA}) and was calculated to be 0.04 for sYFP2. S_3 is the contribution of the donor alone to the acceptor signal (I_{AA}/I_{DD}) and was calculated to be 0.04 for mTQ2.

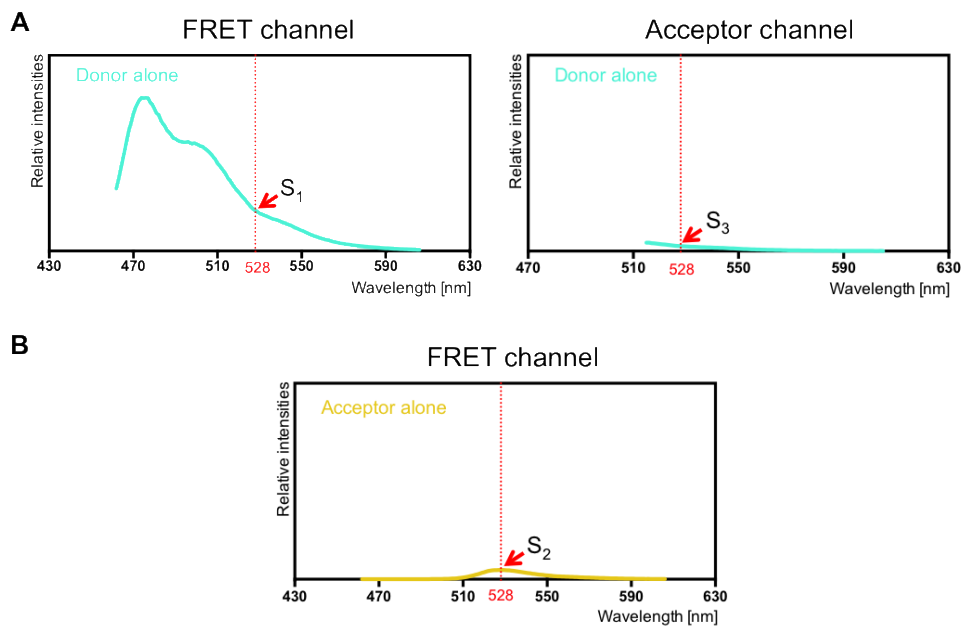


Figure 2.8. Fluorescence spectra showed spill-over factors between channels. **(A)** The fluorescence intensity contribution of donor only sample in the FRET and acceptor channels (S_1 and S_3). **(B)** The fluorescence intensity contribution of acceptor only sample in the FRET channel (S_2).

The FRET efficiency is the quantum yield of the energy transfer transition. The rate of relative detection sensitivity of the excited acceptor compared to the excited donor is described by the alpha factor (α), which was determined to be 1.37 for our mTQ2/sYFP2 FRET pair (Nagy et al., 1998) (Table 2.1).

Table 2.1. Alpha Factor calculation with mTQ2 and sYFP2 fluorescent proteins alone.

$$\text{efr}^1 = \text{ExC}^2 \text{ at max } \lambda \sim \text{QY}^3 \text{ at donor excitation.}$$

		ExC at max	QYmax at acceptor excitation	QY at donor excitation	ExC at donor Excitation
Donor	mTQ2	6055.82	n.a.	0.9300	5631.91
Acceptor	sYFP2	23466.86	0.68	0.0312	732.21
				Ratio efr	7.69

$$\text{Alpha factor: } I_{\text{DA}}(\text{acceptor alone}) * \text{efr} / I_{\text{DD}}(\text{donor alone})$$

¹ efr: FRET efficiency, ² ExC: extinction coefficient, ³ QY: quantum yield

The FRET efficiency (E) is calculated by the following formula:

$$E = \frac{A}{1 + A}$$

$$\text{with } A = \frac{1}{\alpha} \times \frac{I_{\text{DA}} - (I_{\text{DD}} \times S_1) - (I_{\text{AA}} \times S_2) + (I_{\text{DD}} \times S_2 \times S_3)}{I_{\text{DD}}}$$

2.4. *In vitro* high-throughput screening with Biosensor 1

2.4.1. Optimization of Biosensor 1 FRET measurements

To investigate the effect of DMSO, FRET measurements were performed on 0.2 μM Fusion and Biosensor 1 proteins in 50 mM NaCl GF buffer containing various concentrations of DMSO (0.5-5 % DMSO). To evaluate the stability of the biosensor, FRET measurements of 0.2 μM Biosensor 1 in presence of DMSO (0.5 and 1.3 %) were repeated every 10 minutes for 2 hours. A dose response curve was prepared with 12nt THF dsDNA oligonucleotide (see Annex for sequence) to find the concentration needed for inhibition of the interaction in order to use as our positive control for our assay. Minimal FRET values were obtained by adding 0.5 μM 12nt THF dsDNA oligonucleotide to the reactions.

We performed high-throughput screening with 0.2 μ M Biosensor 1 in GF buffer containing 50 mM NaCl (20 mM Tris pH 8.0, 50 mM NaCl, 0.2 mM EDTA, 1 mM TCEP, 10 % glycerol). The final reaction volume was 50 μ l. The FRET efficiency was determined by measuring the emission of excited mTQ2 and sYFP2 (excitation filter at 435/15 nm for mTQ2 and at 485/15 nm for sYFP2) at their maximal emission wavelengths (emission filter at 477/20 nm for mTQ2 and 528/20 nm for sYFP2) (endpoint measurements). FRET efficiencies were calculated as described above. FRET efficiencies of Prestwick Chemical Library second screening were calculated after subtraction of the fluorescence values of the compounds alone.

For a reliable screening assay, there must be a significant separation between the "Max" and "Min" signals. The Z' factor can be used to evaluate this signal separation. We performed a Z' factor assay with 30 samples with 0.2 μ M Biosensor 1 in 50 mM NaCl (our "Max" signal) and 30 samples with 0.2 μ M Biosensor 1 in 50 mM NaCl in the presence of 0.5 μ M 12nt THF dsDNA oligonucleotide (our "Min" signal). The FRET measurements were performed on both the Clariostar and the TECAN microplate reader to determine the Z' factors for both plate readers.

2.4.2. Chemical library screening at CMBA platform

High-throughput chemical library screening was performed on the Center for the screening for BioActive Molecules (CMBA) platform at the CEA, Grenoble. Two chemical libraries were screened: the PPI library from Life Chemicals (800 compounds) and the Prestwick library (1280 compounds). All chemical compounds used in our chemical screens were dissolved in 100 % DMSO. Test compounds from Life Chemicals and Prestwick Chemicals were delivered at 3.8 mM and 10 mM, respectively in 100 % DMSO. For the screening, reactions were carried out in 50 μ l final volume in GF buffer containing 50 mM NaCl. First, 40 μ l 0.25 μ M Biosensor 1 was added to the wells of Corning 384 well plates, then 10 μ l of 5 times concentrated compound stock solution was added to Biosensor 1. After mixing by pipetting, emission wavelengths of excited mTQ2 and sYFP2 were measured on a TECAN microplate reader at different time

points after mixing: 15, 30 and 60 min. All reactions were performed in triplicate at 50 μ M final concentration of inhibitor for the first screening, and then 30 selected test compounds were further tested in a secondary screen in triplicate at 50, 10 and 1 μ M final concentrations. All assay plates contained multiple negative (Biosensor 1 without test compounds) and positive controls (Biosensor 1 with 12nt THF oligonucleotide, 5 M NaCl or 2.5 M NaCl) (Figure 2.9).

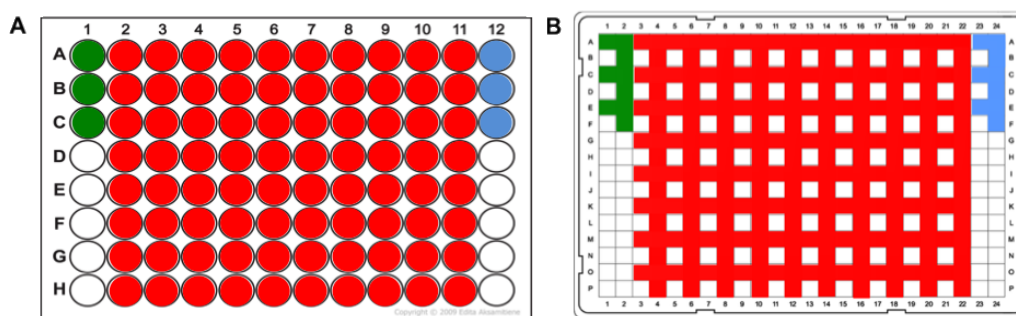


Figure 2.9. Illustration of screening plates. **(A)** 96-well plate containing 5x stock solutions. Green wells: 2.5 % DMSO in buffer containing 50 mM NaCl. Red wells: Total 80 compounds at 250 μ M concentration for each plate. Blue wells: Positive controls; from top to bottom 2.5 μ M 12nt THF oligonucleotide in 50 mM NaCl, 5 M NaCl, and 2.5 M NaCl respectively. **(B)** 384-well plate used for screening every test compounds in triplicate.

A large batch of Biosensor 1 was purified, so that all the tests and screens were performed with the same protein stock. For Life Chemicals PPI fragment library first screening, 3.2 mg Biosensor 1 (110 ml at 0.25 μ M concentration), 20 μ l at 50 μ M concentration 12nt THF oligonucleotide, and 10 Corning 384-well plates were used. For Prestwick Chemicals first screening, 5.4 mg Biosensor 1 (175 ml, at 0.25 μ M concentration), 28 μ l at 50 μ M concentration 12nt THF oligonucleotide, and 16 Corning 384-well plates were used. For second screenings of 30 selected compounds, 0.4 mg Biosensor 1 (14 ml, at 0.25 μ M concentration), 7.5 μ l at 50 μ M concentration 12nt THF oligonucleotide, and 1 Corning 384-well plates were used.

The FRET efficiencies of all compounds were calculated and compared to the maximal FRET control to determine the percent inhibition for each compound with the following formula:

$$\% \text{ inhibition} = 100 \times \left[1 - \frac{(X - \text{MIN})}{(\text{MAX} - \text{MIN})} \right]$$

Various validation tests were performed on selected compounds displaying significant FRET inhibition in our secondary screens. Powders were purchased from Sigma and were solubilized in 100 % DMSO before storing them at -20°C or 4°C. We checked the fluorescence of these compounds by measuring their fluorescence at 435 and 528 nm after dilution in GF buffer containing 50 mM NaCl. To evaluate the effects of these compounds on our Fusion construct (sYFP2-mTQ2), 40 µl 0.25 µM Fusion was mixed with 10 µl of test compounds (at 250 µM) prior to fluorescence reading.

Selected compounds were further tested on the Biosensor 1 with dose response experiments, in which increasing concentrations of compounds (all prepared at a final DMSO concentration of 1%) were added to Biosensor 1. The various compound concentrations were prepared by serial (1:2) dilutions of 500 µM stock solution. The data points corresponding to the means of triplicate measurements were fitted to a standard sigmoidal inhibition model in GraphPad Prism 6 using the following formula:

$$Y = \text{Bottom} + \frac{(\text{Top} - \text{Bottom})}{(1 + 10^{(\text{LogIC}_{50} - \text{Log}(X)) \times H})}$$

X: Compound concentration

Y: Response, decreasing as X increases

Top and Bottom: Plateaus in same units as Y

IC₅₀: Concentration of compound causing half maximal inhibition

H: Hill slope.

2.5. AlphaScreen Assay

Potential hits identified from our HTS with Biosensor 1 were further validated with another technique known as AlphaScreen. We used donor beads coated with streptavidin and AlphaLisa acceptor beads coated with anti-His antibodies. These beads were used to bind biotinylated YB1ΔC and His-tagged hNTH1, respectively. AlphaScreen assays were performed in white, flat-bottom, small volume 384-well plates (Perkin Elmer). The final reaction volume was 20 μ l. All reagents were diluted in AlphaScreen buffer (AS buffer) composed of 20 mM Tris pH 7.5, 150 mM NaCl, 0.01 % Triton X-100, 0.01 % Tween 20, 0.5 mM EDTA, 1 mM β ME and 0.1 mg/ml BSA. First, 8 μ l of the compounds diluted in AS buffer supplemented with 2.5 % DMSO (or the buffer alone for controls without compounds) were transferred to the wells. Then 2 μ l of biotinylated YB1ΔC at 100 nM (10 nM final concentration) and 2 μ l of His-tagged full-length hNTH1 at 1 μ M (100 nM final concentration) were added to the wells. After a 30 min incubation at room temperature, 4 μ l of anti-His AlphaLisa acceptor beads diluted to 0.1 mg/ml in AS buffer were added to the wells and the reaction was left to incubate for a further 45 min at room temperature and protected from light with aluminium foil. Finally, 4 μ l of streptavidin-coated donor beads diluted to 0.1 mg/ml in AS buffer were added to the wells and after 45-60 min incubation, the plate was read on the Clariostar plate-reader fitted with an aperture spoon (to avoid excitation of neighbouring wells) and the appropriate filters (excitation filter at 680/40 nm and emission filter at 570/100 nm). Reactions were prepared in triplicate. The data points corresponding to the means of triplicate measurements were fitted in GraphPad Prism 6 to the same sigmoidal inhibition model as described above.

2.6. DNA relaxation activity assays

Supercoiled plasmid relaxation assays were carried out in 10 μ l final volume containing 1 μ l purified hTopoI enzyme, 250 ng supercoiled pUC19 plasmid in reaction buffer (20 mM Tris pH 8.0, 72 mM KCl, 5 mM MgCl₂, 0.1 % BSA). Reactions were started by addition of the enzyme. The reaction mixture was incubated at 37°C for 30 min. Reactions were terminated with one volume of stop buffer (0.1 M EDTA, 4 % SDS, 0.1 % bromophenol blue, 30 % glycerol) and relaxation products were separated on 0.8 % agarose gel in 1xTBE buffer (89 mM Tris-borate, pH 8.0, 2 mM EDTA) in a horizontal electrophoresis apparatus (5 V/cm) at 4°C and photographed under UV light after staining in water containing Gel Green (Biotium) for 20 min. The TopoI inhibitor, CPT was used as a control in our reactions (Beidler and Cheng, 1995). To check the stimulation of hTopoI relaxation activity by YB1 Δ C protein, hTopoI and YB1 Δ C were preincubated at room temperature for 10 minutes before starting the relaxation reactions (Osherooff and Bjornsti, 2001; Senarisoy et al., 2013).

Substrate plasmid DNA pUC19 was purified from *E. coli* using a Qiagen Plasmid Maxi Kit. The purified plasmid was free of contaminating protein and was primarily composed of negatively supercoiled covalently closed circular DNA molecules (form I DNA), with nicked circles (form II DNA) representing no more than 20 % of the total DNA (Figure 2.10) (Bjornsti and Osherooff, 1999).

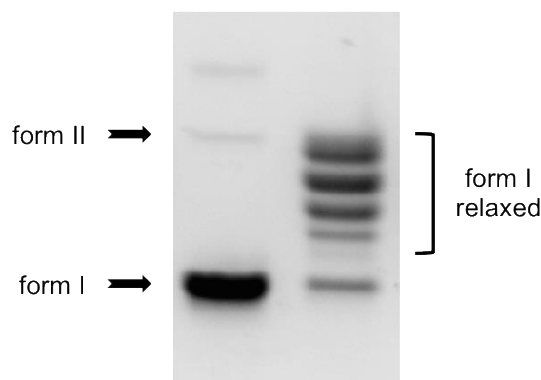


Figure 2.10. Representative agarose gel image to show the mobility of the supercoiled substrate (form I), the nicked circles (form II), and the relaxed topoisomers (form I relaxed).

2.7. Maintenance and transfection of mammalian cells

We used the MCF7 cell line to investigate the interaction of YB1ΔC and hNTH1. MCF7 cells were maintained as subconfluent monolayer cultures in Dulbecco's Modified Eagle's Medium (DMEM) with Glutamax-I (Life Technologies) supplemented with 10 % fetal bovine serum, 100 units/ml penicillin, and 100 µg/ml streptomycin, 0.1 mM non-essential amino acids, 1 mM sodium pyruvate at 37°C under a humidified 5 % CO₂ atmosphere. For passage, cell layers were detached by trypsinization and reseeded upon dilution (1:6).

To detect the interaction of YB1ΔC and hTopoI, we used HeLa, MCF7 and PC3 cells. HeLa cells were grown in 35 mm dishes using DMEM (Life Technologies) supplemented with 10 % fetal bovine serum, 100 units/ml penicillin, and 100 µg/ml streptomycin and the cells were maintained in a 37°C incubator supplied with 5 % CO₂. PC-3 cell line was obtained from the European Collection of Authenticated Cell Cultures (ECACC). PC3 cells were maintained in Coon's Modification of Ham's F-12 (Sigma) supplemented with 10 % fetal bovine serum, 100 units/ml penicillin, and 100 µg/ml streptomycin at 37°C under a humidified 5 % CO₂ atmosphere. For passage, cell layers were detached by trypsinization and reseeded upon dilution (1:10).

For all three cell lines, 24 h before transfection a monolayer culture covering 80 % of the substratum (i.e. 80 % confluent) was divided 1:3 into 35 mm dishes containing two microscope coverslips. Cells were transfected with 1 µg plasmid DNAs using FuGENE HD transfection reagent (Promega) in accordance with the manufacturer's instructions. Cells were grown on microscope coverslips for 24 h post transfection before being washed in PBS, fixed in 2 % paraformaldehyde in PBS (37°C, 15 min) and then washed again three times for 5 min in PBS. Slides were finally mounted in DABCO, and immediately inspected under the microscope.

2.8. FRET measurements in mammalian cells

Fluorescence microscopy – particularly exploiting genetically expressed fluorescent proteins – can be applied directly to map and quantify protein interactions in live or fixed cells and preserve information concerning the inhomogeneous cellular distribution of molecules, with typical spatial resolution below $0.5\text{ }\mu\text{m}$ (Jares-Erijman and Jovin, 2006).

The epifluorescence microscope on the M4D imaging platform of IBS was used to check for cell localisation and transfection efficiency before acceptor photobleaching experiments. For acceptor photobleaching experiments, the cells were monitored after fixation using an Olympus IX81 confocal spinning disk microscope equipped with a FRAPPA device on the M4D imaging platform of IBS (Figure 2.11). The images were acquired with a 60x objective and with appropriate filter sets for the two channels (CFP and YFP). Exposure times were typically of 100ms and laser powers of CFP (445 nm) and YFP (515 nm) were 80 %, and 5 %, respectively.

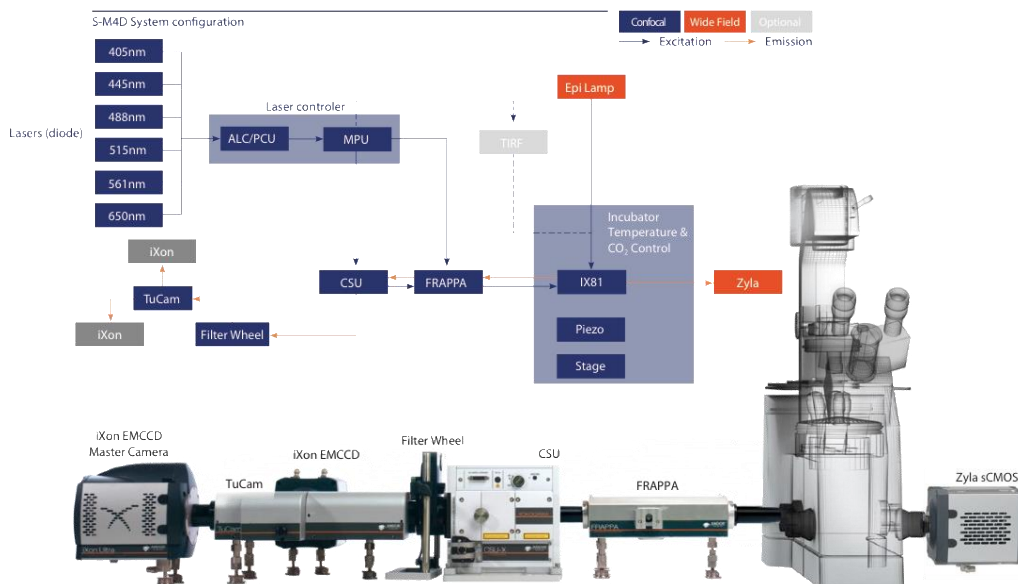


Figure 2.11. Illustration of the confocal, spinning disk microscopy platform setup used for the acceptor photobleaching experiments on fixed cells.

Acceptor photobleaching is one of the methods for detecting FRET in cells. In FRET, the acceptor fluorophore quenches the donor fluorescence by taking its energy. Photobleaching the acceptor fluorophore releases this quenching and in case of FRET, the donor fluorescence increases when the acceptor is bleached. For acceptor photobleaching experiments, we acquired 50 sequential images (100 ms exposure time, laser 445 nm for CFP with 80 % power and laser 515 nm for YFP with 5 % power). After 10 acquired images, the acceptor was gradually photobleached (100 ms exposure time, laser 515 nm and 1-3 % power) in a selected area of the nucleus. The imaging scans were acquired with a laser power attenuated to 0.1 – 1 % of the bleach intensity. For quantitative acceptor photobleaching analysis, fluorescence intensities of the bleached region (ROI 1), the entire cell nucleus (ROI 2) and background (ROI 3) were measured at each time point. Data were corrected for extracellular background intensity and for the overall loss in total intensity as a result of the bleach pulse itself and the imaging scans. Images were analysed with Volocity software and the FRET efficiency was calculated using the acceptor photobleaching (donor dequenching) method described in Roszik et al., 2013 which is independent of the donor-to-acceptor ratio.

Chapter 3. Results

Summary

FRENCH

Partie I. Complexe de YB-1/hNTH1

Du signal FRET a été détecté en utilisant la technique de photoblanchiment de l'accepteur dans des cellules MCF7 transfectées de manière stable avec hNTH1-mTQ2 et exprimant de manière transitoire YB-1ΔC-sYFP2. Afin de surmonter la faible efficacité de co-transfection et d'étudier les conditions dans lesquelles interagissent hNTH1 et YB-1, nous avons créé une seule chaîne polypeptidique, qui contient les protéines sYFP2, YB-1ΔC, hNTH1 et mTQ2 reliées par des liaisons d'acides aminés (entre 5 et 10). Nous n'avons pas observé de signal FRET significatif avec les cellules MCF7 exprimant le Biosenseur 1 nucléaire.

Toutes les protéines utilisées pour des expériences de FRET *in vitro* ont été purifiées avec succès. Le signal FRET a pu être détecté lors du mélange de protéines individuelles à une concentration de protéine de 5 μM dans du tampon contenant 50 mM de NaCl. A cette concentration de NaCl, l'efficacité de FRET du Biosenseur 1 est également très élevée (39%) et comparable à celle obtenue avec notre construction Fusion dans laquelle sYFP2 et mTQ2 sont associées en une même chaîne polypeptidique (~ 40%). Nous avons effectué des mesures FRET sur les 7 constructions de Biosenseur à différentes concentrations de NaCl (50 mM - 1 M), indiquant que l'interaction entre YB-1ΔC et hNTH1 est spécifique, mais semble être très sensible au sel. Toutes les constructions de Biosenseur ont montré des efficacités de FRET minimales similaires en présence d'urée 6 M. Nous avons effectué des mesures de FRET en présence d'un substrat ADN non clivable de hNTH1. Nous avons observé un effet similaire à celui du sel. Lorsque la concentration d'oligonucléotide augmente, l'efficacité de FRET diminue. Nous avons également effectué les mesures FRET dans du NaCl 50 mM à différentes concentrations de protéines du Biosenseur 1 (allant de 0,01 à 2 μM). Nous avons observé que l'efficacité de FRET du Biosenseur 1 diminuait rapidement lorsque la concentration était inférieure à 0,2 μM.

La caractérisation des différentes constructions de Biosensor et de nos expériences d'optimisation de tampon a clairement indiqué que notre Biosenseur était un outil approprié pour examiner l'interaction de hNTH1-YB-1 et également pour cribler les inhibiteurs potentiels de cette interaction. Le DMSO n'a pas affecté significativement les niveaux de FRET du Biosenseur. Pour tester la robustesse de notre test, nous avons effectué un test de facteur Z' sur 30 échantillons en l'absence et la présence d'oligonucléotide dsDNA 12nt THF. Les valeurs du facteur Z' issues des mesures effectuées dans notre laboratoire sur le lecteur de plaques Clariostar et sur la plateforme CMBA sont respectivement de 0,83 et 0,90, ce qui montre que notre Biosenseur 1 est un outil très fiable pour détecter les inhibiteurs potentiels de l'interaction YB-1 Δ C/hNTH1. Nous avons utilisé notre Biosenseur 1 pour réaliser un criblage à haut débit de la chimiothèque Life Chemicals PPI (Interactions protéine-protéine) et de la chimiothèque Prestwick Chemical sur la plateforme CMBA en collaboration avec Dr. Caroline Barette. Le premier criblage à haut débit a été effectué avec 0,2 μ M de Biosenseur 1 et une concentration de composé fixée à 50 μ M en triplicatas dans un volume final de 50 μ l. Après ce premier HTS, 30 composés sélectionnés présentant des taux réduits de FRET ont été testés à trois concentrations différentes (50, 10 et 1 μ M). Nous avons trouvé trois composés de la chimiothèque Life Chemicals PPI qui présentaient une inhibition de 30-60% à une concentration de 50 μ M et avaient toujours un effet inhibiteur à une concentration de 1 μ M. 8 composés de la chimiothèque de Prestwick se sont avérés être des inhibiteurs potentiels affichant une inhibition claire et dépendante de la concentration sur le signal FRET. Les composés de la chimiothèque Life Chemicals PPI ont montré une fluorescence intrinsèque. Les inhibiteurs potentiels de la chimiothèque Prestwick ont été sélectionnés parmi ceux qui ne présentaient pas de signal de fluorescence intrinsèque. Les 7 composés Prestwick n'ont eu aucun effet sur le signal FRET de la fusion, alors que les composés Life Chemicals ont réduit le signal FRET de 6 à 9%, indiquant que leur fluorescence intrinsèque, relativement élevée, peut interférer avec le processus de FRET. L'efficacité réduite de FRET peut ainsi résulter de la fluorescence intrinsèque du composé et non de l'inhibition de l'interaction hNTH1/YB-1. Trois composés d'essai identifiés à partir de la chimiothèque Life Chemicals PPI semblent donc être des faux positifs. Nos expériences de validation des composés Prestwick à partir de poudre achetés chez

Sigma suggèrent que plusieurs composés obtenus à partir de la plate-forme CMBA pourraient être dégradés ou modifiés en raison de la congélation-décongélation répétée avant utilisation dans le criblage haut débit. Leur effet inhibiteur sur l'interaction hNTH1/YB-1ΔC peut donc être le résultat de leur dégradation ou altération. Des expériences AlphaScreen ont validé l'effet inhibiteur de certains composés Prestwick.

Partie II. Complexe de YB-1/hTopoI

Nous avons exprimé et purifié deux formes de la topoisomérase I humaine : hTopoI-FL et hTopoI-70 à partir de la purification de l'hTopoI marquée par His à l'extrémité C-terminale. Les activités de relaxation de hTopoI-FL et de hTopoI-70 étaient similaires. Camptothécine a montré un effet inhibiteur similaire sur l'activité de hTopoI-FL et hTopoI-70 avec des IC_{50} dans la gamme de 5-10 μ M. YB-1ΔC stimule clairement l'activité de hTopoI-FL et de hTopoI-70, très probablement par une interaction directe, ce qui suggère que le domaine N-terminal de hTopoI n'est pas essentiel pour l'interaction avec YB-1ΔC.

Les constructions de fusion de hTopoI ont été purifiées avec de faibles rendements. Nous avons réussi à mesurer du signal de FRET avec des constructions de fusion hTopoI à une concentration finale de seulement 1 μ M de protéine dans du tampon contenant 50 mM de NaCl. Le signal le plus élevé a été obtenu quand à la fois mTQ2 et sYFP2 ont été fusionnés aux extrémités C-terminales de hTopoI et YB-1ΔC. Les efficacités de FRET étaient plus faibles dans le cas de hTopoI-70, mais significativement plus élevées qu'avec le contrôle négatif (mTQ2 seul), indiquant que la région N-terminale est importante, mais pas essentielle pour l'interaction avec YB-1ΔC, en accord avec nos mesures d'activité de relaxation qui ont montré que YB-1ΔC pouvait également stimuler hTopoI-70. Nous avons observé que des quantités accrues de sel conduisent à des efficacités de FRET réduites en affectant l'interaction.

Nous avons ensuite étudié l'interaction entre YB-1 et hNTH1 dans plusieurs lignées cellulaires (HeLa, MCF7 et PC-3). Nous avons détecté un faible signal de FRET avec les cellules MCF7 et PC-3 co-transfectées avec mTQ2-hTopoI et YB-

1ΔC-sYFP2, mais des études plus approfondies seront nécessaires pour confirmer ces résultats préliminaires.

Özet

TURKISH

Bölüm I. YB-1/hNTH1 kompleksi

FRET sinyali, hNTH1-mTQ2 proteinini stabil olarak eksprese eden ve YB-1ΔC-sYFP2 ile geçici olarak transfekte edilmiş MCF7 hücrelerinde akseptör foto-ağartma tekniği kullanılarak tespit edilmiştir. Düşük ko-transfeksiyon etkinliğinin üstesinden gelmek ve hNTH1 ve YB-1'in etkileştiği koşulları araştırmak için, kısa amino asitlerle bağlanan sYFP2, YB-1ΔC, hNTH1 ve mTQ2 proteinlerini içeren tek bir polipeptit yapısı olan Biyosensör 1 oluşturuldu. Biyosensör 1'i nükleuslarında eksprese eden MCF7 hücreleri ile anlamlı bir FRET sinyali gözlemlenmemiştir.

In vitro FRET deneylerinde kullanılacak olan tüm rekombinant proteinler başarıyla saflaştırılmıştır. FRET sinyali, 50 mM NaCl içeren tampon içinde 5 μM protein konsantrasyonunda proteinlerin karıştırılmasıyla tespit edilebilmiştir. Biyosensör 1'in FRET etkinliği 50 mM'lik bir tuz konsantrasyonunda çok yüksektir (% 39) ve FRET kontrolü olan sYFP2-mTQ2 Füzyon proteinimizle (% 40) elde edilen değere yakındır. Oluşturduğumuz 7 farklı biyosensör yapısıyla artan tuz konsantrasyonlarında (50 mM NaCl-1 M NaCl) FRET ölçümleri gerçekleştirilmiş ve YB-1ΔC ile hNTH1 arasındaki etkileşimin yüksek tuz konsantrasyonlarına duyarlı olduğu görülmüştür. Tüm biyosensör yapıları, 6 M üre varlığında benzer minimal FRET verimliliği göstermiştir. FRET ölçümleri, hNTH1'in hidrolize edilemeyen substratı (12nt THF dsDNA oligo) varlığında gerçekleştirilmiş ve tuz konsantrasyonuna benzer bir etki gözlemlenmiştir. Oligonükleotid konsantrasyonu arttığında FRET verimliliği azalmaktadır. Aynı zamanda FRET ölçümleri farklı Biyosensör 1 protein konsantrasyonlarında (0.01 ila 2 μM arasında) 50 mM NaCl içeren tamponda gerçekleştirilmiştir. Biosensor 1'in FRET verimliliğinin, 0.2 μM'nin altındaki konsantrasyonlarında hızla düştüğünü gözlemlenmiştir.

Farklı biyosensör yapılarının karakterizasyonu ve tampon optimizasyon deneylerimiz, biyosensörümüzün hNTH1-YB-1 etkileşimini araştırmak ve aynı zamanda bu etkileşimin potansiyel inhibitörlerini taramak için uygun bir araç olduğunu açıkça göstermektedir. Kimyasal kütüphanelerindeki bileşiklerde kullanılan DMSO, Biyosensörün FRET seviyelerini önemli ölçüde etkilememiştir. Tarama testinin güvenilirliğini test etmek için, pozitif kontrolümüz olan 12nt THF küt uçlu çift iplikli DNA oligonükleotidin yokluğunda ve varlığında 30'ar örnek üzerinden bir Z' faktör testi gerçekleştirilmiştir. Laboratuvarımızda Clariostar microplaka okuyucu ve CMBA platformu üzerinde yapılan ölçümlerden elde edilen Z' faktör değerleri, sırasıyla 0.83 ve 0.90'dır. 1'e yakın olan bu değerler, Biyosensör 1'in YB-1ΔC/hNTH1 etkileşiminin potansiyel inhibitörlerini tespit etmek için güvenilir bir araç olduğunu göstermektedir. Life Chemicals Protein-protein Etkileşimleri (PPI) kimyasal kütüphanesinin ve Prestwick Chemical kimyasal kütüphanesinin CMBA platformunda yüksek verimli taramasını gerçekleştirmek için Biyosensör 1'i kullandık. İlk yüksek verimli tarama (HTS), 50 µl'lik son hacimde, üç tekrar şeklinde 0.2 µM Biyosensör 1 ve 50 µM bileşik konsantrasyonu ile gerçekleştirilmiştir. Bu ilk HTS'den sonra, azaltılmış FRET seviyeleri gösteren 30 seçilmiş bileşik, üç farklı konsantrasyonda (50, 10 ve 1 µM) tekrar test edilmiştir. Life Chemicals PPI kimyasal kütüphanesinden 50 µM konsantrasyonunda % 30-60 inhibisyon gösteren ve 1 µM konsantrasyonunda hala inhibitör etki gösteren üç bileşik bulunmuştur. Prestwick Chemical kimyasal kütüphanesinden 8 bileşik, FRET sinyalini konsantrasyona bağlı bir inhibe edebilen potansiyel inhibitörler olarak belirlenmiştir.

Life Chemicals PPI kimyasal kütüphane isabetleri içsel bir floresan göstermiştir. Prestwick Kütüphanesi'nden potansiyel isabetler, içsel bir floresan sinyali göstermeyenler arasından seçilmiştir. 7 Prestwick bileşiğinin Füzyon'un FRET sinyali üzerinde hiçbir etkisi bulunmamaktadır, ancak Life Chemicals bileşikleri FRET sinyalini % 6 ila 9 oranında düşürmüştür; bu, nispeten yüksek içsel floresansın FRET sürecine müdahale edebileceğini göstermiştir. Dolayısıyla, azaltılmış FRET verimliliği, hNTH1/YB-1 etkileşiminin inhibisyonundan değil, bileşiğin içsel floresansından kaynaklanabilir. Life Chemicals PPI kimyasal kütüphanesinden tanımlanan üç test bileşiği yanlış pozitif gibi görünmektedir. Elde ettiğimiz sonuçlar, CMBA platformundan elde edilen birkaç bileşiğin

kimyasal taramada kullanılmadan önce tekrarlanan donma-çözülme nedeniyle bozulabileceğini veya modifiye olabileceğini göstermektedir. Bu nedenle, hNTH1/YB-1ΔC etkileşimi üzerindeki inhibitör etkileri, bozulmalarının veya değiştirilmelerinin bir sonucu olabilir. AlphaScreen deneyleri bazı Prestwick bileşiklerinin inhibitör etkisini doğrulamıştır.

Bölüm II. YB-1/hTopoI kompleksi

C-terminal His-etiketli hTopoI'nin saflaştırılmasından iki protein formu hTopoI-FL ve hTopoI-70 elde edilmiştir. hTopoI-FL ve hTopoI-70'in relaksasyon aktiviteleri benzer çıkmıştır. Camptothecin, 5-10 μ M aralığında IC₅₀ değerleri ile hTopoI-FL ve hTopoI-70'in aktivitesi üzerinde benzer bir inhibitör etki göstermiştir. YB-1ΔC, hTopoI-FL ve hTopoI-70'in aktivitesini, büyük olasılıkla doğrudan etkileşim yoluyla benzer şekilde uyarmaktadır; bu da, hTopoI'nin N-terminal alanının YB-1ΔC ile etkileşim için tek bölge olmadığını düşündürmüştür.

Floresan proteinlerle füzyon hTopoI proteinleri, düşük verimle saflaştırılmıştır. FRET sinyali, 50 mM NaCl içeren tamponda sadece 1 μ M protein konsantrasyonunda floresan proteinlerle füzyon olan hTopoI ve YB-1ΔC proteinleri ile ölçülebilmektedir. En yüksek sinyal, hem mTQ2 hem de sYFP2'nin, hTopoI ve YB-1ΔC'nin C terminallerine füzyonundan elde edilmiştir. FRET verimliliği hTopoI-70-mTQ2 durumunda azalmış, ancak yine de negatif kontrol (mTQ2) ile karşılaştırıldığında anlamlı olarak daha yüksek çıkmıştır. Bu N-terminal bölgesinin önemli olduğunu, ancak hTopoI-70'in de YB-1 ile uyarılabildiğini gösteren relaksasyon aktivite ölçümleri ile uyumlu olarak etkileşim için zorunlu olmadığını göstermiştir. Artan tuz konsantrasyonlarının, etkileşimi etkileyerek düşük FRET verimliliğine yol açtığı gözlemlenmiştir.

YB-1 ve hTopoI arasındaki etkileşim, birçok hücre hattında (HeLa, MCF7 ve PC-3) araştırılmıştır. mTQ2-hTopoI ve YB-1ΔC-sYFP2 ile birlikte transfekte edilmiş MCF7 ve PC-3 hücreleri ile bir miktar FRET sinyali saptanmıştır ancak bu ön sonuçları doğrulamak için daha ileri çalışmalara ihtiyaç duyulmaktadır.

Part I. YB-1/hNTH1 complex

Before my arrival in Grenoble, Dr. J. Timmins' team had shown that hNTH1 and YB-1 interact *in vitro* (AlphaScreen assay) as described in the "Introduction". Moreover, using *in vitro* DNA repair activity measurements using purified hNTH1 and YB-1, YB-1 had been shown to specifically stimulate the lyase activity of hNTH1, but not the glycosylase activity. The objectives of my work were to further investigate the YB-1/hNTH1 complex formation *in vivo* and to design and optimise a FRET-based biosensor to detect the interaction of hNTH1 with YB-1, which could be used for high-throughput chemical library screening for potential inhibitors of the YB-1/hNTH1 complex in order to use for sensitizing cisplatin-resistant mammalian cells.

3.1. YB-1/hNTH1 interaction in mammalian cells

YB-1 and hNTH1 had previously been shown to interact in MCF7 breast cancer cells (Guay et al., 2008). We thus set out to further study this interaction in cells using the FRET method. First, we prepared mammalian expression vectors, encoding for either hNTH1 fused to the cyan fluorescent protein, mTurquoise2 (mTQ2) (Goedhart et al., 2012) or YB-1 fused to the yellow fluorescent protein, sYFP2 (Kremers et al., 2006). mTQ2 and sYFP2 are high brilliance, FRET-compatible fluorescent proteins (Kremers et al., 2006) (see Annex for list of constructs). Two constructs of YB-1 were prepared: one of them corresponding to the intact protein, and the other one corresponding to the nuclear form of YB-1 that is missing the C-terminal region (YB-1 Δ C). We checked the expression and cellular localisation of these constructs after transfection into the breast cancer cell line, MCF7 (Figure 3.1). As expected, hNTH1 and the truncated YB-1 (YB-1 Δ C) were found to localise to the nucleus, while the full-length YB-1 mostly localised to the cytoplasm (Figure 3.1). For subsequent experiments, we thus used only the nuclear form of YB-1, which is more relevant for the study of its interaction with hNTH1.

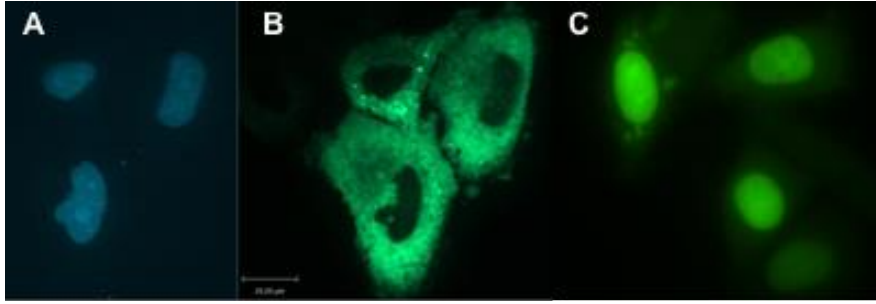


Figure 3.1. MCF7 cells transfected with hNTH1-mTQ2 (A), YB-1-sYFP2 (B) and YB-1ΔC-sYFP2 (C).

For *in vivo* FRET assays, MCF7 cells were transfected with both hNTH1 fused to mTQ2 and YB-1ΔC fused to sYFP2. However, the co-transfection efficiency was very low (<1 %) and it was difficult to find cells expressing both constructs. To overcome this problem, we developed two strategies in parallel, which are described below. First, we established a stable MCF7 cell line, which expressed hNTH1-mTQ2 and could be used for transfection with YB-1ΔC fused to sYFP2. Second, we designed a Biosensor construct encoding sYFP2, YB-1ΔC, hNTH1 and mTQ2 proteins in a single polypeptide chain connected by short amino acid linkers.

3.1.1. FRET measurements in hNTH1-mTQ2 expressing MCF7 cells

We created a stable MCF7 cell line, which ubiquitously expresses hNTH1-mTQ2. To perform *in vivo* FRET assays, we transiently transfected this stable cell line with either sYFP2 alone, sYFP2-YB-1ΔC or YB-1ΔC-sYFP2. Cells were fixed one day after transfection and the FRET signal was detected by performing gradual acceptor photobleaching using a FRAPPA device (Van Munster et al., 2005). In this procedure, the acceptor (sYFP2) is bleached, causing the donor (mTQ2) signal to increase in case of FRET. The increase in mTQ2 intensity upon acceptor (sYFP2) photobleaching is visible by eye in these cells (Figure 3.2). Expression levels of YB-1ΔC constructs were variable. We only detected clear FRET signal in MCF7 cells, which overexpressed the YB-1ΔC protein. The FRET efficiencies measured on MCF7 cells stably transfected with hNTH1-mTQ2 and transiently expressing sYFP2 alone, sYFP2-YB-1ΔC or YB-1ΔC-sYFP2 were 1.3 %, 15.4 % and 22.0 % respectively (Figure 3.2 D). The strongest FRET signal was

obtained from stably transfected MCF7 cells transiently expressing YB-1ΔC-sYFP2 in which both mTQ2 and sYFP2 were fused to the C-termini of hNTH1 and YB-1ΔC, respectively. In this configuration, the FRET efficiency was significantly higher than that of the negative control (transiently transfected with sYFP2-NLS, a nuclear form of sYFP2), and clearly indicated that hNTH1 and YB-1ΔC interact in the nuclei of MCF7 cells.

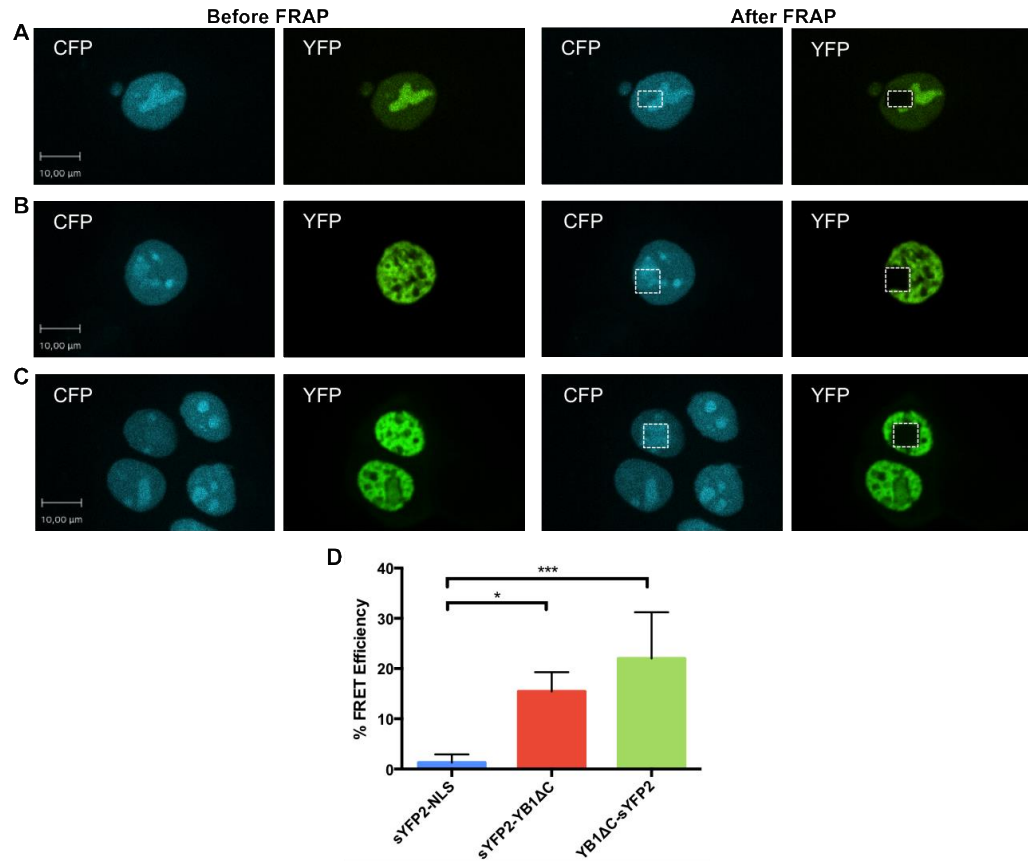


Figure 3.2. hNTH1-YB-1 FRET measurements in transfected MCF7 cells. MCF7 stable cell line-expressing hNTH1-mTQ2 and transfected with sYFP2 alone (A), sYFP2-YB-1ΔC (B) and YB-1ΔC-sYFP2 (C). mTQ2 is seen in the CFP channel (blue). sYFP2 is seen in the YFP channel (green). The white rectangle indicates the area of the nucleus that was photobleached. Scale bar: 10 μm. (D) FRET efficiencies in the MCF7 stable cell line expressing hNTH1-mTQ2 and transfected with sYFP2-NLS, sYFP2-YB-1ΔC and YB-1ΔC-sYFP2. The presented data are the mean of at least three replicates.

3.1.2. Design of Biosensor construct

In order to overcome the low co-transfection efficiency and to investigate the conditions under which hNTH1 and YB-1 interact, we created a single polypeptide construct, which contains sYFP2, YB-1 Δ C, hNTH1 and mTQ2 proteins connected by short amino acid linkers (Figure 3.3).

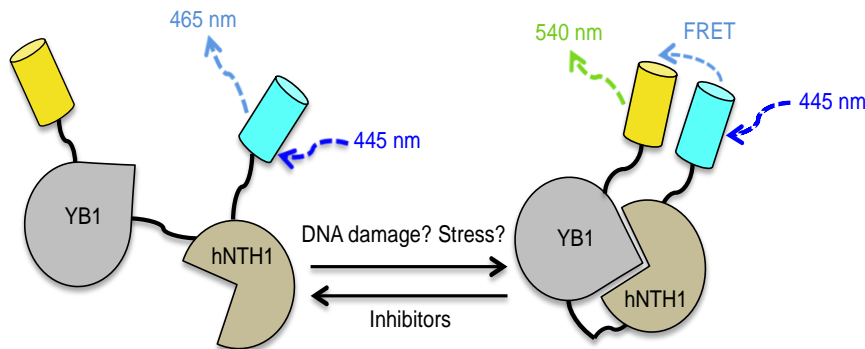


Figure 3.3. Biosensor design. The yellow and blue cylinders represent sYFP2 and mTQ2 proteins, respectively. Upon interaction of hNTH1 with YB-1, mTQ2 and sYFP2 come close together and FRET signal can be measured.

The Biosensor 1 construct was cloned into a mammalian expression vector and transfected into MCF7 cells. Only a subset of cells showed nuclear expression of the Biosensor (*i.e.* both mTQ2 and sYFP2 were expressed in the nucleus). A majority of cells showed cytoplasmic expression of the biosensor and some cells also showed differential expression of mTQ2 and sYFP2 in different cell compartments, suggesting the Biosensor 1 had been cleaved *in vivo*. We nonetheless performed acceptor photobleaching experiments on selected MCF7 cells expressing nuclear Biosensor 1 and the FRET efficiency was found as ~7% in these cells (Figure 3.4). This relatively low FRET efficiency compared to that obtained with our stably transfected MCF7 cell line (Figure 3.2) could be due to the orientation of the proteins in the Biosensor 1 construct. Our *in vivo* FRET experiments using the individual constructs indicated that FRET was more efficient when both fluorescent proteins were fused to the C-termini of hNTH1 and YB-1. Also, little is known concerning the stoichiometry of the hNTH1/YB-1 complex; a one to one hNTH1:YB-1 Δ C ratio as is the case in the Biosensor may

not be enough for efficient complex assembly. To verify this, we thus decided to further characterise the Biosensor 1 *in vitro*.

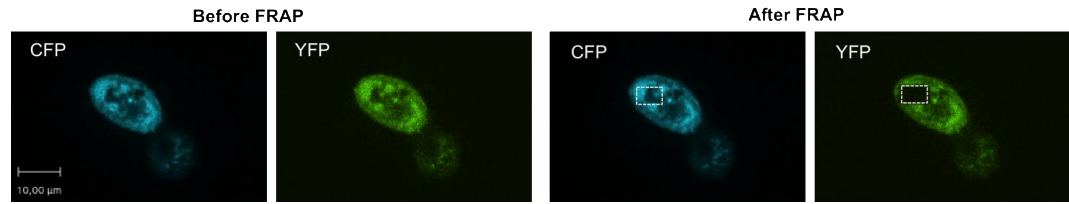


Figure 3.4. Example of a hNTH1-YB-1 FRET measurement in MCF7 cells transfected with Biosensor 1. mTQ2 is seen in the CFP channel (blue). sYFP2 is seen in the YFP channel (green). The white rectangle indicates the area of the nucleus that was photobleached. Scale bar: 10μm.

3.2. YB-1ΔC/hNTH1 interaction *in vitro*

3.2.1. Purification of fluorescent protein fusion constructs

3.2.1.1. Fluorescent proteins

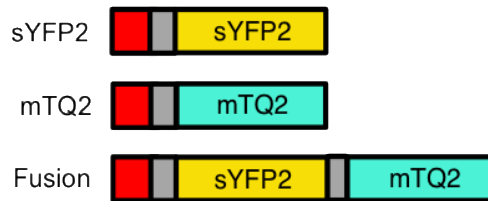


Figure 3.5. Illustration of fluorescent proteins used in our work. Red: N-terminal, cleavable His-tag. Grey: short linker sequences.

sYFP2, mTQ2, and Fusion (sYFP2-mTQ2) constructs (Figure 3.5) were successfully expressed in *E. coli* BL21 cells with cleavable N-terminal His-tags and were purified with Ni-IDA sepharose column followed by gel filtration (Figure 3.6).

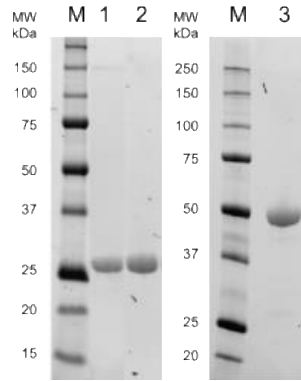


Figure 3.6. Example of Stain-Free gel image of fluorescent proteins. M: Biorad SDS-PAGE broad range protein marker, 1-3: sYFP2 (28 kDa), mTQ2 (28 kDa), Fusion (57 kDa), respectively.

3.2.1.2. YB-1ΔC fusion constructs

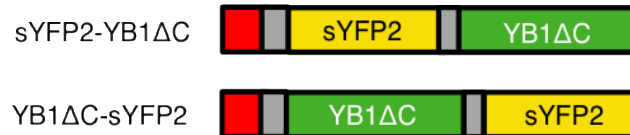


Figure 3.7. Illustration of YB-1ΔC constructs fused to sYFP2 used in our work. Red: N-terminal, cleavable His-tag. Grey: short linker sequences.

sYFP2-YB-1ΔC and YB-1ΔC-sYFP2 constructs (Figure 3.7) were cloned into pProEX-HTb for expression in *E. coli* BL21 cells with cleavable N-terminal His-tags and were purified using three chromatographic steps: a nickel affinity column, a heparin column and a size-exclusion chromatography. Although the proteins were relatively free of other protein contaminants after the Nickel column, they were highly contaminated with nucleic acids. We thus used a heparin column and a first size-exclusion chromatography in high salt (1 M NaCl) to remove this nucleic acid contamination (Figure 3.8). In the end, we recovered between 1.5 and 2.5 mg/L of pure sYFP2-YB-1ΔC and YB-1ΔC-sYFP2 proteins, which was sufficient for further experiments.

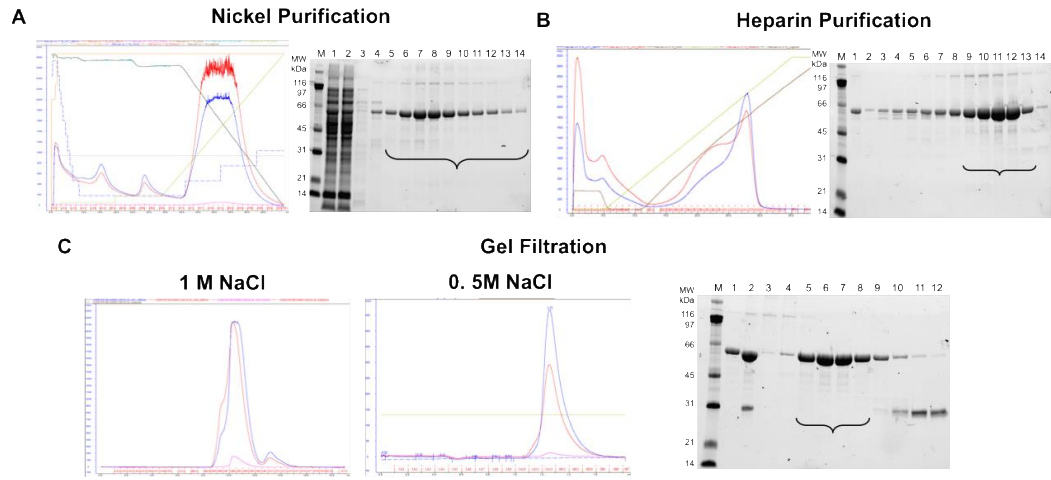


Figure 3.8. Illustration of the different chromatographic steps used to purify YB-1ΔC fusion constructs (53 kDa). Curly brackets indicate the pooled fractions. **(A)** Chromatogram and Stain-Free gel of nickel purification; **(B)** Chromatogram and Stain-Free gel of heparin purification; **(C)** Chromatograms and Stain-Free gel of gel filtration at 1 M NaCl and 0.5 M NaCl.

3.2.1.3. hNTH1 fusion constructs

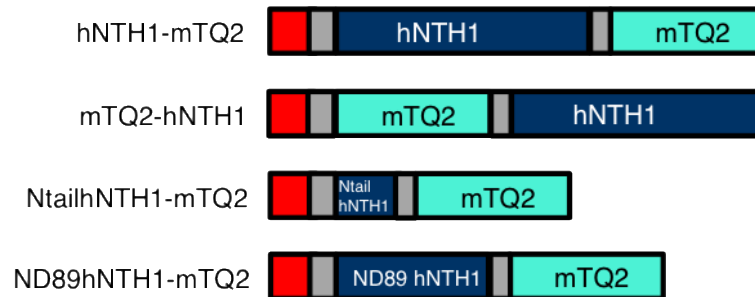


Figure 3.9. Illustration of hNTH1 constructs fused to mTQ2 used in our work. Red: N-terminal, cleavable His-tag. Grey: short linker sequences.

All hNTH1 fusion constructs (Figure 3.9) were cloned into pProEX-HTb for expression in *E. coli* BL21 cells with cleavable N-terminal His-tags and were purified using three chromatographic steps. All constructs produced similar chromatographic profiles on His-Trap columns (Figure 3.10). Since hNTH1 possesses a [4Fe-4S] cluster and absorbs at 410 nm, we used this wavelength for tracking our protein (Ikeda et al., 1998).

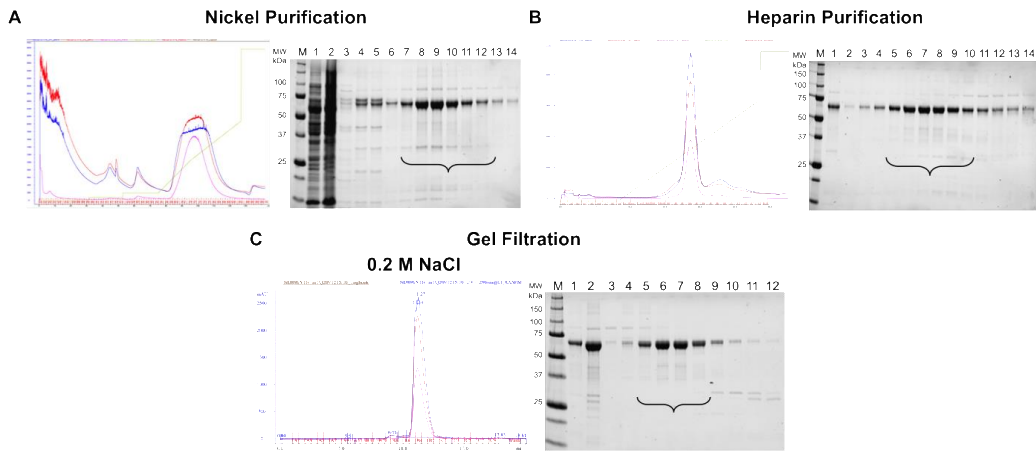


Figure 3.10. Illustration of the different chromatographic steps used to purify hNTH1 fusion constructs. Curly brackets indicate the pooled fractions. **(A)** Chromatogram and Stain-Free gel of nickel purification; **(B)** Chromatogram and Stain-Free gel of heparin purification; **(C)** Chromatogram and Stain-Free gel of gel filtration.

For hNTH1-mTQ2 and ND89hNTH1-mTQ2, we performed a heparin affinity chromatography step to remove contaminating DNA. NtailhNTH1 construct was not contaminated with DNA therefore we exchanged the Heparin affinity purification step with an ion-exchange chromatography to eliminate other contaminants (Figure 3.11). As a last purification step, all hNTH1 constructs were loaded on a Superdex 75 size exclusion column equilibrated in a buffer containing 200 mM NaCl (Figure 3.10). In the end, we recovered pure hNTH1 fusion constructs at a sufficient concentration for further experiments (Table 3.1).

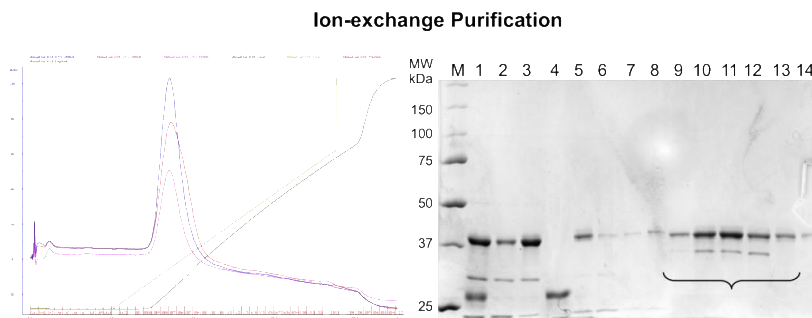


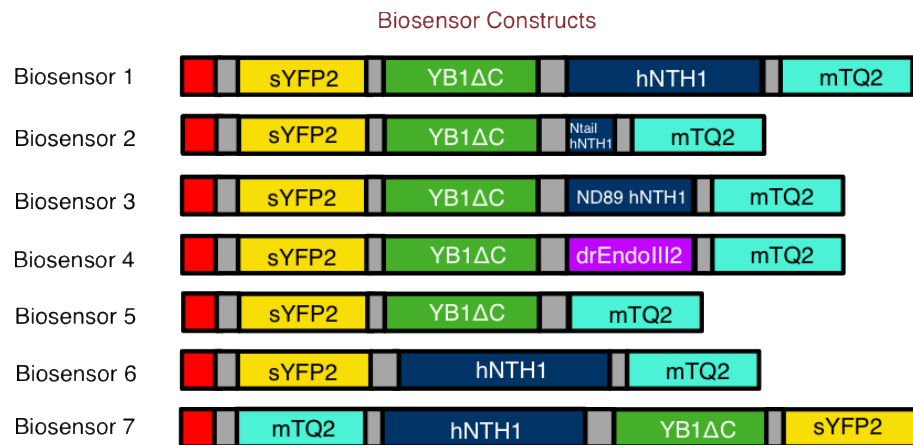
Figure 3.11. NtailhNTH1-mTQ2 ion-exchange chromatography. Chromatogram of HiTrapQ FF column with 50mM NaCl and 10% Stain-Free gel analysis of fractions. Curly bracket shows the pooled fractions.

Table 3.1. Properties of purified hNTH1 fusion proteins.

Name of proteins	Size (kDa)	Purification Yield/L culture (mg)	Concentration (mg/ml)
hNTH1-mTQ2	63	1	0.9
mTQ2-hNTH1	63	3.5	7
NtailhNTH1-mTQ2	38.5	0.5	2
ND89hNTH1-mTQ2	54	1.4	4.2

3.2.1.4. Biosensor constructs

Figure 3.12 illustrates all the Biosensor constructs that we prepared and used for *in vitro* FRET measurements. As for the individual constructs, the Biosensor constructs were cloned into pProEX-HTb vector for expression in *E. coli* BL21 cells with a cleavable N-terminal His-Tag. Cloning of these constructs was facilitated by introducing a *NdeI* restriction site within the central linker sequence between YB-1ΔC and hNTH1.

**Figure 3.12.** Illustration of the Biosensor constructs used in our work. Red: N-terminal, cleavable His-tag. Grey: short linker sequences.

The Biosensor constructs were overproduced with a His-tag allowing us to purify them by a nickel affinity column. All of the biosensors showed similar chromatographic profiles. Despite previous treatments eluted Biosensors from

nickel affinity column were heavily contaminated with nucleic acids. We performed a heparin affinity purification and a gel filtration with 1 M NaCl containing GF buffer to eliminate nucleic acid contamination. In order to reduce the salt concentration in the final sample for further analysis, we used a second gel filtration column equilibrated in a GF Buffer containing 500 mM NaCl (Figure 3.13). In the end, we recovered pure Biosensor proteins (Figure 3.14) at a sufficient concentration for further experiments (Table 3.2).

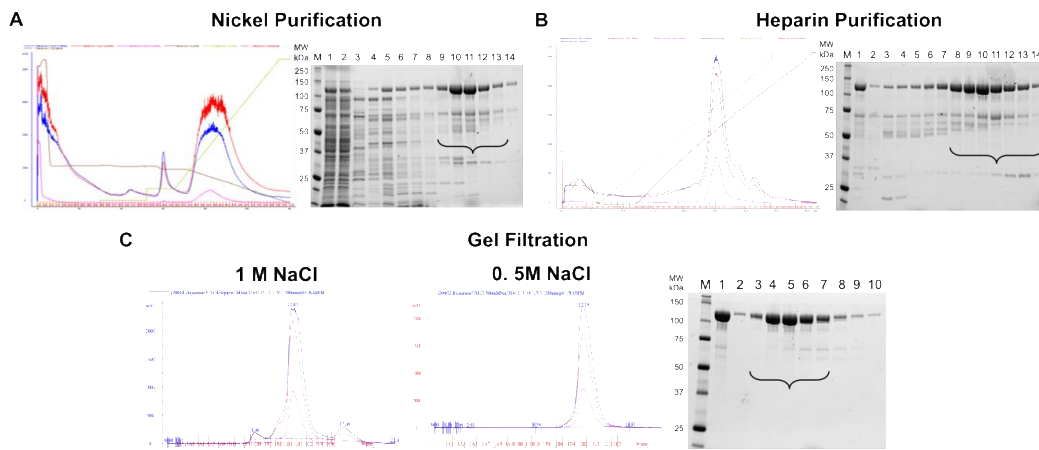


Figure 3.13. Representative gels and chromatograms of Biosensor 1 (116 kDa) purification. Curly brackets indicate the pooled fractions. **(A)** Chromatogram and Stain-Free gel of nickel purification; **(B)** Chromatogram and Stain-Free gel of heparin purification; **(C)** Chromatograms at 1 M NaCl and 0.5 M NaCl and Stain-Free gel of gel filtration.

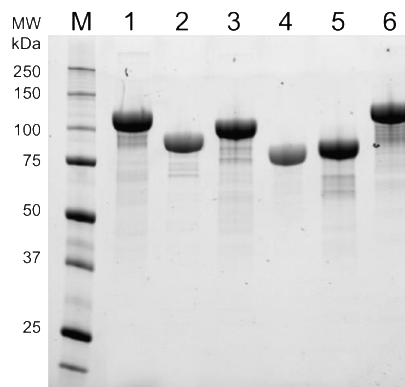


Figure 3.14. Stain-free gel analysis of purified Biosensor constructs. M: Biorad Precision Plus unstained protein marker, 1-6: Biosensor 1 (116 kDa), Biosensor 2 (91 kDa), Biosensor 3 (106 kDa), Biosensor 5 (80 kDa), Biosensor 6 (91 kDa), Biosensor 7 (116 kDa), respectively.

Table 3.2. Properties of purified Biosensor proteins.

Name of proteins	Size (kDa)	Purification Yield/L culture (mg)	Concentration (mg/ml)
Biosensor 1	116	2	2.6
Biosensor 2	91	1	1.9
Biosensor 3	106	0.9	1.5
Biosensor 4	105	0.15	5
Biosensor 5	80	1.4	3
Biosensor 6	91	4.5	3
Biosensor 7	116	1.5	5.5

3.2.2. FRET measurements

3.2.2.1. Mixture of individual proteins

We used the fluorescent proteins alone (sYFP2 and mTQ2) as negative controls and the sYFP2-mTQ2 Fusion as a positive control (Figure 3.15) throughout our FRET measurements. These measurements were also used for our calculations of the FRET efficiency (see Chapter 2 Materials & Methods).

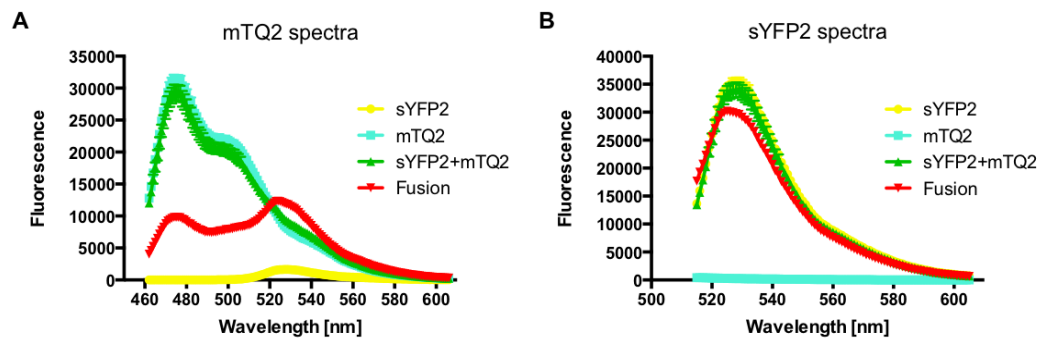


Figure 3.15. mTQ2 and sYFP2 spectra of the sYFP2 and mTQ2 alone and mixed in a 1:1 ratio, and sYFP2-mTQ2 fusion construct at 1.5 μ M in 200mM NaCl GF buffer. (A) Emission spectra obtained after exciting mTQ2 at 435nm. (B) Emission spectra obtained after exciting sYFP2 at 485nm.

We did not observe any FRET signal when mixing the individual fluorescent proteins sYFP2 and mTQ2 (FRET efficiency $\sim 0\%$), but the fluorescent protein Fusion construct had a significant FRET signal (FRET efficiency $\sim 40\%$). When measuring FRET after mixing individual hNTH1 and YB-1 Δ C proteins fused to mTQ2 and sYFP2, respectively no significant FRET signal was detected using a protein concentration of $1.5\ \mu\text{M}$ and buffer containing $200\ \text{mM}$ NaCl. Since high salt concentrations are known to interfere with ionic interactions, we tried to decrease the salt concentration, and also tried to increase the protein concentration to make sure that we were above the estimated K_d value ($\sim 0.5\ \mu\text{M}$) determined previously in the laboratory. Finally, FRET signal could be detected when mixing individual proteins at $5\ \mu\text{M}$ protein concentration in $50\ \text{mM}$ NaCl buffer (Figure 3.16 A).

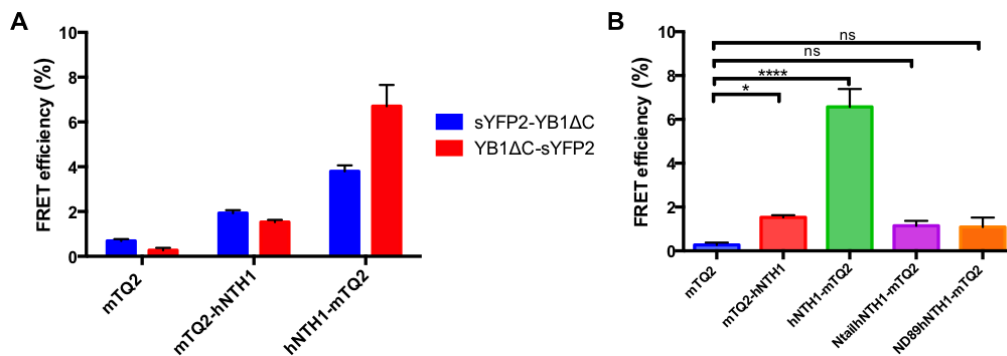


Figure 3.16. FRET efficiencies of individual protein mixes of hNTH1 and YB-1 Δ C constructs. **(A)** FRET efficiencies of protein mixtures containing mTQ2 alone, mTQ2-hNTH1 or hNTH1-mTQ2 mixed with sYFP2-YB-1 Δ C or YB-1 Δ C-sYFP2 at $5\ \mu\text{M}$ final concentration in $50\ \text{mM}$ NaCl GF buffer. The highest FRET signal was obtained with the fluorescent proteins fused to the C-termini of hNTH1 and YB-1 Δ C. **(B)** FRET efficiencies of YB-1 Δ C-sYFP2 mixed with various constructs of hNTH1 fused to mTQ2 at $5\ \mu\text{M}$ in $50\ \text{mM}$ NaCl GF buffer. The highest FRET efficiency was obtained with full-length hNTH1 fused to the N-terminus of mTQ2.

As in our *in vivo* FRET measurements (Figure 3.3), the highest signal was obtained when both mTQ2 and sYFP2 were fused to the C-termini of hNTH1 and YB-1 Δ C, respectively. We also evaluated other constructs of hNTH1 (Ntail and ND89) with YB-1 Δ C-sYFP2, but these truncated forms of hNTH1 did not show any significant FRET signal (Figure 3.16 B).

3.2.2.2. Biosensors

We then set out to determine the optimal buffer conditions for FRET with our Biosensor 1 construct. We changed the NaCl concentration (500 mM NaCl, 250 mM NaCl, 100 mM NaCl, and 50 mM NaCl) and evaluated its effect on the FRET signal (Figure 3.17 A). When we decreased the salt, we observed an increase in the FRET signal, illustrated by the increase in emission at 525 nm (corresponding to the sYFP2 peak) as a result of energy transfer from the donor to the acceptor. The interaction between YB-1 Δ C and hNTH1 thus appears to be highly salt-sensitive. At a salt concentration of 50 mM, however, the FRET efficiency is very high (39 %) and comparable to that obtained with our Fusion construct (~40 %) (Figure 3.17 B).

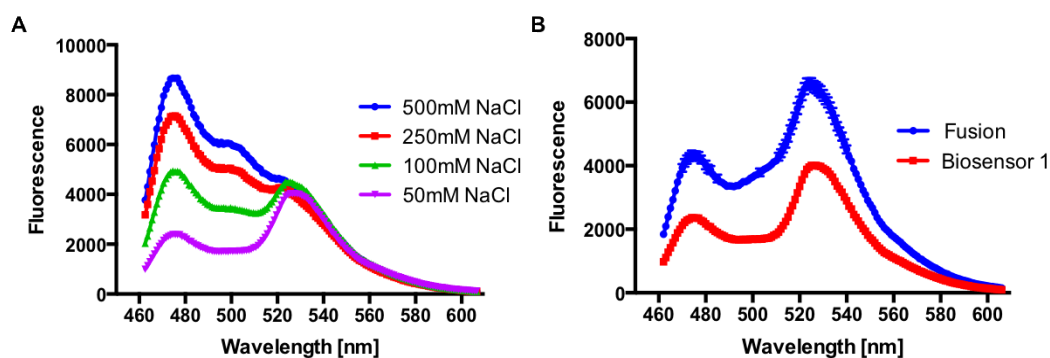


Figure 3.17. FRET measurements of Biosensor 1 and its comparison with Fusion construct. **(A)** mTQ2 spectra of 1 μ M Biosensor 1 at different NaCl (50, 100, 250, and 500 mM) concentrations. The highest FRET signal of Biosensor 1 was obtained in buffer containing 50 mM NaCl **(B)** mTQ2 spectra of 1 μ M Fusion and Biosensor 1 in buffer containing 50 mM NaCl. Fusion and Biosensor 1 showed similar FRET efficiencies in buffer containing 50 mM NaCl.

Then we carried out FRET measurements on all 7 Biosensor constructs at different concentrations of salt (50 mM NaCl-1 M NaCl) in order to observe the difference between the constructs (Figure 3.18 A). Since the biosensor is a single polypeptide chain, all constructs show a basal FRET signal of ~10 %. The relative change in FRET efficiency (Δ FRET efficiency) when going from 500 mM NaCl to 50 mM NaCl is thus a better measure of the interaction than the absolute FRET measurement (Figure 3.18 B).

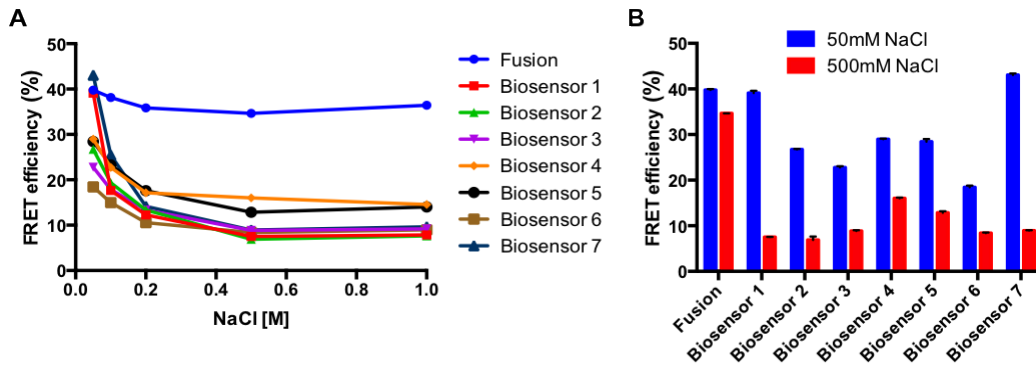


Figure 3.18. FRET measurements of all Biosensors and Fusion construct at different NaCl concentrations. **(A)** FRET efficiencies of Biosensor constructs at different NaCl concentrations (50 mM NaCl - 1 M NaCl). All Biosensor constructs had a basal FRET signal. Biosensors 1 and 7 showed a considerable change between salt concentrations of 50 mM and 500 mM. **(B)** Comparison of the FRET efficiencies of Biosensor constructs at 50 mM and 500 mM NaCl concentrations.

There was a small effect of salt on our positive control (Fusion of sYFP2-mTQ2). We observed a slight decrease (5 %), which could be due to changes in the chromophore conformation or non-specific interactions between fluorescent proteins. Salt concentration considerably affects the FRET efficiencies of the Biosensor 1 and 7, suggesting that it specifically interferes with the interaction between hNTH1 and YB-1.

Compared to Biosensors 1 and 7, the other Biosensor constructs (Biosensors 2-6) showed either reduced FRET signals at low salt and/or increased FRET signals at high salt concentration, resulting in overall reduced Δ FRET efficiencies. This indicates that the interaction between YB-1 and hNTH1 is largely lost when truncated forms of hNTH1 or the bacterial homologue of hNTH1 (*Deinococcus radiodurans* EndoIII2 protein) are used. These findings are in agreement with our FRET measurements performed on the individual constructs (Fig. 3.16). Biosensors 5 and 6, which are missing one of the two protein partners (hNTH1 in Biosensor 5 and YB-1 Δ C in Biosensor 6), also displayed significantly reduced Δ FRET efficiency. A high Δ FRET efficiency is thus a strong indication that hNTH1 and YB-1 interact within the biosensor constructs.

To determine the minimal FRET level for each Biosensor construct, we performed our FRET measurements in the presence of 6 M urea that efficiently denatures hNTH1 and YB-1, but not the fluorescent proteins (Figure 3.19) as judged by their unaffected fluorescent intensity. All Biosensor constructs showed similar minimal FRET efficiencies. Interestingly, we noticed that the FRET efficiency of the Fusion is also reduced in comparison with the 40 % FRET efficiency in 50 mM NaCl, even though the fluorescence intensity measurements were unchanged.

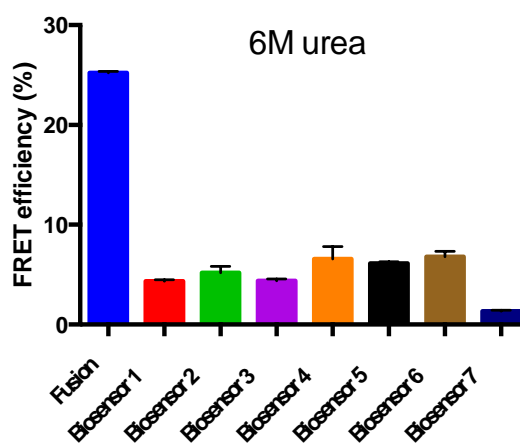


Figure 3.19. FRET efficiencies of Fusion and Biosensor constructs at 1 μ M concentration in 50 mM NaCl in the presence of 6 M urea. All Biosensor constructs showed similar minimal FRET efficiencies.

Previous experiments in our laboratory showed that hNTH1 binds with high affinity ($K_d \sim 2$ nM) a 12 mer double-stranded oligonucleotide containing a tetrahydrofuran (THF) synthetic AP site paired with guanine (G) (Figure 3.20 A). We thus performed FRET measurements in the presence of this uncleavable substrate of hNTH1 (Figure 3.20 B). We observed a similar effect as with NaCl. When the concentration of oligonucleotide increased, the FRET efficiency decreased (Figure 3.20 C). But unlike NaCl concentration, there was no effect on the Fusion. This suggests that the FRET signal results from a specific interaction between hNTH1 and YB-1 that has been disrupted by binding of hNTH1 to its DNA substrate.

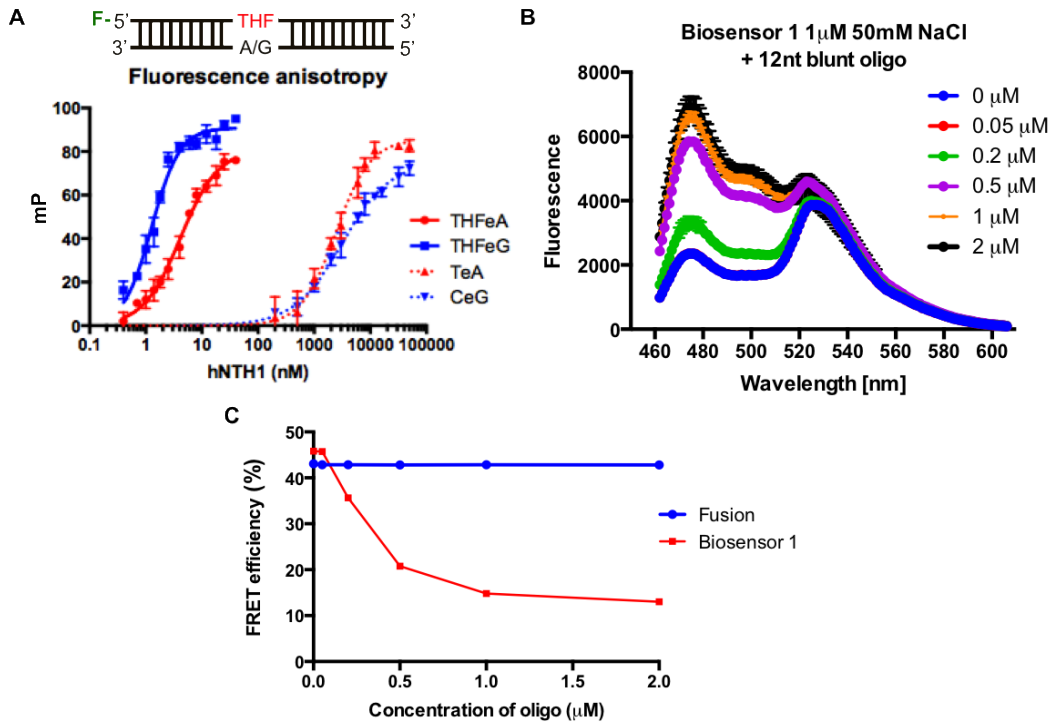


Figure 3.20. FRET measurements in order to find a potential competitor of YB-1/hNTH1 interaction for Biosensor 1 construct. **(A)** hNTH1 affinity to different oligonucleotides containing a stable THF abasic site paired with either guanine (G) or adenine (A). hNTH1 showed a higher affinity to the oligonucleotide containing a stable THF abasic site paired with guanine **(B)** mTQ2 spectra of 1 μ M Biosensor 1 in 50 mM NaCl in the presence of increasing concentrations of 12nt THF blunt dsDNA oligonucleotide. Increasing concentrations of 12nt THF blunt dsDNA oligonucleotide decreased the FRET signal of Biosensor 1. **(C)** FRET efficiencies of Fusion and Biosensor 1 at 1 μ M concentration in 50mM NaCl as a function of 12nt THF blunt dsDNA oligonucleotide concentration (0-2 μ M). 12nt THF blunt dsDNA oligonucleotide did not decrease the FRET signal of Fusion construct.

We also performed the FRET measurements in 50 mM NaCl at different Biosensor 1 protein concentrations (ranging from 0.01 to 2 μ M) to check whether this had any influence on the FRET efficiency (Figure 3.21). We observed that the FRET efficiency of the Biosensor 1 rapidly dropped when lowering the concentration below 0.2 μ M. This was not the case with the Fusion protein, which exhibited a constant FRET efficiency irrespective of its concentration, as expected for intramolecular FRET.

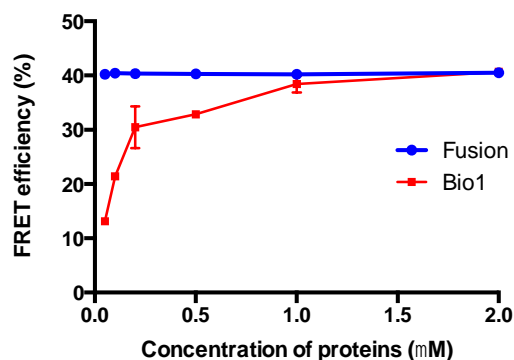


Figure 3.21. FRET measurements of Fusion and Biosensor constructs at different protein concentrations in buffer containing 50mM NaCl. The FRET signal of Fusion did not change according to protein concentrations. However, the FRET signal of Biosensor 1 decreased below 0.2 μ M protein concentration.

3.3. High-throughput chemical library screening with Biosensor 1

Protein-protein interactions (PPI) are important in most cellular processes and, as such, are the focus of many probe- and drug-discovery programs (Roche and Morelli, 2010). However, it has been difficult to identify small molecule or peptide inhibitors of PPI that bind stoichiometrically to a single site on the protein surface. In the absence of high-resolution structures of targeted proteins, *in silico* drug design and approaches based on molecular docking to find protein-protein interaction inhibitors (2P2I) are not suitable. In such cases, FRET can be a useful method high-throughput screening for protein-protein interaction inhibitors (Song et al., 2011; Rogers et al., 2012; Schaap et al., 2013).

The characterisation of the different Biosensor constructs and our buffer optimisation experiments clearly indicated that our Biosensor was a suitable tool for probing the hNTH1-YB-1 interaction and also for screening potential inhibitors of this interaction. We chose Biosensor 1 construct for the subsequent screening experiments because this construct was more stable and robust compared to Biosensor 7 and could be produced at high yields. The robotic chemical screening assay was performed in collaboration with Caroline BARETTE from the Center for the screening for BioActive Molecules (CMBA) platform, located at the Biosciences and Biotechnology Institute of Grenoble (BIG).

We checked the quality and reliability of our FRET-based assay before starting the chemical library screening.

3.3.1. Optimization of Biosensor 1

Compounds in chemical libraries are typically dissolved in DMSO (Dimethyl sulfoxide). We thus evaluated the FRET levels of the Biosensor in the presence of a range of DMSO concentrations to ensure that it didn't significantly affect our assay (Figure 3.22). We observed only a slight decrease (~ 5 %) in the FRET efficiency at the highest DMSO concentrations indicating that low concentrations of DMSO were compatible with our assay.

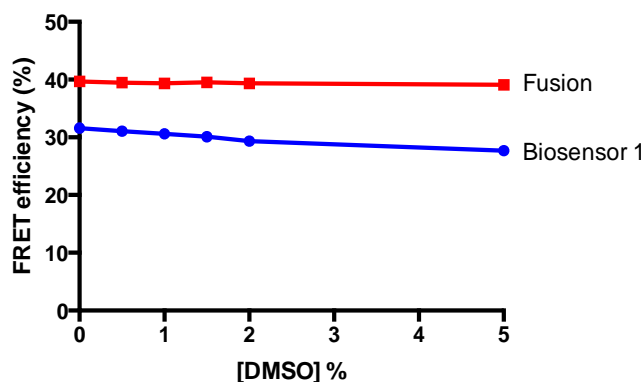


Figure 3.22. Stability of FRET signal of 0.2 μ M Fusion and Biosensor 1 construct in presence of increasing amounts of DMSO (0.5, 1, 1.5, 2, and 5 %). A slight decrease (~5 %) in the FRET efficiency of Biosensor 1 was observed at 5 % DMSO concentration.

Before performing high-throughput chemical library screening, several quality control analyses had to be done to assess the reliability of our assay. First, based on our experiments presented in Figure 3.21, we decreased the Biosensor 1 concentration to 0.2 μ M in order to screen more chemicals with a minimal amount of protein. At this concentration, the FRET efficiency of Biosensor 1 was close to 30 %. Then we performed a dose response assay (Figure 3.23) with the 12nt THF blunt dsDNA oligonucleotide, which we planned to use as a positive control for inhibition in our screening experiments. We found the IC_{50} value of the 12nt THF dsDNA oligonucleotide to be 0.13 μ M. We thus chose to fix the concentration of the oligo at 0.5 μ M which produces the minimal FRET level (~ 10 %).

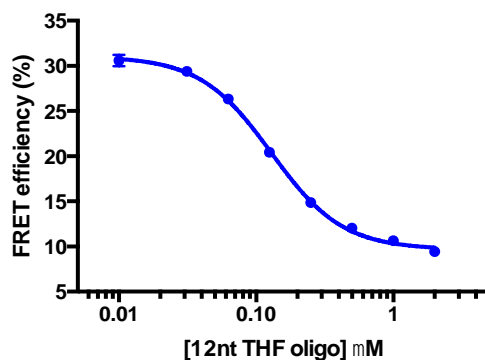


Figure 3.23. Inhibition of Biosensor 1 FRET by addition of hNTH1 DNA substrate. Dose response of 12nt THF blunt dsDNA oligonucleotide (at 0.01, 0.03, 0.06, 0.13, 0.25, 0.5, 1, and 2 μ M) on 0.2 μ M Biosensor 1 in buffer containing 50mM NaCl. The data points corresponding to the means of triplicate measurements were fitted to a standard sigmoidal inhibition model in GraphPad Prism.

Finally, we checked the stability of the Biosensor 1 and the FRET signal over a 2-hour period (Figure 3.24). We compared the stability of the Biosensor in its optimal buffer, in the presence of DMSO (0.5 % and 1.3 %) and in the presence of 0.5 μ M 12nt THF blunt dsDNA oligonucleotide. The FRET signal of Biosensor 1 was relatively stable at 0.2 μ M in 50 mM NaCl. A slight decrease in the signal is observed, but a significant and reproducible difference in FRET efficiency for Biosensor 1 was detected in the absence and presence of 0.5 μ M 12nt THF blunt dsDNA oligonucleotide. Again addition of DMSO did not significantly affect the FRET signal.

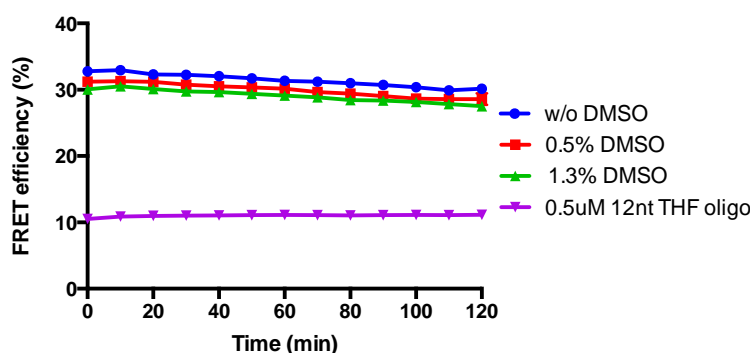


Figure 3.24. Stability of FRET signal of Biosensor 1 construct during 2 hours. The FRET efficiency of Biosensor 1 was monitored over a 2 hour period in 50 mM GF buffer (blue), supplemented with either 0.5 % DMSO (red), 1.3 % DMSO (green) or 0.5 μ M 12nt THF oligo (purple).

Our maximum (Max) FRET values detected for 0.2 μM Biosensor 1 in GF buffer containing 50 mM NaCl were found to be $\sim 30\%$ on the Clariostar fluorescence plate reader and $\sim 40\%$ on the TECAN microplate reader present on the CMBA screening platform. Our minimum (Min) FRET values obtained with 0.2 μM Biosensor 1 in GF buffer containing 50 mM NaCl in the presence of 0.5 μM 12nt THF oligonucleotide were found to be $\sim 10\%$ on the Clariostar and $\sim 18\%$ on the TECAN microplate reader. On both plate readers, the ΔFRET efficiency (Max – Min) was thus very similar and close to 20% .

To test the robustness of our screening assay, we performed a Z' factor test on 30 samples in the absence and presence of 12nt THF blunt dsDNA oligonucleotide. The Z' factor is a statistical parameter to determine the suitability of an assay for high-throughput screening (Zhang et al., 1999). The equation we used for the determination of the Z' factor and the categorization of our screening assay is given in Figure 3.25.

$$Z' = 1 - \frac{(3\sigma_{c+} + 3\sigma_{c-})}{|\mu_{c+} - \mu_{c-}|}$$

σ : standard deviation, μ : mean, c+ : positive control, c- : negative control

<i>Z'-factor value</i>	<i>Structure of assay</i>	<i>Related to screening</i>
1	SD = 0 (no variation), or the dynamic range $\rightarrow \infty$	An ideal assay
$1 > Z \geq 0.5$	Separation band is large	An excellent assay
$0.5 > Z > 0$	Separation band is small	A double assay
0	No separation band, the sample signal variation and control signal variation bands touch	A "yes/no" type assay
<0	No separation band, the sample signal variation and control signal variation bands overlap	Screening essentially impossible

Figure 3.25. Equation of Z' factor and categorization of screening assay by the value of the Z' factor (Zhang et al., 1999).

The Z' factor values derived from measurements performed in our laboratory on the Clariostar plate reader and on the CMBA platform are presented in Table 3.3.

Table 3.3. Z' factor values obtained for our Biosensor 1 assay.

Plate reader, Laboratory	Z' factor
Clariostar, IBS	0.83
TECAN, CMBA platform	0.90

As seen in Figure 3.25, the value of the Z' factor is expected to be between 0.5 and 1 in a robust assay. Our results show that our Biosensor 1 is a very reliable tool to detect the potential inhibitors of the YB-1 Δ C/hNTH1 interaction.

3.3.2. Life Chemicals Protein-Protein Interaction Fragment Library

We used our Biosensor 1 to perform a high-throughput screen of the Life Chemicals Protein-protein Interactions (PPI) library on the CMBA platform. This chemical library contains 800 compounds that have been specifically selected to target protein-protein interactions. All stock compounds in this library were provided at 3.8 mM in 100 % DMSO.

The first high-throughput screening was performed with 0.2 μ M Biosensor 1 and 50 μ M compound concentration in triplicate in a final volume of 50 μ l. The 12nt THF oligonucleotide at 0.5 μ M final concentration was used as a positive control (Figure 3.26). The percentage inhibition of the compounds was calculated by comparing the Biosensor 1 FRET efficiencies in the absence and presence of 12nt THF oligonucleotide (see Material and Methods for detailed description of calculation).

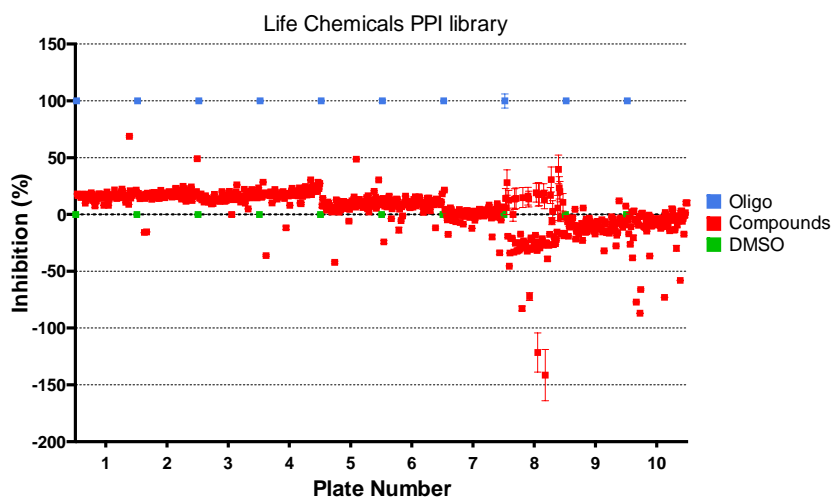


Figure 3.26. Overall results obtained from the first HTS of Life Chemicals PPI library. The FRET of Biosensor 1 in DMSO (green dots) was set to 0% inhibition, while the FRET of Biosensor 1 in the presence of 12nt THF oligonucleotide (blue dots) was set to 100% inhibition. Test compounds from ten 384-well plates are shown as red dots in the graph. The values presented are the mean of triplicate measurements recorded 1h after mixing the Biosensor 1 with the compounds.

Due to an error in the calculation of the required Biosensor 1 volume, the robot pipetted the wrong volumes of Biosensor 1 in the 8th plate and as a result FRET calculations derived from these measurements are highly variable and unreliable. After this first HTS, 30 selected compounds exhibiting reduced FRET levels (> 25 % inhibition) were further tested at three different concentrations (50, 10 and 1 μ M) (Figure 3.27). Of these 30 compounds, 22 of them were from plate 8 in order to repeat them correctly, and 8 of them showed reduced FRET signal with a small standard deviation.

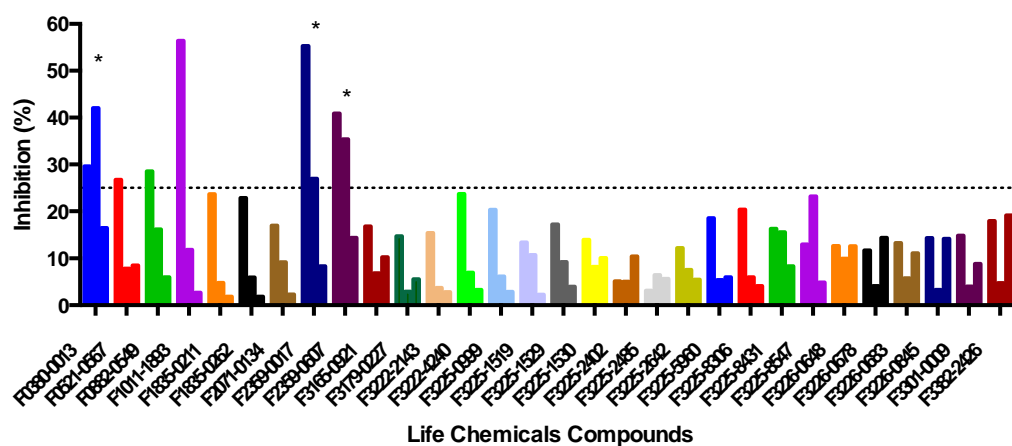


Figure 3.27. Overall results obtained from the second HTS of Life Chemicals PPI library with selected 30 compounds. Inhibition percentages of Biosensor 1 in presence of 30 selected Life Chemicals compounds at 50, 10 and 1 μ M (three columns of the same colour side by side, respectively). Horizontal dashed line represents 25 % inhibition on Biosensor 1. Selected compounds used in further validation tests are marked with an asterisk (*).

We found three compounds, which showed 30-60 % inhibition at 50 μ M concentration and had still an inhibitory effect at 10 μ M concentration (Figure 3.27 and 3.28 D). Two of these display similar chemical structures (Figure 3.28 B, C).

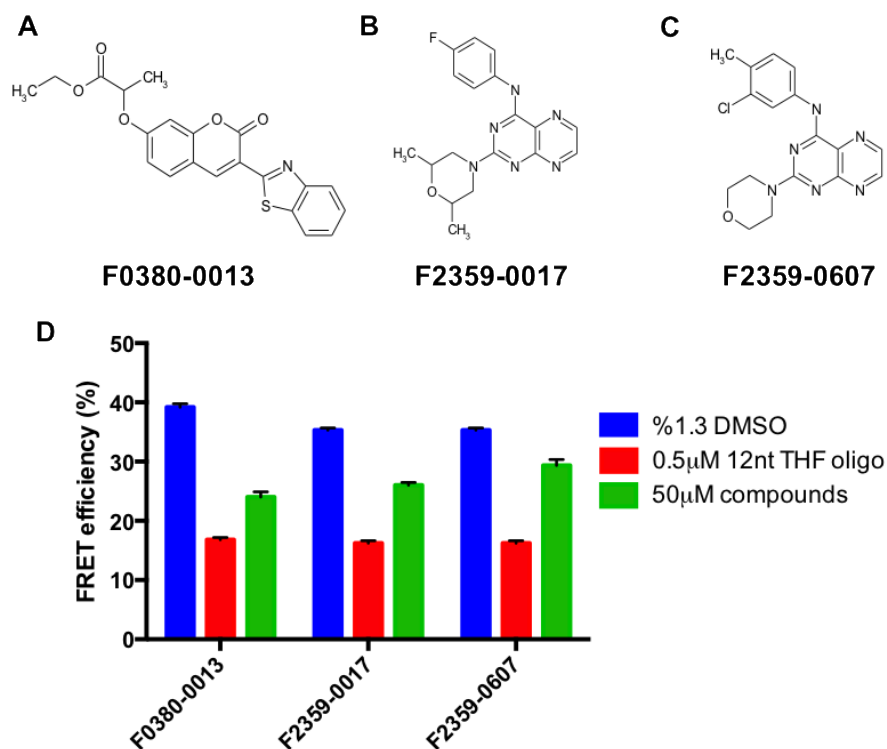


Figure 3.28. Potential hits identified in Life Chemicals PPI library. (A-C) Chemical structures and names of three potential hits identified from the high-throughput screening of the Life Chemical PPI library (D) FRET efficiencies of three potential hits identified from the Life Chemicals PPI library with Biosensor 1. Blue: Biosensor 1 + 1.3 % DMSO; Red: Biosensor 1 + 0.5 μ M 12nt THF DNA; Green: Biosensor 1 + 50 μ M compounds.

3.3.3. Prestwick Chemical Library

Next, we performed a second HTS on the CMBA platform using the Prestwick Chemical Library. This library is a unique collection composed of 1280 small molecules, 95 % approved drugs (FDA, EMA and other agencies). All stock compounds in this library were at 10 mM in 100% DMSO. As before, the screen was performed with 0.2 μ M Biosensor 1 and 50 μ M compound in triplicate.

After this first high-throughput screening (Figure 3.29), we found 20 compounds showing higher than 50 % inhibition. Some of them also increased the FRET signal, but a majority of compounds did not show any significant effect on Biosensor 1.

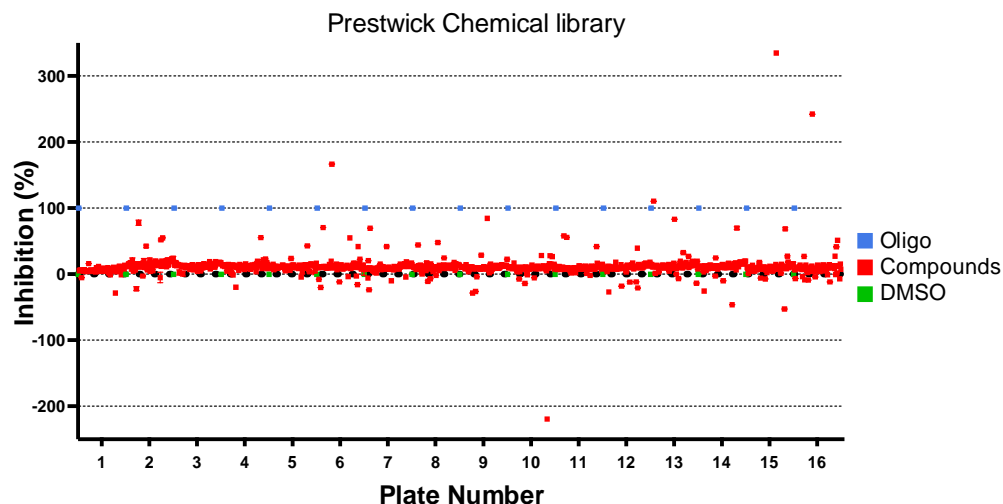


Figure 3.29. Overall results obtained from the first HTS of Prestwick Chemical library. The FRET of Biosensor 1 in DMSO (green dots) was set to 0% inhibition, while the FRET of Biosensor 1 in the presence of 12nt THF oligonucleotide (blue dots) was set to 100% inhibition. Test compounds from 16 384-well plates are shown as red dots in the graph. The values presented are the mean of triplicate measurements recorded 1h after mixing the Biosensor 1 with the compounds.

30 compounds were selected for a second screening at three different concentrations (50, 10 and 1 μM). Of these, 28 compounds showed higher than 30 % inhibition in the primary screen, with 3 compounds reducing the FRET levels of the Biosensor more severely than the 12nt THF oligonucleotide (and hence appear as >100 % inhibition in Figure 3.29), while two of them increased the FRET efficiency of Biosensor 1 (negative inhibition in Figure 3.29). Several of these compounds strongly affected the measured fluorescence intensities. Two of them showed 15 times higher mTQ2 signal, which indicates that the compounds themselves may emit strong fluorescence at 477 nm. Half of them showed similar effects on fluorescence intensities of mTQ2 and sYFP2. The rest of them decreased both fluorescence intensities of mTQ2 and sYFP2. In this second screening, we therefore, decided to include wells corresponding to the test compounds alone diluted in the Biosensor buffer to check for the intrinsic fluorescence of the compounds. The results of the secondary screen are shown in Figure 3.30.

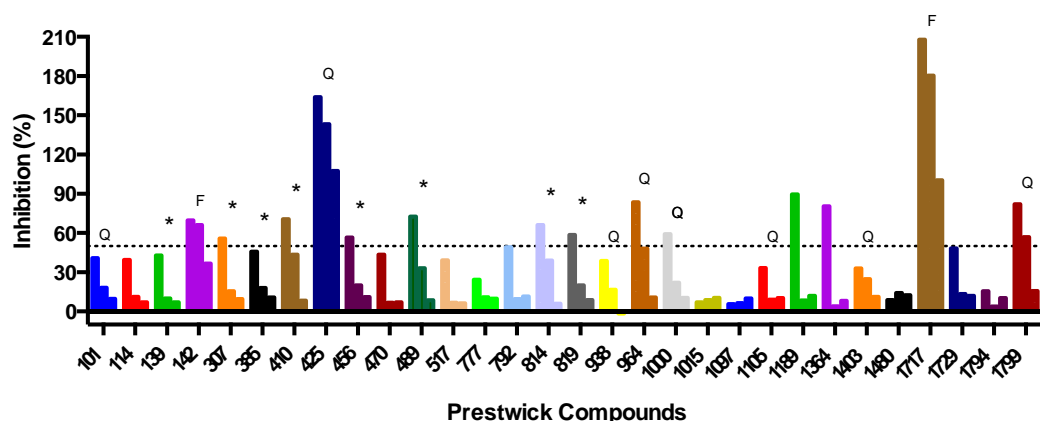


Figure 3.30. Overall results obtained from the secondary HTS of Prestwick Chemical library with 30 selected compounds. Inhibition percentages of Biosensor 1 in presence of 30 selected Life Chemicals compounds at 50, 10 and 1 μ M (three columns of the same colour side by side, respectively). Horizontal dashed line represents 50 % inhibition of Biosensor 1. Selected compounds used in further validation tests are marked with an asterisk (*). F indicates the compounds, which showed high intrinsic fluorescence signal alone. Q indicates the compounds that quench the fluorescence signal.

8 compounds from the Prestwick Chemical Library were found to be potential inhibitors displaying a clear, concentration-dependent inhibition of the FRET signal (Figure 3.31).

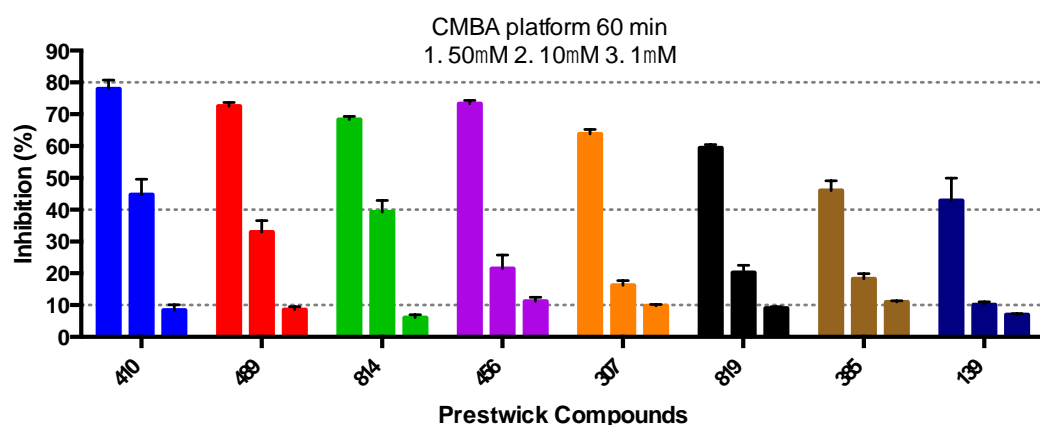
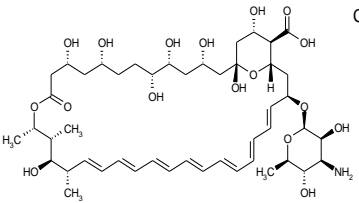
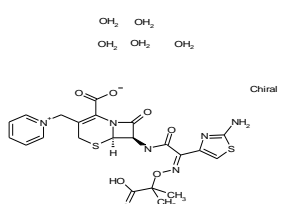
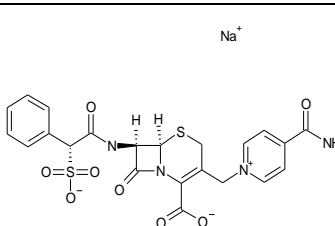
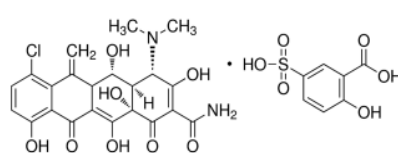
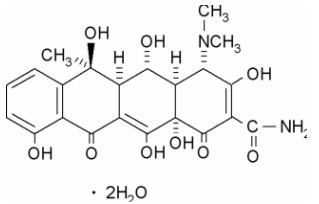
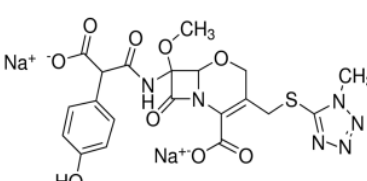
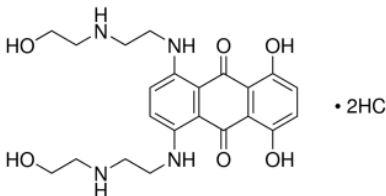
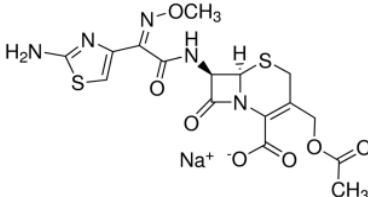


Figure 3.31. Characterisation of the top 8 hits identified from the Prestwick chemical library. Extent of Biosensor FRET inhibition by 8 Prestwick compounds (at 50, 10 and 1 μ M) identified in the secondary screening on the CMBA platform. The values are derived from the 1h measurement.

The names, properties and molecular structures of these 8 compounds from the Prestwick Chemical Library are given in Table 3.4.

Table 3.4. List of compounds from Prestwick Chemical Library after second screening.

Cpd id	Chemical name	Formula	Molecular weight (g/mol)	Molecular Structure
410	Amphotericin B	$C_{47}H_{73}NO_{17}$	924	 Chiral
489	Ceftazidime pentahydrate	$C_{22}H_{32}N_6O_{12}S_2$	637	 Chiral
814	Cefsulodin sodium salt	$C_{22}H_{19}N_4NaO_8S_2$	555	 Na ⁺
456	Meclocycline sulfosalicylate	$C_{29}H_{27}ClN_2O_{14}S$	695	 • HO-SO ₂ -C ₆ H ₃ (OH)-COOH
307	Oxytetracycline dihydrate	$C_{22}H_{28}N_2O_{11}$	497	 • 2H ₂ O
819	Moxalactam disodium salt	$C_{20}H_{18}N_6Na_2O_9S$	564	 Na ⁺ Na ⁺

385	Mitoxantrone dihydrochloride	$C_{22}H_{30}Cl_2N_4O_6$	517	
139	Cefotaxime sodium salt	$C_{16}H_{16}N_5NaO_7S_2$	478	

Amphotericin B is a polyene antifungal antibiotic produced by *Streptomyces nodosus*, with antifungal activity. Ceftazidime pentahydrate, Cefsulodin sodium, Moxalactam disodium and Cefotaxime sodium are beta-lactams and cephalosporin antibiotics with bactericidal activity. Meclocycline sulfosalicylate and Oxytetracycline are tetracycline derivative antibiotics. Mitoxantrone is an anthracenedione antibiotic with antineoplastic activity and a topoisomerase II inhibitor.

3.4. Validation of hits from screening

In order to validate these initial hits, we ordered the powders corresponding to the three hits from Life Chemicals (F0380-0013, F2359-0017 and F2359-0607) and to seven of the eight Prestwick compounds (Amphotericin B, Meclocycline sulfosalicylate, Moxalactam disodium, Cefsulodin sodium, Mitoxantrone, Ceftazidime and Oxytetracycline) from Sigma for further analyses. We did not purchase the 8th compound (Cefotaxime) for the first validation tests because it was the least effective of the four beta-lactam antibiotics.

3.4.1. Autofluorescence of compounds

First, we checked the fluorescence spectra of the compounds identified in the Life Chemicals PPI library alone in buffer. The test compound that showed the highest inhibition (F0380-0013) showed a high level of fluorescence in the mTQ2 channel, which if uncorrected, largely affected the FRET efficiency calculation making it appear as a false positive result. The other two compounds showed low

levels of intrinsic fluorescence. Potential hits from the Prestwick Library were selected from those that did not show intrinsic fluorescence signal (Table 3.5).

Table 3.5. The level of intrinsic fluorescence of potential hits from Life Chemicals and Prestwick Chemical Library at 50 μ M concentration.

Name of compounds	mTQ2 channel (ex 435/em 477)	sYFP2 channel (ex 485/em 528)
F0380-0013	15112	354
F2359-0017	1364	28
F2359-0607	3078	20
Amphotericin B	75	57
Meclocycline	266	16
Moxalactam	16	10
Cefsulodin	100	26
Mitoxantrone	-2	22
Ceftazidime	23	11
Oxytetracycline	122	13

3.4.2. Effect of compounds on the FRET signal of the Fusion construct

We then tested the effect of our selected compounds on the FRET signal of 0.2 μ M Fusion (Figure 3.32) to verify that their effects on Biosensor 1 were not due to an interference with the FRET process itself. In these new measurements performed with the purchased compounds from Sigma, the FRET efficiencies were calculated after correcting for the intrinsic fluorescence of the test compounds. The 7 Prestwick compounds had no effect on the FRET signal of the Fusion, whereas the Life Chemical compounds reduced FRET signal by 6 to 9 % indicating that their intrinsic fluorescence, which is relatively high, may interfere with the FRET process.

We also performed the same experiments with Prestwick compounds obtained from the CMBA platform and after storage at 4°C during 2 days and 3 months. The results did not change indicating Prestwick compounds do not interfere with the FRET process.

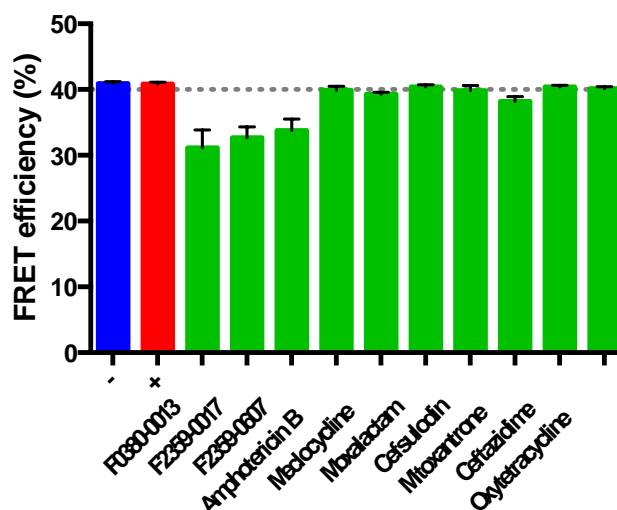


Figure 3.32. Effect of selected compounds on the FRET efficiency of the Fusion construct. FRET efficiencies of 0.2 μ M Fusion in the absence (blue) and presence (red) 12nt THF-DNA and 50 μ M test compounds (green). Reduced FRET signal of Fusion was observed in the presence of Life Chemicals compounds. No significant change was detected on Fusion FRET signal in the presence of Prestwick compounds.

3.4.3. Effect of compounds on the FRET signal of Biosensor 1

Next, we tested the inhibitory effects of these identified compounds on the FRET signal of 0.2 μ M Biosensor 1. Life Chemicals compounds prepared from powders were tested at two different concentrations (50 μ M and 10 μ M) (Figure 3.33).

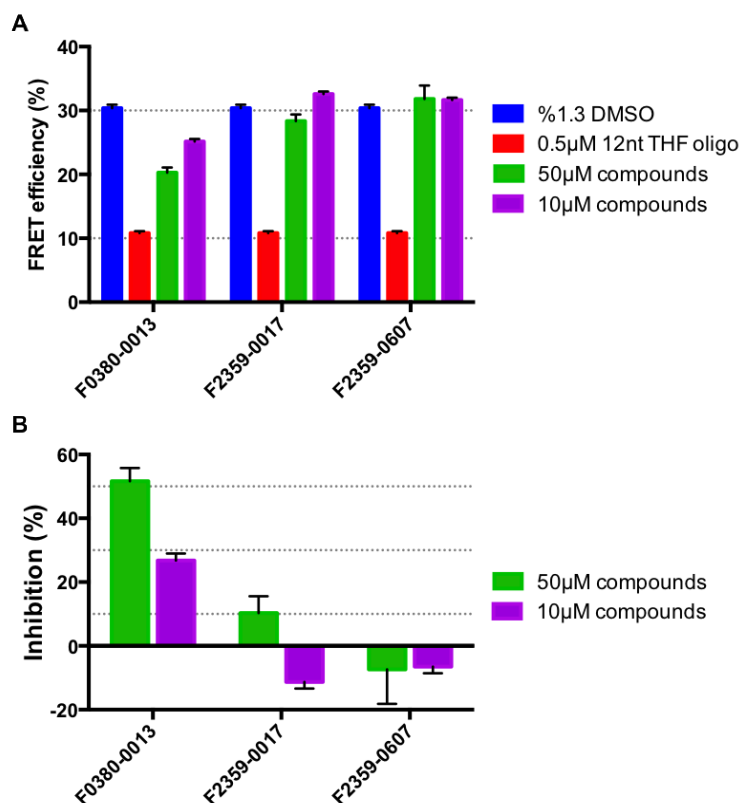


Figure 3.33. Inhibition of Biosensor 1 FRET by Life Chemicals test compounds. **(A)** FRET efficiencies of Biosensor 1 at 0.2µM concentration in buffer containing 50mM NaCl in the presence of DMSO alone (blue), 12nt THF oligonucleotide (red) and either 10 (purple) or 50 µM (green) of Life Chemicals test compounds. **(B)** Extent of inhibition of Life Chemicals test compounds at 10 (purple) or 50 µM (green). Horizontal dashed lines indicate 10, 30, and 50 % values, respectively.

Compounds F2359-0017 and F2359-0607 had little effect on the FRET signal of Biosensor 1. Compound F0380-0013 caused a decrease in Biosensor 1 FRET similar to that seen with the Fusion construct (Figure 3.32). The reduced FRET efficiency may thus result from the intrinsic fluorescence of the compound and not from inhibition of the hNTH1/YB-1 interaction. These three test compounds identified from the Life Chemicals PPI library thus appear to be false-positives.

We then tested the seven selected compounds from the Prestwick Chemical library freshly prepared from Sigma powders on 0.2 µM Biosensor 1 (Figure 3.34). Initial measurements were performed at a single compound concentration of 50 µM.

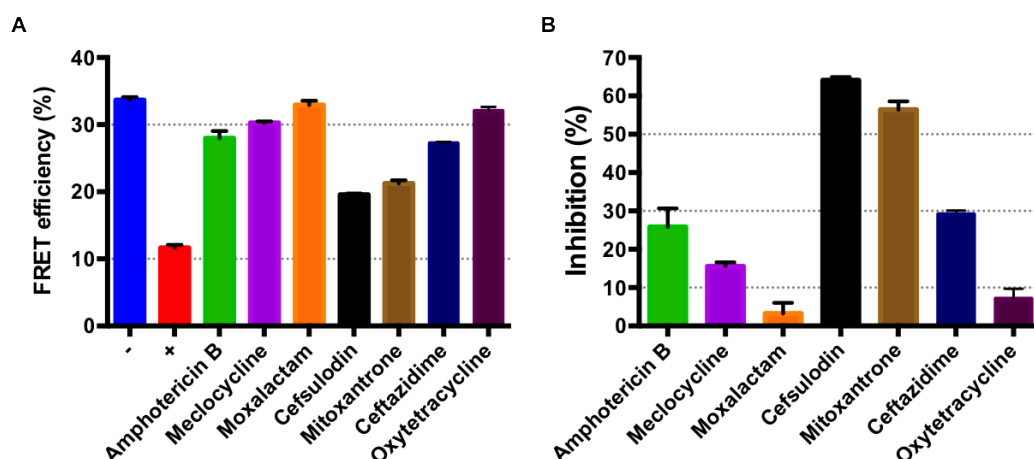


Figure 3.34. Inhibition of Biosensor 1 FRET by seven Prestwick compounds. **(A)** FRET efficiencies of Biosensor 1 at 0.2 μ M concentration in buffer containing 50mM NaCl in the presence of DMSO alone (blue), 12nt THF oligonucleotide (red) or 50 μ M Prestwick test compounds. **(B)** Inhibition percentages of Prestwick test compounds at 50 μ M. Horizontal dashed lines indicate 10, 30, and 50 % values, respectively.

The results obtained for Cefsulodin and Mitoxantrone ordered from Sigma showed similar inhibitory effects to those seen in our second screening on the CMBA platform. However, the other compounds showed little or no effects. We repeated these measurements after a few days and to our surprise the effects of the compounds were different indicating that the solubility of the compounds may be an issue. To verify this, Caroline Barette from the CMBA platform also kindly provided us with a small volume of the compound stock solutions used in the robotic screens allowing us to test these compounds stocks on our Biosensor construct in parallel. We performed these comparative measurements on the 7 of Prestwick compounds (Figure 3.35).

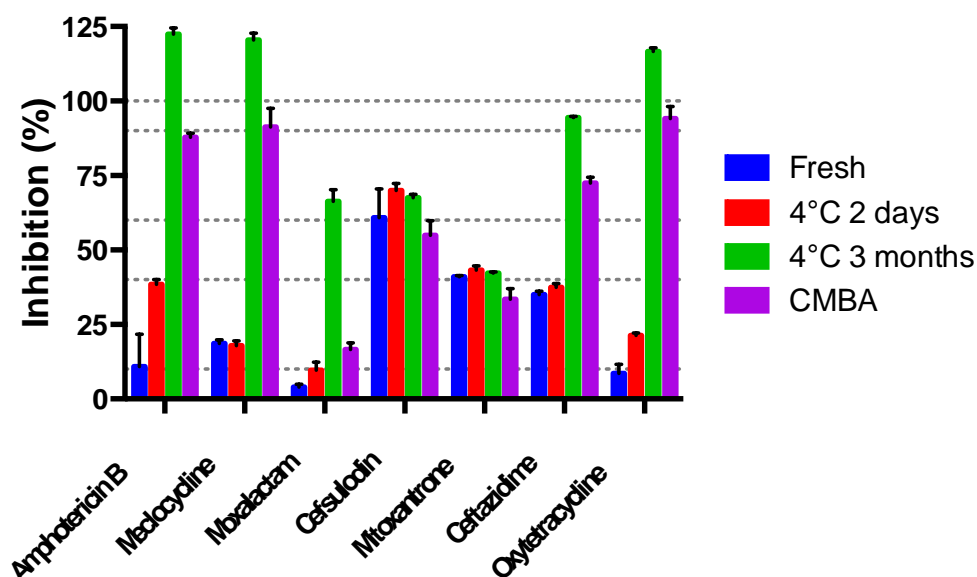


Figure 3.35. Comparison of the extent of inhibition of seven selected Prestwick compounds from different sources. Extent of inhibition of Prestwick compounds at 50 μ M, either freshly prepared from powders (blue), stored at 4°C for 2 days after preparation (red) or for 3 months (green), and provided by the CMBA platform as a 10mM stock solution (purple). Storage at 4°C for three months improved their ability to inhibit the Biosensor FRET levels even more potently than compounds provided by the CMBA platform. Horizontal dashed lines indicate 10, 40, 60, 90, and 100 % values, respectively.

Cefsulodin and Mitoxantrone were found to be potent inhibitors irrespective of their source and mode of preparation and storage with inhibitions of ~ 65 and ~ 45 % respectively. Meclocycline and Oxytetracycline ordered from Sigma did not show any significant inhibition using freshly prepared solutions and after storage of these chemicals at 4°C for 2 days. This is in marked contrast with the effect of these compounds provided by the CMBA platform, which caused around 90 % inhibition. Interestingly, after storage of the solubilized compounds at 4°C for three months, we observed an even stronger inhibition effect with these two compounds, which surpassed the inhibitory effect of the 12nt THF oligonucleotide (> 100 % inhibition). In the case of Amphotericin B and Moxalactam, storing the compounds at 4°C significantly improved their ability to inhibit the Biosensor FRET levels. Storage at 4°C for three months improved their inhibitory potential to levels beyond those obtained with the compounds provided by the CMBA platform. A similar behaviour was seen for Ceftazidime, even though its inhibitory potential was quite strong already using freshly prepared solutions (40

%). These measurements confirm that all seven of these compounds strongly inhibit the Biosensor 1 FRET signal as seen in our primary and secondary HTS, but this effect may be caused by degraded or altered compounds.

In view of these differences in inhibition depending on the source and storage conditions of the compounds, we decided to check the UV/Vis absorbance spectra of our various compounds (Figure 3.36).

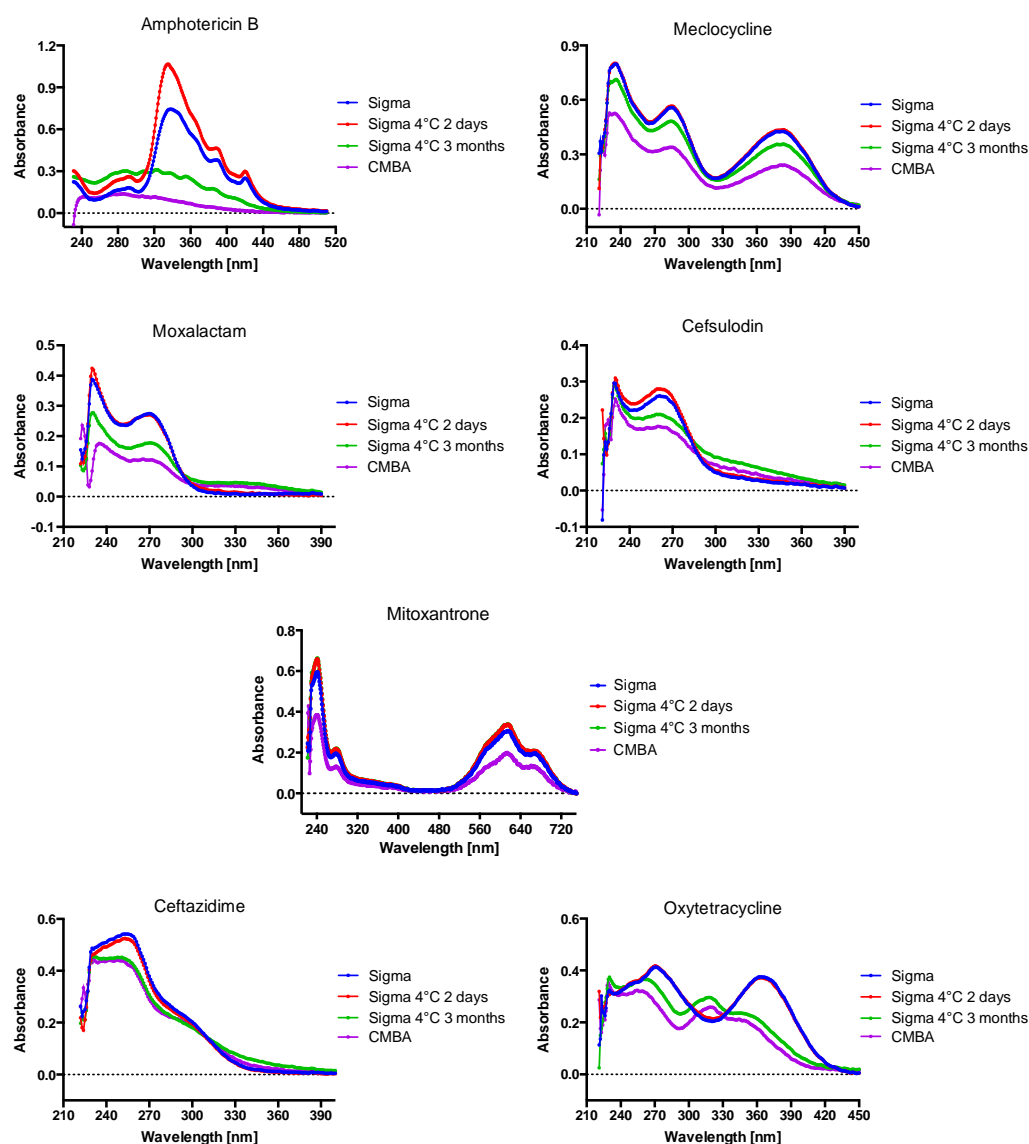


Figure 3.36. Spectral analysis of Prestwick compounds. Comparison of spectra of seven selected Prestwick compounds freshly prepared from Sigma powders (blue), stored at 4°C for 2 days after preparation (red) or for 3 months (green) and provided by the CMBA platform (purple).

Here again, these absorbance spectra reveal some clear differences between Prestwick compounds freshly prepared from powder (blue lines) and those obtained from CMBA platform (purple lines) or stored at 4°C for 3 months (green lines). Interestingly, there are similarities between the spectra obtained from the Prestwick compounds provided by the CMBA platform (purple lines) and those prepared from Sigma powder and stored at 4°C for 3 months (green lines), which clearly suggests that several of the compounds are unstable and no longer correspond to the initial solubilized compound.

Finally, we performed dose response assays with the seven Prestwick hits. We used the freshly prepared solutions after 2 days of storage at 4°C for Cefsulodin and Mitoxantrone and used solutions stored at 4°C for 3 months for the other compounds (Figure 3.37).

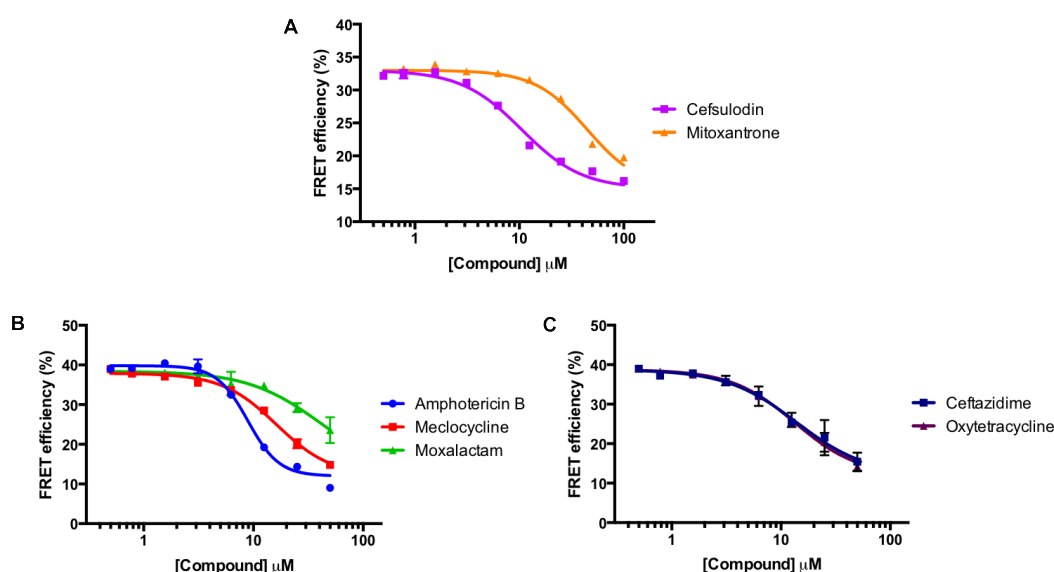


Figure 3.37. Dose response curves of selected Prestwick hits ordered from Sigma, dissolved in DMSO and stored at 4°C for 2 days or 3 months prior to measurements. The data points corresponding to the means of triplicate measurements were fitted to a standard sigmoidal inhibition model in GraphPad Prism. (A) Cefsulodin and mitoxantrone (2 days at 4°C), (B) Amphotericin B, Meclocycline and Moxalactam, (C) Ceftazidime and Oxytetracycline.

IC₅₀ values of Prestwick hits ordered from Sigma are given in Table 3.6. Amphotericin B, Ceftazidime, Oxytetracycline and Cefsulodin were found to be the more potent inhibitors of the hNTH1/YB-1ΔC interaction with IC₅₀ values

between 8 and 14 μM . Mecloxyline is also a potential inhibitor with an IC_{50} of 16 μM . Mitoxantrone and Moxlactam exhibit higher IC_{50} values ($> 40 \mu\text{M}$) and appear to be poorer inhibitors.

Table 3.6. IC_{50} values of Prestwick hits ordered from Sigma.

	Ampho- tericin B	Meclo- cycline	Moxa- lactam	Cefsul- lodin	Mitoxan- trone	Ceftazi- dime	Oxytetra- cycline
IC_{50} (μM)	8.91	16.26	41.50	10.47	44.67	13.93	13.34
R^2 of fits	0.99	0.99	0.92	0.99	0.97	0.96	0.98

Lastly, for comparison we performed limited dose response assays with the small amounts of compounds provided by the CMBA platform (Figure 3.38).

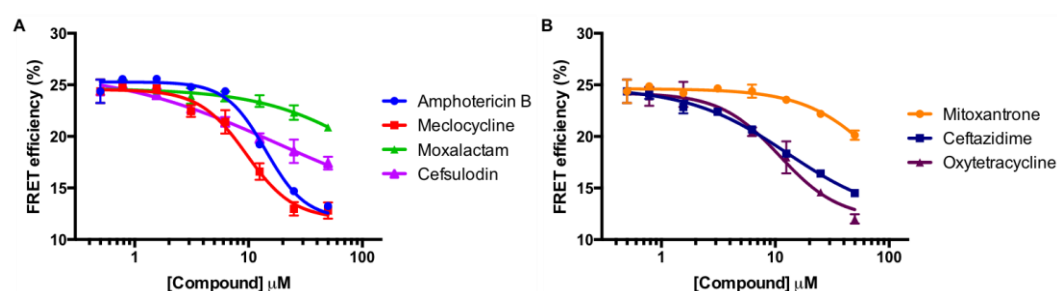


Figure 3.38. Dose response curves of seven Prestwick hits provided by CMBA platform. (A) Amphotericin B, Mecloxyline, Moxalactam and Cefsulodin, (B) Mitoxantrone, Ceftazidime, and Oxytetracycline. The data points corresponding to the means of triplicate measurements were fitted to a standard sigmoidal inhibition model in GraphPad Prism.

IC_{50} values of the seven Prestwick hits provided by CMBA platform are given in Table 3.7. These data confirm that Mitoxantrone and Moxalactam are less potent as Biosensor 1 FRET inhibitors, while the other compounds have IC_{50} values between 9 and 18 μM .

Table 3.7. IC_{50} values of Prestwick hits provided by CMBA platform.

	Ampho- tericin B	Meclo- cycline	Moxa- lactam	Cefsul- lodin	Mitoxan- trone	Ceftazi- dime	Oxytetra- cycline
IC_{50} (μM)	14.16	9.58	128.83	18.20	92.26	12.79	10.97
R^2 of fits	0.98	0.97	0.83	0.94	0.91	0.98	0.96

Amphotericin B, Meclocycline, Ceftazidime and Oxytetracycline from Sigma and the CMBA platform inhibited the interaction in the similar range 9 to 16 μ M. Moxalactam showed a higher inhibitory effect after incubation at 4°C for 3 months than obtained from the CMBA platform (Table 3.6 and 3.7), confirming our previous results (Figure 3.35). Cefsulodin and in particular Mitoxantrone provided by the CMBA platform showed significantly reduced inhibitory effect than Sigma powders, suggesting the fresh solutions of these compounds in contrast with other Prestwick chemicals are more potent inhibitors (Table 3.6 and 3.7).

Our results suggest that several compounds obtained from the CMBA platform may be degraded or modified due to repeated freeze-thawing prior to use in chemical screening. Their inhibitory effect on hNTH1/YB-1 Δ C interaction may therefore be the result of their degradation or alteration.

3.4.4. AlphaScreen Assay

To further validate these initial hits, we tested the effects of five of these compounds using an alternative protein-protein interaction assay that had previously been used to study the hNTH1/YB-1 interaction in the laboratory, namely the AlphaScreen technology, which is a bead-based luminescence assay. Dose-response measurements were performed for compounds Amphotericin B, Meclocycline, Moxalactam, Mitoxantrone and Cefsulodin prepared from Sigma powders and stored at 4°C for 2 days (Figure 3.39). Mitoxantrone, which is a darkly coloured compound, was found to significantly quench the luminescence signal produced by the AlphaScreen beads and could therefore not be evaluated using this technique. The other four compounds showed dose-dependent inhibition of the hNTH1/YB-1 Δ C interaction with IC₅₀ values between 30 and 160 μ M, which are a little higher but in the similar range to those determined using our FRET-based Biosensor 1 (Table 3.8).

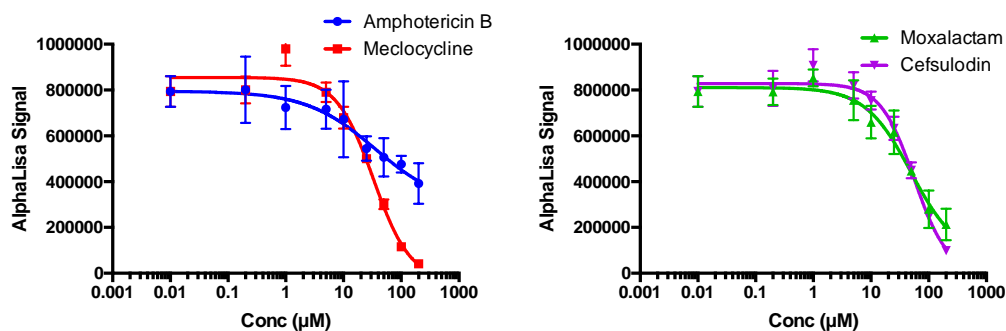


Figure 3.39. Dose response curves of selected Prestwick hits ordered from Sigma and stored at 4°C for 2 days determined by AlphaScreen assay. The data points corresponding to the means of triplicate measurements were fitted to a standard sigmoidal inhibition model in GraphPad Prism.

Table 3.8. IC₅₀ values of Prestwick hits determined by AlphaScreen assay.

	Amphotericin B	Cefsulodin	Meclocycline	Moxalactam
IC ₅₀ (µM)	160.9	55.48	30.77	49.66
R ² of fits	0.74	0.97	0.96	0.93

Part II. YB-1-hTopoI complex

In addition to its interaction with hNTH1, YB-1 has also been shown to interact with hTopoI and to function as an endogenous regulator of hTopoI-dependent DNA relaxation. In particular, YB-1 is able to interact with hTopoI during CPT-induced oxidative stress and this process increases cellular sensitivity to this drug in PC-3 cells (Wu et al., 2014). The objective of my work was thus to investigate and further characterise the interaction between hTopoI and YB-1 *in vitro* and in diverse mammalian cell lines using FRET to evaluate its potential as an anticancer drug target.

3.5. YB-1-hTopoI interaction *in vitro*

3.5.1. Expression and purification of human Topoisomerase I (hTopoI)

Initially the complete hTopoI and two N-terminally truncated forms of hTopoI were cloned into pProEX-HTb for expression in *E. coli* BL21 cells with cleavable N-terminal His-tags (Figure 3.40 and see Annex). The two truncated forms showed no expression and for the intact hTopoI protein, it was successfully expressed, but partially degraded and two forms of hTopoI were recovered. The first pool contained a degraded form of hTopoI, while the second pool contained mostly full-length hTopoI. In both cases, the protein yield was very low and the protein concentration could not be determined reliably, but the protein could nonetheless be used to perform initial relaxation activity tests. To overcome these difficulties, we decided to tag the protein at its C-terminus with a non-cleavable hexa-histidine tag (Figure 3.40).

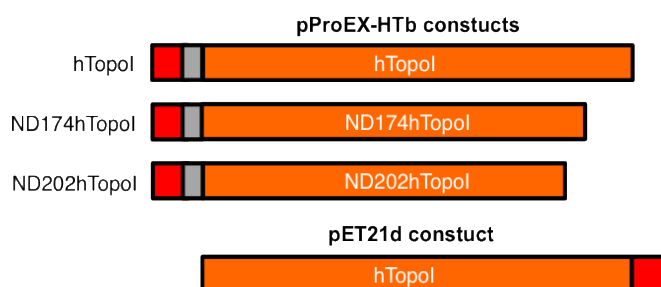


Figure 3.40. Illustration of hTopoI constructs used in our work. Red: His-tag. Grey: short linker sequences.

For this C-terminally His-tagged hTopoI, we also observed partial degradation of the protein after the first Ni-affinity purification, but the protein yield was much higher (Figure 3.41). A major band ~70 kDa (hTopoI-70) was eluted in the 50 mM imidazole wash and full-length hTopoI (hTopoI-FL) was eluted mostly during the imidazole gradient.

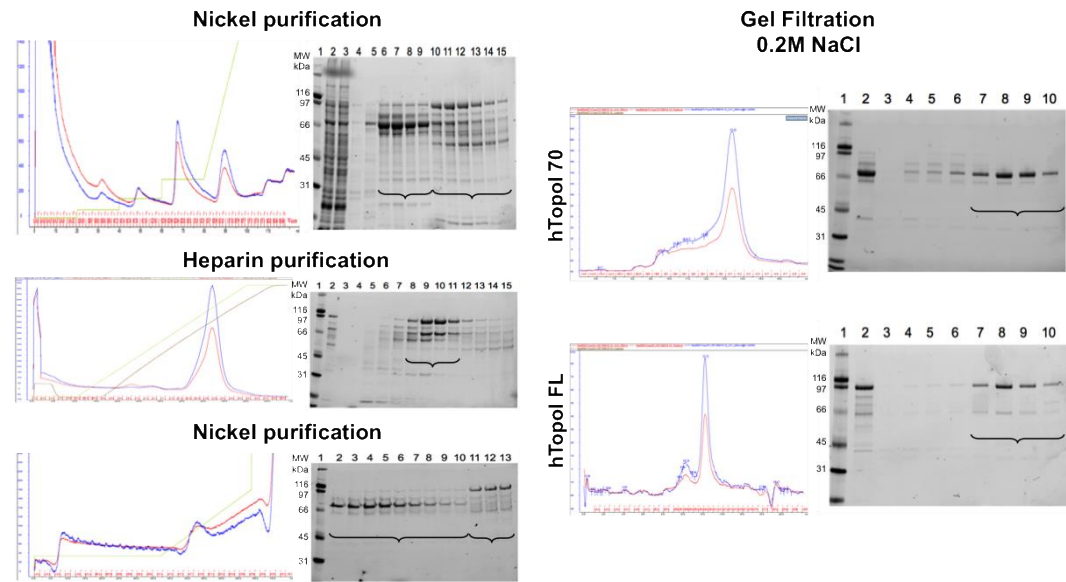


Figure 3.41. Purification of hTopoI-FL and hTopoI-70. Illustration of the various chromatographic steps involved in the purification of C-terminally His-tagged hTopoI full-length and hTopoI-70 from bacterial cell lysates.

Both forms were collected separately for further purifications. We tried to separate contaminants from the hTopoI-FL using a Heparin column, but this step was unsuccessful. Instead, we found that performing a second Nickel affinity column with a long (8-10 CV) 50 mM imidazole wash to separate hTopoI-70 and hTopoI-FL was successful. This way we achieved to largely separate the two forms of hTopoI. For the last purification step, the samples were loaded on a Biorad SEC 650 size exclusion column and hTopoI-FL and hTopoI-70 were eluted with GF buffer containing 200 mM NaCl. In the end, we recovered pure hTopoI-70 and hTopoI-FL at 3.5 mg/ml and 0.75 mg/ml protein concentrations, respectively starting from a 6 L culture. The yield was low (Table 3.9), but significantly higher than with the N-terminally His-tagged hTopoI.

We characterised the purified hTopoI-FL and hTopoI-70 by mass spectrometry analysis. hTopoI-FL displayed the expected mass for the full-length protein (91.8 kDa) and we determined that hTopoI-70 (71.2 kDa) is an N-terminally truncated form of hTopoI (missing residues 1-172) (Figure 3.42).

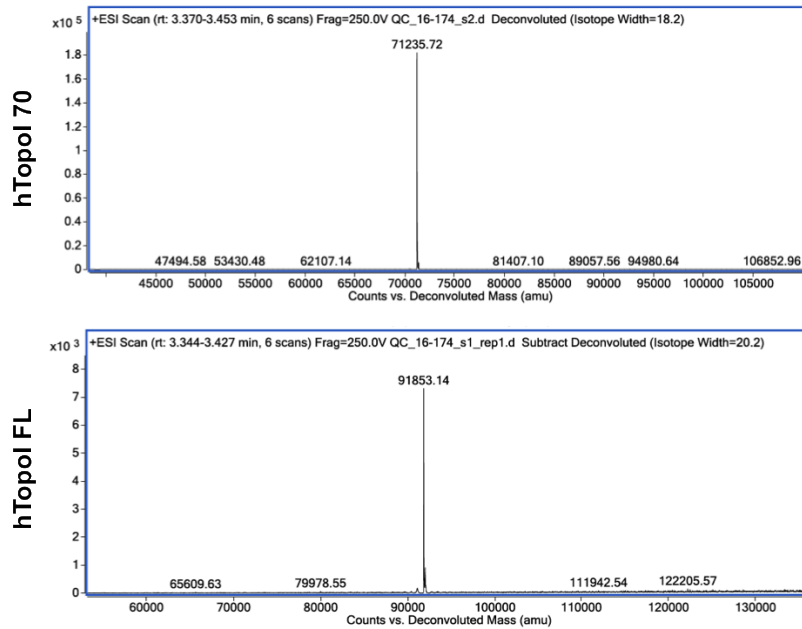


Figure 3.42. Mass spectrometry analysis of hTopoI-FL and hTopoI-70 fractions.

To attempt to reduce this degradation, we designed a mutant in which K172 was mutated to alanine. However, hTopoI-FL-K172A showed a similar purification and degradation profile as wild-type protein.

Table 3.9. Properties of purified hTopoI proteins.

Name of proteins	Size (kDa)	Purification Yield/ L culture (mg)	Concentration (mg/ml)
His-hTopoI-FL	93.5	-	-
hTopoI-FL-His	92	0.009	0.75
hTopoI-70-His	71	0.06	3.5

3.5.2. DNA relaxation activity assays

We performed relaxation assays using both hTopoI-FL and hTopoI-70 (with C-terminal His-tags) purified from *E. coli* (Figure 3.43).

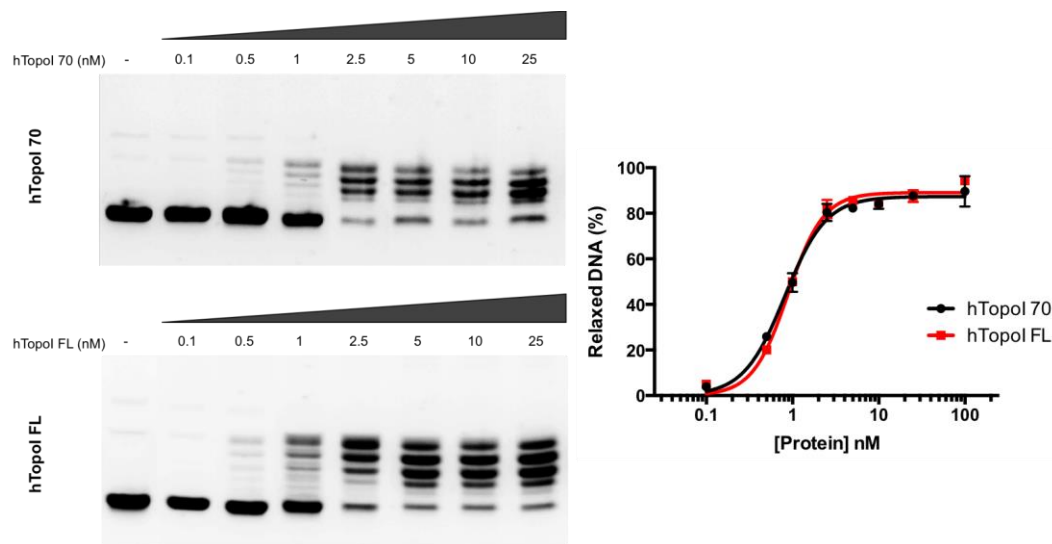


Figure 3.43. DNA relaxation activity of purified hTopoI. Left: Representative agarose gel images of relaxation activity of hTopoI-70 and hTopoI-FL on supercoiled pUC19 plasmid (0.1-25 nM). Right: Extent of DNA relaxation as a function of hTopoI-70 (black) or hTopoI-FL (red) concentration (nM). Experiments were performed in triplicate and the means and standard deviations were plotted and fitted to a simple sigmoidal model using GraphPad Prism.

The relaxation activities of hTopoI-FL and hTopoI-70 are similar as expected and reported previously (Lance Stewart et al., 1996), since both constructs possess an intact catalytic domain. We compared the relaxation activity of hTopoI-FL wild type (wt) and mutant K172A. There was no difference in their relaxation, suggesting that the mutation does not affect hTopoI (Figure 3.44).

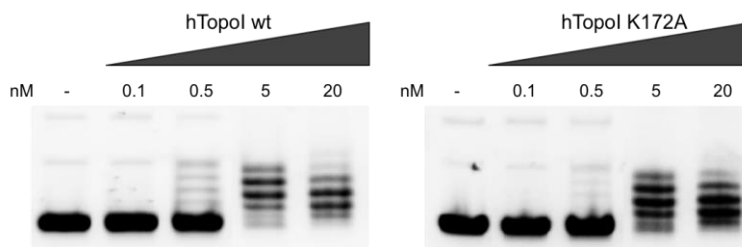


Figure 3.44. DNA relaxation activity of wild-type and K172A hTopoI. Representative agarose gel images of the relaxation activity of hTopoI wt and mutant K172A (0.1-20 nM) on supercoiled pUC19 plasmid.

We then investigated the effect of the hTopoI poison CPT, on the relaxation activity of hTopoI-FL and hTopoI-70. CPT showed a similar inhibitory effect on the activity of hTopoI-FL and hTopoI-70 with IC_{50} values in the range of 5-10 μ M (Figure 3.45).

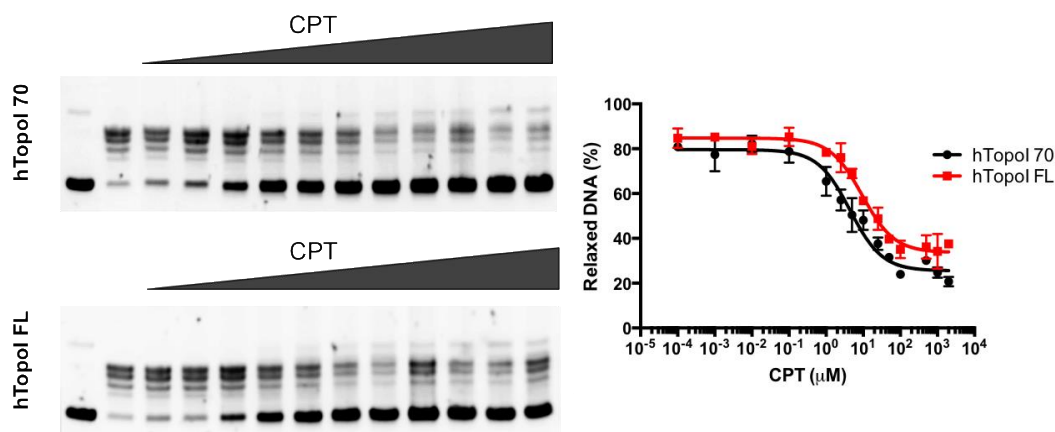


Figure 3.45. Inhibition of the DNA relaxation activity of hTopoI by CPT. Left: Representative agarose gel images of relaxation activity of 20 nM hTopoI-70 and hTopoI-FL on supercoiled pUC19 plasmid in the presence of increasing concentrations of CPT (0-2 mM). Right: Extent of DNA relaxation by 20 nM hTopoI-70 (black) and hTopoI-FL (red) in the presence of increasing CPT concentrations (0-2 mM). Experiments were performed in triplicate and the means and standard deviations were plotted and fitted to a simple inhibition model using GraphPad Prism.

3.5.3. Stimulation of hTopoI's relaxation activity by YB-1

We chose to investigate the effect of YB-1 on the hTopoI relaxation activity using a hTopoI concentration of 0.5 nM, which relaxes ~ 10-20 % of supercoiled plasmid. We checked the effect of the nuclear form of YB-1, YB-1ΔC, on the relaxation activity of hTopoI-FL and hTopoI-70 by pre-incubating the proteins together before adding them to the supercoiled DNA reaction mix (Figure 3.46). YB-1ΔC clearly stimulates the activity of both hTopoI-FL and hTopoI-70, most likely through a direct interaction, which suggests that the N-terminal domain of hTopoI is not essential for the interaction with YB-1ΔC. To further explore this, we thus performed interaction studies using FRET.

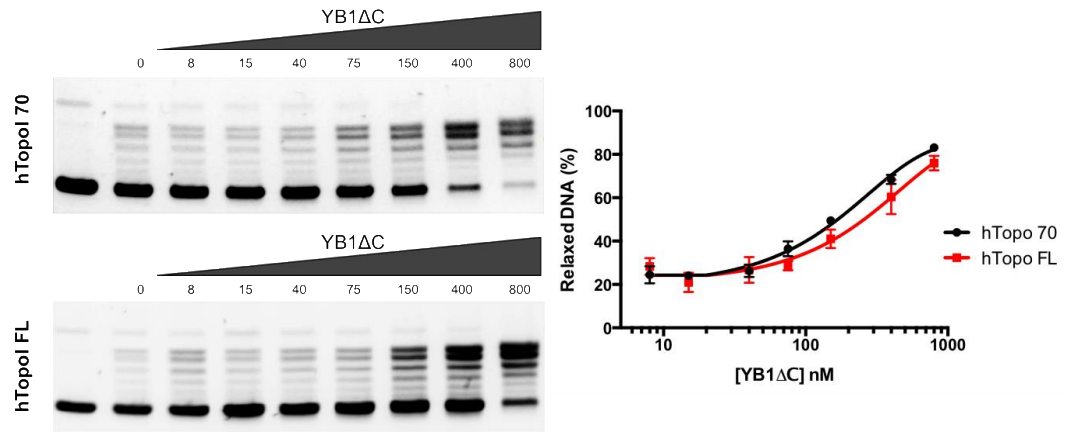


Figure 3.46. Stimulation of hTopoI DNA relaxation activity by YB-1ΔC. Left: Representative agarose gel images showing the stimulatory effect of YB-1ΔC (8-800 nM) on 0.5 nM hTopoI-FL and hTopoI-70 enzymatic activity. Right: Extent of DNA relaxation by 0.5 nM hTopoI-70 (black) and hTopoI-FL (red) in the presence of increasing amounts of YB-1ΔC. Experiments were performed in triplicate and the means and standard deviations were plotted and fitted to a one-phase association model using GraphPad Prism.

3.5.4. *In vitro* FRET measurements

3.5.4.1. Expression and purification of hTopoI fusion constructs

To investigate the interaction of hTopoI with YB-1 by FRET, we fused hTopoI to mTQ2. As for hTopoI-FL, two constructs were prepared with either the His-tag at the N- or the C-terminus (Figure 3.47). After the Ni-affinity purification of His-mTQ2-hTopoI, the protein was partially degraded and very low amounts of mTQ2-hTopoI were recovered, allowing us to make just one FRET measurement. Then we purified the C-terminally His-tagged hTopoI-mTQ2 starting from a 6 L bacterial culture. Figure 3.48 summarizes all purification steps. We found that the protein was partially degraded during the Ni-affinity purification and as with hTopoI-His we ended up purifying two forms of hTopoI: hTopoI-70-mTQ2 and hTopoI-FL-mTQ2.



Figure 3.47. Illustration of hTopoI fusion constructs used in our work. Red: His-tag, grey: short linker sequences, orange: hTopoI, cyan: mTurquoise2 (mTQ2).

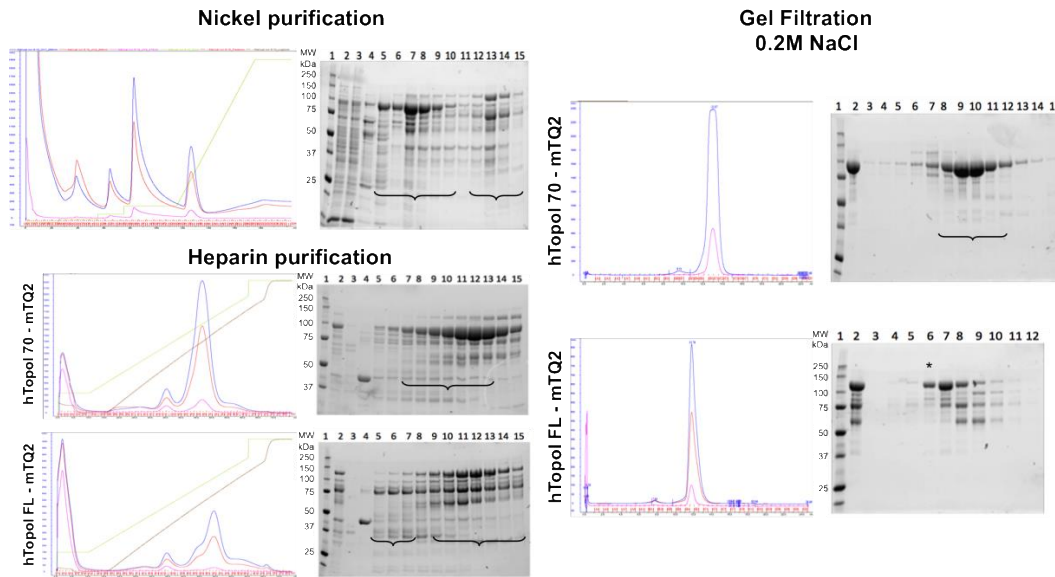


Figure 3.48. Purification of hTopoI-mTQ2. Illustration of the various chromatographic steps involved in the purification of C-terminally his-tagged hTopoI-mTQ2 and hTopoI-70-mTQ2.

After a final gel filtration step, we recovered sufficient hTopoI-70-mTQ2 protein for FRET measurements and a small amount of hTopoI-FL-mTQ2 construct (Table 3.10).

Table 3.10. Properties of purified hTopoI fused to mTQ2 proteins.

Name of proteins	Size (kDa)	Purification Yield/ L culture (mg)	Concentration (mg/ml)
His-mTQ2-hTopoI	122	0.004	1
TopoI-mTQ2-His	120	0.015	3.0
TopoI70-mTQ2-His	99	0.500	1.8

We tried to create a Biosensor construct containing hTopoI-FL (see Annex). We successfully obtained the clone of pProEX-HTb-mTQ2-hTopoI-YB1 Δ C-sYFP2 for overexpression in *E.coli* BL21 cells, but by gel electrophoresis and Western blotting we could not detect a band at ~172 kDa corresponding to our intact Biosensor construct. We performed a small-scale purification, which revealed that the hTopoI Biosensor construct was degraded in the bacteria.

3.5.4.2. Mixture of individual proteins

Purified hTopoI and YB-1 Δ C fusion proteins used for FRET measurements are shown in Figure 3.49.

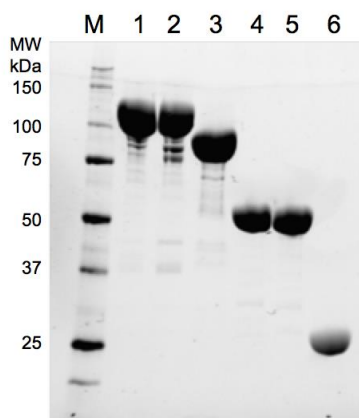


Figure 3.49. Representative gel of the purified proteins for *in vitro* FRET measurements. M: Biorad Precision Plus unstained protein marker, 1-6: hTopoI-mTQ2 (120 kDa), hTopoI-mTQ2 contaminated (120 kDa), hTopoI-70-mTQ2 (99 kDa), YB-1 Δ C-sYFP2 (53 kDa), sYFP2-YB-1 Δ C (53 kDa), sYFP2 (28 kDa), respectively.

Despite very low amounts of protein, we succeeded in measuring FRET with hTopoI fusion constructs at a final concentration of only 1 μ M protein in GF buffer containing 50 mM NaCl (Figure 3.50). For comparison, no FRET signal was detected for hNTH1 constructs at such low protein concentrations.

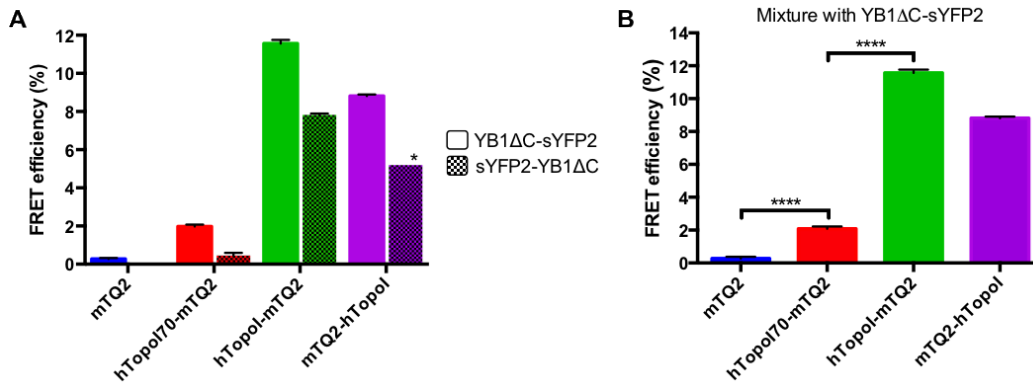


Figure 3.50. FRET efficiencies of individual protein mixes of hTopoI and YB-1ΔC constructs. (A) FRET efficiencies of hTopoI and YB-1ΔC mixtures at 1μM in buffer containing 50mM NaCl. *Single measurement (B) FRET efficiencies of individual protein mixtures with YB-1ΔC-sYFP2 at 1μM in buffer containing 50mM NaCl.

Our FRET measurements confirmed that hTopoI interacts directly with nuclear YB-1ΔC. The highest signal was obtained when both mTQ2 and sYFP2 were fused to the C-termini of hTopoI and YB-1ΔC. The FRET efficiencies were decreased in the case of hTopoI-70, but still significantly higher than with the negative control (mTQ2 alone), indicating that the N-terminal region is important, but not essential for the interaction with YB-1ΔC, in agreement with our relaxation activity measurements that showed that YB-1ΔC could also stimulate hTopoI-70. The FRET levels were seen to vary according to the purity of purified protein construct. When hTopoI-FL-mTQ2 was contaminated with small amounts of hTopoI-70 form (Figure 2.49, lane 2), the FRET efficiency measured for the hTopoI-FL-mTQ2 mixture with YB-1ΔC-sYFP2 was reduced compared with that obtained using the more pure sample (Figure 2.49, lane 1).

We investigated the effect of salt concentration on the hTopoI/YB-1 interaction (Figure 3.51) and observed that increased amounts of salt lead to reduced FRET efficiencies by affecting the interaction.

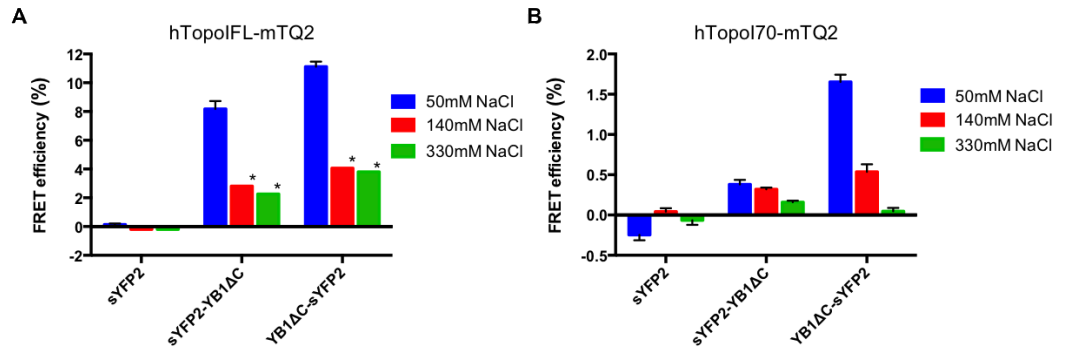


Figure 3.51. Effect of salt concentration on YB-1/hTopoI interaction. **(A)** FRET efficiencies of hTopoIFL and YB-1ΔC mixtures at 1μM in buffer containing 50mM, 140mM, and 330mM NaCl. *Single measurement **(B)** FRET efficiencies of hTopoI70 and YB-1ΔC mixtures at 1μM in buffer containing 50mM, 140mM, and 330mM NaCl.

3.6. YB-1/hTopoI interaction in mammalian cells

After confirming that hTopoI and YB-1 interact directly *in vitro*, we set out to investigate their interaction *in vivo*, in different human cell lines and several fusion constructs were prepared for these experiments (Figure 3.52).

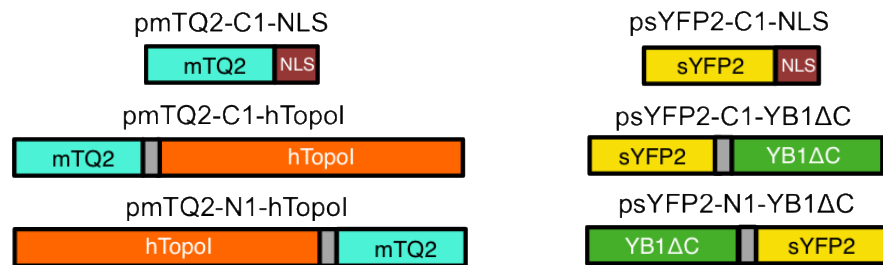


Figure 3.52. Schematic illustration of mammalian expression vector constructs used for *in vivo* FRET experiments.

3.6.1. FRET measurements in HeLa cells

We first evaluated the interaction of YB-1ΔC with hTopoI in HeLa cells. Before performing FRET experiments, we checked the expression and cellular localisation of mTQ2 fused hTopoI constructs (Figure 3.53).

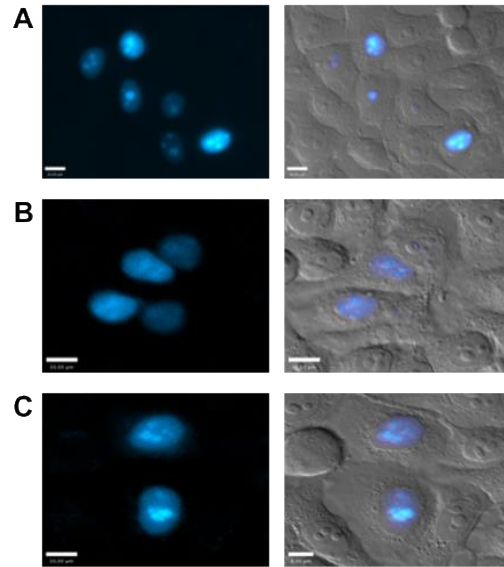


Figure 3.53. Nuclear localisation of hTopoI-mTQ2 in HeLa cells. Representative epifluorescence microscopy images of HeLa cells transfected with pmTQ2-NLS (**A**), pmTQ2-C1-hTopoI (**B**) and pmTQ2-N1-hTopoI (**C**). Right column, CFP channel; left column, DIC channel overlaid with CFP channel.

We observed expression of both N-terminally and C-terminally mTQ2 fused hTopoI in HeLa cells, however the transfection efficiencies were very low for both constructs. The mTQ2-hTopoI construct showed better transfection efficiency and donor fluorescent intensity than the hTopoI-mTQ2 construct. When we performed co-transfection experiments with mTQ2-hTopoI and YB-1-sYFP2, we were unable to find cells co-expressing both constructs. Moreover, attempts to establish a stable HeLa cell line expressing mTQ2-hTopoI failed (surviving cells no longer showed any detectable expression of mTQ2-hTopoI), probably due to toxicity of hTopoI overexpression.

To overcome the low co-transfection efficiency, we tried the 2A self-cleaving peptide based co-expression system (Wang et al., 2015). The Foot-and-mouth disease virus 2A peptide regulates the simultaneous expression and cleavage of multiple gene targets in cells. We inserted the 2A peptide in between our YB-1 Δ C-sYFP2 and mTQ2-hTopoI sequences to ensure the two constructs were expressed at similar levels *in vivo*. As a negative control, we prepared a construct in which sYFP2-YB-1 Δ C was replaced by sYFP2-NLS (Figure 3.54).

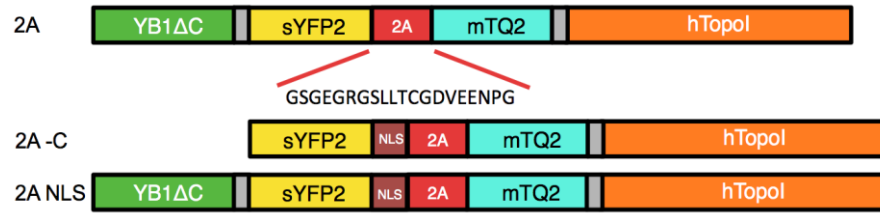


Figure 3.54. Schematic illustration of 2A co-expression constructs used in mammalian cells. 2A - C is a negative control, missing YB-1ΔC, in which sYFP2-NLS and mTQ2-hTopoI are co-expressed in the nucleus. 2A NLS is a variant of the 2A construct in which an additional NLS signal was added to the C-terminus of sYFP2 to favour the nuclear localisation of YB1-ΔC-sYFP2.

We transfected our HeLa cells with these co-expression constructs. The images of fixed samples were acquired one day after transfection (Figure 3.55).

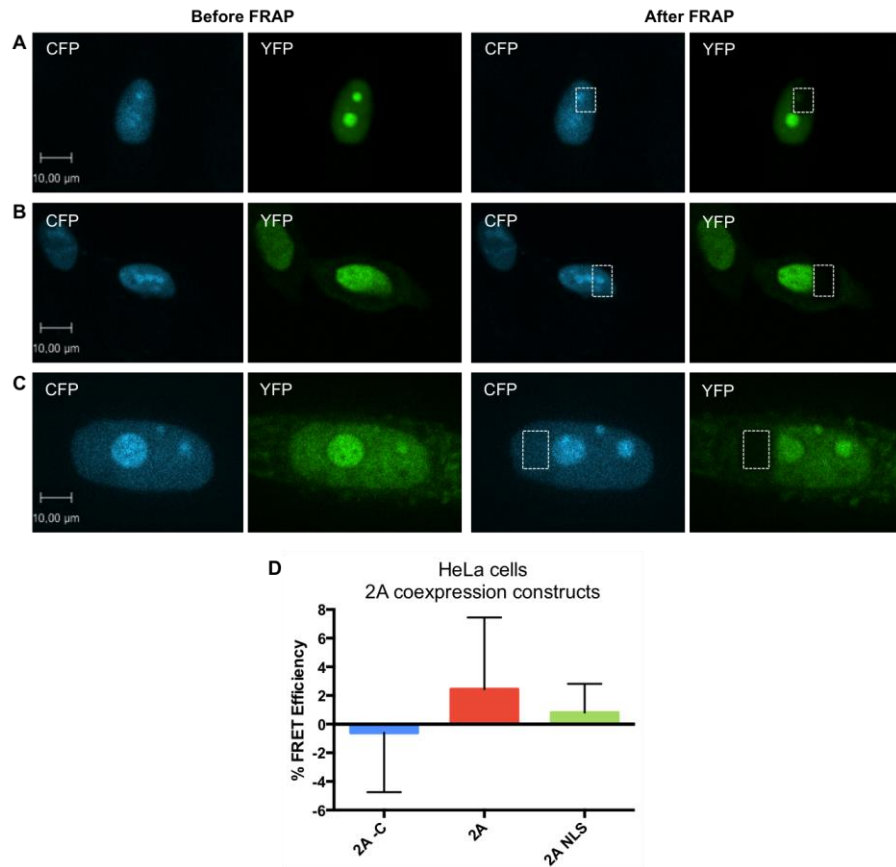


Figure 3.55. FRET measurements between YB-1ΔC and hTopoI in HeLa cells. Representative epifluorescence microscopy images of HeLa cells transfected with psYFP2-NLS-2A-mTQ2-hTopoI (A), pYB-1ΔC-sYFP2-2A-mTQ2-hTopoI (B), pYB-1ΔC-sYFP2-NLS-2A-mTQ2-hTopoI (C). mTQ2 is seen in the CFP channel (blue). sYFP2 is seen in the YFP channel (green). The white rectangle indicates the area of the nucleus that was photobleached. Scale bar: 10μm. (D) FRET efficiencies measured in HeLa cells transfected with the various 2A constructs. The presented data are the mean of at least eight replicates.

We observed co-expression of YB-1 Δ C-sYFP2 and mTQ2-hTopoI, but the cellular localisation of YB-1 Δ C-sYFP2 was variable in these cells. Some cells showed nuclear localisation, others showed cytoplasmic staining and some showed both of these localisations. In contrast, the sYFP2-NLS and mTQ2-hTopoI proteins were found to localise correctly in the nucleus. To overcome cytoplasmic diffusion of YB-1 Δ C-sYFP2, we added a Nuclear Localisation Signal (NLS) at the C-terminus of sYFP2 (Figure 3.54). Some cytoplasmic staining was still observed even in the presence of an additional NLS sequence (Figure 3.55 C). After performing Acceptor Photobleaching, no significant FRET signal could be detected with these different 2A constructs in HeLa cells (Figure 3.55 D).

3.6.2. FRET measurements in MCF7 cells

We then decided to study the hTopoI/YB-1 Δ C interaction in the breast cancer cell line, MCF7 cells. We transfected the cells with the 2A co-expression constructs and used the acceptor photobleaching method to detect FRET signal (Figure 3.56).

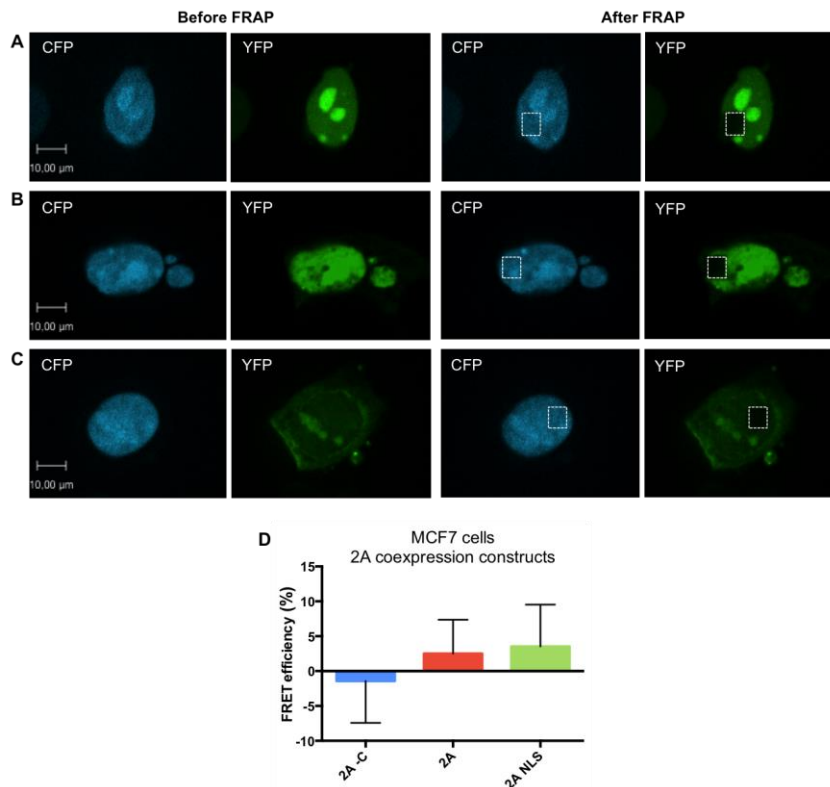


Figure 3.56. FRET measurements between YB-1 Δ C and hTopoI in MCF7 cells using the 2A constructs. Representative epifluorescence microscopy images of MCF7 cells transfected with

psYFP2-NLS-2A-mTQ2-hTopoI (A), pYB-1ΔC-sYFP2-2A-mTQ2-hTopoI (B), pYB-1ΔC-sYFP2-NLS-2A-mTQ2-hTopoI (C). mTQ2 is seen in the CFP channel (blue). sYFP2 is seen in the YFP channel (green). The white rectangle indicates the area of the nucleus that was photobleached. Scale bar: 10μm. (D) FRET efficiencies measured in MCF7 cells transfected with the various 2A constructs. The presented data are the mean of at least five replicates.

In MCF7 cells transfected with the 2A -C negative control, both mTQ2-hTopoI and sYFP2-NLS were detected in the nuclei (Figure 3.56 A). In MCF7 cells transfected with 2A constructs containing YB-1ΔC, YB-1ΔC-sYFP2 was both in the nucleus and in the cytoplasm (Figure 3.56 B and C). Acceptor photobleaching experiments were performed on cells co-expressing nuclear YB-1ΔC and mTQ2-hTopoI and as in the case of HeLa cells, the FRET levels measured were very variable and no significant FRET signal could be detected with these 2A constructs in the MCF7 cell line (Figure 3.56 D).

We also performed co-transfection experiments in MCF7 cells and the co-transfection efficiency was higher than in HeLa cells, allowing us to perform acceptor photobleaching experiments on co-transfected cells (Figure 3.57). This allowed us to test different YB-1ΔC and hTopoI constructs to determine whether the position of the fluorescent protein influenced the FRET efficiency. A significant FRET signal was obtained from MCF7 cells co-transfected with mTQ2-hTopoI and YB-1ΔC-sYFP2, when YB-1ΔC-sYFP2 was highly expressed, thus indicating that hTopoI and YB-1ΔC can interact in the nuclei of MCF7 cells (Figure 3.57 D). In contrast, no FRET was detected when sYFP2 was fused to the N-terminus of YB-1ΔC. The orientation of the two fluorescent proteins is thus critical for detecting the interaction as was observed in our *in vitro* measurements (Figure 3.50 A).

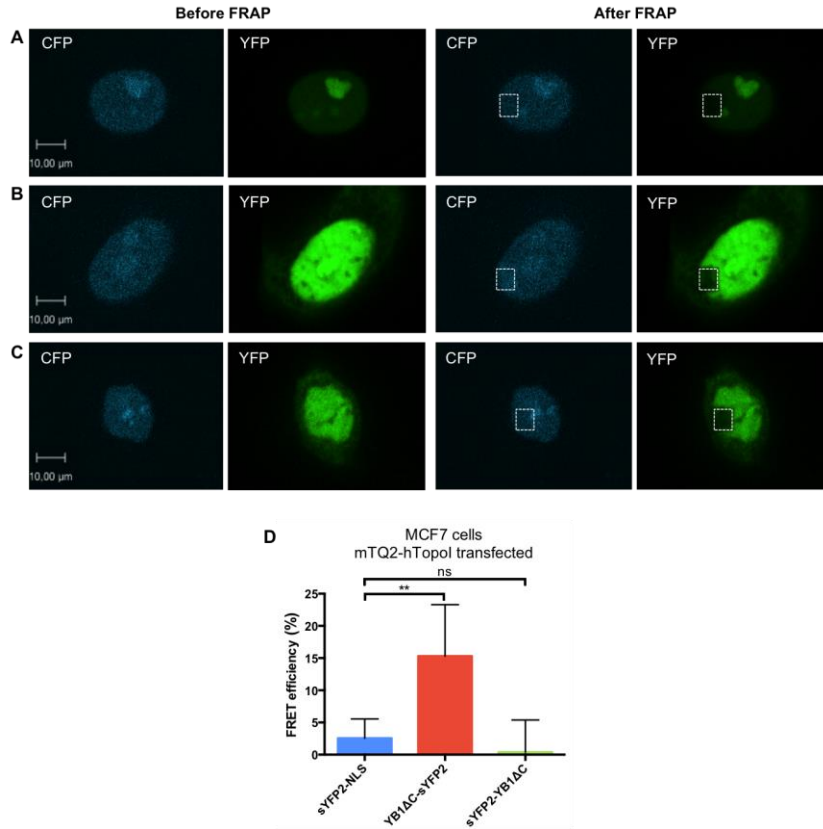


Figure 3.57. FRET measurements in MCF7 cells co-transfected with YB-1 Δ C and hTopoI. Representative epifluorescence microscopy images of MCF7 cells co-transfected with mTQ2-hTopoI and with sYFP2-NLS (A), YB-1 Δ C- sYFP2 (B) and sYFP2-YB-1 Δ C (C). mTQ2 is seen in the CFP channel (blue). sYFP2 is seen in the YFP channel (green). The white rectangle indicates the area of the nucleus that was photobleached. Scale bar: 10 μm . (D) FRET efficiencies measured in MCF7 cells co-transfected with mTQ2-hTopoI and sYFP2 fusion constructs. The presented data are the mean of at least five replicates.

3.6.3. FRET measurements in PC-3 cells

In the literature, the interaction between hTopoI and YB-1 had previously been detected in the prostate cancer cell line, PC-3 (Wu et al., 2014). We thus set out to investigate whether we could also detect FRET in PC-3 cells co-expressing hTopoI and YB-1. First, we transfected our PC-3 cells with 2A constructs. We observed co-expression of sYFP2-NLS and mTQ2-hTopoI in the nucleus (Figure 3.58 A), but all cells transfected with either the 2A or 2A NLS construct (containing YB-1 Δ C) showed mostly cytoplasmic staining for the sYFP2 (Figure 3.58 B and C). Therefore, we could not perform acceptor photobleaching experiments.

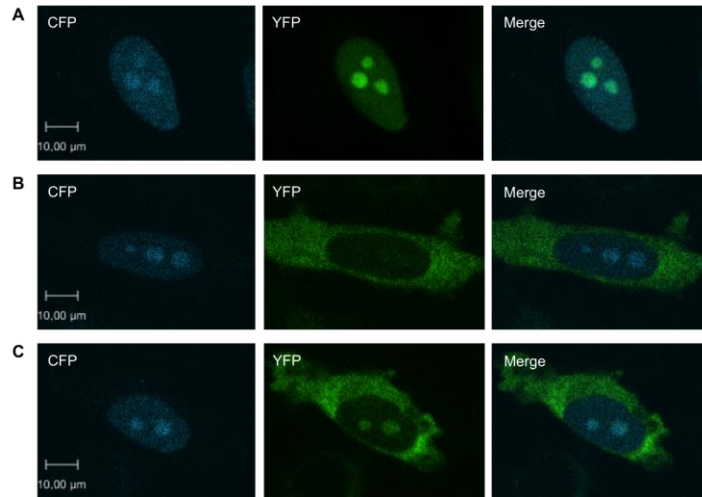


Figure 3.58. Cellular distribution of sYFP2 and mTQ2 signals in PC-3 cells transfected with 2A constructs. Representative epifluorescence microscopy images of PC-3 cells transfected with pYFP2-NLS-2A-mTQ2-hTopoI (A), pYB-1ΔC-sYFP2-2A-mTQ2-hTopoI (B), pYB-1ΔC-sYFP2-NLS-2A-mTQ2-hTopoI (C). mTQ2 is seen in the CFP channel (blue). sYFP2 is seen in the YFP channel (green). The last column shows merged images. Scale bar: 10μm.

We then performed co-transfection and acceptor photobleaching experiments with the individual constructs in PC-3 cells (Figure 3.59). The expression levels of hTopoI constructs fused with mTQ2 in PC-3 cells were very low.

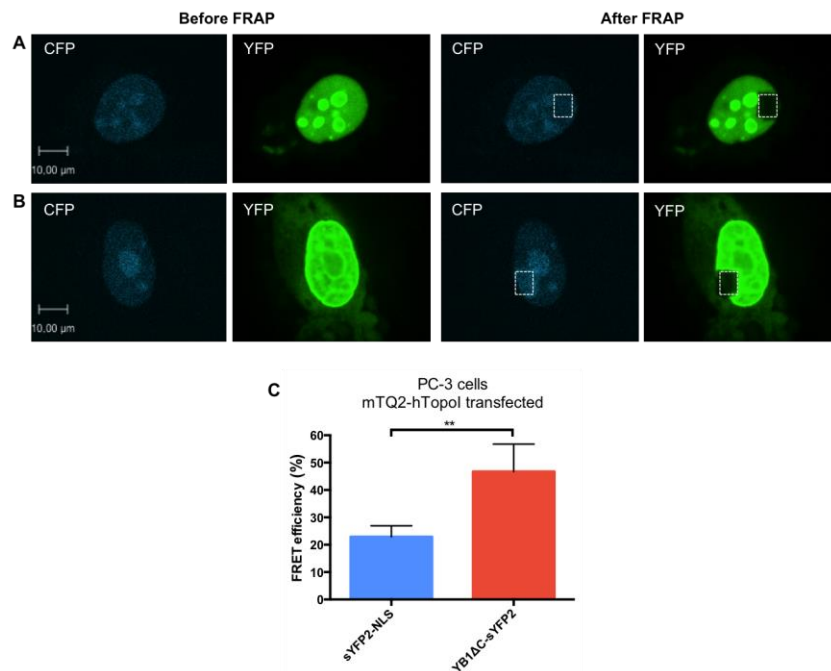


Figure 3.59. FRET measurements in PC-3 cells co-transfected with YB-1ΔC and hTopoI. Representative epifluorescence microscopy images of PC-3 cells co-transfected with mTQ2-

hTopoI and either sYFP2-NLS (**A**) or YB-1 Δ C-sYFP2 (**B**). mTQ2 is seen in the CFP channel (blue). sYFP2 is seen in the YFP channel (green). The white rectangle indicates the area of the nucleus that was photobleached. Scale bar: 10 μ m. (**C**) FRET efficiencies measured in PC-3 cells co-transfected with mTQ2-hTopoI and sYFP2 fusion constructs. The presented data are the mean of at least five replicates.

Our negative control (PC-3 cells co-transfected with mTQ2-hTopoI and sYFP2-NLS) showed a higher FRET efficiency compared to other cell lines. However, the PC-3 cells co-transfected with mTQ2-hTopoI and YB-1 Δ C-sYFP2 showed significantly higher FRET efficiency compared to the negative control suggesting hTopoI and YB-1 Δ C may interact in PC-3 cells (Figure 3.59 C). The FRET signal varied a lot from cell to cell, suggesting the interaction may require a special condition. We also performed the same experiments in PC-3 cells with the hTopoI-mTQ2 construct (with mTQ2 fused to the C-terminus of hTopoI), and obtained high FRET efficiencies (around ~54 %) for both the negative control (co-transfected with sYFP2-NLS) and the interaction experiment (co-transfected with YB-1 Δ C-sYFP2). No reliable conclusions could thus be drawn from these experiments in PC-3 cells.

Chapter 4. Discussion

Summary

FRENCH

Partie I. Complexe de YB-1/hNTH1

La variation d'une cellule à l'autre du signal FRET émanant de l'interaction entre hNTH1 et YB-1 dans les cellules MCF7 suggère que certaines cellules sont exposées au stress dû au processus de transfection ou à la surexpression YB-1 Δ C, qui peut influencer la signalisation cellulaire et d'autres processus cellulaires, ce qui peut favoriser l'interaction entre YB-1 Δ C et hNTH1. Nous avons seulement détecté de faibles niveaux de FRET dans les cellules MCF7 exprimant le Biosenseur 1 dans le noyau; ceci résulte peut-être du ratio 1:1 des protéines dans la construction du Biosenseur 1. Il n'y a aucune information sur la stœchiométrie du complexe YB-1/hNTH1, mais peut-être que l'oligomérisation de YB-1 est nécessaire pour une liaison efficace à hNTH1, ce qui expliquerait pourquoi le signal FRET fort a été détecté seulement dans les cellules MCF7 surexprimant YB-1. YB-1 peut fonctionner de manière similaire à p53, qui est connu pour sa capacité à adopter différentes formes oligomériques qui stimulent différents processus. Contrairement aux expériences de FRET *in vivo*, le signal FRET obtenu en mélangeant des protéines fluorescentes fusionnées à YB-1 et hNTH1 était stable et reproductible. Des concentrations de sel plus élevées bloquent les interactions ioniques entre les surfaces protéine-protéine et l'interaction entre YB-1 et hNTH1 est sensible à la force ionique du tampon de réaction. En raison de la haute sensibilité du FRET et de son aptitude à la spectroscopie et à l'analyse par imagerie, de nombreux efforts ont été déployés pour développer des expériences quantitatives et des tests de criblage à haut débit (HTS). D'autres techniques, telles que le FRET résolu dans le temps et l'AlphaScreen, sont également utilisées pour l'HTS. Chaque méthode a ses avantages et ses inconvénients. En l'absence d'informations structurelles concernant le complexe YB-1/hNTH1, nous avons choisi de développer un test de criblage FRET à haut débit pour rechercher des inhibiteurs potentiels du complexe. Bien que l'utilisation d'une quantité réduite de Biosenseur 1 nous ait permis de cribler plus de composés avec une quantité donnée de protéines, cela a affecté dans une certaine mesure la reproductibilité de

notre test. Il est difficile de trouver un bon contrôle positif lors du développement d'un test d'activité. Nous avons utilisé un substrat spécifique de hNTH1 pour perturber le signal FRET provenant de l'interaction YB-1/hNTH1. L'ajout de substrat de hNTH1 (oligonucléotide dsDNA de 12nt THF) réduit les efficacités FRET des Biosenseurs, mais n'affecte pas le signal de fusion de sYFP2-mTQ2.

En HTS, l'obtention d'une seule mesure de chaque composé pour le criblage primaire est associée à une proportion élevée de faux positifs. Dans notre cas, nous avons effectué des mesures une seule concentration de composé (50 μ M) en triplicatas pour minimiser le nombre de faux positifs. Ensuite, au cours du criblage secondaire de 30 composés sélectionnés, nous avons réalisé des HTS avec des concentrations de composés à 50, 10 et 1 μ M afin d'étudier leurs profils de dose-réponse pour éliminer les inhibiteurs faibles. Lors de la dernière étape, validation des "hits", nous avons rencontré plusieurs problèmes. Les composés identifiés comme inhibiteurs de la bibliothèque Life Chemicals ont émis une fluorescence à une longueur d'onde similaire à celle du donneur, conduisant à une augmentation apparente du signal mTQ2 du Biosenseur 1, qui apparaît comme une diminution du taux de FRET. Notre analyse spectrale des composés Prestwick inhibiteurs du FRET Biosenseur 1 et la comparaison des effets de ces composés provenant de différentes sources ont révélé que ces impacts initiaux identifiés par la plateforme CMBA peuvent ne pas correspondre aux composés attendus, mais plutôt à des formes dégradées ou modifiées de ces produits chimiques. La perte ou l'instabilité du composé pendant le stockage à long terme et plusieurs cycles de congélation-décongélation peuvent expliquer pourquoi nous n'avons pas réussi à reproduire les effets inhibiteurs de certains des composés Prestwick sélectionnés lorsque nous préparions des solutions fraîches à partir de poudres commandées chez Sigma. Dans certains cas, le stockage des composés à 4°C pendant 2 à 3 jours a amélioré leur effet, ce qui pourrait aussi résulter d'une lente solubilisation de ces composés.

À l'avenir, la nature chimique exacte de ces inhibiteurs potentiels devra être déterminée et les valeurs de IC₅₀ de ces composés actifs déterminées avec précision en utilisant le test Biosenseur 1, mais aussi avec un test alternatif tel que l'AlphaScreen.

Partie II. Complexe de YB-1/hTopoI

Pour purifier hTopoI, plusieurs systèmes d'expression ont été utilisés, le système baculovirus-cellule d'insecte étant le plus largement utilisé pour les analyses structurales. Nous avons exprimé hTopoI dans des cellules *E. coli* BL21 en utilisant un ADNc optimisé par codon avec des marqueurs His N-terminaux ou C-terminaux. Nous avons observé plusieurs formes dégradées après la purification par affinité sur résine nickel, avec une forme tronquée majeure avec un poids moléculaire proche de 70 kDa. Ces multiples espèces pourraient être expliquées par des éléments promoteurs procaryotes et/ou des signaux d'initiation de traduction procaryotes conduisant à l'expression et/ou à la traduction de formes hTopoI tronquées. Elles peuvent également provenir de la protéolyse de la protéine après traduction, bien que notre mutant hTopoI dans lequel K172 a été remplacé par de l'alanine a également été soumis à un clivage, ce qui suggère que cela ne soit pas la cause principale de la troncation. Notre hTopoI-70 étant dépourvue des résidus 1-172, l'obtention de la même activité que hTopoI-FL était un résultat attendu et confirme que les 172 résidus N-terminaux sont dispensables pour l'activité de relaxation de l'ADN de hTopoI. Dans la littérature, les résidus 191-206 dans le domaine N-terminal de hTopoI se sont révélés être impliqués dans le contrôle de l'étape de rotation des brins de la catalyse et la médiation des contacts à l'ADN en aval du site de clivage. Nous avons démontré que la forme nucléaire de YB-1, YB-1 Δ C, stimule spécifiquement l'activité de relaxation de l'ADN de hTopoI-FL et hTopoI-70, indiquant que les 172 premiers résidus du domaine N-terminal ne sont pas essentiels pour cette stimulation YB-1 Δ C-dépendante.

Nous avons démontré une interaction directe de YB-1 Δ C avec hTopoI en mélangeant des protéines marquées par fluorescence purifiée à une concentration de 1 μ M en utilisant des mesures de FRET *in vitro*, suggérant que l'affinité de l'interaction entre YB-1/hTopoI peut être supérieure à celle de l'interaction YB-1/hNTH1. Parce que le signal FRET avec hTopoI-70 n'a pas été complètement perdu, d'autres régions de hTopoI peuvent également être nécessaires pour l'interaction, comme suggéré par nos expériences de relaxation d'ADN dans lesquelles hTopoI-70 a également été stimulée par YB-1 Δ C.

Dans des expériences de co-transfection, un signal FRET considérable a été observé dans les cellules MCF7 et PC-3 transfectées avec mTQ2-hTopoI et YB1 Δ C-sYFP2 comparées aux cellules témoins négatives transfectées avec mTQ2-hTopoI et sYFP2-NLS. Cependant, comme dans le cas de YB-1/hNTH1, la surexpression de YB1 Δ C-sYFP2 était nécessaire pour détecter un signal FRET clair, indiquant que des formes oligomériques supérieures de YB-1 pourraient être nécessaires pour interagir avec hTopoI, comme cela a été observé pour p53.

Il a été montré que PARP-1, un régulateur clé des événements de réparation de l'ADN, peut inhiber l'activité de relaxation de hTopoI par pADP-ribosylation *in vitro*. Pour cette raison, les inhibiteurs de PARP sont maintenant utilisés dans des essais cliniques pour améliorer la cytotoxicité de la caomptothécine (CPT). La stimulation de PARP-1 par YB-1 a également été démontrée récemment et cette stimulation diminue la sensibilité des cellules aux inhibiteurs de PARP-1. Si YB-1 augmente l'activité de PARP-1, ceci pourrait à son tour provoquer une inhibition de l'activité catalytique de hTopoI par la ribosylation de pADP. YB-1 semble donc jouer un rôle régulateur complexe dans les cellules via ses différents partenaires d'interaction, et ces résultats apparemment contradictoires peuvent résulter de différents mécanismes régulateurs dans les cellules et/ou différents niveaux d'expression des protéines dans différentes cellules tumorales.

Effectuer des expériences EMSA pour étudier l'effet de YB-1 sur la liaison à l'ADN de hTopoI fournira plus d'informations sur l'effet stimulant de YB-1 sur l'activité de relaxation de hTopoI. D'autres méthodes biochimiques et biophysiques, telles que la résonance plasmonique de surface (SPR), la calorimétrie par titration isotherme (ITC) et AlphaScreen, pourraient également être utilisées pour étudier davantage l'interaction de YB-1 avec hTopoI.

Özet

TURKISH

Bölüm I. YB-1/hNTH1 kompleksi

FRET sinyalinin hücreden hücreye farklılık göstermesinin nedenlerinden biri, tüm hücrelerde gerçekleşmezken bazı hücrelerin transfeksiyon sürecine veya hücre sinyallerini ve diğer hücresel süreçleri etkileyebilen YB-1ΔC aşırı ekspresyonuna bağlı olarak strese maruz kalması, bunların da YB-1ΔC ve hNTH1 arasındaki etkileşimi desteklemesi olabilir. Biosensör 1'i hücre çekirdeğinde eksprese eden MCF7 hücrelerinde düşük FRET seviyeleri gözlenmiştir. Bu durum Biosensor 1'deki proteinlerin bire bir oranında olmasından kaynaklanabilir. YB-1/hNTH1 kompleksinin stokiometrisi hakkında herhangi bir bilgi yoktur, fakat güçlü FRET sinyalinin sadece YB-1'i aşırı eksprese eden MCF7 hücrelerinde tespit edilmesi belki de YB-1'in oligomerizasyonunun, hNTH1'e etkili bağlanma için gerekli olduğunu düşündürmektedir. YB-1, farklı süreçleri uyaran farklı oligomerik formları olduğu bilinen p53'e benzer bir şekilde işlev görebilir. *In vivo* FRET deneylerinin aksine, saflaştırılmış floresan proteinlerle füzyon olan hNTH1 ve YB-1ΔC proteinlerinin karıştırılması ile yapılan FRET ölçümlerinden elde edilen FRET sinyali stabil ve tekrarlanabilir. Yüksek tuz konsantrasyonları protein-protein yüzeyleri arasındaki iyonik etkileşimleri bloke eder bu nedenle YB-1 ile hNTH1 arasındaki etkileşim, reaksiyon tamponunun iyonik şiddetine duyarlıdır. FRET'in yüksek hassasiyeti ve hem spektroskopi hem de görüntüleme analizi için uygunluğu nedeniyle, kantitatif deneyler ve yüksek verimli tarama (HTS) analizleri geliştirmek için çokça kullanılmaktadır. Zaman çözümlü FRET ve AlphaScreen gibi diğer teknikler de HTS için kullanılmaktadır. Her yöntemin avantajları ve dezavantajları vardır. YB-1/hNTH1 kompleksine ilişkin yapısal bilgilerin yokluğundan, kompleksin potansiyel inhibitörlerini araştırmak için yüksek verimli FRET-bazlı bir tarama testi geliştirilmesi düşünülmüştür. Biosensor 1'in düşük konsantrasyonda kullanılması, belirli bir miktarda protein ile daha fazla bileşiğin taranmasına izin verse de, çalışmamızın tekrarlanabilirliğini bir dereceye kadar etkilemiştir. Bir tarama testi geliştirirken iyi bir pozitif kontrol bulmak zordur. YB-1/hNTH1 etkileşiminden gelen FRET sinyalini bozmak için

hNTH1'in hidrolize edemediği bir substratı kullanılmıştır. hNTH1 substratının (12nt THF dsDNA oligonükleotid) eklenmesi, biyosensörlerin FRET verimini azaltırken sYFP2-mTQ2 füzyon proteinin sinyalini etkilemez.

HTS'de, birincil tarama için her bir bileşiğin tek bir ölçümünün elde edilmesi, yüksek oranda yanlış pozitiflerle ilişkilendirilmiştir. Bizim durumumuzda, yanlış pozitiflerin sayısını en aza indirmek için tek bir bileşik konsantrasyonunun (50µM) ölçümlerini üç kez gerçekleştirdik. Daha sonra, seçilen 30 bileşiğin ikincil taraması sırasında, zayıf inhibitörleri elemek amacıyla konsantrasyon-cevap profillerini araştırmak için 50, 10 ve 1 µM'lik bileşik konsantrasyonları ile HTS gerçekleştirilmiştir. Son adım olan “isabetlerin” doğrulanması sırasında birkaç problemle karşılaşmıştır. Life Chemicals kimyasal kütüphanesinden inhibitör olarak tanımlanan bileşikler, donöre benzer bir dalga boyunda floresan yaymıştır bu da Biosensor 1'in mTQ2 sinyalinde belirgin bir artışa neden olmuştur. Bunun sonucunda da FRET seviyesini azalttıkları belirlenmiştir. Biyosensör 1 FRET sinyalini inhibe eden seçilmiş Prestwick bileşiklerinin spektral analizleri ve bu bileşiklerin farklı kaynaklardan gelenlerinin etkilerinin karşılaştırılması, CMBA platformu tarafından belirlenen bu başlangıç isabetlerinin beklenen bileşiklere karşılık gelmediğini, bunun yerine bozulmuş veya modifiye olmuş formlarından meydana geldiğini ortaya çıkarmaktadır. Uzun süreli depolama ve çoklu donma-çözülme döngüleri sırasında bileşik kaybı veya kararsızlığı, Sigma'dan sipariş edilen tozları kullanarak taze çözeltiler hazırladığımız zaman, seçilen Prestwick bileşiklerinin bazılarının önleyici etkilerini neden yeniden üretemediğimizi açıklayabilir. Bazı durumlarda bileşiklerin 4°C'de 2-3 gün saklanması etkilerini geliştirmiş, bu bileşiklerin yavaş çözünmesinden kaynaklanabilmektedir.

Gelecekte, bu potansiyel inhibitörlerin tam kimyasal yapısı belirlenmeli ve bu aktif bileşiklerin IC₅₀ değerleri, Biyosensör 1 testi kullanılarak ve aynı zamanda AlphaScreen gibi alternatif bir deneyle de belirlenmelidir.

Bölüm II. YB-1/hTopoI kompleksi

hTopoI'yi saflaştırmak için, çeşitli ekspresyon sistemleri kullanılmıştır ve bakulovirüs ekspresyon sistemi, yapısal analizler için gerekli protein eldesi için en yaygın olarak kullanılanıdır. *E. coli* BL21 hücrelerinde, N veya C terminali His-etiketleriyle kodonu optimize edilmiş cDNA kullanılarak hTopoI'i ifade etmeyi başardık. Nikel afinite saflaştırması sonucunda, 70 kDa'ya yakın bir moleküler ağırlığa sahip, büyük bir degrade form ile birkaç değişik degrade form gözlemlenmiştir. Bu değişik degrade formlar, prokaryotik promoter elementler ve/veya prokaryotik translasyon başlatma sinyallerinin bölünmüş hTopoI formlarının ekspresyonuna ve/veya translasyonuna yol açması sonucu ortaya çıkabilmektedir. Ayrıca bu durum, proteolitik bozunmadan da kaynaklanabilirler. Ancak lizin172'nin alanin ile değiştirildiği hTopoI mutantımızın da degradasyona maruz kalmasından dolayı bu degradasyonun ana nedeni olmayabileceği düşünülmektedir. hTopoI-70'in 1-172 arasındaki amino asit kalıntıları eksiktir, ancak hTopoI-FL ile aynı aktiviteyi göstermektedir. Bu literatürde olduğu gibi beklenen bir sonuçtur, N-terminal domaininde bulunan 172 amino asit kalıntılarının hTopoI'nin DNA relaksasyon aktivitesi için gerekli olmadığını teyit etmektedir. Literatürde, hTopoI'nin N-terminal alanındaki 191-206 amino asit kalıntılarının, enzimin iplik döndürme adımının kontrol edilmesinde ve kesim bölgesinin aşağısındaki DNA'ya temasında rol oynadığı gösterilmiştir. YB-1ΔC, YB-1'nin nükleer formu, hem hTopoI-FL'nin hem de hTopoI-70'in DNA relaksasyon aktivitesini spesifik olarak uyardığı ve N-terminal domainin ilk 172 amino asit kalıntısının bu YB-1ΔC bağımlı stimülasyon için gerekli olmadığını gösterilmiştir.

YB-1ΔC'nin hTopoI ile doğrudan etkileşimini, saflaştırılmış floresan proteinlerle füzyon olan hTopoI ve YB-1ΔC proteinlerinin 1 μM konsantrasyonunda karıştırmak suretiyle FRET ölçümleri ile gösterilmiş ve bu da YB-1/hTopoI etkileşim afinitesinin YB-1/hNTH1 etkileşiminden daha yüksek olabileceğini düşündürmektedir. hTopoI-70 ile FRET sinyali azalıp ancak tamamen kaybolmadığından, hTopoI-70'in de YB-1ΔC tarafından uyarıldığı DNA relaksasyon deneyleri tarafından da önerildiği için, etkileşim için başka hTopoI bölgeleri de gerekmektedir.

Ko-transfeksiyon deneylerinde, mTQ2-hTopoI ve sYFP2-NLS ile transfeke edilen negatif kontrol hücreleri ile karşılaştırıldığında mTQ2-hTopoI ve YB1ΔC-sYFP2 ile transfeke edilen MCF7 ve PC-3 hücrelerinde anlamlı bir FRET sinyali gözlenmiştir. Bununla birlikte, YB-1/hNTH1 durumunda olduğu gibi, net bir FRET sinyalinin saptanması için YB1C-sYFP2'nin aşırı ekspresyonu gereklidir, bu da p53'de gözlemlendiği gibi, hTopoI ile etkileşime girmek için YB-1'in daha yüksek oligomerik formlarının gerekli olabileceğini göstermektedir.

DNA onarım olaylarının anahtar regülatörü olan PARP-1'in, *in vitro* olarak pADP-ribosilasyonu ile hTopoI relaksasyon aktivitesini inhibe ettiği gösterilmiştir. Bu nedenle, PARP inhibitörleri CPT'nin sitotoksitesini artırmak için klinik çalışmalarda kullanılmaktadır. PARP-1'in son zamanlarda YB-1 ile uyarıldığı gösterilmiştir ve bu uyarım hücrelerin PARP-1 inhibitörlerine olan duyarlılığını azaltmaktadır. YB-1, PARP-1'in aktivitesini arttırırsa, bu durum, hTopoI'nin katalitik aktivitesinin pADP-ribosilasyonu ile engellenmesine neden olabilmektedir. Dolayısıyla YB-1, çeşitli etkileşim partnerleri aracılığıyla hücrelerde karmaşık bir düzenleyici rol oynamaktadır ve literatürdeki çelişkili bulgular, farklı tümör hücrelerindeki farklı düzenleyici mekanizmalardan ve/veya farklı protein ekspresyon seviyelerinden kaynaklanabilmektedir.

YB-1'in hTopoI'nin DNA bağlanması üzerindeki etkisini araştırmak için EMSA deneylerinin yapılması, YB-1'in hTopoI'nin relaksasyon aktivitesi üzerindeki uyarıcı etkisi hakkında daha fazla bilgi sağlayacaktır. Yüzey Plazmon Rezonansı (SPR), İzotermal titrasyon kalorimetrisi (ITC) ve AlphaScreen gibi diğer biyokimyasal ve biyofiziksel yöntemler, YB-1'in hTopoI ile etkileşimini daha fazla araştırmak için kullanılabilir.

Part I. YB-1/hNTH1 complex

We successfully demonstrated the YB-1/hNTH1 interaction using FRET method in MCF7 cells and *in vitro* with purified proteins. We created a robust and reliable FRET-based assay using our Biosensor 1 construct, for high throughput screening in order to find potential inhibitors of the YB-1/hNTH1 complex. We identified several promising compounds in the Prestwick Chemical library that significantly reduced the FRET signal of our Biosensor 1.

We obtained a significant FRET signal with a MCF7 stable cell line expressing hNTH1-mTQ2 and transfected with YB1ΔC-sYFP2, but only in cells in which YB-1ΔC was strongly overexpressed (Figure 3.2). This observation is not surprising because YB-1 has been reported to interact and regulate the activity of hNTH1 under genotoxic stress conditions, such as cisplatin treatment in the MCF7 cells (Guay et al., 2008). During acceptor photobleaching experiments, FRET signal varied from cell to cell. It is possible that some cells are exposed to stress due to the transfection process or YB-1ΔC overexpression, which can influence cell signalling and other cellular processes, which in turn may favour the interaction between YB-1ΔC and hNTH1.

We encountered cellular localisation problems during transfection of MCF7 cells with the Biosensor 1 construct. A possible reason for this could be that the endogenous NLS signals of YB-1ΔC and hNTH1 were no longer accessible when the proteins were joined together in the Biosensor construct. Changing the relative positions of the proteins within the biosensor construct may overcome this problem. In some cases, Biosensor 1 was also degraded and CFP and YFP staining were observed in the nucleus and cytoplasm, respectively. This suggests that the linkers between the proteins and particularly between YB-1ΔC and hNTH1, are protease-sensitive. This could be avoided or minimised by changing the sequence of these linker regions. When we performed acceptor photobleaching experiments in MCF7 cells expressing the Biosensor 1 in the nucleus, we only detected low levels of FRET. This may result from the 1:1 ratio of the proteins in the Biosensor 1 construct. There is no information about the stoichiometry of the YB-1/hNTH1 complex, but maybe the oligomerization of

YB-1 is needed for efficient binding to hNTH1, which would explain why strong FRET signal was only detected in YB-1 overexpressing MCF7 cells. YB-1 may function similarly to p53, which is known to adopt different oligomeric forms that stimulate different processes (Søe and Grosse, 2003).

FRET measurements by mixing fluorescent proteins fused to YB-1 and hNTH1 confirmed our FRET experiments in MCF7 cells. Contrary to *in vivo* FRET experiments, the obtained FRET signal was stable and reproducible. Because FRET is a distance-sensitive method (less than 10 nm), the positions and orientations of fluorescent proteins are important in obtaining a FRET signal. The FRET efficiencies of mixtures were affected by the position of the fluorescent protein, as in the *in vivo* FRET experiments. The highest FRET signal was obtained when both mTQ2 and sYFP2 were fused to the C-termini of hNTH1 and YB-1 Δ C, respectively. In this condition, a FRET signal of ~ 7% could be reproducibly measured which is significantly higher than our negative control (YB-1 Δ C-sYFP2 mixed with mTQ2 alone) (Figure 3.16). The concentration of mixture was also important. Below 5 μ M concentration no FRET signal was detected. This may reflect the affinity or the stoichiometry of the complex. As we observed in MCF7 cells, an excess of YB-1 may be necessary for complex formation. Optimal buffer conditions were also critical to detect the FRET signal. At NaCl concentrations higher than 50 mM, we could not detect a significant FRET signal. This indicates that the interaction between YB-1 and hNTH1 is sensitive to the ionic strength of the reaction buffer. Higher salt concentrations block ionic interactions between protein-protein surfaces (Dumetz et al., 2007). The purity of protein samples is also very important, especially for nucleic acid-binding proteins. A contamination of RNA and/or DNA can affect the interaction of these proteins. For this reason, we performed several chromatographic steps to ensure complete elimination of nucleic acid contamination in our purification procedure (Figure 2.5). Some biochemical methods for investigation of protein-protein interaction, like co-immuno precipitation, may give misleading results with nucleic acid-binding proteins even after nuclease treatment where nucleic acid contaminations are still present.

Biosensor 1 FRET signal is robust and reproducible. It is a very simple assay, which does not require mixing different reagents or long incubation periods. Because of the FRET's high sensitivity and its suitability for both spectroscopy and imaging analysis, much effort has been made to develop quantitative experiments and HTS assays (Song et al., 2011; Rogers et al., 2012; Schaap et al., 2013; Chakraborty et al., 2014; Wei et al., 2014). However, due to the low FRET yield of fluorescent proteins and the complexity of fluorescence emissions from the donor and acceptor, it has been a very difficult process to evolve FRET into a quantitative assay. Nevertheless, with promising improvements in fluorescent proteins, researchers have tried to overcome these problems (Kremers et al., 2006; Mastop et al., 2017). The cross-talk in the fluorescent protein-based FRET can be corrected for, which minimises these issues for example. FRET is usually performed as ratiometric assays, which reduces the effects of autofluorescence and spectral interference of media and test compounds. But in some cases, if the autofluorescence of compounds overlaps with donor emission signal, it may lead to false positive results as we encountered with the three compounds from Life Chemicals PPI fragment library. Some compounds that strongly absorb UV light can inhibit excitation of the FRET donor, which absorbs in the far-UV region (ca. 350 nm).

FRET methods are relatively easy to automate and to miniaturize. They can be used with a wide range of protein sizes, with the provision that the FRET pairs must come within a few nanometers from each other. The size of the complex can be limited by the distance and the orientation of the fluorescent proteins. For very large complexes, the AlphaScreen assay that allows detection of interactions within a distance of 200 nm may be more suitable. Alpha technologies are adaptable to many assay types, are very sensitive, and are active over long distances (200 nm vs 10-20 nm for TR-FRET). The central limitations to AlphaScreen and AlphaLisa are the increased expense compared with other mix-and-read formats and the sensitivity of the materials to ambient light.

Glickman et al., 2002, compared AlphaScreen, time-resolved fluorescence resonance energy transfer (TR-FRET), and time-resolved fluorescence (TRF), and concluded that the AlphaScreen format had the best sensitivity, dynamic range,

and decreased plate-reading time. These techniques varied in the detection reagents and optical plate-reading system used. Of the three formats, TR-FRET assay had the least inter-well variation, most likely because it is a ratiometric type of measurement. Both FRET-type and AlphaScreen formats can measure a wide range of affinities (K_d 's ranging from low pM to low mM concentrations) because there are no wash steps. It is noteworthy that AlphaScreen beads have 300-3000 proteins/bead, and the protein density can be varied. This multi-valency can significantly increase sensitivity, because one PPI per bead pair leads to the maximal signal. With FRET methods, each binding partner carries a single label so that if some beads are unbound, a lower signal will be generated. However, monovalency also implies that the signal will be proportional to the number of binding interactions.

In the absence of structural information regarding the YB-1/hNTH1 complex, we chose to develop a high throughput FRET-based screening assay to search for potential inhibitors of the complex (Figure 4.1).

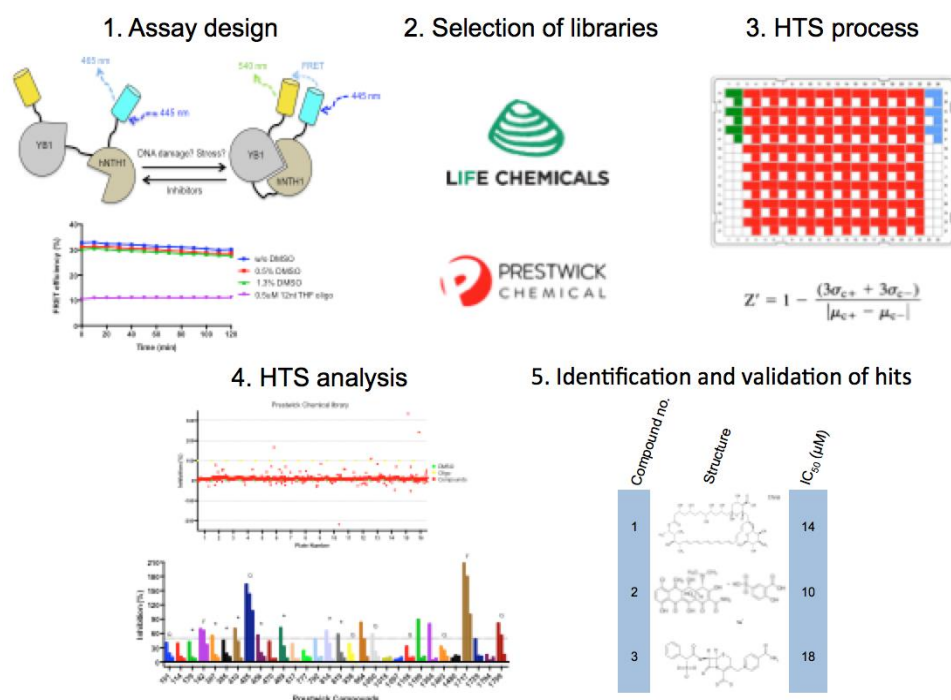


Figure 4.1. The steps of high throughput chemical library screening with Biosensor 1 in order to find potential inhibitors of YB-1/hNTH1 complex. Inspired from Inglese et al., 2007. The first step was the development and optimization of our robust and reliable Biosensor 1 assay. In the second step, Life Chemicals and Prestwick Chemical libraries were selected for HTS to find potential YB-

1/hNTH1 complex. Then, Robotic HTS was performed at CMBA platform with a 0.9 Z' factor value. The results obtained from our first and second screenings were analysed for the extent of inhibition. The last step is the validation of the hits by dose-response curves in order to obtain IC₅₀ values.

As with our FRET measurements on protein mixtures, higher salt concentrations significantly affected the FRET efficiencies of the biosensor, confirming that salt interferes with the interaction between hNTH1 and YB-1. High ionic strength was also found to reduce the FRET of our positive control (sYFP2-mTQ2 fusion) most likely as a result of non-specific effects (change in chromophore conformation, non-specific interactions between fluorescent proteins) (Figure 3.18). To our surprise, the biosensor concentration used also affected the levels of FRET. This was in marked contrast with the Fusion construct which produced a stable FRET signal regardless of its concentration in the reactions, as would be expected for intramolecular FRET. This finding suggests that the FRET signal of the biosensor may result from dimerization and intermolecular FRET.

We also observed variable FRET levels of the Biosensor 1 from day to day when preparing diluted samples (at 0.2 μ M) using different stocks of NaCl solutions and different tubes. Using untreated 384-well plates (without non-binding property) also affected the FRET signal of our Biosensor 1. So although using a reduced amount of Biosensor 1 allowed us to screen more compounds with a given amount of protein, it did affect to some extent the reproducibility of our assay. To minimise the impact of this variability on our screening results, we included both positive (0.5 μ M 12nt THF oligo) and negative (DMSO) controls in each 384-well plate during HTS and alongside all our subsequent measurements during validation experiments. In this way, our FRET levels could always be compared to those of our controls.

It is difficult to find a good bioactive control while developing a screening assay. High concentrations of detergent and/or urea have been showed to disrupt protein interactions (Song et al., 2011), but are not specific to the interaction and can affect the fluorescent proteins too. We used a specific substrate of hNTH1 to disrupt the FRET signal coming from YB-1/hNTH1 interaction. Addition of

hNTH1 substrate (12nt THF dsDNA oligonucleotide) reduces the FRET efficiencies of biosensors, but does not affect the signal of sYFP2-mTQ2 fusion (Figure 3.20 C). This suggests that the FRET signal results from a specific interaction between hNTH1 and YB-1 that has been disrupted by the interaction of hNTH1 with its DNA substrate. This may either result from competition for a shared binding site on hNTH1 or from a conformational change in hNTH1 upon DNA binding that leads to reduced FRET. Small angle X-ray scattering measurements performed in J. Timmins' team have indeed shown that hNTH1 undergoes a major conformational change upon DNA binding that involves its NTD, the region that we have shown to be important for YB-1 binding (unpublished data). The hNTH1 substrate was thus used to evaluate the robustness of our assay, which based on its Z' factor values was found to be highly robust and well suited to screen chemical libraries (Table 3.3).

We chose two relatively small libraries (~ 1000 compounds) for our initial screens for potential inhibitors of the YB-1/hNTH1 complex: the Life Chemicals PPI fragment library and the Prestwick Chemical library. These screens were well adapted to test the usefulness of our Biosensor 1 as a screening assay and were sufficiently diverse to provide us with some initial, promising hits. Moreover, the advantage of the Prestwick Chemical library is that it contains 95 % approved drugs (FDA, EMA and other agencies), which can facilitate and accelerate subsequent drug development processes.

In HTS, obtaining a single measurement of each compound for the primary screen has been associated with a high proportion of false positives (Malo et al., 2006). In our case, we performed our measurements at a single compound concentration (50 μ M) in triplicate to minimize the number of false positives. Then, during the secondary screening of 30 selected compounds, we performed HTS with 50, 10 and 1 μ M compound concentrations in order to investigate their concentration-response profiles eliminating weak inhibitors.

During the last step, validation of the "hits", we encountered several problems. The compounds identified as inhibitors from the Life Chemicals library emitted fluorescence at a similar wavelength as the donor (Table 3.5), leading to

an apparent increase in Biosensor 1's mTQ2 signal, which appears as a decreased FRET level. Determining the intrinsic fluorescence of compounds is thus very important to avoid false positive results and we therefore integrated this step into our secondary screening of the Prestwick compounds. This is not only a problem in FRET; in AlphaScreen/AlphaLisa assays the compounds can also interfere with the assay technology by four mechanisms, including those mimicking biotin, quenching singlet oxygen, quenching light, and scattering light (Yasgar et al., 2016). We observed a drastic AlphaLisa signal decrease with Mitoxantrone (even at very low concentrations) during validation tests, suggesting Mitoxantrone, which is a dark solution, was quenching the light produced by the AlphaLisa beads.

Our spectral analysis of the selected Prestwick compounds that inhibited Biosensor 1 FRET (Figure 3.36) and the comparison of the effects of these compounds from different sources (Figure 3.35) revealed that these initial hits identified by the CMBA platform may not correspond to the expected compounds, but rather to degraded or modified forms of these chemicals. The degraded/modified forms of these Prestwick compounds appear to be in most cases more active as inhibitors of the YB-1/hNTH1 interaction than their native formula. Only Cefsulodin and Mitoxantrone were not affected by long storage times and gave similar results when tested from freshly dissolved powders as those obtained from the CMBA platform. On HTS platforms, the use of solvents, and typically a single solvent (DMSO), for preparation of chemical libraries is a necessity for automated screenings. The solvent in which the compounds are dissolved may catalyse or participate in certain reactions, leading to the degradation of the compounds. There are several studies investigating the stability of compounds in DMSO. One of them showed that there is no significant degradation after 25 freeze/thaw cycles by high-performance liquid chromatography–mass spectrometry analysis, but compound loss was observed (Kozikowski et al., 2003). In another study, humidity was shown to be an important factor affecting compound stability. The degradation of target compounds was showed after treatment at 40°C in water-free DMSO by UV chromatogram. (Cheng et al., 2003). Compound loss or instability during long-term storage and multiple freeze-thaw cycles may explain why we failed to

reproduce the inhibitory effects of some of the selected Prestwick compounds when we prepared fresh solutions using powders ordered from Sigma. In some cases, storage of the compounds at 4°C for 2-3 days improved their potency, which could also result from slow solubilization of these compounds.

Additional experiments that might contribute to strengthen our data could be achieved by employing gas chromatography-tandem mass spectrometry (GC-MS/MS) and/or nuclear magnetic resonance (NMR) spectroscopy for further clarification of the exact chemical nature of these potential inhibitors. This might also be helpful in initiating an advanced structure-activity relationship study. The IC₅₀ values of these identified active compounds should be precisely determined using the Biosensor 1 assay, but also with an alternative assay such as the AlphaScreen. Cytotoxicity tests, like 3-(4,5-dimethylthiazol-2-yl)-2,5-diphenyl-2H-tetrazolium bromide (MTT) assay, should also be performed with the potential hits, before testing their ability to inhibit the interaction in cells using our FRET assay in our stably transfected MCF7 cells expressing mTQ2-hNTH1. It would also be interesting to create a cisplatin-resistant MCF7 cell line to evaluate the FRET signal and test for the ability of our potential inhibitors to sensitize this cell line. To further explore the importance of the YB-1:hNTH1 stoichiometry on complex formation, we could also create 2A co-expression constructs for hNTH1 and YB-1.

A manuscript describing these results is in preparation. It will present the characterization of the YB-1/hNTH1 interaction *in vitro* and *in vivo* using FRET, the design and optimization of our Biosensor constructs and the use of Biosensor 1 as a robust tool for HTS in order to find potential inhibitors for YB-1/hNTH1 complex.

Part II. YB-1/hTopoI complex

In this work, we have showed that YB-1 Δ C stimulates the DNA relaxation activity of both the full-length hTopoI and a N-terminally truncated form of hTopoI (hTopoI-70) *in vitro* using purified proteins produced in *E. coli*. We demonstrated a direct interaction of YB-1 with hTopoI by FRET and investigated the interaction between YB-1 and hTopoI in several cell lines (HeLa, MCF7, and PC-3). We detected some FRET signal with MCF7 and PC-3 cells co-transfected with mTQ2-hTopoI and YB-1 Δ C-sYFP2, but further studies will be needed to confirm these preliminary results.

To purify hTopoI, several expression systems have been used in the past, with the baculovirus-insect cell system being the most widely used for structural analyses (Stewart and Champoux, 1999; Peixoto et al., 2010; Tsai et al., 2010). The purification yields reported in these studies were of 250 μ g of purified hTopoI from 10^9 HeLa cells and ~ 10 mg of purified hTopoI from 3×10^9 insect cells (L. Stewart et al., 1996). In Dr. Joanna Timmins' lab, this system is not commonly used, so we decided to express hTopoI in *E. coli* BL21 cells using a codon-optimized cDNA with either N- or C-terminal His-tags. We observed several degraded forms after the nickel affinity purification, with a major truncated form with a molecular weight close to 70 kDa. We separated these fractions and obtained two active forms of hTopoI (FL and 70) from a single purification (Figure 3.41). Our purification yield for the C-terminal His-tagged proteins was low with ~ 55 μ g for hTopoI-FL and ~ 360 μ g for hTopoI-70 (Table 3.9) from 6 L of *E. coli* cells, but this was enough for our relaxation activity tests. To identify interaction domains of hTopoI, cloning of additional N-terminally truncated forms (Figure 3.40) was also performed, but we did not observe any expression of these truncated constructs in *E. coli* BL21 cells. In literature, multiple hTopo I-related protein species smaller than the full-length product were identified in *E. coli* expression (Madden and Champoux, 1992). These multiple species could be explained by prokaryotic promoter elements and/or prokaryotic translation initiation signals leading to expression and/or translation of truncated hTopoI forms. They may also arise from proteolytic degradation, although our hTopoI mutant in which K172 was replaced with alanine was also subject to

cleavage, suggesting this may not be the main cause of the truncation. In *E. coli*, overexpression of *hTopoI* gene has also been reported to be highly toxic (Madden and Champoux, 1992), which could explain why *E. coli* cells process the protein very rapidly after its production. Multiple degraded species of hTopoI could indeed be detected in cell extracts before cell lysis. The overexpression of the biosensor construct containing hTopoI in *E. coli* BL21 cells most likely failed because of these major degradation problems.

Our relaxation activity tests demonstrated that purified hTopoI-FL and hTopoI-70 had similar enzymatic activities even at low protein concentration. In literature, amino acid residues 191–206 in the N-terminal domain of hTopoI have been shown to be involved in controlling the strand rotation step of catalysis and mediating contacts to DNA downstream of the cleavage site (Lisby et al., 2001; Fröhlich et al., 2004). Our hTopoI-70 is lacking amino acid residues 1-172, therefore obtaining the same activity as hTopoI-FL was an expected result and confirms that the N-terminal 172 residues are dispensable for hTopoI's DNA relaxation activity. Both forms of hTopoI also exhibited similar sensitivities to the TopoI poison, CPT. The intrinsic sensitivity of hTopoI to CPT has been reported to be determined by the composition of the conserved core and active site Tyr 723 containing C-terminal domain (Wright et al., 2015), both of which are present in the two purified forms of hTopoI. Finally, we confirmed that YB-1 enhances the DNA relaxation by hTopoI (Wu et al., 2014), and additionally demonstrated that the nuclear form of YB-1, YB-1 Δ C, specifically stimulates the DNA relaxation activity of both hTopoI-FL and hTopoI-70, indicating the first 172 amino acid residues of the N-terminal domain of hTopoI are not essential for this YB-1 Δ C-dependent stimulation (Figure 3.46).

We then demonstrated a direct interaction of YB-1 Δ C with hTopoI by mixing purified fluorescently tagged proteins at 1 μ M concentration using FRET measurements (Figure 3.50). Obtaining a clear FRET signal at 1 μ M protein concentration, suggests that the YB-1/hTopoI interaction affinity may be higher than that of the YB-1/hNTH1 interaction. The FRET efficiencies of the mixtures were affected by the position of the fluorescent proteins, as seen for the YB-1/hNTH1 complex, but to a lesser extent. The highest signal was obtained when

both mTQ2 and sYFP2 were fused to the C-termini of hTopoI and YB-1 Δ C. The FRET signal significantly decreased in the absence of the N-terminal extension of hTopoI (hTopoI-70), indicating the first 172 amino acid residues of N-terminal domain play an important role in the direct interaction with YB-1 Δ C. Because the FRET signal with hTopoI-70 was not completely lost, other regions of hTopoI may also be needed for the interaction, as suggested by our DNA relaxation experiments in which hTopoI-70 was also stimulated by YB-1 Δ C. Alternatively, we cannot rule out that the relative orientation of the fluorescent proteins was more favourable for FRET in the case of hTopoI-FL compared to hTopoI-70. The purity of protein isolates was also critical for FRET measurements. We observed a significantly decreased FRET signal when the hTopoI-mTQ2 sample was contaminated with small amounts of hTopoI-70-mTQ2. YB-1 has been proposed to interact with hTopoI via its cold shock and C-terminal domains and this direct interaction is needed for enhancement of hTopoI's DNA relaxation activity (Wu et al., 2014). Our FRET studies clearly show that YB-1 Δ C, missing amino acid residues 219-324, was potent at interacting with hTopoI and stimulating its activity.

The interaction of YB-1 and hTopoI had previously been detected by co-immunoprecipitation experiments from human gastric cancer HGC-27, pancreatic cancer PANC-1, and human prostate cancer PC-3 cells (Wu et al., 2014). We tried to investigate this interaction by fluorescence microscopy using acceptor photobleaching method. We were able to express hTopoI constructs (hTopoI-mTQ2 and mTQ2-hTopoI) in three different mammalian cell lines (HeLa, MCF7 and PC-3) with low transfection efficiencies. The mTQ2-hTopoI construct showed better transfection efficiency and donor fluorescence intensity than the hTopoI-mTQ2 construct. Co-transfection of HeLa cells with mTQ2-hTopoI and with YB-1 Δ C constructs to perform FRET experiments did not work. The creation of a stable cell line, which expresses mTQ2-hTopoI constitutively, also failed, suggesting that maybe overexpression of hTopoI is toxic to cells. We therefore decided to use the 2A self-cleaving peptide-based multi-gene expression system (Wang et al., 2015) (Figure 3.54). No significant FRET signal could be detected with 2A constructs in HeLa and MCF7 cells (Figure 3.55 and 3.56). In PC-3 cells, we did not perform acceptor photobleaching experiments with the

cells transfected with the 2A constructs because a majority of cells showed YB-1 Δ C-sYFP2 expression in the cytoplasm instead of in the nucleus (Figure 3.58). In theory this 2A construct should provide equal expression (1:1 ratio) of both proteins. But a recent study suggests that protein expression decreases by ~70% at the second gene position compared to the first gene position in bi-cistronic 2A constructs (Liu et al., 2017). An incorrect stoichiometry of the produced YB-1/hTopoI complex, may explain why no FRET signal was detected with these 2A constructs. It is unclear at present why in some cases the YB-1 Δ C-sYFP2 expressed in these 2A constructs was sometimes mislocalised to the cytoplasm. Addition of an extra nuclear localisation signal (NLS) did not improve this, suggesting that it is not due to a poorly accessible NLS peptide.

In co-transfection experiments, a considerable FRET signal was observed in both MCF7 and PC-3 cells transfected with mTQ2-hTopoI and YB1 Δ C-sYFP2 compared to negative control cells transfected with mTQ2-hTopoI and sYFP2-NLS (Figure 3.57 and 3.59). However, as in the case of YB-1/hNTH1, the overexpression of YB1 Δ C-sYFP2 was required to detect a clear FRET signal, indicating that higher oligomeric forms of YB-1 may be needed to interact with hTopoI, as has been observed for p53 (Søe and Grosse, 2003). In PC-3 cells, many cells expressed sYFP2 constructs at very high levels and a relatively high FRET signal could also be measured in negative control samples (Figure 3.59 D). The high nuclear protein abundance in PC-3 cells may cause this increased, unspecific FRET signal.

PARP-1, a key regulator of DNA repair events, has been shown to inhibit the hTopoI relaxation activity by pADP-ribosylation *in vitro* (Kasid et al., 1989). For this reason, PARP inhibitors are now being used in clinical trials to enhance the cytotoxicity of CPT (Das et al., 2016). PARP-1 has also recently been shown to be stimulated by YB-1 and this stimulation decreases the sensitivity of cells to PARP-1 inhibitors (Alemasova et al., 2018). If YB-1 enhances the activity of PARP-1, this could in turn cause inhibition of hTopoI's catalytic activity by pADP-ribosylation. YB-1 thus appears to be playing a complex regulatory role in cells via its various interaction partners, and these apparently contradictory

findings may result from different regulatory mechanisms in cells and/or different protein expression levels in different tumour cells.

Performing EMSA experiments using labelled DNA substrates to investigate the effect of YB-1 on the DNA-binding of hTopoI will provide more information about YB-1's stimulatory effect on the relaxation activity of hTopoI. Other biochemical and biophysical methods, such as Surface Plasmon Resonance (SPR), Isothermal titration calorimetry (ITC), and AlphaScreen, could also be used to further investigate the interaction of YB-1 with hTopoI. We failed to produce a functional biosensor with YB-1 and hTopoI for inhibitor screening; however, alternative approaches such as HTRF could be used for chemical library screening. FRET studies of the YB-1/hTopoI complex should be pursued *in vivo* and it would be interesting to investigate the effect of CPT on the interaction in cells.

A manuscript reporting our data regarding the YB-1/hTopoI complex will be prepared in the near future.

Part III. Both hNTH1 and hTopoI complexes with YB-1

The intrinsically disordered structure of YB-1 is critical for its interactions with several partners and for the different functions it performs in the cell (Lyabin et al., 2014). Moreover, post-translational modifications of YB-1 (phosphorylation, acetylation, and ubiquitylation) resulting from the specific activation of signalling pathways in tumour cells may also regulate its functions in the cell (Kohn et al., 2003). An increase of the amount of YB-1 in the cell or its translocation from the cytoplasm to the nucleus have been shown to cause an increase or decrease of mRNAs or proteins encoded by many genes involved in cell proliferation, differentiation, multiple drug resistance and DNA repair (Eliseeva et al., 2011).

In MCF7 cells, we observed that YB-1 interacts with both hNTH1 and hTopoI, which clearly shows that YB-1 plays a complex, but central role and may regulate different cellular processes within a given cell type via its interactions with different proteins. In response to genotoxic stress, YB-1 is known to translocate into the nucleus and activate the expression of some genes, which are responsible for DNA repair, replication and other signalling pathways. It also interacts with nuclear proteins to regulate different processes like transcription and DNA repair. DNA topoisomerase I plays a role in the pause-release of transcription machinery by removing the positive supercoils, which represent a mechanical barrier in front of the RNA polymerase II (Baranello et al., 2016). Interactions between YB-1 and hTopoI are increased when tumour cells are exposed to drug-induced oxidative stress (Wu et al., 2014). By enhancing the relaxation activity of hTopoI, YB-1 may facilitate the initiation of gene transcription needed for the response to genotoxic stress. This YB-1/hTopoI complex formation increased cellular sensitivity to CPT. Meanwhile, the stimulation of hNTH1's AP-lyase activity by YB-1 would result in more efficient DNA repair to protect cells from death thereby allowing tumour cells to become more resistant to DNA damaging drugs (like cisplatin). The cellular response may be different according to the drug used for treatment.

Part IV. Conclusions and Future Prospects

FRET is a versatile method that can be applied both *in vitro* and *in vivo*. However, compared to a test tube containing purified proteins, cells are much more complex systems with a lot of protein-protein, nucleic acid-protein, and receptor-ligand interactions. In our acceptor photobleaching experiments, we observed varying FRET efficiencies *in vivo*, but *in vitro* the FRET signal was stable. Further studies will be needed to better understand the molecular mechanisms tightly regulating the interactions of YB-1 with its multiple cellular partners *in vivo*. Characterizing the YB-1 complexes formed under genotoxic stress conditions may offer novel treatment strategies against drug-resistant tumour cells.

In the future, the hNTH1/YB-1 Biosensor 1 will be used for screening a much larger chemical library (10,000 compounds) in order to identify potent inhibitors of the hNTH1/YB-1 interaction. Although it has not worked for hTopoI due to degradation problems, our designed Biosensor construct offers a new strategy to study protein-protein interactions and to perform HTS for potential inhibitors. Several teams at IBS have already shown interest in adapting the Biosensor to their needs and a collaboration with Dr. Cécile Morlot will be initiated later this year.

ANNEX

1. Original and optimized cDNA sequences of our proteins

hNTH1 Original cDNA	1	ATGTGTAAGTCCGAGGAGTCCGGCATGACCGCCTTGAGCGCGAGGATGCT	50
		
hNTH1 Optimized cDNA	1	ATGTGCTCTCCGAGGAATCTGGTATGACCGCTGTCTGCTCGTATGCT	50
hNTH1 Original cDNA	51	GACCCGGAGCCGAGCCTGGGACCCGGGGCTGGGCCGCGGGGTGTAGGG	100
		
hNTH1 Optimized cDNA	51	GACCCGTTCTCGTTCTCTGGGTCCGGGTGCTGGTCCGCTGGTTGCCGTG	100
hNTH1 Original cDNA	101	AGGAGCCCGGGCCTCTCCGGAGAAGAGAGGCTGCAGCAGAAGCGAGGAAA	150
		
hNTH1 Optimized cDNA	101	AAGAACCAGGTCCTGCTGCGTCGTCGTAAGCTGCTGCTGAAGCTCGTAAA	150
hNTH1 Original cDNA	151	AGCCACAGCCCCGTGAAGCGTCCGCGGAAAGCACAGAGACTGCGTGTGGC	200
		
hNTH1 Optimized cDNA	151	TCTCACTCTCCGGTTAAACGTCCGCGTAAAGCTCAGCGTCTGCGTGTGTC	200
hNTH1 Original cDNA	201	CTATGAGGGCTCGGACAGTGAGAAAGGTGAGGGGGCTGAGCCCCCAAGG	250
		
hNTH1 Optimized cDNA	201	TTACGAAGGTCTCTGACTCTGAAAAAGGTGAAGGTGCTGAACCGCTGAAAG	250
hNTH1 Original cDNA	251	TGCCAGTCTGGGAGCCCCAGGACTGGCAGCAACAGCTGGTCAACATCCGT	300
		
hNTH1 Optimized cDNA	251	TTCCGGTTTGGGAACCGCAGGACTGGCAGCAGCAGCTGGTTAACATCCGT	300
hNTH1 Original cDNA	301	GCCATGAGGAACAAAAAGGATGCACCTGTGGACCATCTGGGGACTGAGCA	350
		
hNTH1 Optimized cDNA	301	GCTATGCGTAACAAAAAGACGCTCCGGTTGACCACCTGGGTACCGAACA	350
hNTH1 Original cDNA	351	CTGTATGACTCCAGTGCCCCCAAGGTACGCAGGTACCAGGTGCTGTC	400
		
hNTH1 Optimized cDNA	351	CTGCTACGACTCTTCTGCTCCGCCGAAAGTTCGTCGTTACCAGGTTCTGC	400
hNTH1 Original cDNA	401	TGTCACTGATGCTCTCCAGCCAAACCAAGACCAGGTGACGGCGGGCGCC	450
		
hNTH1 Optimized cDNA	401	TGTCTCTGATGCTGTCTTCTCAGACCAAGACCAGGTTACCGCTGGTGCT	450
hNTH1 Original cDNA	451	ATGCAGCGACTGCGGGCGGGGCCTGACGGTGGACAGCATCTGCAGAC	500
		
hNTH1 Optimized cDNA	451	ATGCAGCGTCTGCGTCTGCTGGTCTGACCGTTGACTCTATCTGCAGAC	500
hNTH1 Original cDNA	501	AGATGATGCCACGCTGGGCAAGCTCATCTACCCCGTCGGTTTCTGGAGGA	550
		
hNTH1 Optimized cDNA	501	CGACGACGCTACCCCTGGGTAAACTGATCTACCCGGTTGGTTTCTGGCGTT	550
hNTH1 Original cDNA	551	GCAAGGTGAAATACATCAAGCAGACCAGCGCCATCCTGCAGCAGCACTAC	600
		
hNTH1 Optimized cDNA	551	CTAAAGTTAAATACATCAAACAGACCTCTGCTATCCTGCAGCAGCACTAC	600
hNTH1 Original cDNA	601	GGTGGGGACATCCCAGCCTCTGTGGCCGAGCTGGTGGCGCTGCCGGGTGT	650
		
hNTH1 Optimized cDNA	601	GGTGGTGACATCCCGGCTTCTGTTGCTGAAGTGGTTGCTCTGCCGGGTGT	650
hNTH1 Original cDNA	651	TGGGCCCAAGATGGCACACCTGGCTATGGCTGTGGCCTGGGGCACTGTGT	700
		
hNTH1 Optimized cDNA	651	TGGTCCGAAAATGGCTCACCTGGCTATGGCTGTGCTTGGGGTACCGTTT	700

hNTH1 Original cDNA	701	CAGGCATTGCAGTGGACACGCATGTGCACAGAATCGCCAACAGGCTGAGG	750
		. .	
hNTH1 Optimized cDNA	701	CTGGTATCGCTGTTGACACCCACGTTACCGTATCGCTAACCGTCTGCGT	750
hNTH1 Original cDNA	751	TGGACCAAGAAGGCAACCAAGTCCCCAGAGGAGACCCGCGCCGCCCTGGA	800
		. .	
hNTH1 Optimized cDNA	751	TGGACCAAAAAAGCTACCAATCTCCGAAGAAACCGTGCTGCTCTGGA	800
hNTH1 Original cDNA	801	GGAGTGGCTGCCTAGGGAGCTGTGGCACGAGATCAATGGACTCTTGGTGG	850
		. .	
hNTH1 Optimized cDNA	801	AGAATGGCTGCCGCGTGAACGTGTGGCACGAAATCAACGGTCTGCTGGTTG	850
hNTH1 Original cDNA	851	GCTTCGGCCAGCAGACCTGTCTGCCTGTGCACCCTCGCTGCCACGCCTGC	900
		. .	
hNTH1 Optimized cDNA	851	GTTTCGGTCAGCAGACCTGCCTGCCGCTTACCCGCGTTGCCACGCTTGC	900
hNTH1 Original cDNA	901	CTCAACCAAGCCCTCTGCCCGCGCCAGGGTCTCTGA	939
		
hNTH1 Optimized cDNA	901	CTGAACCAAGGCTCTGTGCCCGGCTGCTCAGGGTCTGTAA	939

Figure A.1. hNTH1 sequence alignment of Original cDNA and Optimized cDNA.

YB1 Original cDNA	1	ATGAGCAGCGAGGCCGAGACCCAGCAGCCGCCCGCCCCCCCCCGCCG	50
		
YB1 Optimized cDNA	1	ATGTCTTCTGAAGCTGAAACCAaCAGCCaCCGGCTGCcCCGCCGGCTGC	50
YB1 Original cDNA	51	CCCCGCCCTCAGCGCCGCCGACACCAAGCCCGGCACTACGGGCAGCGCG	100
		. .	
YB1 Optimized cDNA	51	TCCGGCTCTGTCTGTCTGCTGACACAAACCGGGTACCACCGGTTCcGGcG	100
YB1 Original cDNA	101	CAGGGAGCGGTGGCCCGGGCGGCCTCACATCGGCGGCGCCTGCCGGCGGG	150
		. .	
YB1 Optimized cDNA	101	CTGGTTCTGGTGGTCCaGcGGTCTGACCTCTGCTGCTCCGGCTGGTGGT	150
YB1 Original cDNA	151	GACAAGAAGGTCATCGCAACGAAGGTTTGGGAACAGTAAATGGTTCAA	200
		
YB1 Optimized cDNA	151	GACAAAAAAGTTATCGCTACCAAAGTTCTGGGTACCGTTAAATGGTTCAA	200
YB1 Original cDNA	201	TGTAAGGAACGGATATGGTTTTCATCAACAGGAATGACACCAAGGAAGATG	250
		. .	
YB1 Optimized cDNA	201	CGTTCGTAACGGTTACGGTTTTCATCAACCGTAACGACACCAAGAAGACG	250
YB1 Original cDNA	251	TATTTGTACACCAGACTGCCATAAAGAAGAATAACCCAGGAAGTACCTT	300
		
YB1 Optimized cDNA	251	TTTTCTGTTACACAGACCGCTATCAAAAAAACAACCCGCGTAAATACCTG	300
YB1 Original cDNA	301	CGCAGTGTAGGAGATGGAGAGACTGTGGAGTTTGATGTTGTTGAAGGAGA	350
		
YB1 Optimized cDNA	301	CGTTCTGTTGGTGACGGTGAAACCGTTGAATTCGACGTTGTTGAAGGTGA	350
YB1 Original cDNA	351	AAAGGGTGCAGGAGGCAGCAAAATGTTACAGGTCCTGGTGGTGTCCAGTTC	400
		
YB1 Optimized cDNA	351	AAAAGGTGCTGAAGCTGCTAACGTTACCGGTCCGGGTGGTGTCCGGTTC	400
YB1 Original cDNA	401	AAGGCAGTAAATATGCAGCAGACCGTAACCATTTATAGACGCTATCCACGT	450
		
YB1 Optimized cDNA	401	AGGGTTCTAAATACGCTGCTGACCGTAACCACTACCGTCGTTACCCGCGT	450
YB1 Original cDNA	451	CGTAGGGGTCTCCACGCAATTACCAGCAAAATTACCAGAATAGTGAGAG	500
		
YB1 Optimized cDNA	451	CGTCGcGGTCCaCctCGTAACtACCAGCAGAACTACCAGAATCTGAgTC	500

YB1 Original cDNA	501	TGGGGAAAAAGAACGAGGGATCGGAGAGTGCTCCCGAAGGCCAGGCCAAC	550
		
YB1 Optimized cDNA	501	TGGTGAAAAAACGAAGGTTCTGAATCTGCTCCGGAAGGTCTAGGCTCAGC	550
YB1 Original cDNA	551	AACGCCGGCCCTACCGCAGGCGAAGGTTCCACCTTACTACATGCGGAGA	600
		
YB1 Optimized cDNA	551	AGCGTCGcCCaTACCGTCGcCGTCGTTCCCGCCGTACTACATGCGTCGT	600
YB1 Original cDNA	601	CCCTATGGGCGTCGACCACAGTATTCCAACCTCCTGTGCAGGAGAAGT	650
		
YB1 Optimized cDNA	601	CCGTACGGTCGTCGTCCGCACTACTAACC CGCCGGTTCAGGTTGAAGT	650
YB1 Original cDNA	651	GATGGAGGGTGCTGACAACAGGGTGCAGGAGAACAAGGTAGACCAGTGA	700
		
YB1 Optimized cDNA	651	TATGGAAGGTGCTGACAACAGGGTGTGGTGAACAGGGTCGTCCGGTTC	700
YB1 Original cDNA	701	GGCAGAATATGTATCGGGGATATAGACCACGATTCCGCGAGGGCCCTCCT	750
		
YB1 Optimized cDNA	701	GTCAGAACATGTACCGTGGTTACCGTCCGCGTTTCCGTCGTGGTCCGCCG	750
YB1 Original cDNA	751	CGCCAAAGACAGCCTAGAGAGGACGGCAATGAAGAAGATAAAGAAAATCA	800
		
YB1 Optimized cDNA	751	CGTCAGCGTCAGCCGCGTGAAGACGGcAACGAAGAAGACAAAGAAAACCA	800
YB1 Original cDNA	801	AGGAGATGAGACCAAGGTCTAGCAGCCACCTCAACGTCGGTACCGCCGCA	850
		
YB1 Optimized cDNA	801	GGGTGACGAAACCCAGGGTCAaCAGCCGCCGAGCGTCGTTACCGTCGTA	850
YB1 Original cDNA	851	ACTTCAATTACCGACGCAGACGCCAGAAAACCTAAACCACAAGATGGC	900
		
YB1 Optimized cDNA	851	ACTTCAACTACCGTCGcCGcCGTCCGGAACCCGAAACCGCAGGACGGT	900
YB1 Original cDNA	901	AAAGAGACAAAAGCAGCCGATCCACCAGCTGAGAATTTCGTCCGCTCCCGA	950
		
YB1 Optimized cDNA	901	AAAGAAACCAAAGCTGCTGACCCGCCGCTGAAAACCTCTTCTGCTCCGGA	950
YB1 Original cDNA	951	GGCTGAGCAGGGCGGGGCTGAGTAA	975
		
YB1 Optimized cDNA	951	AGCTGAACAGGGTGGTGTGAATAA	975

Figure A.2. YB1 sequence alignment of Original cDNA and Optimized cDNA.

hTopol Original cDNA	1	ATGAGTGGGGACCACCTCCACAAACGATTCCCAGATCGAAGCGGATTTCCG	50
hTopol Optimized cDNA	1	ATGAGTGGGGACCACCTGCACAAACGATTCCCAGATCGAAGCCGATTTCCG	50
hTopol Original cDNA	51	ATTGAATGATTCTCATAAACACAAAGATAAAACACAAAGATCGAGAACACC	100
		.	
hTopol Optimized cDNA	51	GTTGAATGATTCTCATAAACACAAAGATAAAACACAAAGATCGCGAACACC	100
hTopol Original cDNA	101	GGCACAAAGAACACAAGAAGGAGAAGGACCGGGAAGTCCAAGCATAGC	150
hTopol Optimized cDNA	101	GGCACAAAGAACACAAGAAGGAGAAGGACCGTGAAGTCCAAGCATAGC	150
hTopol Original cDNA	151	AACAGTGAACATAAAGATTCTGAAAAGAAACACAAAGAGAAGGAGAAGAC	200
hTopol Optimized cDNA	151	AACAGTGAACATAAAGATTCTGAAAAGAAACACAAAGAGAAGGAGAAGAC	200
hTopol Original cDNA	201	CAAAACACAAAGATGGAAGCTCAGAAAAGCATAAAGACAAACATAAAGACA	250
hTopol Optimized cDNA	201	CAAAACACAAAGATGGCAGCTCAGAAAAGCATAAAGACAAACATAAAGACC	250
hTopol Original cDNA	251	GAGACAAGGAAAAACGAAAAGAGGAAAAGGTTTCGAGCCTCTGGGGATGCA	300
		
hTopol Optimized cDNA	251	GCGACAAGGAAAAACGCAAAGAGGAAAAGGTTTCGGGCCTCTGGGGATGCA	300

hTopol Original cDNA	301	AAAATAAAGAAGGAGAAGGAAAATGGCTTCTCTAGTCCACCACAAATTAA	350
		. .	
hTopol Optimized cDNA	301	AAAATCAAGAAAGAGAAGGAAAATGGCTTCTCTAGTCCACCACAAATTAA	350
hTopol Original cDNA	351	AGATGAACCTGAAGATGATGGCTATTTTGTTCCTCCTAAAGAGGATATAA	400
		. . .	
hTopol Optimized cDNA	351	AGATGAACCTGAAGATGATGGCTATTTTGTTCCTCCGAAAGAGGATATCA	400
hTopol Original cDNA	401	AGCCATTAAAGAGACCTCGAGATGAGGATGATGCTGATTATAAACCTAAG	450
		
hTopol Optimized cDNA	401	AGCCATTGAAGCGGCCTCGCGATGAGGATGATGCGGATTATAAACCTAAG	450
hTopol Original cDNA	451	AAAATTAAAACAGAAGATACCAAGAAGGAGAAGAAAAGAAAAGTAGAAGA	500
		
hTopol Optimized cDNA	451	AAAATTAAAACAGAAGATACCAAGAAGGAGAAGAAACGCAAACTGGAAGA	500
hTopol Original cDNA	501	AGAAGAGGATGGTAAATTGAAAAAACCCAAGAATAAAGATAAAGATAAAA	550
		. . .	
hTopol Optimized cDNA	501	AGAAGAGGATGGTAAATTGAAAAAACCAAGAATAAAGATAAAGATAAAA	550
hTopol Original cDNA	551	AAGTTCCTGAGCCAGATAACAAGAAAAAGAAGCCGAAGAAAGAAGAGGAA	600
		. . .	
hTopol Optimized cDNA	551	AAGTTCCTGAGCCAGATAACAAGAAAAAGAAGCCGAAGAAAGAAGAGGAA	600
hTopol Original cDNA	601	CAGAAGTGGAAATGGTGGGAAGAAGAGCGCTATCCTGAAGGCATCAAGTG	650
		. . .	
hTopol Optimized cDNA	601	CAGAAGTGGAAATGGTGGGAAGAAGAGCGCTATCCTGAAGGCATCAAGTG	650
hTopol Original cDNA	651	GAAATTCCTAGAACATAAAGGTCCAGTATTTGCCCCACCATATGAGCCTC	700
		
hTopol Optimized cDNA	651	GAAATTCCTGGAACATAAAGGTCCAGTGTTTGCCCCACCTTATGAGCCGC	700
hTopol Original cDNA	701	TTCCAGAGAATGTCAAGTTTTATTATGATGGTAAAGTCATGAAGCTGAGC	750
		
hTopol Optimized cDNA	701	TCCCAGAGAATGTCAAGTTTTATTATGATGGTAAAGTCATGAAGCTGAGC	750
hTopol Original cDNA	751	CCCAAAGCAGAGGAAGTAGCTACGTTCTTTGCAAAAATGCTCGACCATGA	800
		
hTopol Optimized cDNA	751	CCAAAAGCAGAGGAAGTCGCTACGTTCTTTGCAAAAATGTTGGACCATGA	800
hTopol Original cDNA	801	ATATACTACCAAGGAAATATTTAGGAAAAATTTCTTTAAAGACTGGAGAA	850
		
hTopol Optimized cDNA	801	ATATACTACCAAGGAAATCTTTCGCAAAAATTTCTTTAAAGACTGGCGGA	850
hTopol Original cDNA	851	AGGAAATGACTAATGAAGAGAAGAATATTATCACCAACCTAAGCAAATGT	900
		. . .	
hTopol Optimized cDNA	851	AGGAAATGACTAATGAAGAGAAGAATATTATCACCAACCTGAGCAAATGT	900
hTopol Original cDNA	901	GATTTTACCCAGATGAGCCAGTATTTCAAAGCCCAGACGGAAGCTCGGAA	950
		
hTopol Optimized cDNA	901	GATTTTACCCAGATGAGTCAGTATTTCAAAGCCCAGACGGAAGCGCGTAA	950
hTopol Original cDNA	951	ACAGATGAGCAAGGAAGAGAAAAGTGAATCAAAGAGGAGAATGAAAAAT	1000
		. . .	
hTopol Optimized cDNA	951	ACAGATGAGCAAGGAAGAGAAAAGTGAATCAAAGAGGAGAATGAAAAAT	1000
hTopol Original cDNA	1001	TACTGAAAGAATATGGATTCTGTATTATGGATAACCACAAAGAGAGGATT	1050
		
hTopol Optimized cDNA	1001	TGCTGAAAGAATATGGGTTCTGTATTATGGATAACCACAAAGAGCGCATT	1050
hTopol Original cDNA	1051	GCTAACTTCAAGATAGAGCCTCCTGGACTTTTCCGTGGCCGCGGCAACCA	1100
		
hTopol Optimized cDNA	1051	GCCAACTTCAAGATCGAGCCTCCCGGCCTTTTCCGGGGCCGCGGCAACCA	1100
hTopol Original cDNA	1101	CCCCAAGATGGGCATGCTGAAGAGACGAATCATGCCCGAGGATATAATCA	1150
		
hTopol Optimized cDNA	1101	CCCCAAAATGGGTATGCTGAAGCGCGGTATCATGCCAGAGGATATCATT	1150
hTopol Original cDNA	1151	TCAACTGTAGCAAAGATGCCAAGGTTCTTCTCTCTCCAGGACATAAG	1200
		
hTopol Optimized cDNA	1151	TCAACTGTAGCAAAGATGCCAAGTTCCATCTCTCTCCGCCAGGCCATAAG	1200

hTopol Original cDNA	1201	TGGAAAGAAGTCCGGCATGATAACAAGGTTACTTGGCTGGTTTCCTGGAC	1250
hTopol Optimized cDNA	1201	TGGAAAGAAGTCCGGCATGATAACAAGGTTACCTGGCTGGTTTCCTGGAC	1250
hTopol Original cDNA	1251	AGAGAACATCCAAGGTTCCATTAAATACATCATGCTTAACCCTAGTTCAC	1300
		.	
hTopol Optimized cDNA	1251	GGAGAACATCCAAGGTTCCATTAAATACATCATGCTCAACCCTAGCTCAC	1300
hTopol Original cDNA	1301	GAATCAAGGTTGAGAAGGACTGGCAGAAATACGAGACTGCTCGGCGGCTG	1350
		. .	
hTopol Optimized cDNA	1301	GCATCAAAGGGGAGAAGGACTGGCAGAAATACGAGACTGCACGTCGGCTG	1350
hTopol Original cDNA	1351	AAAAATGTGTGGACAAGATCCGGAACCAGTATCGAGAAGACTGGAAGTC	1400
hTopol Optimized cDNA	1351	AAAAATGTGTGGACAAGATCCGGAACCAGTATCGCGAAGACTGGAAGTC	1400
hTopol Original cDNA	1401	CAAAGAGATGAAAGTCCGGCAGAGAGCTGTAGCCCTGTACTTCATCGACA	1450
hTopol Optimized cDNA	1401	CAAAGAGATGAAAGTCCGTCAGCGCGCAGTGGCCCTGTACTTCATCGACA	1450
hTopol Original cDNA	1451	AGCTTGCTCTGAGAGCAGGCAATGAAAAGGAGGAAGGAGAAACAGCGGAC	1500
		. .	
hTopol Optimized cDNA	1451	AACTTGCTCTGCGCGCGGGCAATGAAAAGGAGGAAGGTGAAACCGCCGAC	1500
hTopol Original cDNA	1501	ACTGTGGGCTGCTGCTCACTTCGTGTGGAGCACATCAATCTACACCCAGA	1550
hTopol Optimized cDNA	1501	ACTGTGGGCTGCTGCTCACTTCGTGTGGAGCACATCAATCTGCACCCAGA	1550
hTopol Original cDNA	1551	GTTGGATGGTCAGGAATATGTGGTAGAGTTTGACTTCCTCGGGAAGGACT	1600
hTopol Optimized cDNA	1551	GTTGGATGGTCAGGAATATGTGGTCGAGTTTGACTTCCTCGGGAAGGACT	1600
hTopol Original cDNA	1601	CCATCAGATACTATAACAAGGTCCCTGTTGAGAAACGAGTTTAAAGAAC	1650
		.	
hTopol Optimized cDNA	1601	CCATCCGCTACTATAACAAGGTCCCTGTTGAGAAACGCGTTTAAAGAAC	1650
hTopol Original cDNA	1651	CTACAATATTTATGGAGAACAAGCAGCCCGAGGATGATCTTTTGTATAG	1700
		. .	
hTopol Optimized cDNA	1651	CTGCAATGTTTATGGAGAACAACAGCCAGAGGATGATCTTTTGTATCG	1700
hTopol Original cDNA	1701	ACTCAATACTGGTATTCTGAATAAGCATCTTCAGGATCTCATGGAGGGCT	1750
		
hTopol Optimized cDNA	1701	GTTGAATACGGGTATTCTGAATAAGCATCTCCAGGATCTGATGGAGGGCT	1750
hTopol Original cDNA	1751	TGACAGCCAAGGTATTCGTACATACAATGCCTCCATCACGTACAGCAG	1800
		. . .	
hTopol Optimized cDNA	1751	TGACCGCCAAAGTGTTCCGCACCTACAATGCAAGCATCACGTTCAGCAA	1800
hTopol Original cDNA	1801	CAGCTAAAAGAACTGACAGCCCCGGATGAGAACATCCAGCGAAGATCCT	1850
		.	
hTopol Optimized cDNA	1801	CAGTTGAAAGAACTGACTGCCCGGATGAGAACATCCAGCAAAGATCCT	1850
hTopol Original cDNA	1851	TTCTTATAACCGTGCCAATCGAGCTGTTGCAATTCTTTGTAACCATCAGA	1900
hTopol Optimized cDNA	1851	TTCTTATAACCGCGCCAATCGTGCGGTTGCAATTCTTTGTAACCATCAGC	1900
hTopol Original cDNA	1901	GGGCACCACCAAAAACCTTTTGAGAAGTCTATGATGAACTTGCAAACTAAG	1950
hTopol Optimized cDNA	1901	GGGCACCACCGAAAACCTTTTGAGAAGTCTATGATGAACTTGCAAACTAAG	1950
hTopol Original cDNA	1951	ATTGATGCCAAGAAGGAACAGCTAGCAGATGCCCGGAGAGACCTGAAAAG	2000
hTopol Optimized cDNA	1951	ATTGATGCCAAGAAGGAACAGCTCGCAGATGCCCGGCGGACCTGAAAAG	2000
hTopol Original cDNA	2001	TGCTAAGGCTGATGCCAAGGTCATGAAGGATGCAAAGACGAAGAAGGTAG	2050
		. .	
hTopol Optimized cDNA	2001	CGCGAAGGCTGATGCCAAGGTCATGAAGGATGCAAAAACGAAAAGGTGG	2050
hTopol Original cDNA	2051	TAGAGTCAAAGAAGAAGGCTGTTCAGAGACTGGAGGAACAGTTGATGAAG	2100
		. .	
hTopol Optimized cDNA	2051	TCGAGTCAAAGAAAAAGGCCGTTTCAGCGCCTGGAGGAACAGTTGATGAAG	2100

hTopoI Original cDNA	2101	CTGGAAGTTCAAGCCACAGACCGAGAGGAAAAATAACAGATTGCCCTGGG	2150
hTopoI Optimized cDNA	2101	CTGGAAGTTCAAGCCACCGACCGAGGAAAAATAACAGATTGCCCTGGG	2150
hTopoI Original cDNA	2151	AACCTCCAAACTCAATTATCTGGACCTAGGATCACAGTGGCTTGGTGCA	2200
		.	
hTopoI Optimized cDNA	2151	CACCTCCAAATTGAATTATCTGGACCTCGGATCACGGTGGCATGGTGCA	2200
hTopoI Original cDNA	2201	AGAAGTGGGGTGTCCCAATTGAGAAGATTTACAACAAAACCCAGCGGGAG	2250
hTopoI Optimized cDNA	2201	AGAAATGGGGTGTCCCAATTGAGAAGATTTACAACAAAACCCAGCGTGAG	2250
hTopoI Original cDNA	2251	AAGTTTGCCTGGGCCATTGACATGGCTGATGAAGACTATGAGTTTATAG	2298
hTopoI Optimized cDNA	2251	AAGTTTGCCTGGGCCATTGACATGGCGGATGAAGACTATGAGTTTAA	2298

Figure A.3. hTopoI sequence alignment of Original cDNA and Optimized cDNA.

2. PCR primers used and cloning fragments prepared in this work

Table A.1. Oligonucleotides used as PCR-primers for assembly of three *hTopoI* fragments. Lowercase letters show oligonucleotide tails not identical to the target sequence.

Primer name	Primer Sequence
pEX-A2-hTopoI	
F_ pEX-A2-FragA	5' – ACCTGCTTTTGCTCGCTTGGATCC – 3'
R_ pEX-A2-FragA	5' – CTTCCTCTGCTTTTGGGCTCAGC – 3'
F_ FragAB	5' – gagcccaaaagcagaggaag TCGCTACGTTCTTTGCAAAAATGTTGGA – 3'
R_ FragB	5' – cagattgatg TGCTCCACACGAAGGCTACAGC – 3'
F_ FragBC	5' – gtgtggagca CATCAATCTGCACCCAGAGTTGGAT – 3'
R_ FragC	5' – ccaagcgagcaaaagcaggt TTAAAACTCGTAGTCTTCATCCGCCCATG – 3'

Table A.2. Assembling the full length *hTopoI*

Construct	Insert 1 / bp	Insert 2 / bp	Plasmid / bp	Final Product (bp)
	FragB	FragC	pEX-A2-FragA	
pEX-A2-hTopoI	796	796	3216	4748

Table A.3. Oligonucleotides used as PCR-primers for mammalian expression vectors. Green coloured letters: restriction enzyme site; red coloured letters: gene specific region; pink colored letters: 2A linker. Lowercase letters show oligonucleotide tails not identical to the target sequence.

Primer name	Primer Sequence
pmTQ2-N1-hNTH1	
For_ hNTH1_N1	5'– AACTCGAGATGTGCTCTCCGCAGGAATCTGG –3'
Rev_ hNTH1_N1	5'– TTGGATCCGACAGACCCTGAGCAGCCGGG –3'
pmTQ2-C1-hNTH1	
For_ hNTH1_C1	5'– AACTCGAGCTATGTGCTCTCCGCAGGAATCTGG –3'
Rev_ hNTH1_C1	5'– TTGGATCCTCACAGACCCTGAGCAGCCGGG –3'
psYFP2-C1-YB1	
For_ YB1_C1	5'– AACTCGAGCTATGTCTTCTGAAGCTGAAACCCAACAG –3'
Rev_ YB1_C1	5'– TTGGATCCTTATTTCAGCACCACCCTGTTTCAGCTT –3'
psYFP2-N1-YB1ΔC	
For_ YB1_N1	5'– AACTCGAGATGTCTTCTGAAGCTGAAACCCAACAG –3'
Rev_ YB1dC_N1	5'– TTGGATCCGATTCCATAACTTCACCCTGAACCGGC –3'
psYFP2-C1-YB1ΔC	
For_ YB1_C1	5'– AACTCGAGCTATGTCTTCTGAAGCTGAAACCCAACAG –3'
Rev_ YB1dC_C1	5'– TTGGATCCTTATTCCATAACTTCACCCTGAACCGGC –3'
pmTQ2-N1-hTopoI	
F_hTopoI	5' – AACTCGAGCTATGAGCGGCGACCACCTGCAC – 3'
R_hTopoI-N1	5' – TTGGATCCGAAAACCTCGTAGTCTTCATCCGCC – 3'
pmTQ2-C1-hTopoI	
R_hTopoI-C1	5' – TTGGATCCGATTAAAACTCGTAGTCTTCATCC – 3'
pYB1ΔC-sYFP2-2A-mTQ2-hTopoI	
F_ pmTQ2-C1-hTopoI	5' – gtcgaggagaatcctggcccaATGGTGAGCAAGGGCGAGGAG – 3'
R_ pmTQ2-C1-hTopoI	5' – AGAAGACATGGTGGCGACCGGTAGCGC – 3'
F_ YB1dC-sYFP2-2A	5' – ccggtcgccaccATGTCTTCTGAAGCTGAAACCCAACAG – 3'
R1_YB1dC-sYFP2-2A	5' – tcctetgcctcTCCGCTTCCCTTGTACAGCTCGTCCATGCC – 3'
R2_2A	5' – gtcaccgatgttagcagactTCCTCTGCCCTCTCCGCTTCC – 3'
R3-2A	5' – tggccaggattctcctcgacGTCACCGCATGTTAGCAGACT – 3'
psYFP2-NLS-2A-mTQ2-hTopoI	
F_ sYFP2-NLS	5' – CCGGTCGCCACCATGGTGAGCAAGGGCGAGGA – 3'
R_ sYFP2-NLS	5' – tcctetgcctcTCCGCTTCCCTCTAGATCCGGTGGATCCTACC – 3'

Table A.4. Cloning of constructs for mammalian expression.

Construct	Insert / bp	Plasmid / bp	RE couple used	Final Product (bp)
pmTQ2-N1-hNTH1	950	4690	<i>XhoI</i> / <i>BamHI</i>	5640
pmTQ2-C1-hNTH1	963	4668	<i>XhoI</i> / <i>BamHI</i>	5631
psYFP2-N1-YB1	989	4678	<i>XhoI</i> / <i>BamHI</i>	5667
psYFP2-N1-YB1ΔC	671	4680	<i>XhoI</i> / <i>BamHI</i>	5351
psYFP2-C1-YB1ΔC	674	4678	<i>XhoI</i> / <i>BamHI</i>	5352
pmTQ2-N1-hTopoI	2315	4674	<i>XhoI</i> / <i>BamHI</i>	6989
pmTQ2-C1-hTopoI	2318	4674	<i>XhoI</i> / <i>BamHI</i>	6992
pYB1ΔC-sYFP2-2A-mTQ2-hTopoI	7022	1470	-	8450
psYFP2-NLS-2A-mTQ2-hTopoI	7022	861	-	7883
pYB1ΔC -sYFP2-NLS-2A-mTQ2-hTopoI	7022	1539	-	8561

Table A.5. Oligonucleotides used as PCR-primers for fluorescent protein coupled proteins cloning. Green coloured letters: restriction enzyme site; red coloured letters: gene specific region; bleu coloured letters: linker sequence between two protein genes. Lowercase letters show oligonucleotide tails not identical to the target sequence.

Primer name	Primer Sequence
pProEX-HTb-hNTH1-mTQ2 /NtailhNTH1-mTQ2	
F_hNTH1	5' – AAGTCGACGATGTGCTCTCCGAGGAATCTGG – 3'
R_mTQ2	5' – TTAAGCTTTCACCTTGACAGCTCGTCCATGCCGAG – 3'
pProEX-HTb-ND89hNTH1-mTQ2	
F_ND89hNTH1	5' – AAGTCGACGATGCAGGACTGGCAGCAGCAGCTG – 3'
pProEX-HTb-mTQ2-hNTH1	
R_hNTH1	5' – TTAAGCTTTCACAGACCCTGAGCAGCCGGG – 3'
pProEX-HTb-sYFP2-YB1ΔC	
F_sYFP2	5' – AAGTCGACGATGGTGAGCAAGGGCGAGGAG – 3'
R_YB1ΔC	5' – TTAAGCTTTCATTCCATAACTTCACCCTGAACCGGC – 3'
pProEX-HTb-YB1ΔC-sYFP2	
F_YB1ΔC	5' – AAGTCGACGATGTCTTCTGAAGCTGAAACCCAACAG – 3'
pProEX-HTb-hTopoI	
F_hTopoI	5' – AACCATGGGAATGAGCGGCGACCACTGCAC – 3'
R_hTopoI	5' – TTCTCGAGTTAAACTCGTAGTCTTCATCC – 3'

pET21d-hTopoI	
R_hTopoI_CterHis	5' – TTCTCGAGAAACTCGTAGTCTTCATCCGCC – 3'
pET21d-mTQ2-hTopoI	
F_Linkers-hTopoI	5' – tccggactcagatctcgagctATG AGC GGC GAC CAC CTG – 3'
R_pET21d	5' – TCCCATGGTATATCTCCTTCTTAAAGTTAAAC – 3'
F_pET21d-mTQ2	5' – ttaagaaggagatataccatgggaATGGTGAGCAAGGGCGAG – 3'
R_Linkers-mTQ2	5' – AGCTCGAGATCTGAGTCCGGACTT – 3'
pET21d-hTopoI-mTQ2	
F_mTQ-pET21	5' – atggacgagctgtacaagCTCGAGCACCACCACCACC – 3'
R_Linkers-hTopoI	5' – ggtggcgaccggtggatccgaAAACTCGTAGTCTTCATCCGCC – 3'
F_Linkers	5' – TCGGATCCACCGGTCGCCAC – 3'
R_mTQ2	5' – ctcgagCTTGTACAGCTCGTCCATGCCGAG – 3'

Table A.6. Cloning of fluorescent protein coupled constructs for bacterial expression.

Construct	Insert / bp	Plasmid / bp	RE couple used	Final Product (bp)
pProEX-HTb-hNTH1-mTQ2	1694	4702	<i>SalI</i> / <i>HindIII</i>	6396
pProEX-HTb-NtailhNTH1-mTQ2	1025	4702	<i>SalI</i> / <i>HindIII</i>	5727
pProEX-HTb-ND89hNTH1-mTQ2	1430	4702	<i>SalI</i> / <i>HindIII</i>	6132
pProEX-HTb-mTQ2-hNTH1	1694	4702	<i>SalI</i> / <i>HindIII</i>	6396
pProEX-HTb-sYFP2-YB1ΔC	1415	4702	<i>SalI</i> / <i>HindIII</i>	6117
pProEX-HTb-YB1ΔC- sYFP2	1415	4702	<i>SalI</i> / <i>HindIII</i>	6117
pProEX-HTb-hTopoI	2316	4674	<i>NcoI</i> / <i>XhoI</i>	6990
pET21d-hTopoI	2313	5354	<i>NcoI</i> / <i>XhoI</i>	7667
pET21d-mTQ2-hTopoI	762	7688	-	8405
pET21d-hTopoI-mTQ2	744	7706	-	8405

Table A.7. Oligonucleotides used as PCR-primers for Biosensors cloning. Green coloured letters: restriction enzyme site; red coloured letters: gene specific region; bleu coloured letters: linker sequence between two protein genes.

Primer name	Primer Sequence
Biosensor 1	
For_SYFP2-YB1ΔC	5' – AAGTCGACGATGGTGAGCAAGGGCGAGGAG – 3'
R_SYFP2-YB1ΔC Bio	5' – TTGCTAGCACCTCCGCCGCTTTCCATAACTTCACCCTGAACCGGC – 3'
F_hNTH1-mTQ2_Bio	5' – AAGCTAGCGGAGGCGGGACGATGTGCTCTCCGCAGGAATCTGG – 3'
R_hNTH1-mTQ2	5' – TTAAGCTTTCACTTGTACAGCTCGTCCATGCCGAG – 3'
Biosensor 3	
F_ND89NT H1-mTQ2_Bio	5'-AAGCTAGCGGAGGCGGGACGATGCAGGACTGGCAGCAGCAGCTG -3'
Biosensor 4	
F_drEndoIII-mTQ2_Bio	5' – AAGCTAGCGGAGGCGGGACGATGACTCGCAATTCTGCCTCCCC – 3'
Biosensor 5	
F_mTQ2_Bio	5'-AAGCTAGCGGAGGCGGGACGATGGTGAGCAAGGGCGAGGAGCTG-3'
Biosensor 6	
R_sYFP2_Bio	5' – TTGCTAGCACCTCCGCCGCTCTTGTACAGCTCGTCCATGCCGAG – 3'
Biosensor 7	
R_mTQ2-hNTH1_Bio	5' – TTGCTAGCACCTCCGCCGCTCAGACCCTGAGCAGCCGG – 3'
For_YB1ΔC-sYFP2_Bio	5'-AAGCTAGCGGAGGCGGGACGATGTCTTCTGAAGCTGAAACCCAACAG-3'
Biosensor hTopoI	
Rev_mTQ2-hTopoI_Bio	5' – TTGCTAGCACCTCCGCCGCTAAACTCGTAGTCTTCATCCGCC – 3'

Table A.8. Cloning of Biosensor constructs for bacterial expression.

Construct	Insert / bp	Plasmid / bp	RE couple used	Final Product (bp)
pProEX-HTb-sYFP2-YB1ΔC-hNTH1-mTQ2	1424 1705	4692	<i>SalI</i> / <i>NheI</i> <i>NheI</i> / <i>HindIII</i>	7821
pProEX-HTb-sYFP2-YB1ΔC-NtailhNTH1-mTQ2	1424 1036	4692	<i>SalI</i> / <i>NheI</i> <i>NheI</i> / <i>HindIII</i>	7152
pProEX-HTb-sYFP2-YB1ΔC-ND89hNTH1-mTQ2	1424 1441	4692	<i>SalI</i> / <i>NheI</i> <i>NheI</i> / <i>HindIII</i>	7557
pProEX-HTb-sYFP2-YB1ΔC-drEndoIII2-mTQ2	1424 1444	4692	<i>SalI</i> / <i>NheI</i> <i>NheI</i> / <i>HindIII</i>	7560
pProEX-HTb-sYFP2-YB1ΔC-mTQ2	1424 748	4692	<i>SalI</i> / <i>NheI</i> <i>NheI</i> / <i>HindIII</i>	6864
pProEX-HTb-sYFP2-hNTH1-mTQ2	746 1705	4692	<i>SalI</i> / <i>NheI</i> <i>NheI</i> / <i>HindIII</i>	7143
pProEX-HTb-mTQ2-hNTH1-YB1ΔC-sYFP2	1703 1426	4692	<i>SalI</i> / <i>NheI</i> <i>NheI</i> / <i>HindIII</i>	7821
pProEX-HTb-mTQ2-hTopoI-YB1ΔC-sYFP2	3062 1426	4692	<i>SalI</i> / <i>NheI</i> <i>NheI</i> / <i>HindIII</i>	9180

3. Protein sequences and properties obtained from ProtParam tool on the ExPASy Proteomics Server

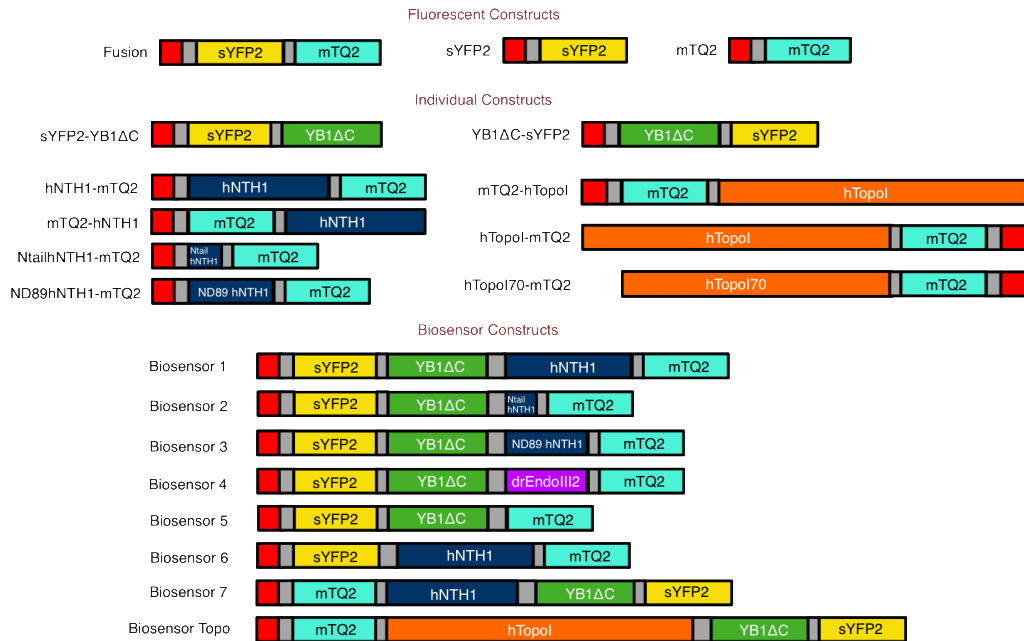


Figure A.4. Schematic illustration of all purified protein constructs in this work.

pProEX-HTb-sYFP2-mTQ2 (Fusion)

MSYYHHHHHDYDIPTTENLYFQAMGSGIQRPTSTMVSKGEELFTGVVPILVELDGDVN
 GHKFSVSGEGEGDATYGKLTCLKICTTGKLPVPWPTLVTTTLGYGVQCFAFYPDHMKQHDF
 FKSAMPEGYVQERTIFFKDDGNYKTRAEVKFEGDTLVNRIELKGIDFKEDGNILGHKLEY
 NYNSHNVIYITADKQKNGIKANFKIRHNIEDGGVQLADHYQQNTPIGDGPVLLPDNHYSY
 QSKLSKDPNEKRDHMLLEFVTAAGITLGMDELYKSGLRSRAMVSKGEELFTGVVPILVE
 LDGDVNGHKFSVSGEGEGDATYGKLTCLKICTTGKLPVPWPTLVTTLSWGVQCFAFYPDH
 MKQHDFFKSAMPEGYVQERTIFFKDDGNYKTRAEVKFEGDTLVNRIELKGIDFKEDGNIL
 GHKLEYNYFSDNVYITADKQKNGIKANFKIRHNIEDGGVQLADHYQQNTPIGDGPVLLPD
 NHYLSTQSKLSKDPNEKRDHMLLEFVTAAGITLGMDELYK-

Number of amino acids: 498

Molecular weight: 55747.04

Theoretical pI: 5.82

Extinction coefficients:

Extinction coefficients are in units of $M^{-1} \text{ cm}^{-1}$, at 280 nm measured in water.

Ext. coefficient 49530

Abs 0.1% (=1g/l) 0.888, assuming all pairs of Cys residues form cystines

Ext. coefficient 49280

Abs 0.1% (=1g/l) 0.884, assuming all Cys residues are reduced

pProEX-HTb-sYFP2

MSYYHHHHHHDYDIPTTENLYFQGAMGSGIQRPTSTMVSKGEELFTGVVPILVELDGDVN
GHKFSVSGEGEGDATYGKLTCLKICTTGKLPVPWPTLVTTLG YGVQCFARYPDHMKQHDF
FKSAMPEGYVQERTIFFKDDGNYKTRAEVKFEGDTLVNRIELKGIDFKEDGNILGHKLEY
NYNSHN VYITADKQKNGIKANFKIRHNIEDGGVQLADHYQQNTPIGDGPVLLPDNHYLSY
QSKLSKDPNEKRDHMLLEFVTAAGITLGMDELYK-

Number of amino acids: 252

Molecular weight: 28122.80

Theoretical pI: 5.86

Extinction coefficients:

Extinction coefficients are in units of $M^{-1} \text{ cm}^{-1}$, at 280 nm measured in water.

Ext. coefficient 23505

Abs 0.1% (=1g/l) 0.836, assuming all pairs of Cys residues form cystines

Ext. coefficient 23380

Abs 0.1% (=1g/l) 0.831, assuming all Cys residues are reduced

pProEX-HTb-mTQ2

MSYYHHHHHHDYDIPTTENLYFQGAMGSGIQRPTSTMVSKGEELFTGVVPILVELDGDVN
GHKFSVSGEGEGDATYGKLTCLKFICTTGKLPVPWPTLVTTLSWGVQCFARYPDHMKQHDF
FKSAMPEGYVQERTIFFKDDGNYKTRAEVKFEGDTLVNRIELKGIDFKEDGNILGHKLEY
NYFSDNVYITADKQKNGIKANFKIRHNIEDGGVQLADHYQQNTPIGDGPVLLPDNHYLST
QSKLSKDPNEKRDHMLLEFVTAAGITLGMDELYK-

Number of amino acids: 252

Molecular weight: 28158.83

Theoretical pI: 5.63

Extinction coefficients:

Extinction coefficients are in units of $M^{-1} \text{ cm}^{-1}$, at 280 nm measured in water.

Ext. coefficient 26025

Abs 0.1% (=1g/l) 0.924, assuming all pairs of Cys residues form cystines

Ext. coefficient 25900

Abs 0.1% (=1g/l) 0.920, assuming all Cys residues are reduced

Figure A.5. Protein sequences and properties after cleavage of His-tag obtained from ProtParam tool on the ExPASy Proteomics Server of fluorescent constructs. Red coloured letters, hexa-His tag; pink coloured letters, TEV cleavage site; yellow coloured letters, sYFP2; cyan coloured letters, mTQ2.

pProEX-HTb-sYFP2-YB1ΔC

MSYYHHHHHHDYDIPTTENLYFQGAMGSGIQRPTSTMVSKGEELFTGVVPILVELDGDVN
GHKFSVSGEGEGDATYGKLTCLKICTTGKLPVPWPTLVTTLG YGVQCFARYPDHMKQHDF
FKSAMPEGYVQERTIFFKDDGNYKTRAEVKFEGDTLVNRIELKGIDFKEDGNILGHKLEY
NYNSHN VYITADKQKNGIKANFKIRHNIEDGGVQLADHYQQNTPIGDGPVLLPDNHYLSY
QSKLSKDPNEKRDHMLLEFVTAAGITLGMDELYKSGLRSRAMSSEAETQQPPAAPPAAP
ALSAADTKPGTTGSGAGSGGPGGLTSAAPAGGDKKVIATKVLGTVKWFNVRNGYGFINRN
DTKEDV FVHQTAIKKNNPRKYLR SVGDGETVEFDVVEGEKGAEAAANTGPGGVPVQGSKY

AADRNHYRRYPRRRGPPRNYQQNYQNSESGEKNEGSESAPEGQAQRRPYRRRRFPYYM
RRPYGRRPQYSNPPVQGEVME-

Number of amino acids: 478

Molecular weight: 52672.89

Theoretical pI: 8.99

Extinction coefficients:

Extinction coefficients are in units of $M^{-1} cm^{-1}$, at 280 nm measured in water.

Ext. coefficient 46885

Abs 0.1% (=1g/l) 0.890, assuming all pairs of Cys residues form cystines

Ext. coefficient 46760

Abs 0.1% (=1g/l) 0.888, assuming all Cys residues are reduced

pProEX-HTb-YB1ΔC-sYFP2

MSYYHHHHHDYDIPTTENLYFQAMGSGIQRPTSTMSSEAETQPPAAPPAPALSAAD
TKPGTTGSGAGSGGPGGLTSAAPAGGDKKVIATKVLGTVKWFNVRNGYGFINRNDTKEDV
FVHQTAIKNNPRKYLRVGDGETVEFDVVEGEKGAEANVTGPGGVPVQGSKYAADRNH
YRRYPRRRGPPRNYQQNYQNSESGEKNEGSESAPEGQAQRRPYRRRRFPYYMRRPYGR
RPQYSNPPVQGEVMESDPPVATMVSKGEELFTGVVPILVELDGDVNGHKFSVSGEGEGDA
TYGKLTCLKICTTGKLPVPWPTLVTTLGYGVCFAFYDPDHMKQHDFFKSAMPEGYVQERT
IFFKDDGNYKTRAEVKFEGDTLVNRIELKGIDFKEDGNILGHKLEYNNSHNVIYITADKQ
KNGIKANFKIRHNIEDGGVQLADHYQQNTPIGDGPVLLPDNHYSYQSKLSKDPNEKRDH
MVLLEFVTAAGITLGMDELYK-

Number of amino acids: 478

Molecular weight: 52612.78

Theoretical pI: 8.65

Extinction coefficients:

Extinction coefficients are in units of $M^{-1} cm^{-1}$, at 280 nm measured in water.

Ext. coefficient 46885

Abs 0.1% (=1 g/l) 0.891, assuming all pairs of Cys residues form cystines

Ext. coefficient 46760

Abs 0.1% (=1 g/l) 0.889, assuming all Cys residues are reduced

Figure A.6. Protein sequences and properties after cleavage of His-tag obtained from ProtParam tool on the ExPASy Proteomics Server of YB1ΔC constructs. Red coloured letters, hexa-His tag; pink coloured letters, TEV cleavage site; yellow coloured letters, sYFP2; green coloured letters, YB1ΔC.

pProEX-HTb-hNTH1-mTQ2

MSYYHHHHHDYDIPTTENLYFQAMGSGIQRPTSTMCS PQESGMTALSARMLTRSRSLG
PGAGPRGCREEPGPLRRREAAAEARKSHSPVKRPRKAQRLRVAYEGSDSEKGEAEPLKV
PVWEPQDWQQQLVNIRAMRNKKDAPVDHLGTEHCYDSSAPPKVRRYQVLLSLMLSSQTKD
QVTAGAMQRLRARGLTVDLSILQTDDATLGKLIYPVGFWRSKVKYIKQTSAILQQHYGGDI
PASVAELVALPGVGPKMAHLAMAVAWGTVSGIAVDTHVHRIANRLRWTKKATKSPEETRA
ALEEWLPRELWHEINGLLVGFGQQTCLPVHPRCHACLNQALCPAAQGLSDPPVATMVSKG
EELFTGVVPILVELDGDVNGHKFSVSGEGEGDATYGKLTCLKFICTTGKLPVPWPTLVTTL

SWGVCQFARYPDHMKQHDFFKSAMPEGYVQERTIFFKDDGNYKTRAEVKFEGDTLVNRIE
LKGIDFKEDGNILGHKLEYNYFSDNVYITADKQKNGIKANFKIRHNIEDGGVQLADHYQQ
NTPIGDGPVLLPDNHYLSTQSKLSKDPNEKRDHMLLEFVTAAGITLGMDELYK-

Number of amino acids: 571

Molecular weight: 63198.11

Theoretical pI: 8.75

Extinction coefficients:

Extinction coefficients are in units of M⁻¹ cm⁻¹, at 280 nm measured in water.

Ext. coefficient 73840

Abs 0.1% (=1 g/l) 1.168, assuming all pairs of Cys residues form cystines

Ext. coefficient 73340

Abs 0.1% (=1 g/l) 1.160, assuming all Cys residues are reduced

pProEX-HTb-mTQ2- hNTH1

MSYYHHHHHDYDIPTTENLYFQAMGSGIQRPTSTMVSKGEELFTGVVPILVELDGDVN
GHKFSVSGEGEGDATYGKLTCLKFICTTGKLPVPWPTLVTTLSWGVQCFARYPDHMKQHDF
FKSAMPEGYVQERTIFFKDDGNYKTRAEVKFEGDTLVNRIELKGIDFKEDGNILGHKLEY
NYFSDNVYITADKQKNGIKANFKIRHNIEDGGVQLADHYQQNTPIGDGPVLLPDNHYLST
QSKLSKDPNEKRDHMLLEFVTAAGITLGMDELYKSGLRSRAMCSPQESGMTALSARMLT
RSRSLGPGAGPRGCREEPGPLRRREAAAEARKSHSPVKRPRKAQRLRVAYEGSDSEKGE
AEPLKVPVWEPQDWWQQLVNIRAMRNKKDAPVDHLGTEHCYDSSAPPKVRRYQVLLSLML
SSQTKDQVTAGAMQRLRARGLTVDLSILQTDDATLGKLIYPVGFWRSKVKYIKQTSAILQQ
HYGGDIPASVAELVALPGVGPMAHLAMAVAWGTVSGIAVDTHVHRIANRLRWTKKATKS
PEETRAALEEWLPRELWHEINGLLVGFGQQTCLPVHPRCHACLNQALCPAAQGL-

Number of amino acids: 571

Molecular weight: 63258.22

Theoretical pI: 8.97

Extinction coefficients:

Extinction coefficients are in units of M⁻¹ cm⁻¹, at 280 nm measured in water.

Ext. coefficient 73840

Abs 0.1% (=1 g/l) 1.167, assuming all pairs of Cys residues form cystines

Ext. coefficient 73340

Abs 0.1% (=1 g/l) 1.159, assuming all Cys residues are reduced

pProEX-HTb-NtailhNTH1-mTQ2

MSYYHHHHHDYDIPTTENLYFQAMGSGIQRPTSTMCSPPQESGMTALSARMLTRSRSLG
PGAGPRGCREEPGPLRRREAAAEARKSHSPVKRPRKAQRLRVAYEGSDSEKGEAEPLKV
PVWEPSPDPVATMVSKGEELFTGVVPILVELDGDVNGHKFSVSGEGEGDATYGKLTCLKFI
CTTGKLPVPWPTLVTTLSWGVQCFARYPDHMKQHDFFKSAMPEGYVQERTIFFKDDGNYK
TRAEVKFEGDTLVNRIELKGIDFKEDGNILGHKLEYNYFSDNVYITADKQKNGIKANFKI
RHNIEDGGVQLADHYQQNTPIGDGPVLLPDNHYLSTQSKLSKDPNEKRDHMLLEFVTAAG
ITLGMDELYK-

Number of amino acids: 348

Molecular weight: 38503.57

Theoretical pI: 6.84

Extinction coefficients:

Extinction coefficients are in units of M⁻¹ cm⁻¹, at 280 nm measured in water.

Ext. coefficient 33140
 Abs 0.1% (=1 g/l) 0.861, assuming all pairs of Cys residues form cystines
 Ext. coefficient 32890
 Abs 0.1% (=1 g/l) 0.854, assuming all Cys residues are reduced

pProEX-HTb- ND89hNTH1-mTQ2

MSYYHHHHHHDYDIPTT**ENLYFQG**AMGSGIQRPTSTMQDWQQQLVNIRAMRNKKDAPVDH
 LGTEHCYDSSAPPKVRRYQVLLSLMLSSQTKDQVTAGAMQRLRAGLTVDSILQTDATL
 GKLIYPVGFWRSKVKYIKQTSAILQQHYGGDIPASVAELVALPGVGPKMAHLAMAVAWGT
 VSGIAVDTHVHRIANRLRWTKKATKSPEETRAALEEWLPRELWHEINGLLVGFQQOTCLP
 VHPRCHACLNQALCPAAQGLSDPPVAT**MSVSKGEELFTGVVPIILVELDGDVNGHKFSVSGE**
GEGDATYGKLTCLKFICTTGKLPVPWPTLVTTLSWGVQCFARYPDHMKQHDFFKSAMPEGY
VQERTIFFKDDGNYKTRAEVKFEGDTLVNRIELKGIDFKEDGNILGHKLEYNYFSDNVYI
TADKQKNGIKANFKIRHNIEDGGVQLADHYQQNTPIGDGPVLLPDNHYLSTQSKLSKDPN
EKRDMVLEFVTAAGITLGMDELYK-

Number of amino acids: 483

Molecular weight: 53652.28

Theoretical pI: 7.37

Extinction coefficients:

Extinction coefficients are in units of M⁻¹ cm⁻¹, at 280 nm measured in water.

Ext. coefficient 66725

Abs 0.1% (=1 g/l) 1.244, assuming all pairs of Cys residues form cystines

Ext. coefficient 66350

Abs 0.1% (=1 g/l) 1.237, assuming all Cys residues are reduced

Figure A.7. Protein sequences and properties after cleavage of His-tag obtained from ProtParam tool on the ExPASy Proteomics Server of hNTH1 constructs. Red coloured letters, hexa-His tag; pink coloured letters, TEV cleavage site; cyan coloured letters, mTQ2; blue coloured letters, hNTH1.

pProEX-HTb-mTQ2- hTopoI

MSYYHHHHHHDYDIPTT**ENLYFQG**AMGSGIQRPTSTMVSKGEELFTGVVPIILVELDGDVN
 GHKFSVSGEGEGDATYGKLTCLKFICTTGKLPVPWPTLVTTLSWGVQCFARYPDHMKQHDF
 FKSAMPEGYVQERTIFFKDDGNYKTRAEVKFEGDTLVNRIELKGIDFKEDGNILGHKLEY
 NYFSDNVYITADKQKNGIKANFKIRHNIEDGGVQLADHYQQNTPIGDGPVLLPDNHYLST
 QSKLSKDPNEKRDMVLEFVTAAGITLGMDELYK**SGLRSRAMSGDHLHND****SQIEAD****FRL**
NDSHKHKDKHKDREHRHKEHKKEKDREKSKHSNSEHKDSEKKHKEKEKTKHKDGSSEKHK
DKHKDRDKEKRKEEKVRASGDAIKKEKENGFSPPQIKDEPEDDGYFVPPKEDIKPLKR
PRDEDDADYKPKKIKTEDTKKEKKRKLEEEEDGKLKPKNKDKDKVPEPDNKKKPKKE
EEQKWKWWEERYPEGIKWKFLHKGVPFAPPYEPLPENVKFYDGVKMLSPKAEVAT
FFAKMLDHEYTTKEIFRKNFFKDWKEMTNEEKNIITNLKSCDFTQMSQYFKAQTEARKQ
MSKEEKLKIKEENEKLLKEYGFCIMDNHKERIANFKIEPPGLFRGRGNHPKMGMMLKRRIM
PEDIIINCSKDAKVPSPPPGHKWKEVRHDNKVTWLVSWTENIQGSIKYIMLNPSRIKGE
KDWQKYETARRLKKCVDKIRNQYREDWKSKEMKVRQRAVALYFIDKLALRAGNEKEEGET
ADTVGCCSLRVEHINLHPELDGQEYVVEFDFLGKDSIRYYNKVPVEKRVFKNLQLFMENK

QPEDDLFDRNLNTGILNKHQLDLMEGLTAKVFRTYNASITLQQQLKELTAPDENIPAKILSYN
 RANRAVAAILCNHQRAPPKTFEKSMMNLQTKIDAKKEQLADARRDLKSAKADAKVMKDA
 KTKKVVESKKKAVQRLEEQLMKLEVQATDREENKQIALGTSKLNYLDPRITVAWCKKWGV
 PIEKIYNKTQREKFAWAIDMADEDYEF-

Number of amino acids: 1024

Molecular weight: 119594.36

Theoretical pI: 9.13

Extinction coefficients:

Extinction coefficients are in units of M⁻¹ cm⁻¹, at 280 nm measured in water.

Ext. coefficient 129315

Abs 0.1% (=1 g/l) 1.081, assuming all pairs of Cys residues form cystines

Ext. coefficient 128690

Abs 0.1% (=1 g/l) 1.076, assuming all Cys residues are reduced

pET21d-hTopoI-mTQ2

MGMSGDHLHNDSQLIADFRNLNDSHKHKDKHKDREHRHKEHKKEKDREKSKHSNSEHKDSE
 KKHKEKEKTKHKDGSSEKHKDKHKDRDKEKRKEEKVRASGDAKIKKEKENGFSPPQIKD
 EPEDDGYFVPPKEDIKPLKRPRDEDDADYKPKIKTEDTKKEKKRKLEEEEDGKLKPKN
 KDKDKKVPEPDNKKKKPKKEEQKWKWEEERYPEGIKWKFLHKGPFVAPPYEPLPENV
 KFYDYGKVMKLSPKAEVATFFAKMLDHEYTTKEIFRKNFFKDWRKEMTNEEKNIITNLS
 KCDFTQMSQYFKAQTEARKQMSKEEKLKIKEENEKLLKEYGFCIMDNHKERIANFKIEPP
 GLFRGRGNHPKMGMLKRRIMPEDIIINCSKDAKVPSPPPGHKWKEVRHDNKVTWLVSWE
 NIQGSIKYIMLNPSRIKGEKDQKYETARRLKKCVDKIRNQYREDWKSSEMKVQRARA
 LYFIDKLALRAGNEKEEGETADTVGCCSLRVEHINLHPELDGQEYVVEFDLFGKDSIRYY
 NKVPVEKRVFKNLQLFMENKQPEDDLFDRNLNTGILNKHQLDLMEGLTAKVFRTYNASITL
 QQQLKELTAPDENIPAKILSYNANRAVAAILCNHQRAPPKTFEKSMMNLQTKIDAKKEQL
 ADARRDLKSAKADAKVMKDAKTKKVVESKKKAVQRLEEQLMKLEVQATDREENKQIALGT
 SKLNYLDPRITVAWCKKWGVPIEKIYNKTQREKFAWAIDMADEDYEFSDPPVATMVSKGE
 ELFTGVVPILVELDGDVNGHKFSVSGEGEGDATYGLTLKFICTTGKLPVPWPTLVTTLS
 WGVQCFARYPDHMKQHDFFKSAMPEGYVQERTIFFKDDGNYKTRAEVKFEGDTLVNRIEL
 KGIDFKEDGNILGHKLEYNYFSDNVYITADKQKNGIKANFKIRHNIEDGGVQLADHYQQN
 TPIGDGPVLLPDNHYLSTQSKLSKDPNEKRDHMLLEFVTAAGITLGMDELYKLEHHHHH
 H-

Number of amino acids: 1020

Molecular weight: 119412.04

Theoretical pI: 9.03

Extinction coefficients:

Extinction coefficients are in units of M⁻¹ cm⁻¹, at 280 nm measured in water.

Ext. coefficient 129315

Abs 0.1% (=1 g/l) 1.083, assuming all pairs of Cys residues form cystines

Ext. coefficient 128690

Abs 0.1% (=1 g/l) 1.078, assuming all Cys residues are reduced

hTopoI70-mTQ2

LKKPKNKDKDKKVPEPDNKKKKPKKEEQKWKWEEERYPEGIKWKFLHKGPFVAPPYE
 PLPENVKFYDYGKVMKLSPKAEVATFFAKMLDHEYTTKEIFRKNFFKDWRKEMTNEEKNI

IITNLSKCDFTQMSQYFKAQTEARKQMSKEEKLKIKEENEKLLKEYGFCIMDNHKERIAN
 FKIEPPGLFRGRGNHPKMGMLKRRIMPEDIIINCSKDAKVPSPPPGHKWKEVRHDNKVTW
 LVSWTENIQGSIKYIMLNPSSRIKGEKDWQKYETARRLKKCVDKIRNQYREDWKSSEMKV
 RQRAVALYFIDKLALRAGNEKEEGETADTVGCCSLRVEHINLHPELDGQEYVVEFDLFGK
 DSIRYYNKVPVEKRVFKNLQLFMENKQPEDDLFDRLNTGILNKHLLQDLMEGLTAKVFRTY
 NASITLQQQLKELTAPDENIPAKILSYNRANRAVAILCNHQRAPPKTFEKSMMNLQTKID
 AKKEQLADARRDLKSAKADAKVMKDAKTKKVVESKKKAVQRLLEEQLMKLEVQATDREENK
 QIALGTSKLNYLDPRITVAWCKKWGVPIEKIYNKTQREKFAWAIDMADEDYEFSDPPVAT
 MVSKGEELFTGVVPIILVELDGDVNGHKFSVSGEGEGDATYGKLTCLKFICTTGKLPVPWPPT
 LVTTLSWGVQCFARYPDHMKQHDFFKSAMPEGYVQERTIFFKDDGNYKTRAEVKFEGDTL
 VNRIELKGIDFKEDGNILGHKLEYNYFSDNVYITADKQKNGIKANFKIRHNIEDGGVQLA
 DHYQQNTPIGDGPVLLPDNHYLSTQSKLSKDPNEKRDHMLLEFVTAAGITLGMDELYKL
 EHHHHHH-

Number of amino acids: 847

Molecular weight: 98778.29

Theoretical pI: 8.98

Extinction coefficients:

Extinction coefficients are in units of M⁻¹ cm⁻¹, at 280 nm measured in water.

Ext. coefficient 126335

Abs 0.1% (=1 g/l) 1.279, assuming all pairs of Cys residues form cystines

Ext. coefficient 125710

Abs 0.1% (=1 g/l) 1.273, assuming all Cys residues are reduced

Figure A.8. Protein sequences and properties after cleavage of His-tag obtained from ProtParam tool on the ExPASy Proteomics Server of hTopoI constructs. Red coloured letters, hexa-His tag; pink coloured letters, TEV cleavage site; cyan coloured letters, mTQ2; orange coloured letters, hTopoI.

Biosensor 1

pProEX-HTb-sYFP2-YB1ΔC-hNTH1-mTQ2

MSYYHHHHHHDYDIPTTENLYFQCAMGSGIQRPTSTMVSKGEELFTGVVPIILVELDGDVN
 GHKFSVSGEGEGDATYGKLTCLKFICTTGKLPVPWPPTLVTTLSWGVQCFARYPDHMKQHDF
 FKSAMPEGYVQERTIFFKDDGNYKTRAEVKFEGDTLVNRIELKGIDFKEDGNILGHKLEY
 NYNSHNVIYITADKQKNGIKANFKIRHNIEDGGVQLADHYQQNTPIGDGPVLLPDNHYLSY
 QSKLSKDPNEKRDHMLLEFVTAAGITLGMDELYKSGLSRAMSSEAETQQPPAAPAAP
 ALSAADTKPGTTGSGAGSGGPGGLTSAAPAGGDKKVIATKVLGTVKWFNVRNGYGFINRN
 DTKEDVVFVHQTAIKKNNPRKYLRVGDGETVEFDVVEGEKGAEANVTGPGGVPVQGSKY
 AADRNYHRRYPRRRGPPRNYQQNYQNSESGEKNESGESAPEGQAQQRRPYRRRRFPYYM
 RRPYGRRPQYSNPPVQGEVMESSGGASGGTMCSPQESGMTALSARMLTRSRLGPGAGP
 RGCREEPGPLRRREAAAEARKSHSPVKRPRKAQRLRVAYEGSDSEKGEAEPLKVPVWEP
 QDWQQQLVNIRAMRNKKDAPVDHLGTEHCYDSSAPPKVRRYQVLLSLMLSSQTKDQVTAG
 AMQRLRLRAGLTVDSILQTDATLGKLIYPVGFWRSKVKYIKQTSAILQQHYGGDIPASVA
 ELVALPGVGPKMAHLAMAVAWGTVSGIAVDTHVHRIANRLRWTKKATKSPEETRAALEEW
 LPRELWHEINGLLVGFGQQTCLPVHPRCHACLNQALCPAAQGLSDPPVATMVSKGEELFT
 GVVPIILVELDGDVNGHKFSVSGEGEGDATYGKLTCLKFICTTGKLPVPWPPTLVTTLSWGVQ
 CFARYPDHMKQHDFFKSAMPEGYVQERTIFFKDDGNYKTRAEVKFEGDTLVNRIELKGID

FKEDGNILGHKLEYNYFSDNVYITADKQKNGIKANFKIRHNIEDGGVQLADHYQQNTPIG
DGPVLLPDNHYLSTQSKLSKDPNEKRDHMLLEFVTAAGITLGMDELYK-

Number of amino acids: 1046

Molecular weight: 115297.25

Theoretical pI: 8.86

Extinction coefficients:

Extinction coefficients are in units of M⁻¹ cm⁻¹, at 280 nm measured in water.

Ext. coefficient 120725

Abs 0.1% (=1 g/l) 1.047, assuming all pairs of Cys residues form cystines

Ext. coefficient 120100

Abs 0.1% (=1 g/l) 1.042, assuming all Cys residues are reduced

Biosensor 2

pProEX-HTb-sYFP2-YB1ΔC-NtailhNTH1-mTQ2

MSYYHHHHHHDYDIPTTENLYFQGAMGSGIQRPTSTMVSKGEELFTGVVPILVELDGDVN
GHKFSVSGEGEGDATYGKLTCLKICTTGKLPVPWPTLVTTLG YGVQCFARYPDHMKQHDF
FKSAMPEGYVQERTIFFKDDGNYKTRAEVKFEGDTLVNRIELKGIDFKEDGNILGHKLEY
NYNSHNVYITADKQKNGIKANFKIRHNIEDGGVQLADHYQQNTPIGDGPVLLPDNHYLSY
QSKLSKDPNEKRDHMLLEFVTAAGITLGMDELYKSGLRSRAMSSEAETQQPPAAPPAAP
ALSAADTKPGTTGSGAGSGGPGGLTSAAPAGGDKKVIATKVLGTVKWFNVRNGYGFINRN
DTKEDV FVHQTAIKKNNPRKYLRSVGDGETVEFDVVEGEKGAEANVTGPGGVPVQGSKY
AADRNH YRRYPRRRGPPRNYQQNYQNSESGEKNESGESAPEGQAQQRRPYRRRRFPYYM
RRPYGRRPQYSNPPVQGEVMESGGGASGGGTMCSPQESGMTALSARMLTRSRLGPGAGP
RGCREEPGPLRRREAAAEARKSHSPVKRPRKAQRLRVAYEGSDSEKGEAEPLKVPVWEP
SDPPVATMVSKGEELFTGVVPILVELDGDVNGHKFSVSGEGEGDATYGKLTCLKFICTTGK
LPVPWPTLVTTLSWG VQCFARYPDHMKQHDFFKSAMPEGYVQERTIFFKDDGNYKTRAEV
KFEGDTLVNRIELKGIDFKEDGNILGHKLEYNYFSDNVYITADKQKNGIKANFKIRHNIE
DGGVQLADHYQQNTPIGDGPVLLPDNHYLSTQSKLSKDPNEKRDHMLLEFVTAAGITLG
MDELYK-

Number of amino acids: 823

Molecular weight: 90602.70

Theoretical pI: 8.48

Extinction coefficients:

Extinction coefficients are in units of M⁻¹ cm⁻¹, at 280 nm measured in water.

Ext. coefficient 80025

Abs 0.1% (=1 g/l) 0.883, assuming all pairs of Cys residues form cystines

Ext. coefficient 79650

Abs 0.1% (=1 g/l) 0.879, assuming all Cys residues are reduced

Biosensor 3

pProEX-HTb-sYFP2-YB1ΔC-ND89hNTH1-mTQ2

MSYYHHHHHHDYDIPTTENLYFQGAMGSGIQRPTSTMVSKGEELFTGVVPILVELDGDVN
GHKFSVSGEGEGDATYGKLTCLKICTTGKLPVPWPTLVTTLG YGVQCFARYPDHMKQHDF
FKSAMPEGYVQERTIFFKDDGNYKTRAEVKFEGDTLVNRIELKGIDFKEDGNILGHKLEY
NYNSHNVYITADKQKNGIKANFKIRHNIEDGGVQLADHYQQNTPIGDGPVLLPDNHYLSY
QSKLSKDPNEKRDHMLLEFVTAAGITLGMDELYKSGLRSRAMSSEAETQQPPAAPPAAP
ALSAADTKPGTTGSGAGSGGPGGLTSAAPAGGDKKVIATKVLGTVKWFNVRNGYGFINRN

DTKEDV FVHQTA I K K N N P R K Y L R S V G D G E T V E F D V V E G E K G A E A A N V T G P G G V P V Q G S K Y
 A A D R N H Y R R Y P R R R G P P R N Y Q Q N Y Q N S E S G E K N E G S E S A P E G Q A Q Q R R P Y R R R R F P P Y Y M
 R R P Y G R R P Q Y S N P P V Q G E V M E S G G G A S G G G T M Q D W Q Q L V N I R A M R N K K D A P V D H L G T E H
 C Y D S S A P P K V R R Y Q V L L S L M L S S Q T K D Q V T A G A M Q R L R A R G L T V D S I L Q T D D A T L G K L I Y
 P V G F W R S K V K Y I K Q T S A I L Q Q H Y G G D I P A S V A E L V A L P G V G P K M A H L A M A V A W G T V S G I A
 V D T H V H R I A N R L R W T K K A T K S P E E T R A A L E E W L P R E L W H E I N G L L V G F G Q Q T C L P V H P R C
 H A C L N Q A L C P A A Q G L S D P P V A T M V S K G E E L F T G V V P I L V E L D G D V N G H K F S V S G E G E G D A
 T Y G K L T L K F I C T T G K L P V P W P T L V T T L S W G V Q C F A R Y P D H M K Q H D F F K S A M P E G Y V Q E R T
 I F F K D D G N Y K T R A E V K F E G D T L V N R I E L K G I D F K E D G N I L G H K L E Y N Y F S D N V Y I T A D K Q
 K N G I K A N F K I R H N I E D G G V Q L A D H Y Q Q N T P I G D G P V L L P D N H Y L S T Q S K L S K D P N E K R D H
 M V L L E F V T A A G I T L G M D E L Y K -

Number of amino acids: 958

Molecular weight: 105751.42

Theoretical pI: 8.48

Extinction coefficients:

Extinction coefficients are in units of M⁻¹ cm⁻¹, at 280 nm measured in water.

Ext. coefficient 113610

Abs 0.1% (=1 g/l) 1.074, assuming all pairs of Cys residues form cystines

Ext. coefficient 113110

Abs 0.1% (=1 g/l) 1.070, assuming all Cys residues are reduced

Biosensor 4

pProEX-HTb-sYFP2-YB1ΔC-drEndoIII2-mTQ2

MSYY H H H H H D Y D I P T T E N L Y F Q G A M G S G I Q R P T S T M V S K G E E L F T G V V P I L V E L D G D V N
 G H K F S V S G E G E G D A T Y G K L T L K L I C T T G K L P V P W P T L V T T L G Y G V Q C F A R Y P D H M K Q H D F
 F K S A M P E G Y V Q E R T I F F K D D G N Y K T R A E V K F E G D T L V N R I E L K G I D F K E D G N I L G H K L E Y
 N Y N S H N V Y I T A D K Q K N G I K A N F K I R H N I E D G G V Q L A D H Y Q Q N T P I G D G P V L L P D N H Y L S Y
 Q S K L S K D P N E K R D H M V L L E F V T A A G I T L G M D E L Y K S G L R S R A M S S E A E T Q Q P P A A P P A A P
 A L S A A D T K P G T T G S G A G S G G P G G L T S A A P A G G D K K V I A T K V L G T V K W F N V R N G Y G F I N R N
 D T K E D V F V H Q T A I K K N N P R K Y L R S V G D G E T V E F D V V E G E K G A E A A N V T G P G G V P V Q G S K Y
 A A D R N H Y R R Y P R R R G P P R N Y Q Q N Y Q N S E S G E K N E G S E S A P E G Q A Q Q R R P Y R R R R F P P Y Y M
 R R P Y G R R P Q Y S N P P V Q G E V M E S G G G A S G G G T M T R N S A S P R L P A G A R A R A P Q V L S A L G R L Y
 P D A R T E L V F N T P F E L L V A T V L S A Q A T D V S V N A A T P A L F A A Y P D A H A L S Q A T A D D I E P Y I R
 S I G L Y R G K A K N L A A L A R L L V E R H G G E V P N D F D A V A L P G A G R K T A N V V L S N A Y D Y P A I A V
 D T H V G R L A R R L G L S V Q T N P D K V E A D L Q K L F P R D R W V F L H H A L I L H G R R V C H A R K P Q C P S C
 E L A S F C P K V G V E H V E G S D P P V A T M V S K G E E L F T G V V P I L V E L D G D V N G H K F S V S G E G E G D
 A T Y G K L T L K F I C T T G K L P V P W P T L V T T L S W G V Q C F A R Y P D H M K Q H D F F K S A M P E G Y V Q E R
 T I F F K D D G N Y K T R A E V K F E G D T L V N R I E L K G I D F K E D G N I L G H K L E Y N Y F S D N V Y I T A D K
 Q K N G I K A N F K I R H N I E D G G V Q L A D H Y Q Q N T P I G D G P V L L P D N H Y L S T Q S K L S K D P N E K R D
 H M V L L E F V T A A G I T L G M D E L Y K -

Number of amino acids: 959

Molecular weight: 105193.50

Theoretical pI: 8.15

Extinction coefficients:

Extinction coefficients are in units of M⁻¹ cm⁻¹, at 280 nm measured in water.

Ext. coefficient 87600

Abs 0.1% (=1 g/l) 0.833, assuming all pairs of Cys residues form cystines

Ext. coefficient 87100

Abs 0.1% (=1 g/l) 0.828, assuming all Cys residues are reduced

Biosensor 5

pProEX-HTb-sYFP2-YB1ΔC-mTQ2

MSYYHHHHHHDYDIPTTENLYFQ^{AMGSGIQRP}ST^{MVSKGEELFTGVVPILVELDGDVN}
^{GHKFSVS}GEGEGDATY^{GKLT}TLK^{LICTTGKLPVPWP}TLVTT^{LG}YGVQCFARYPDHMKQHDF
^{FKSAM}PEGYVQERTIFFKDDGNYKTRA^{EVKFEGDTLVNRIELKGIDFKEDGNILGHKLEY}
^{NYN}SHNVYITADKQKNGIKANFKIRHNIEDGGVQLADHYQQNTPIGDGPVLLPDNHYLSY
^{QSKLSKDPNEKRDH}MLLEFVTAAGITLGMDELYK^{SGLRSRAMSSE}AETQQPPAAPPAAP
^{ALSAADTKPGTTGSGAGSGGPGGLTSAAPAGGDKKVIATKVLGTVKWFNVRNGYGF}INRN
^{DTKEDV}FVHQTAIKKNNPRKYLR^{SVGDGETVEFDVVEGEKGAE}AANVTGPGGVFVQGSKY
^{AADR}NHYRRYPRRRGPPRNYQQNYQNSESGEKNEGSESAPEGQAQQRRPYRRRRFPYYM
^{RRPYGRRPQYSNPPVQGEVME}SGGASGGGT^{MVSKGEELFTGVVPILVELDGDVNGHKFS}
^{VSGEGEGDATY}GKLT^{LKFI}CTTGKLPVPWP^{TLVTTLSW}GVQCFARYPDHMKQHDFFKSAM
^{PEGYVQERTIFFKDDGNYKTRA}EVKFEGDTLVNRIELKGIDFKEDGNILGHKLEYNYFSD
^{NVYITADKQKNGIKANFKIRHNIEDGGVQLADHYQQNTPIGDGPVLLPDNHYLSTQSKLS}
^{KDPNEKRDH}MLLEFVTAAGITLGMDELYK-

Number of amino acids: 727

Molecular weight: 80257.9

Theoretical pI: 7.11

Extinction coefficients:

Extinction coefficients are in units of M⁻¹ cm⁻¹, at 280 nm measured in water.

Ext. coefficient 72910

Abs 0.1% (=1 g/l) 0.908, assuming all pairs of Cys residues form cystines

Ext. coefficient 72660

Abs 0.1% (=1 g/l) 0.905, assuming all Cys residues are reduced

Biosensor 6

pProEX-HTb-sYFP2-hNTH1-mTQ2

MSYYHHHHHHDYDIPTTENLYFQ^{AMGSGIQRP}ST^{MVSKGEELFTGVVPILVELDGDVN}
^{GHKFSVS}GEGEGDATY^{GKLT}TLK^{LICTTGKLPVPWP}TLVTT^{LG}YGVQCFARYPDHMKQHDF
^{FKSAM}PEGYVQERTIFFKDDGNYKTRA^{EVKFEGDTLVNRIELKGIDFKEDGNILGHKLEY}
^{NYN}SHNVYITADKQKNGIKANFKIRHNIEDGGVQLADHYQQNTPIGDGPVLLPDNHYLSY
^{QSKLSKDPNEKRDH}MLLEFVTAAGITLGMDELYK^{SGGGASGGGTMCSPQESGMTALSAR}
^{MLTRSRSLGPGAGPRGCREEPGPLRRREAAAEARKSHSPVKRPRKAQRLRVAYEGSDSEK}
^{GEGAEPLKVPVWEPQDWQQQLVNIRAMRNKKDAPVDHLGTEHCYDSSAPPKVRRYQVLLS}
^{LMLSSQTKDQVTAGAMQRLRARGLTVD}SILQTDATLGKLIYPVGFWR^{SKVKYIKQ}TSAI
^{LQQHYGGDIPASVAELVALPGVGPKMAHLAMAVAWGT}VSGIAVDTHVHRIANRLRWTKKA
^{TKSPEETRAALEEWLPRELWHEINGLLVGFGQQTCLPVHPRCHACLNQALCPAAQGLSDP}
^{PVATMVSKGEELFTGVVPILVELDGDVNGHKFSVS}GEGEGDATY^{GKLT}TLK^{LICTTGKLPV}
^{PWPTLVTTLSW}GVQCFARYPDHMKQHDFFKSAMPEGYVQERTIFFKDDGNYKTRA^{EVKFE}
^{GD}TLVNRIELKGIDFKEDGNILGHKLEYNYFSDNVYITADKQKNGIKANFKIRHNIEDGG
^{VQLADHYQQNTPIGDGPVLLPDNHYLSTQSKLSKDPNEKRDH}MLLEFVTAAGITLGMDE
^{LYK-}

Number of amino acids: 820

Molecular weight: 90747.1

Theoretical pI: 7.43

Extinction coefficients:

Extinction coefficients are in units of M⁻¹ cm⁻¹, at 280 nm measured in water.

Ext. coefficient 97345

Abs 0.1% (=1 g/l) 1.073, assuming all pairs of Cys residues form cystines

Ext. coefficient 96720

Abs 0.1% (=1 g/l) 1.066, assuming all Cys residues are reduced

Biosensor 7

pProEX-HTb-mTQ2-hNTH1-YB1ΔC-sYFP2

MSYYHHHHHDYDIPTTENLYFQ^{AMGSGIQRPST}MSVSKGEELFTGVVPILVELDGDVN
GHKFSVSGEGEGDATYGKLT^{LKFICTTGKLPVPWPTLVTTLSWGVQC}FARYPDHMKQHDF
FKSAMPEGYVQERTIFFKDDGNYKTRAEVKFEGDTLVNRIELKGIDFKEDGNILGHKLEY
NYFSDNVYITADKQKNGIKANFKIRHNIEDGGVQLADHYQQNTPIGDGPVLLPDNH^{YLSY}
QSKLSKDPNEKRDH^{MVLL}EFVTAAGITLGMDELYK^{SGLRSRAMCSPQESGMTALSARMLT}
RSRSLGPGAGPRGCREEPGLRRREAAAEARKSHSPVKRPRKAQRLRVAYEGSDSEKGE
AEPLKVPVWEPQDWQQQLVNIRAMRNKKDAPVDHLGTEHCYDSSAPPKVRRYQVLLSLML
SSQTKDQVTAGAMQRLRARGLTVD^{SILQTD}DATLGKLIYPVGFWR^{SKVKYIKQTSAILQQ}
HYGGDIPASVAELVALPGVGPKMAHLAMAVAWGTVSGIAVDTHVHRIANRLRWTKKATKS
PEETRAALEEWLPRELWHEINGLLVGF^{GQQTCLPVHPRCHACLNQALCPAAQGLSGGGAS}
GGGTMSSEAETQQPPAAPPAAPALSAADTKPGTTGSGAGSGGPGGLTSAAPAGGDKKVIA
TKVLGTVKWFNVRNGYGF^{INRNDTKEDVFVHQTAIKNNPRKYLR}SVGDGETVEFDVVEG
EKGAEEANVTGPGGVPVQGSKYAADRNHYRRYPRRRGPPRNYQQNYQNSESGEKNEGSES
APEGQAQQRRPYRRRRFP^{PYYMR}RPYGRRPQYSNPPVQGEVME^{SDPPVAT}MSVSKGEELFT
GVVPILVELDGDVNGHKFSVSGEGEGDATYGKLT^{LKLICTTGKLPVPWPTLVTTLG}YGVQ
CFARYPDHMKQHDFFKSAMPEGYVQERTIFFKDDGNYKTRAEVKFEGDTLVNRIELKGID
FKEDGNILGHKLEY^{NYNSHN}VYITADKQKNGIKANFKIRHNIEDGGVQLADHYQQNTPIG
DGPVLLPDNH^{YLSY}QSKLSKDPNEKRDH^{MVLL}EFVTAAGITLGMDELYK-

Number of amino acids: 1046

Molecular weight: 115297.25

Theoretical pI: 8.86

Extinction coefficients:

Extinction coefficients are in units of M⁻¹ cm⁻¹, at 280 nm measured in water.

Ext. coefficient 120725

Abs 0.1% (=1 g/l) 1.047, assuming all pairs of Cys residues form cystines

Ext. coefficient 120100

Abs 0.1% (=1 g/l) 1.042, assuming all Cys residues are reduced

Biosensor Topo

pProEX-HTb-mTQ2-hTopoI-YB1ΔC-sYFP2

MSYYHHHHHDYDIPTTENLYFQ^{AMGSGIQRPST}MSVSKGEELFTGVVPILVELDGDVN
GHKFSVSGEGEGDATYGKLT^{LKFICTTGKLPVPWPTLVTTLSWGVQC}FARYPDHMKQHDF
FKSAMPEGYVQERTIFFKDDGNYKTRAEVKFEGDTLVNRIELKGIDFKEDGNILGHKLEY
NYFSDNVYITADKQKNGIKANFKIRHNIEDGGVQLADHYQQNTPIGDGPVLLPDNH^{YLSY}
QSKLSKDPNEKRDH^{MVLL}EFVTAAGITLGMDELYK^{SGLRSRAMSGDHLHND}SQIEAD^{FRL}
ND^{SHKHKDKHKDREHRHKEHKKEKDREKSKHSN}SEHKDSEKKHKEKEKTKHKDGSSEKHK
DKHKDRDKEKRKEEKVRASGDAKIKKEKENGFS^{SPQIKDEPEDDGYFVPPKEDIKPLKR}

PRDEDDADYKPKKIKTEDTKKEKKRKLEEEEDGKLKKPKNKDKDKKVPEPDNKKKKPKKE
 EEQKWKWWEERYPEGIKWKFLEHKGPVFAPPYEPLPENVKFYDGVKMLSPKAEVAT
 FFAKMLDHEYTTKEIFRKNFFKDWKEMTNEEKNIITNLSKCDFTQMSQYFKAQTEARKQ
 MSKEEKLKIKEENEKLLKEYGFCIMDNHKERIANFKIEPPGLFRGRGNHPKMGMLKRRIM
 PEDI I INCSKDAKVPSPPPGHKWKEVRHDNKVTWLVSWTENIQGSIKYIMLNPSSRIKGE
 KDWQKYETARRLKKCVDKIRNQYREDWKSKEMKVRQRAVALYFIDKLALRAGNEKEEGET
 ADTVGCCSLRVEHINLHPELDGQEYVVEFDLFGKDSIRYYNKVPVEKRVFKNLQLFMENK
 QPEDDLFDRLNTGILNHLQDLMEGLTAKVFRTYNASITLQQQLKELTAPDENIPAKILS
 YNRANRAVAILCNHQRAPPKTFEKSMMNLQTKIDAKKEQLADARRDLKSAKADAKVMKDA
 KTKKVVESKKKAVQRLEEQLMKLEVQATDREENKQIALGTSKLNYLDPRITVAWCKKWGV
 PIEKIYNKTQREKFAWAIDMADEDYEFSGGGASGGGTMSSEAE TQQPPAAPPAALSAA
 DTKPGTTGSGAGSGGPGGLTSAAPAGGDKKVIATKVLGTVKWFNVRNGYGFINRNDTKED
 VVFVHQTAIKKNNPRKYLRVGDGETVEFDVVEGEKGAEANVTGPGGVPVQGSKYAADRN
 HYRRYPRRRGPPRNYQQNYQNSESGEKNESGESAPEGQAQRRPYRRRRFPYYMRRPYG
 RRPQYSNPPVQGEVME SDPPVATMVSKGEELFTGVVPILVELDGDVNGHKFSVSGEGED
 ATYGKLTCLKICTTGKLPVPWPTLVTTLGYGVCFAFYPDHMKQHDFFKSAMPEGYVQER
 TIFFKDDGNYKTRAEVKFEGDTLVNRIELKGIDFKEDGNILGHKLEYNYNSHNVYITADK
 QKNGIKANFKIRHNIEDGGVQLADHYQQNTPIGDGPVLLPDNHLYSYQSKLSKDPNEKRD
 HMYLLEFVTAAGITLGMDELYK-

Number of amino acids: 1499

Molecular weight: 171633.39

Theoretical pI: 9.05

Extinction coefficients:

Extinction coefficients are in units of M⁻¹ cm⁻¹, at 280 nm measured in water.

Ext. coefficient 176200

Abs 0.1% (=1 g/l) 1.027, assuming all pairs of Cys residues form cystines

Ext. coefficient 175450

Abs 0.1% (=1 g/l) 1.022, assuming all Cys residues are reduced

Figure A.9. Protein sequences and properties after cleavage of His-tag obtained from ProtParam tool on the ExPASy Proteomics Server of Biosensor constructs. Red coloured letters, hexa-His tag; pink coloured letters, TEV cleavage site; yellow coloured letters, sYFP2; green coloured letters, YB1ΔC; blue coloured letters, hNTH1; cyan coloured letters, mTQ2; purple coloured letters, drEndoIII2; orange coloured letters, hTopoI.

4. Sequence of 12nt THF dsDNA oligonucleotide

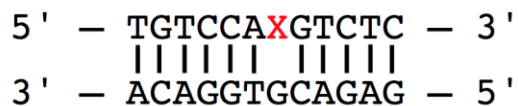


Figure A.10. Illustration of 12nt THF dsDNA oligonucleotide. X: dSpacer, Tetrahydrofuran (THF).

REFERENCES

- Aamann, M.D., Hvitby, C., Popuri, V., Muftuoglu, M., Lemminger, L., Skeby, C.K., Keijzers, G., Ahn, B., Bjørås, M., Bohr, V.A., Stevnsner, T.**, 2014, Cockayne Syndrome group B protein stimulates NEIL2 DNA glycosylase activity, *Mech. Ageing Dev.*, 135, 1–14. <https://doi.org/10.1016/j.mad.2013.12.008>
- Adam, V., Nienhaus, K., Bourgeois, D., Nienhaus, G.U.**, 2009, Structural basis of enhanced photoconversion yield in green fluorescent protein-like protein Dendra2, *Biochemistry (Mosc.)*, 48, 4905–4915. <https://doi.org/10.1021/bi900383a>
- Akbari, M., Peña-Díaz, J., Andersen, S., Liabakk, N.-B., Otterlei, M., Krokan, H.E.**, 2009, Extracts of proliferating and non-proliferating human cells display different base excision pathways and repair fidelity, *DNA Repair*, 8, 834–843. <https://doi.org/10.1016/j.dnarep.2009.04.002>
- Alemasova, E.E., Naumenko, K.N., Kurgina, T.A., Anarbaev, R.O., Lavrik, O.I.**, 2018, The multifunctional protein YB-1 potentiates PARP1 activity and decreases the efficiency of PARP1 inhibitors, *Oncotarget*, 9, 23349–23365. <https://doi.org/10.18632/oncotarget.25158>
- Arkin, M.R., Glicksman, M.A., Fu, H., Havel, J.J., Du, Y.**, 2004, Inhibition of protein-protein interactions: Non-cellular assay formats, in: Sittampalam, G.S., Coussens, N.P., Brimacombe, K., Grossman, A., Arkin, M., Auld, D., Austin, C., Baell, J., Bejcek, B., Chung, T.D.Y., Dahlin, J.L., Devanaryan, V., Foley, T.L., Glicksman, M., Hall, M.D., Hass, J.V., Inglese, J., Iversen, P.W., Kahl, S.D., Kales, S.C., Lal-Nag, M., Li, Z., McGee, J., McManus, O., Riss, T., Trask, O.J., Weidner, J.R., Xia, M., Xu, X. (Eds.), *Assay Guidance Manual*. Eli Lilly & Company and the National Center for Advancing Translational Sciences, Bethesda (MD).
- Arkin, M.R. and Wells, J.A.**, 2004, Small-molecule inhibitors of protein-protein interactions: Progressing towards the dream, *Nat. Rev. Drug Discov.*, 3, 301–317.
- Asakuno, K., Kohno, K., Uchiumi, T., Kubo, T., Sato, S., Isono, M., Kuwano, M.**, 1994, Involvement of a DNA binding protein, MDR-NF1/YB-1, in human MDR1 gene expression by actinomycin D, *Biochem. Biophys. Res. Commun.*, 199, 1428–1435. <https://doi.org/10.1006/bbrc.1994.1390>
- Ba, X. and Boldogh, I.**, 2018, 8-Oxoguanine DNA glycosylase 1: Beyond repair

of the oxidatively modified base lesions, *Redox Biol.*, 14, 669–678.
<https://doi.org/10.1016/j.redox.2017.11.008>

Bajar, B.T., Wang, E.S., Zhang, S., Lin, M.Z., Chu, J., 2016, A guide to fluorescent protein FRET pairs, *Sensors*, 16.
<https://doi.org/10.3390/s16091488>

Bandyopadhyay, K., Li, P., Gjerset, R.A., 2012, CK2-mediated hyperphosphorylation of topoisomerase I targets serine 506, enhances topoisomerase I–DNA binding, and increases cellular Camptothecin sensitivity *PLOS ONE*, 7, e50427.
<https://doi.org/10.1371/journal.pone.0050427>

Baranello, L., Wojtowicz, D., Cui, K., Devaiah, B.N., Chung, H.-J., Chan-Salis, K.Y., Guha, R., Wilson, K., Zhang, X., Zhang, H., Piotrowski, J., Thomas, C.J., Singer, D.S., Pugh, B.F., Pommier, Y., Przytycka, T.M., Kouzine, F., Lewis, B.A., Zhao, K., Levens, D., 2016, RNA Polymerase II regulates topoisomerase 1 activity to favor efficient transcription, *Cell*, 165, 357–371. <https://doi.org/10.1016/j.cell.2016.02.036>

Bargou, R.C., Jürchott, K., Wagener, C., Bergmann, S., Metzner, S., Bommert, K., Mapara, M.Y., Winzer, K.J., Dietel, M., Dörken, B., Royer, H.D., 1997, Nuclear localization and increased levels of transcription factor YB-1 in primary human breast cancers are associated with intrinsic MDR1 gene expression, *Nat. Med.*, 3, 447–450.

Basse, M.-J., Betzi, S., Morelli, X., Roche, P., 2016, 2P2Idb v2: update of a structural database dedicated to orthosteric modulation of protein–protein interactions, Database 2016. <https://doi.org/10.1093/database/baw007>

Beard, W.A., Prasad, R., Wilson, S.H., 2006, Activities and mechanism of DNA polymerase beta, *Methods Enzymol.*, 408, 91–107.
[https://doi.org/10.1016/S0076-6879\(06\)08007-4](https://doi.org/10.1016/S0076-6879(06)08007-4)

Beck, W.T., Morgan, S.E., Mo, Y.-Y., Bhat, U.G., 1999, Tumor cell resistance to DNA topoisomerase II inhibitors: new developments, *Drug Resist. Updat.*, 2, 382–389. <https://doi.org/10.1054/drup.1999.0110>

Beidler, D.R. and Cheng, Y.C., 1995, Camptothecin induction of a time- and concentration-dependent decrease of topoisomerase I and its implication in camptothecin activity, *Mol. Pharmacol.*, 47, 907–914.

Beretta, G.L., Gatti, L., Perego, P., Zaffaroni, N., 2013, Camptothecin resistance in cancer: insights into the molecular mechanisms of a DNA-

- damaging drug, *Curr. Med. Chem.*, 20, 1541–1565.
- Berggård, T., Linse, S., James, P.**, 2007, Methods for the detection and analysis of protein-protein interactions, *Proteomics*, 7, 2833–2842. <https://doi.org/10.1002/pmic.200700131>
- Bertram, J.S.**, 2000, The molecular biology of cancer, *Mol. Aspects Med.*, 21, 167–223. [https://doi.org/10.1016/S0098-2997\(00\)00007-8](https://doi.org/10.1016/S0098-2997(00)00007-8)
- Bessho, T.**, 1999, Nucleotide excision repair 3' endonuclease XPG stimulates the activity of base excision repair enzyme thymine glycol DNA glycosylase, *Nucleic Acids Res.*, 27, 979–983.
- Bjornsti, M.-A. and Osheroff, N.** (Eds.), 1999, DNA Topoisomerase Protocols: Volume I: DNA Topology and Enzymes, *Methods in Molecular Biology*, Humana Press.
- Bogan, A.A. and Thorn, K.S.**, 1998, Anatomy of hot spots in protein interfaces, *J. Mol. Biol.*, 280:1–9.
- Boorstein, R.J., Chiu, L.N., Teebor, G.W.**, 1989, Phylogenetic evidence of a role for 5-hydroxymethyluracil-DNA glycosylase in the maintenance of 5-methylcytosine in DNA, *Nucleic Acids Res.*, 17, 7653–7661.
- Bourgeois, D.**, 2017, Deciphering structural photophysics of fluorescent proteins by kinetic crystallography, *Int. J. Mol. Sci.*, 18. <https://doi.org/10.3390/ijms18061187>
- Bowen, C., Stuart, A., Ju, J.-H., Tuan, J., Blonder, J., Conrads, T.P., Veenstra, T.D., Gelmann, E.P.**, 2007, NKX3.1 homeodomain protein binds to topoisomerase I and enhances its activity, *Cancer Res.*, 67, 455–464. <https://doi.org/10.1158/0008-5472.CAN-06-1591>
- Chakrabarti, P. and Janin, J.**, 2002, Dissecting protein–protein recognition sites, *Proteins*, 47, 334–343.
- Chakraborty, S., Núñez, D., Hu, S.-Y., Domingo, M.P., Pardo, J., Karmenyan, A., Gálvez, E.M., Chiou, A.**, 2014, FRET based quantification and screening technology platform for the interactions of Leukocyte Function-Associated Antigen-1 (LFA-1) with InterCellular Adhesion Molecule-1 (ICAM-1), *PLOS ONE*, 9, e102572. <https://doi.org/10.1371/journal.pone.0102572>
- Champoux, J.J.**, 2001, DNA topoisomerases: structure, function, and mechanism, *Annu. Rev. Biochem.*, 70, 369–413. <https://doi.org/10.1146/annurev.biochem.70.1.369>

- Chan, M.K., Ocampo-Hafalla, M.T., Vartanian, V., Jaruga, P., Kirkali, G., Koenig, K.L., Brown, S., Lloyd, R.S., Dizdaroglu, M., Teebor, G.W.,** 2009, Targeted deletion of the genes encoding NTH1 and NEIL1 DNA N-glycosylases reveals the existence of novel carcinogenic oxidative damage to DNA, *DNA Repair*, 8, 786–794. <https://doi.org/10.1016/j.dnarep.2009.03.001>
- Chattopadhyay, R., Das, S., Maiti, A.K., Boldogh, I., Xie, J., Hazra, T.K., Kohno, K., Mitra, S., Bhakat, K.K.,** 2008, Regulatory role of human AP-Endonuclease (APE1/Ref-1) in YB-1-mediated activation of the multidrug resistance gene MDR1, *Mol. Cell. Biol.*, 28, 7066–7080. <https://doi.org/10.1128/MCB.00244-08>
- Cheng, X., Hochlowski, J., Tang, H., Hepp, D., Beckner, C., Kantor, S., Schmitt, R.,** 2003, Studies on repository compound stability in DMSO under various conditions, *J. Biomol. Screen.*, 8, 292–304. <https://doi.org/10.1177/1087057103008003007>
- Cohen, S.B., Ma, W., Valova, V.A., Algie, M., Harfoot, R., Woolley, A.G., Robinson, P.J., Braithwaite, A.W.,** 2010, Genotoxic stress-induced nuclear localization of oncoprotein YB-1 in the absence of proteolytic processing, *Oncogene*, 29, 403–410. <https://doi.org/10.1038/onc.2009.321>
- Colmegna, B., Morosi, L., D’Incalci, M.,** 2017, Molecular and pharmacological mechanisms of drug resistance: An evolving paradigm, in: SpringerLink, *Handbook of Experimental Pharmacology*, Springer, Berlin, Heidelberg, pp. 1–12. https://doi.org/10.1007/164_2017_20
- Czubaty, A., Girstun, A., Kowalska-Loth, B., Trzcińska, A.M., Purta, E., Winczura, A., Grajkowski, W., Staroń, K.,** 2005, Proteomic analysis of complexes formed by human topoisomerase I, *Biochim. Biophys. Acta BBA - Proteins Proteomics*, 1749, 133–141. <https://doi.org/10.1016/j.bbapap.2005.03.007>
- Dahl, E., En-Nia, A., Wiesmann, F., Krings, R., Djudjaj, S., Breuer, E., Fuchs, T., Wild, P.J., Hartmann, A., Dunn, S.E., Mertens, P.R.,** 2009, Nuclear detection of Y-boxprotein-1 (YB-1) closely associates with progesterone receptor negativity and is a strong adverse survival factor in human breast cancer, *BMC Cancer*, 9, 410. <https://doi.org/10.1186/1471-2407-9-410>
- Das, S., Chattopadhyay, R., Bhakat, K.K., Boldogh, I., Kohno, K., Prasad, R., Wilson, S.H., Hazra, T.K.,** 2007, Stimulation of NEIL2-mediated oxidized

- base excision repair via YB-1 interaction during oxidative stress, *J. Biol. Chem.*, 282, 28474–28484. <https://doi.org/10.1074/jbc.M704672200>
- Das, S.K., Rehman, I., Ghosh, A., Sengupta, S., Majumdar, P., Jana, B., Das, B.B.**, 2016, Poly(ADP-ribose) polymers regulate DNA topoisomerase I (Top1) nuclear dynamics and camptothecin sensitivity in living cells, *Nucleic Acids Res.*, 44, 8363–8375. <https://doi.org/10.1093/nar/gkw665>
- Day, R.N. and Davidson, M.W.**, 2009, The fluorescent protein palette: tools for cellular imaging, *Chem. Soc. Rev.*, 38, 2887–2921. <https://doi.org/10.1039/b901966a>
- De Las Rivas, J. and Fontanillo, C.**, 2010, Protein–protein interactions essentials: Key concepts to building and analyzing interactome networks, *PLoS Comput. Biol.*, 6. <https://doi.org/10.1371/journal.pcbi.1000807>
- Degorce, F., Card, A., Soh, S., Trinquet, E., Knapik, G.P., Xie, B.**, 2009, HTRF: A technology tailored for drug discovery –A review of theoretical aspects and recent applications, *Curr. Chem. Genomics*, 3, 22–32. <https://doi.org/10.2174/1875397300903010022>
- Dianov, G.L.**, 2011, Base excision repair targets for cancer therapy, *Am. J. Cancer Res.*, 1, 845–851.
- Didier, D.K., Schiffenbauer, J., Woulfe, S.L., Zacheis, M., Schwartz, B.D.**, 1988, Characterization of the cDNA encoding a protein binding to the major histocompatibility complex class II Y box, *Proc. Natl. Acad. Sci. U. S. A.*, 85, 7322–7326.
- Dizdaroglu, M.**, 2015, Oxidatively induced DNA damage and its repair in cancer, *Mutat. Res. Rev. Mutat. Res.*, 763, 212–245. <https://doi.org/10.1016/j.mrrev.2014.11.002>
- Dizdaroglu, M.**, 2005, Base-excision repair of oxidative DNA damage by DNA glycosylases, *Mutat. Res. Mol. Mech. Mutagen., Mechanistic Approaches to Chemoprevention of Mutation and Cancer*, 591, 45–59. <https://doi.org/10.1016/j.mrfmmm.2005.01.033>
- Dizdaroglu, M., Bauche, C., Rodriguez, H., Laval, J.**, 2000, Novel substrates of *Escherichia coli* Nth protein and its kinetics for excision of modified bases from DNA damaged by free radicals, *Biochemistry (Mosc.)*, 39, 5586–5592. <https://doi.org/10.1021/bi9927787>
- Dizdaroglu, M., Karahalil, B., Sentürker, S., Buckley, T.J., Roldán-Arjona, T.**, 1999, Excision of products of oxidative DNA base damage by human

NTH1 protein, *Biochemistry (Mosc.)*, 38, 243–246.
<https://doi.org/10.1021/bi9819071>

Bates A.D. and Maxwell A., 2005, DNA Topology, New Edition. Oxford University Press, Oxford, New York.

Dumetz, A.C., Snellinger-O'brien, A.M., Kaler, E.W., Lenhoff, A.M., 2007, Patterns of protein protein interactions in salt solutions and implications for protein crystallization, *Protein Sci. Publ. Protein Soc.*, 16, 1867–1877.
<https://doi.org/10.1110/ps.072957907>

Dyson, H.J. and Wright, P.E., 2005, Intrinsically unstructured proteins and their functions, *Nat. Rev. Mol. Cell Biol.*, 6, 197–208.
<https://doi.org/10.1038/nrm1589>

Eliseeva, I.A., Kim, E.R., Guryanov, S.G., Ovchinnikov, L.P., Lyabin, D.N., 2011, Y-box-binding protein 1 (YB-1) and its functions, *Biochem. Mosc.*, 76, 1402–1433. <https://doi.org/10.1134/S0006297911130049>

Evdokimova, V.M., Wei, C.-L., Sitikov, A.S., Simonenko, P.N., Lazarev, O.A., Vasilenko, K.S., Ustinov, V.A., Hershey, J.W.B., Ovchinnikov, L.P., 1995, The major protein of messenger ribonucleoprotein particles in somatic cells is a member of the Y-box binding transcription factor family, *J. Biol. Chem.*, 270, 3186–3192. <https://doi.org/10.1074/jbc.270.7.3186>

Farrell, A., 2011, A close look at cancer, *Nat. Med.*, 17, 262–265.
<https://doi.org/10.1038/nm0311-262>

Fröhlich, R.F., Andersen, F.F., Westergaard, O., Andersen, A.H., Knudsen, B.R., 2004, Regions within the N-terminal domain of human topoisomerase I exert important functions during strand rotation and DNA binding, *J. Mol. Biol.*, 336, 93–103. <https://doi.org/10.1016/j.jmb.2003.12.007>

Fromme, J.C. and Verdine, G.L., 2003, Structure of a trapped endonuclease III-DNA covalent intermediate, *EMBO J.*, 22, 3461–3471.
<https://doi.org/10.1093/emboj/cdg311>

Gaudreault, I., Guay, D., Lebel, M., 2004, YB-1 promotes strand separation in vitro of duplex DNA containing either mispaired bases or cisplatin modifications, exhibits endonucleolytic activities and binds several DNA repair proteins, *Nucleic Acids Res.*, 32, 316–327.
<https://doi.org/10.1093/nar/gkh170>

Glavinas, H., Krajcsi, P., Cserepes, J., Sarkadi, B., 2004, The role of ABC transporters in drug resistance, metabolism and toxicity, *Curr. Drug Deliv.*,

1, 27–42.

- Glickman, J.F., Wu, X., Mercuri, R., Illy, C., Bowen, B.R., He, Y., Sills, M.,** 2002, A comparison of ALPHAScreen, TR-FRET, and TRF as assay methods for FXR nuclear receptors, *J. Biomol. Screen.*, 7, 3–10. <https://doi.org/10.1177/108705710200700102>
- Gobert, C., Bracco, L., Rossi, F., Olivier, M., Tazi, J., Lavelle, F., Larsen, A.K., Riou, J.F.,** 1996, Modulation of DNA topoisomerase I activity by p53, *Biochemistry (Mosc.)*, 35, 5778–5786. <https://doi.org/10.1021/bi952327w>
- Goedhart, J., von Stetten, D., Noirclerc-Savoye, M., Lelimosin, M., Joosen, L., Hink, M.A., van Weeren, L., Gadella, T.W.J., Royant, A.,** 2012, Structure-guided evolution of cyan fluorescent proteins towards a quantum yield of 93%, *Nat. Commun.*, 3, 751. <https://doi.org/10.1038/ncomms1738>
- Gottesman, M.M., Fojo, T., Bates, S.E.,** 2002, Multidrug resistance in cancer: role of ATP-dependent transporters, *Nat. Rev. Cancer*, 2, 48–58. <https://doi.org/10.1038/nrc706>
- Graumann, P. and Marahiel, M.A.,** 1996, A case of convergent evolution of nucleic acid binding modules, *BioEssays News Rev. Mol. Cell. Dev. Biol.*, 18, 309–315. <https://doi.org/10.1002/bies.950180409>
- Guay, D., Garand, C., Reddy, S., Schmutte, C., Lebel, M.,** 2008, The human endonuclease III enzyme is a relevant target to potentiate cisplatin cytotoxicity in Y-box-binding protein-1 overexpressing tumor cells, *Cancer Sci.*, 99, 762–769. <https://doi.org/10.1111/j.1349-7006.2008.00739.x>
- Hanahan, D. and Weinberg, R.A.,** 2011, Hallmarks of cancer: The next generation, *Cell*, 144, 646–674.
- Hasegawa, S.L., Doetsch, P.W., Hamilton, K.K., Martin, A.M., Okenquist, S.A., Lenz, J., Boss, J.M.,** 1991, DNA binding properties of YB-1 and dbpA: binding to double-stranded, single-stranded, and abasic site containing DNAs, *Nucleic Acids Res.*, 19, 4915–4920.
- Helleday, T., Petermann, E., Lundin, C., Hodgson, B., Sharma, R.A.,** 2008, DNA repair pathways as targets for cancer therapy, *Nat. Rev. Cancer*, 8, 193–204. <https://doi.org/10.1038/nrc2342>
- Hilbert, T.P., Boorstein, R.J., Kung, H.C., Bolton, P.H., Xing, D., Cunningham, R.P., Teebor, G.W.,** 1996, Purification of a mammalian homologue of Escherichia coli endonuclease III: identification of a bovine

pyrimidine hydrate-thymine glycol DNase/AP lyase by irreversible cross linking to a thymine glycol-containing oligoxynucleotide, *Biochemistry (Mosc.)*, 35, 2505–2511. <https://doi.org/10.1021/bi952516e>

Hilbert, T.P., Chaung, W., Boorstein, R.J., Cunningham, R.P., Teebor, G.W., 1997, Cloning and expression of the cDNA encoding the human homologue of the DNA repair enzyme, Escherichia coli endonuclease III, *J. Biol. Chem.*, 272, 6733–6740.

Hoeijmakers, J.H.J., 2001, Genome maintenance mechanisms for preventing cancer, *Nature*, 17, 411:366–74. <https://doi.org/10.1038/35077232>

Holden, J.A., 2001, DNA topoisomerases as anticancer drug targets, from the laboratory to the clinic, *Curr. Med. Chem. Anticancer Agents*, 1, 1–25. <https://doi.org/info:doi/10.2174/1568011013354859>

Horie, K., Tomida, A., Sugimoto, Y., Yasugi, T., Yoshikawa, H., Taketani, Y., Tsuruo, T., 2002, SUMO-1 conjugation to intact DNA topoisomerase I amplifies cleavable complex formation induced by camptothecin, *Oncogene*, 21, 7913–22. <https://doi.org/10.1038/sj.onc.1205917>

Housman, G., Byler, S., Heerboth, S., Lapinska, K., Longacre, M., Snyder, N., Sarkar, S., 2014, Drug resistance in cancer: an overview, *Cancers*, 6, 1769–1792. <https://doi.org/10.3390/cancers6031769>

Ikeda, S., Biswas, T., Roy, R., Izumi, T., Boldogh, I., Kurosky, A., Sarker, A.H., Seki, S., Mitra, S., 1998, Purification and characterization of human NTH1, a homolog of Escherichia coli endonuclease III. Direct identification of Lys-212 as the active nucleophilic residue, *J. Biol. Chem.*, 273, 21585–21593.

Inglese, J., Shamu, C.E., Guy, R.K., 2007, Reporting data from high-throughput screening of small-molecule libraries, *Nat. Chem. Biol.*, 3, 438–441. <https://doi.org/10.1038/nchembio0807-438>

Ise, T., Nagatani, G., Imamura, T., Kato, K., Takano, H., Nomoto, M., Izumi, H., Ohmori, H., Okamoto, T., Ohga, T., Uchiumi, T., Kuwano, M., Kohno, K., 1999, Transcription factor Y-box binding protein 1 binds preferentially to cisplatin-modified DNA and interacts with proliferating cell nuclear antigen, *Cancer Res.*, 59, 342–346.

Izumi, H., Imamura, T., Nagatani, G., Ise, T., Murakami, T., Uramoto, H., Torigoe, T., Ishiguchi, H., Yoshida, Y., Nomoto, M., Okamoto, T., Uchiumi, T., Kuwano, M., Funa, K., Kohno, K., 2001, Y box-binding

protein-1 binds preferentially to single-stranded nucleic acids and exhibits 3' → 5' exonuclease activity, *Nucleic Acids Res.*, 29, 1200–1207.

Jacobs, A.L. and Schär, P., 2012, DNA glycosylases: in DNA repair and beyond, *Chromosoma*, 121, 1–20. <https://doi.org/10.1007/s00412-011-0347-4>

Janz, M., Harbeck, N., Dettmar, P., Berger, U., Schmidt, A., Jürchott, K., Schmitt, M., Royer, H.-D., 2002, Y-box factor YB-1 predicts drug resistance and patient outcome in breast cancer independent of clinically relevant tumor biologic factors HER2, uPA and PAI-1, *Int. J. Cancer*, 97, 278–282.

Jares-Erijman, E.A. and Jovin, T.M., 2006, Imaging molecular interactions in living cells by FRET microscopy, *Curr. Opin. Chem. Biol.*, 10, 409–416. <https://doi.org/10.1016/j.cbpa.2006.08.021>

Juan, C.C., Hwang, J.L., Liu, A.A., Whang-Peng, J., Knutsen, T., Huebner, K., Croce, C.M., Zhang, H., Wang, J.C., Liu, L.F., 1988, Human DNA topoisomerase I is encoded by a single-copy gene that maps to chromosome region 20q12-13.2, *Proc. Natl. Acad. Sci. U. S. A.*, 85, 8910–8913.

Kasid, U.N., Halligan, B., Liu, L.F., Dritschilo, A., Smulson, M., 1989, Poly(ADP-ribose)-mediated post-translational modification of chromatin-associated human topoisomerase I. Inhibitory effects on catalytic activity, *J. Biol. Chem.*, 264, 18687–18692.

Kauvar, L.M., Morgan, A.S., Sanderson, P.E., Henner, W.D., 1998, Glutathione based approaches to improving cancer treatment, *Chem. Biol. Interact.*, 111–112, 225–238. [https://doi.org/10.1016/S0009-2797\(97\)00163-4](https://doi.org/10.1016/S0009-2797(97)00163-4)

Kim, J.H., Lee, S.-R., Li, L.-H., Park, H.-J., Park, J.-H., Lee, K.Y., Kim, M.-K., Shin, B.A., Choi, S.-Y., 2011, High cleavage efficiency of a 2A peptide derived from porcine teschovirus-1 in human cell lines, zebrafish and mice, *PloS One*, 6, e18556. <https://doi.org/10.1371/journal.pone.0018556>

Kloks, C.P.A.M., Spronk, C.A.E.M., Lasonder, E., Hoffmann, A., Vuister, G.W., Grzesiek, S., Hilbers, C.W., 2002, The solution structure and DNA-binding properties of the cold-shock domain of the human Y-box protein YB-1, *J. Mol. Biol.*, 316, 317–326. <https://doi.org/10.1006/jmbi.2001.5334>

Klungland, A., Höss, M., Gunz, D., Constantinou, A., Clarkson, S.G., Doetsch, P.W., Bolton, P.H., Wood, R.D., Lindahl, T., 1999, Base

excision repair of oxidative DNA damage activated by XPG protein, *Mol. Cell*, 3, 33–42.

Klungland, A. and Lindahl, T., 1997, Second pathway for completion of human DNA base excision-repair: reconstitution with purified proteins and requirement for DNase IV (FEN1), *EMBO J.*, 16, 3341–3348. <https://doi.org/10.1093/emboj/16.11.3341>

Kohno, K., Izumi, H., Uchiumi, T., Ashizuka, M., Kuwano, M., 2003, The pleiotropic functions of the Y-box-binding protein, YB-1, *BioEssays News Rev. Mol. Cell. Dev. Biol.*, 25, 691–698. <https://doi.org/10.1002/bies.10300>

Koike, K., Uchiumi, T., Ohga, T., Toh, S., Wada, M., Kohno, K., Kuwano, M., 1997, Nuclear translocation of the Y-box binding protein by ultraviolet irradiation, *FEBS Lett.*, 417, 390–394.

Kojima, A., Hackett, N.R., Crystal, R.G., 1998, Reversal of CPT-11 resistance of lung cancer cells by adenovirus-mediated gene transfer of the human carboxylesterase cDNA, *Cancer Res.*, 58, 4368–4374.

Koster, D.A., Crut, A., Shuman, S., Bjornsti, M.-A., Dekker, N.H., 2010, Cellular strategies for regulating DNA supercoiling: A single-molecule perspective, *Cell*, 142, 519–530. <https://doi.org/10.1016/j.cell.2010.08.001>

Koster, D.A., Palle, K., Bot, E.S.M., Bjornsti, M.-A., Dekker, N.H., 2007, Antitumour drugs impede DNA uncoiling by topoisomerase I, *Nature*, 448, 213–217. <https://doi.org/10.1038/nature05938>

Kozikowski, B.A., Burt, T.M., Tirey, D.A., Williams, L.E., Kuzmak, B.R., Stanton, D.T., Morand, K.L., Nelson, S.L., 2003, The effect of freeze/thaw cycles on the stability of compounds in DMSO, *J. Biomol. Screen.*, 8, 210–215. <https://doi.org/10.1177/1087057103252618>

Kremers, G.-J., Goedhart, J., van Munster, E.B., Gadella, T.W.J., 2006, Cyan and yellow super fluorescent proteins with improved brightness, protein folding, and FRET Förster radius, *Biochemistry (Mosc.)*, 45, 6570–6580. <https://doi.org/10.1021/bi0516273>

Krokan, H.E. and Bjørås, M., 2013, Base excision repair, *Cold Spring Harb. Perspect. Biol.*, 5, 1–22. <https://doi.org/10.1101/cshperspect.a012583>

Kuwano, M., Oda, Y., Izumi, H., Yang, S.-J., Uchiumi, T., Iwamoto, Y., Toi, M., Fujii, T., Yamana, H., Kinoshita, H., Kamura, T., Tsuneyoshi, M., Yasumoto, K., Kohno, K., 2004, The role of nuclear Y-box binding protein 1 as a global marker in drug resistance, *Mol. Cancer Ther.*, 3, 1485–1492.

- Ladomery, M. and Sommerville, J.**, 1995, A role for Y-box proteins in cell proliferation, *BioEssays News Rev. Mol. Cell. Dev. Biol.*, 17, 9–11. <https://doi.org/10.1002/bies.950170104>
- Lakowicz, J. R.**, 2006, Principles of fluorescence spectroscopy, *Springer Science Publisher*, New York.
- Landsman, D.**, 1992, RNP-1, an RNA-binding motif is conserved in the DNA-binding cold shock domain, *Nucleic Acids Res.*, 20, 2861–2864.
- Lasham, A., Print, C.G., Woolley, A.G., Dunn, S.E., Braithwaite, A.W.**, 2013, YB-1: oncoprotein, prognostic marker and therapeutic target?, *Biochem. J.*, 449, 11–23. <https://doi.org/10.1042/BJ20121323>
- Leshner, D.-T.T., Pommier, Y., Stewart, L., Redinbo, M.R.**, 2002, 8-Oxoguanine rearranges the active site of human topoisomerase I., *Proc. Natl. Acad. Sci. U. S. A.*, 99, 12102–12107. <https://doi.org/10.1073/pnas.192282699>
- Lichtman, J.W. and Conchello, J.-A.**, 2005, Fluorescence microscopy, *Nat. Methods*, 2, 910–919. <https://doi.org/10.1038/nmeth817>.
- Lievens, S., Eyckerman, S., Lemmens, I., Tavernier, J.**, 2010, Large-scale protein interactome mapping: strategies and opportunities, *Expert Rev. Proteomics*, 7, 679–690. <https://doi.org/10.1586/epr.10.30>
- Lisby, M., Olesen, J.R., Skouboe, C., Krogh, B.O., Straub, T., Boege, F., Velmurugan, S., Martensen, P.M., Andersen, A.H., Jayaram, M., Westergaard, O., Knudsen, B.R.**, 2001, Residues within the N-terminal domain of human topoisomerase I play a direct role in relaxation, *J. Biol. Chem.*, 276, 20220–20227. <https://doi.org/10.1074/jbc.M010991200>
- Liu, L.F., Desai, S.D., Li, T.K., Mao, Y., Sun, M., Sim, S.P.**, 2000, Mechanism of action of camptothecin, *Ann. N. Y. Acad. Sci.*, 922, 1–10.
- Liu, X., Choudhury, S., Roy, R.**, 2003, In vitro and in vivo dimerization of human endonuclease III stimulates its activity, *J. Biol. Chem.*, 278, 50061–50069. <https://doi.org/10.1074/jbc.M309997200>
- Liu, X. and Roy, R.**, 2002, Truncation of amino-terminal tail stimulates activity of human endonuclease III (hNTH1), *J. Mol. Biol.*, 321, 265–276.
- Liu, Z., Chen, O., Wall, J.B.J., Zheng, M., Zhou, Y., Wang, L., Ruth Vaseghi, H., Qian, L., Liu, J.**, 2017, Systematic comparison of 2A peptides for cloning multi-genes in a polycistronic vector, *Sci. Rep.*, 7. <https://doi.org/10.1038/s41598-017-02460-2>

- Longley, D.B. and Johnston, P.G.**, 2005, Molecular mechanisms of drug resistance, *J. Pathol.*, 205, 275–292. <https://doi.org/10.1002/path.1706>
- Lyabin, D.N., Eliseeva, I.A., Ovchinnikov, L.P.**, 2014. YB-1 protein: functions and regulation. *Wiley Interdiscip. Rev. RNA* 5, 95–110. <https://doi.org/10.1002/wrna.1200>
- Madden, K.R. and Champoux, J.J.**, 1992, Overexpression of human topoisomerase I in baby hamster kidney cells: hypersensitivity of clonal isolates to camptothecin, *Cancer Res.*, 52, 525–532.
- Madhusudan, S., Smart, F., Shrimpton, P., Parsons, J.L., Gardiner, L., Houlbrook, S., Talbot, D.C., Hammonds, T., Freemont, P.A., Sternberg, M.J.E., Dianov, G.L., Hickson, I.D.**, 2005, Isolation of a small molecule inhibitor of DNA base excision repair, *Nucleic Acids Res.*, 33, 4711–4724. <https://doi.org/10.1093/nar/gki781>
- Malo, N., Hanley, J.A., Cerquozzi, S., Pelletier, J., Nadon, R.**, 2006, Statistical practice in high-throughput screening data analysis, *Nat. Biotechnol.*, 24, 167–175. <https://doi.org/10.1038/nbt1186>
- Malyuchenko, N.V., Kotova, E.Y., Kulaeva, O.I., Kirpichnikov, M.P., Studitskiy, V.M.**, 2015, PARP1 Inhibitors: antitumor drug design, *Acta Naturae*, 7, 27–37.
- Mansoori, B., Mohammadi, A., Davudian, S., Shirjang, S., Baradaran, B.**, 2017, The different mechanisms of cancer drug resistance: a brief review, *Adv. Pharm. Bull.*, 7, 339–348. <https://doi.org/10.15171/apb.2017.041>
- Mao, Y. and Muller, M.T.**, 2003, Down modulation of topoisomerase I affects DNA repair efficiency, *DNA Repair*, 2, 1115–1126. [https://doi.org/10.1016/S1568-7864\(03\)00122-8](https://doi.org/10.1016/S1568-7864(03)00122-8)
- Marenstein, D.R., Chan, M.K., Altamirano, A., Basu, A.K., Boorstein, R.J., Cunningham, R.P., Teebor, G.W.**, 2003, Substrate specificity of human endonuclease III (hNTH1). Effect of human APE1 on hNTH1 activity, *J. Biol. Chem.*, 278, 9005–9012. <https://doi.org/10.1074/jbc.M212168200>
- Marenstein, D.R., Ocampo, M.T., Chan, M.K., Altamirano, A., Basu, A.K., Boorstein, R.J., Cunningham, R.P., Teebor, G.W.**, 2001, Stimulation of human endonuclease III by Y box-binding protein 1 (DNA-binding protein B). Interaction between a base excision repair enzyme and a transcription factor, *J. Biol. Chem.*, 276, 21242–21249. <https://doi.org/10.1074/jbc.M101594200>

- Mastop, M., Bindels, D.S., Shaner, N.C., Postma, M., Gadella, T.W.J., Goedhart, J.**, 2017, Characterization of a spectrally diverse set of fluorescent proteins as FRET acceptors for mTurquoise2, *Sci. Rep.*, 7. <https://doi.org/10.1038/s41598-017-12212-x>
- Mazumder, A., Gerlt, J.A., Absalon, M.J., Stubbe, J., Cunningham, R.P., Withka, J., Bolton, P.H.**, 1991, Stereochemical studies of the .beta.-elimination reactions at aldehydic abasic sites in DNA: endonuclease III from *Escherichia coli*, sodium hydroxide, and Lys-Trp-Lys, *Biochemistry (Mosc.)*, 30, 1119–1126. <https://doi.org/10.1021/bi00218a033>
- Michael, M. and Doherty, M. M.**, 2005, Tumoral drug metabolism: overview and its implications for cancer therapy, *J. Clin. Oncol.*, 23, 205–229. <https://doi.org/10.1200/JCO.2005.02.120>
- Mielke, C., Kalfalah, F.M., Christensen, M.O., Boege, F.**, 2007, Rapid and prolonged stalling of human DNA topoisomerase I in UVA-irradiated genomic areas, *DNA Repair*, 6, 1757–1763. <https://doi.org/10.1016/j.dnarep.2007.06.014>
- Milhas, S., Raux, B., Betzi, S., Derviaux, C., Roche, P., Restouin, A., Basse, M.-J., Rebuffet, E., Lugari, A., Badol, M., Kashyap, R., Lissitzky, J.-C., Eydoux, C., Hamon, V., Gourdell, M.-E., Combes, S., Zimmermann, P., Aurrand-Lions, M., Roux, T., Rogers, C., Müller, S., Knapp, S., Trinquet, E., Collette, Y., Guillemot, J.-C., Morelli, X.**, 2016, Protein-protein interaction inhibition (2P2I)-oriented chemical library accelerates hit discovery, *ACS Chem. Biol.*, 11, 2140–2148. <https://doi.org/10.1021/acschembio.6b00286>
- Mirkin, S.M.**, 2001, DNA topology: fundamentals, *Life Sci.*, 123, 1–11. <https://doi.org/10.1021/ja0156845>
- Roche, P. and Morelli, X.**, 2011, Protein-protein interaction inhibition (2P2I): mixed methodologies for the acceleration of lead discovery, *In In silico lead discovery*, Edited by Miteva M: Bentham; 2010, 118-143.
- Muftuoglu, M., de Souza-Pinto, N.C., Dogan, A., Aamann, M., Stevnsner, T., Rybanska, I., Kirkali, G., Dizdaroglu, M., Bohr, V.A.**, 2009, Cockayne syndrome group B protein stimulates repair of formamidopyrimidines by NEIL1 DNA glycosylase, *J. Biol. Chem.*, 284, 9270–9279. <https://doi.org/10.1074/jbc.M807006200>
- Nagy, P., Vámosi, G., Bodnár, A., Lockett, S.J., Szöllősi, J.**, 1998, Intensity-based energy transfer measurements in digital imaging microscopy, *Eur.*

Biophys. J., 27, 377–389. <https://doi.org/10.1007/s002490050145>

- Newton, P., Harrison, P., Clulow, S.**, 2008, A novel method for determination of the affinity of protein: protein interactions in homogeneous assays, *J. Biomol. Screen.*, 13, 674–682. <https://doi.org/10.1177/1087057108321086>
- Ngounou Wetie, A.G., Sokolowska, I., Woods, A.G., Roy, U., Deinhardt, K., Darie, C.C.**, 2014, Protein-protein interactions: Switch from classical methods to proteomics and bioinformatics-based approaches, *Cell. Mol. Life Sci.*, 71, 205–228. <https://doi.org/10.1007/s00018-013-1333-1>
- Nitiss, J.L., Soans, E., Rogojina, A., Seth, A., Mishina, M.**, 2012, Topoisomerase Assays, *Curr. Protoc. Pharmacol.* CHAPTER, Unit3.3. <https://doi.org/10.1002/0471141755.ph0303s57>
- Oda, Y., Ohishi, Y., Saito, T., Hinoshita, E., Uchiumi, T., Kinukawa, N., Iwamoto, Y., Kohno, K., Kuwano, M., Tsuneyoshi, M.**, 2003, Nuclear expression of Y-box-binding protein-1 correlates with P-glycoprotein and topoisomerase II alpha expression, and with poor prognosis in synovial sarcoma, *J. Pathol.*, 199, 251–258. <https://doi.org/10.1002/path.1282>
- O'Hare, T., Walters, D.K., Stoffregen, E.P., Jia, T., Manley, P.W., Mestan, J., Cowan-Jacob, S.W., Lee, F.Y., Heinrich, M.C., Deininger, M.W.N., Druker, B.J.**, 2005, In vitro activity of Bcr-Abl inhibitors AMN107 and BMS-354825 against clinically relevant imatinib-resistant Abl kinase domain mutants, *Cancer Res.*, 65, 4500–4505. <https://doi.org/10.1158/0008-5472.CAN-05-0259>
- Ohga, T., Koike, K., Ono, M., Makino, Y., Itagaki, Y., Tanimoto, M., Kuwano, M., Kohno, K.**, 1996, Role of the human Y box-binding protein YB-1 in cellular sensitivity to the DNA-damaging agents cisplatin, mitomycin C, and ultraviolet light, *Cancer Res.*, 56, 4224–4228.
- Okamoto, T., Izumi, H., Imamura, T., Takano, H., Ise, T., Uchiumi, T., Kuwano, M., Kohno, K.**, 2000, Direct interaction of p53 with the Y-box binding protein, YB-1: a mechanism for regulation of human gene expression, *Oncogene*, 19, 6194–6202. <https://doi.org/10.1038/sj.onc.1204029>
- Osheroff, N. and Bjornsti, M.-A.** (Eds.), 2001, DNA Topoisomerase Protocols: Volume II: Enzymology and Drugs, *Methods in Molecular Biology*. Humana Press.
- Pecorino, L.**, 2008, Molecular biology of cancer: mechanisms, targets, and

therapeutics. <https://doi.org/10.1038/nchembio840>

- Peixoto, P., Bailly, C., David-Cordonnier, M.-H.**, 2010, Topoisomerase I-mediated DNA relaxation as a tool to study intercalation of small molecules into supercoiled DNA, in: drug-DNA interaction protocols, *Methods in Molecular Biology*, Humana Press, 235–256. https://doi.org/10.1007/978-1-60327-418-0_15
- Piston, D.W. and Kremers, G.-J.**, 2007, Fluorescent protein FRET: the good, the bad and the ugly, *Trends Biochem. Sci.*, 32, 407–414. <https://doi.org/10.1016/j.tibs.2007.08.003>
- Pommier, Y.**, 2014, Drugging topoisomerases: lessons and challenges, *ACS Chem. Biology*, 8, 82–95. <https://doi.org/10.1021/cb300648v>. Drugging
- Pommier, Y.** (Ed.), 2012, DNA topoisomerases and cancer, *Cancer Drug Discovery and Development*. Humana Press.
- Pommier, Y.**, 2006, Topoisomerase I inhibitors: camptothecins and beyond, *Nat. Rev. Cancer*, 6, 789–802. <https://doi.org/10.1038/nrc1977>
- Pommier, Y., Barcelo, J., Rao, V.A., Sordet, O., Jobson, A.G., Thibaut, L., Miao, Z., Seiler, J., Zhang, H., Marchand, C., Agama, K., Redon, C.**, 2006, Repair of topoisomerase I-mediated DNA damage, *Prog. Nucleic Acid Res. Mol. Biol.*, 81, 179–229. [https://doi.org/10.1016/S0079-6603\(06\)81005-6](https://doi.org/10.1016/S0079-6603(06)81005-6)
- Pommier, Y., Sun, Y., Huang, S.-Y.N., Nitiss, J.L.**, 2016, Roles of eukaryotic topoisomerases in transcription, replication and genomic stability, *Nat. Rev. Mol. Cell Biol.*, 17, 703–721. <https://doi.org/10.1038/nrm.2016.111>
- Pourquier, P., Ueng, L.M., Kohlhagen, G., Mazumder, A., Gupta, M., Kohn, K.W., Pommier, Y.**, 1997, Effects of uracil incorporation, DNA mismatches, and abasic sites on cleavage and religation activities of mammalian topoisomerase I, *J. Biol. Chem.*, 272, 7792–7796.
- Prasad, R., Beard, W.A., Strauss, P.R., Wilson, S.H.**, 1998, Human DNA polymerase beta deoxyribose phosphate lyase. Substrate specificity and catalytic mechanism, *J. Biol. Chem.*, 273, 15263–15270.
- Puc, J., Kozbial, P., Li, W., Tan, Y., Liu, Z., Suter, T., Ohgi, K.A., Zhang, J., Aggarwal, A.K., Rosenfeld, M.G.**, 2015, Ligand-dependent enhancer activation regulated by topoisomerase-I activity, *Cell*, 160, 367–380. <https://doi.org/10.1016/j.cell.2014.12.023>
- Rebucci, M. and Michiels, C.**, 2013, Molecular aspects of cancer cell resistance

to chemotherapy, *Biochem. Pharmacol.*, 85, 1219–1226.
<https://doi.org/10.1016/j.bcp.2013.02.017>

Rogers, M.S., Cryan, L.M., Habeshian, K.A., Bazinet, L., Caldwell, T.P., Ackroyd, P.C., Christensen, K.A., 2012, A FRET-based high throughput screening assay to identify inhibitors of anthrax protective antigen binding to capillary morphogenesis gene 2 protein, *PLOS ONE*, 7, e39911.
<https://doi.org/10.1371/journal.pone.0039911>

Roszik, J., Lisboa, D., Szöllosi, J., Vereb, G., 2009, Evaluation of intensity-based ratiometric FRET in image cytometry—approaches and a software solution, *Cytom. Part J. Int. Soc. Anal. Cytol.*, 75, 761–767.
<https://doi.org/10.1002/cyto.a.20747>

Roszik, J., Tóth, G., Szöllösi, J., Vereb, G., 2013, Validating pharmacological disruption of protein-protein interactions by acceptor photobleaching FRET imaging, *Methods Mol. Biol.*, Clifton NJ 986, 165–178.
https://doi.org/10.1007/978-1-62703-311-4_11

Rubinstein, D.B., Stortchevoi, A., Boosalis, M., Ashfaq, R., Guillaume, T., 2002, Overexpression of DNA-binding protein B gene product in breast cancer as detected by in vitro-generated combinatorial human immunoglobulin libraries, *Cancer Res.*, 62, 4985–4991.

Ruffner, H., Bauer, A., Bouwmeester, T., 2007, Human protein-protein interaction networks and the value for drug discovery, *Drug Discov. Today*, 12, 709–716. <https://doi.org/10.1016/j.drudis.2007.07.011>

Sancar, A., Lindsey-Boltz, L.A., Unsal-Kaçmaz, K., Linn, S., 2004, Molecular mechanisms of mammalian DNA repair and the DNA damage checkpoints, *Annu. Rev. Biochem.*, 73, 39–85.
<https://doi.org/10.1146/annurev.biochem.73.011303.073723>

Sánchez-Pérez, I., 2006, DNA repair inhibitors in cancer treatment, *Clin. Transl. Oncol. Off. Publ. Fed. Span. Oncol. Soc. Natl. Cancer Inst. Mex.*, 8, 642–646.

Sarre, A., Ökvist, M., Klar, T., Hall, D.R., Smalås, A.O., McSweeney, S., Timmins, J., Moe, E., 2015, Structural and functional characterization of two unusual endonuclease III enzymes from *Deinococcus radiodurans*, *J. Struct. Biol.*, 191, 87–99. <https://doi.org/10.1016/j.jsb.2015.05.009>

Schaap, M., Hancock, R., Wilderspin, A., Wells, G., 2013, Development of a steady-state FRET-based assay to identify inhibitors of the Keap1-Nrf2

protein-protein interaction, *Protein Sci. Publ. Protein Soc.*, 22, 1812–1819.
<https://doi.org/10.1002/pro.2384>

Senarisoy, M., Canturk, P., Zencir, S., Baran, Y., Topcu, Z., 2013, Gossypol interferes with both type I and type II topoisomerase activities without generating strand breaks, *Cell Biochem. Biophys.*, 66, 199–204.
<https://doi.org/10.1007/s12013-012-9468-5>

Skabkin, M.A., Kiselyova, O.I., Chernov, K.G., Sorokin, A.V., Dubrovin, E.V., Yaminsky, I.V., Vasiliev, V.D., Ovchinnikov, L.P., 2004, Structural organization of mRNA complexes with major core mRNP protein YB-1, *Nucleic Acids Res.*, 32, 5621–5635. <https://doi.org/10.1093/nar/gkh889>

Søe, K. and Grosse, F., 2003, p53 stimulates human topoisomerase I activity by modulating its DNA binding, *Nucleic Acids Res.*, 31, 6585–6592.
<https://doi.org/10.1093/nar/gkg846>

Song, L.-N., Bowen, C., Gelmann, E.P., 2013, Structural and functional interactions of the prostate cancer suppressor protein NKX3.1 with topoisomerase I, *Biochem. J.*, 453, 125–36.
<https://doi.org/10.1042/BJ20130012>

Song, Y., Madahar, V., Liao, J., 2011, Development of FRET assay into quantitative and high-throughput screening technology platforms for protein–protein interactions, *Ann. Biomed. Eng.*, 39, 1224–1234.
<https://doi.org/10.1007/s10439-010-0225-x>

Sorokin, A.V., Selyutina, A.A., Skabkin, M.A., Guryanov, S.G., Nazimov, I.V., Richard, C., Th'ng, J., Yau, J., Sorensen, P.H.B., Ovchinnikov, L.P., Evdokimova, V., 2005, Proteasome-mediated cleavage of the Y-box-binding protein 1 is linked to DNA-damage stress response, *EMBO J.*, 24, 3602–3612. <https://doi.org/10.1038/sj.emboj.7600830>

Stavrovskaya, A., Stromskaya, T., Rybalkina, E., Moiseeva, N., Vaiman, A., Guryanov, S., Ovchinnikov, L., Guens, G., 2012, YB-1 Protein and Multidrug Resistance of Tumor Cells, *Curr Signal Transduct Ther.*, 7, 237–246.

Stewart, L. and Champoux, J.J., 1999, Purification of baculovirus-expressed human DNA topoisomerase I, *Methods Mol. Biol.*, Clifton NJ 94, 223–234.
<https://doi.org/10.1385/1-59259-259-7:223>

Stewart, L., Ireton, G.C., Champoux, J.J., 1996, The domain organization of human topoisomerase I, *J. Biol. Chem.*, 271, 7602–7608.

<https://doi.org/10.1074/jbc.271.13.7602>

- Stewart, L., Ireton, G.C., Parker, L.H., Madden, K.R., Champoux, J.J.**, 1996, Biochemical and biophysical analyses of recombinant forms of human topoisomerase I, *J. Biol. Chem.*, 271, 7593–7601.
- Tafari, S.R. and Wolffe, A.P.**, 1992, DNA binding, multimerization, and transcription stimulation by the *Xenopus* Y box proteins in vitro, *New Biol.*, 4, 349–359.
- Tamura, T. and Hamachi, I.**, 2014, Recent progress in design of protein-based fluorescent biosensors and their cellular applications, *ACS Chem. Biol.*, 9, 2708–2717. <https://doi.org/10.1021/cb500661v>
- Thayer, M.M., Ahern, H., Xing, D., Cunningham, R.P., Tainer, J.A.**, 1995, Novel DNA binding motifs in the DNA repair enzyme endonuclease III crystal structure, *EMBO J.*, 14, 4108–4120.
- Toh, S., Nakamura, T., Ohga, T., Koike, K., Uchiumi, T., Wada, M., Kuwano, M., Kohno, K.**, 1998, Genomic organization of the human Y-box protein (YB-1) gene, *Gene*, 206, 93–97.
- Topcu, Z.**, 2001, DNA topoisomerases as targets for anticancer drugs, *J. Clin. Pharm. Ther.*, 26, 405–416.
- Topcu, Z. and Borden, K.L.B.**, 2000, The yeast two-hybrid system and its pharmaceutical significance, *Pharm. Res.*, 17, 1049–1055. <https://doi.org/10.1023/A:1026493310144>
- Tsai, H.-P., Lin, L.-W., Lai, Z.-Y., Wu, J.-Y., Chen, C.-E., Hwang, J., Chen, C.-S., Lin, C.-M.**, 2010, Immobilizing topoisomerase I on a surface plasmon resonance biosensor chip to screen for inhibitors, *J. Biomed. Sci.*, 17, 49. <https://doi.org/10.1186/1423-0127-17-49>
- Tubbs, A. and Nussenzweig, A.**, 2017, Endogenous DNA damage as a source of genomic instability in cancer, *Cell*, 168, 644–656. <https://doi.org/10.1016/j.cell.2017.01.002>
- Urruticoechea, A., Alemany, R., Balart, J., Villanueva, A., Viñals, F., Capellá, G.**, 2010, Recent advances in cancer therapy: an overview, *Curr. Pharm. Des.*, 16, 3–10.
- Vaiman, A.V., Stromskaya, T.P., Rybalkina, E.Y., Sorokin, A.V., Guryanov, S.G., Zabolotina, T.N., Mechetner, E.B., Ovchinnikov, L.P., Stavrovskaya, A.A.**, 2006, Intracellular localization and content of YB-1 protein in multidrug resistant tumor cells, *Biochem. Biokhimiia*, 71, 146–

154.

- Van Munster, E.B., Kremers, G.J., Abjobo-Hermnas, M.J., Gadella, T.W. Jr.**, 2005, Fluorescence resonance energy transfer (FRET) measurement by gradual acceptor photobleaching, *J. Microsc.*, 218, 253–262. <https://doi.org/10.1111/j.1365-2818.2005.01483.x>
- Wang, J.C.**, 2002, Cellular roles of DNA topoisomerases: a molecular perspective, *Nat. Rev. Mol. Cell Biol.*, 3, 430–440. <https://doi.org/10.1038/nrm831>
- Wang, J.C.**, 1971, Interaction between DNA and an Escherichia coli protein omega, *J. Mol. Biol.*, 55, 523–533.
- Wang, Y., Wang, F., Wang, R., Zhao, P., Xia, Q.**, 2015, 2A self-cleaving peptide-based multi-gene expression system in the silkworm *Bombyx mori*, *Sci. Rep.*, 5, 16273. <https://doi.org/10.1038/srep16273>
- Wei, Z.-H., Chen, H., Zhang, C., Ye, B.-C.**, 2014, FRET-based system for probing protein-protein interactions between σR and RsrA from *Streptomyces Coelicolor* in response to the redox environment, *PLOS ONE*, 9, e92330. <https://doi.org/10.1371/journal.pone.0092330>
- Wells, J.A. and McClendon, C.L.**, 2007, Reaching for high-hanging fruit in drug discovery at protein-protein interfaces, *Nature*, 450, 1001–1009. <https://doi.org/10.1038/nature06526>
- Wistow, G.**, 1990, Cold shock and DNA binding, *Nature*, 344, 823–824. <https://doi.org/10.1038/344823c0>
- Wolffe, A.P.**, 1994, Structural and functional properties of the evolutionarily ancient Y-box family of nucleic acid binding proteins, *BioEssays News Rev. Mol. Cell. Dev. Biol.*, 16, 245–251. <https://doi.org/10.1002/bies.950160407>
- Wolffe, A.P., Tafuri, S., Ranjan, M., Familari, M.**, 1992, The Y-box factors: a family of nucleic acid binding proteins conserved from *Escherichia coli* to man, *New Biol.*, 4, 290–298.
- Wright, C.M., van der Merwe, M., DeBrot, A.H., Bjornsti, M.-A.**, 2015, DNA topoisomerase I domain interactions impact enzyme activity and sensitivity to camptothecin, *J. Biol. Chem.*, 290, 12068–12078. <https://doi.org/10.1074/jbc.M114.635078>
- Wu, S.L., Fu, X., Huang, J., Jia, T.T., Zong, F.Y., Mu, S.R., Zhu, H., Yan, Y., Qiu, S., Wu, Q., Yan, W., Peng, Y., Chen, J., Hui, J.**, 2015, Genome-wide analysis of YB-1-RNA interactions reveals a novel role of YB-1 in miRNA

processing in glioblastoma multiforme, *Nucleic Acids Res.*, 43, 8516–8528.
<https://doi.org/10.1093/nar/gkv779>

- Wu, Y., Wang, K., Li, Z., Liu, Y., Izumi, H., Uramoto, H., Nakayama, Y., Ito, K., Kohno, K.**, 2014, Y-box binding protein 1 enhances DNA topoisomerase 1 activity and sensitivity to camptothecin via direct interaction, *J. Exp. Clin. Cancer Res.*, 33, 1–11.
<https://doi.org/10.1186/s13046-014-0112-7>
- Xu, Y., Villalona-Calero, M.A.**, 2002, Irinotecan: mechanisms of tumor resistance and novel strategies for modulating its activity, *Ann. Oncol. Off. J. Eur. Soc. Med. Oncol.*, 13, 1841–1851.
- Yahata, H., Kobayashi, H., Kamura, T., Amada, S., Hirakawa, T., Kohno, K., Kuwano, M., Nakano, H.**, 2002, Increased nuclear localization of transcription factor YB-1 in acquired cisplatin-resistant ovarian cancer, *J. Cancer Res. Clin. Oncol.*, 128, 621–626. <https://doi.org/10.1007/s00432-002-0386-6>
- Yasgar, A., Jadhav, A., Simeonov, A., Coussens, N.P.**, 2016, AlphaScreen-based assays: ultra-high-throughput screening for small-molecule inhibitors of challenging enzymes and protein-protein interactions, *Methods Mol. Biol.*, Clifton NJ 1439, 77–98. https://doi.org/10.1007/978-1-4939-3673-1_5
- Zahreddine, H. and Borden, K.L.B.**, 2013, Mechanisms and insights into drug resistance in cancer, *Front. Pharmacol.*, 4, 28.
<https://doi.org/10.3389/fphar.2013.00028>
- Zhang, J.H., Chung, T.D., Oldenburg, K.R.**, 1999, A simple statistical parameter for use in evaluation and validation of high throughput screening assays, *J. Biomol. Screen.*, 4, 67–73.
<https://doi.org/10.1177/108705719900400206>
- Zhang, Y.F., Homer, C., Edwards, S.J., Hananeia, L., Lasham, A., Royds, J., Sheard, P., Braithwaite, A.W.**, 2003, Nuclear localization of Y-box factor YB1 requires wild-type p53, *Oncogene*, 22, 2782–2794.
<https://doi.org/10.1038/sj.onc.1206357>

CURRICULUM VITAE

MUGE SENARISOY

Born: Jan 1st 1988
Nationality: Turkish
Marital Status: Single
Address: 1858 street, N°: 23/7, Karsiyaka
 35600 Izmir, Turkey
Telephone: +90 232 311 5133 (Lab)
 +0535 823 5342 (Mobile)
E-mail: muge.senarisoym@ibs.fr
muge.senarisoym@gmail.com



EDUCATION:

- 02.2014 - 09.2018: **Joint Ph.D. in Biotechnology**, Université Grenoble Alpes, Ecole Doctorale Chimie et Sciences du Vivant, Grenoble, France and Ege University, Graduate School of Natural and Applied Sciences, Izmir, Turkey. Thesis defence: 27th Sept. 2018.
Title of thesis: Evaluation of YB-1 transcriptional factor, DNA glycosylase hNTH1 and human topoisomerase I functions in relation to drug resistance and DNA repair mechanisms.
- 09.2010 - 06.2013: **M.Sc. in Biotechnology**, Ege University, Graduate School of Natural and Applied Sciences, Izmir, Turkey.
Title of thesis: Differential characterization of the biological activity of Temozolomide.
- 09.2005 - 06.2010: **B.Sc. in Biology**, Ege University, Faculty of Science, Department of Biology, Molecular Biology and Genetic Program, Izmir, Turkey.
Title of thesis: Telomeric repeat maintenance in experimental renal ischemia/reperfusion model and its relation to apoptosis.

WORK EXPERIENCE:

- 05.04.2018-30.09.2018: PhD student at Ege University, Pharmacy Department, Izmir, Turkey. Supervisor/P.I.: Prof. Dr. Zeki Topcu.
- 04.10.2015-04.04.2018: PhD student at the Institut de Biologie Structurale in Grenoble, France. Fellowships from The Scientific and Technological Research Council of Turkey (TUBITAK) and Labex GRAL. Supervisor/P.I.: Dr. Joanna Timmins.
- 20.02.2013-03.10.2015: PhD student at Ege University, Pharmacy Department, Izmir, Turkey. **Project Assistant**, TUBITAK- SBAG112S492. Supervisor/P.I.: Prof. Dr. Zeki Topcu.
- 17.09.2012-15.02.2013: Master student, **LLP/ Erasmus Exchange Program**, Université Joseph Fourier, Department of Chemistry and Biology, Grenoble, France.
Internship project: Recognition of UV-induced DNA lesions by the UvrA1 and UvrA2 proteins, Institut de Biologie Structurale, Supervisor: Dr. Joanna Timmins
- 11.2010-10.2011: Master student, **Project Assistant**, "Role of the human ADA3 protein in transcriptional regulation and its interactions with other transcriptional regulators", TUBITAK- TBAG108T945; "Differential characterization of the biomolecular interactions of DNA topoisomerase-targeting potential anti-cancer agents", TUBITAK- TBAG 108T548. Supervisor/P.I.: Prof. Dr. Zeki Topcu
- 05.2011: Master student, **Laboratory Trainee**, University of Szeged, Departement of Biochemistry and Molecular Biology, Szeged, Hungary, Supervisor: Dr. Imre Boros

- 02-03.2009: Bachelor student, **Laboratory Trainee**, Laboratory of Molecular Medicine Research, Ege University Children Hospital, Izmir, Turkey.
Internship project: Genetic screening tests of Familial Mediterranean Fever, Supervisor: Prof. Dr. Afig Berdeli

COURSES / CONGRESS:

- 09.2017: EMBO workshop “DNA topoisomerases and DNA topology”, Les Diablerets, Switzerland.
- 06.2016: EMBO workshop “Fluorescence microscopy methods to study protein-protein interactions in living cells”, Rennes, France.
- 11.2015: 11ème rencontre Plasticité et Instabilité du Génome, Gif-sur-Yvette, France.
- 10.2014: GTBio Réunion du Groupe Thématique Biologie de l'Association Française de Cristallographie, Grenoble, France.
-
- 07.2011: 36th FEBS, Federation of European Biochemical Societies Congress, “Biochemistry for Tomorrows Medicine”, Turin, Italy.
- 08.2009: Ege University International 3. Molecular Biology and Genetics Application with Research Platform, Izmir, Turkey.

TECHNICAL EXPERTISE:

Molecular biology: PCR, cloning (using both ligase dependent and ligase independent systems), site directed DNA mutagenesis.

Transformation and protein expression in *E. coli*.

Protein purification using Äkta purification systems (Explorer, FPLC, Basic and Prime), protein analysis using SDS-PAGE.

Functional enzyme assays to measure protein stability, activity and specificity and calculation of kinetic constants.

Protein-protein interactions studies with Yeast Two Hybrid and Fluorescence Resonance Energy Transfer (FRET) method.

Epifluorescence and confocal microscopy techniques (eg. FRAP).

Mammalian cell culture (HeLa, MCF7, PC-3) and transient and stable transfections.

Bioinformatics (database searches, sequence alignments, construct design).

PUBLICATIONS:

1. **Senariso M**, Stelter M, Lacroix F, Kleman JP, Barette C, Fauvarque M-O, Timmins J. A FRET-based biosensor for evaluating the hNTH1-YB1 interface as a potential anti-cancer drug target. (2018) *In preparation*.
2. Caliskan G, Baris IC, Ayaydin F, Dobson MJ, **Senariso M**, Boros IM, Topcu Z, Zencir S (2017). Che1/AATF interacts with subunits of the histone acetyltransferase core module of SAGA complexes. *PLoS One*. 12, e0189193.

3. Istanbul H, **Senarisoy M**, Erciyas E and Topcu Z. (2014) Mannich base derivatives as the potential candidates of human topoisomerase II inhibitors, *Lett Drug Des Discov.* 12, 103-108.

4. **Senarisoy M**, Canturk P, Zencir S, Baran Y and Topcu Z. (2013) Gossypol interferes with both type I and type II topoisomerases without generating strand breaks, *Cell Biochem Biophys.* 66, 199-204.

SELECTED POSTERS PRESENTATIONS:

1. **Senarisoy M**, Lacroix F, Kleman JP, Topcu Z, Timmins J. "Study of the hTopol/YB1 complex in relation to anti-cancer drug resistance". EMBO workshop "DNA topoisomerases and DNA topology", Les Diablerets, Switzerland, September 17-21, 2017.

2. **Senarisoy M**, Stelter M, Godel J, Lacroix F, DeBonis S, Timmins J. "Study of the hNTH1/YB1 complex". 11th Genome Plasticity & Instability Workshop, Gif-sur-Yvette, France, November 24-25, 2015.

3. Canturk P, **Senarisoy M**, Nitiss JL, Topcu Z. "Effects of Gefitinib in the sensitivity of selected *Saccharomyces cerevisiae* strains". 36th FEBS, Federation of European Biochemical Societies Congress, "Biochemistry for Tomorrow's Medicine", Turin, Italy, June 25-30, 2011 *FEBS J.*, 278, 324-324.

ORAL PRESENTATIONS:

1. MolMed Axis seminar, IBS, Grenoble, France, Oct. 2017. Title: Development of a FRET-based biosensor for identification of potential anti-cancer agents.

2. Life Science Switzerland Satellite Meeting to EMBO workshop TOPO2017 Les Diablerets, Switzerland, Sept. 2017. Title: Study of the hTopol/YB1 complex in relation to anti-cancer drug resistance.

3. PhD seminar, Faculty of Pharmacy, Ege University, Izmir, Turkey, Apr. 2015. Title: Roles of DNA topoisomerases in DNA repair.

MEMBERSHIP:

Société Française de Biophysique, 2018-continued.

Turkish Biochemical Society; representative of FEBS. 2011-continued.

REFERENCES:

Prof. Dr. Zeki Topcu, Ege University, Faculty of Pharmacy, Department of Pharmaceutical Biotechnology, Izmir, 35100, Turkey.

Tel: +90 232 311 19 31 E-mail: zeki.topcu@ege.edu.tr

Dr. Joanna Timmins, Institut de Biologie Structurale, 71 Avenue des Martyrs, 38044 Grenoble Cedex 9, France.

Tel: +33 (0)4 57 42 86 78. E-mail: joanna.timmins@ibs.fr